NUCLEAR PROGRAMS

BI-MONTHLY PROGRESS REPORT
CONTRACT AT(29-2)-2831
CONTRACT AT(49-15)-3066

MULTI-HUNDRED WATT RADIOISOTOPE THERMOELECTRIC GENERATOR PROGRAM
LES 8/9 PROGRAM
MJS PROGRAM

Period from 1 July - 31 August 1975

prepared for:

ENERGY RESEARCH AND DEVELOPMENT ADMINISTRATION
ADVANCED NUCLEAR ENERGY SYSTEMS
WASHINGTON, D.C. 20545

SPACE DIVISION
P O Box 8661 • Philadelphia Penna 19101

GENERAL ELECTRIC

DISCLAIMER

NUCLEAR PROGRAMS

BI-MONTHLY PROGRESS REPORT
CONTRACT AT(29-2)-2831
CONTRACT AT(49-15)-3066

MULTI-HUNDRED WATT RADIOISOTOPE THERMOELECTRIC GENERATOR PROGRAM
LES 8/9 PROGRAM
MJS PROGRAM

Period from 1 July - 31 August 1975

prepared for:

ENERGY RESEARCH AND DEVELOPMENT ADMINISTRATION
ADVANCED NUCLEAR ENERGY SYSTEMS
WASHINGTON, D.C. 20545

Approved by: C. W. Whitmore
Program Manager
LES 8/9 Program

Approved by: G. Drenker
Program Manager
MJS Program

Approved by: E. W. Williams
Manager
Nuclear Programs

SPACE DIVISION
P O Box 8661 • Philadelphia, Penna 19101

GENERAL ELECTRIC

page blank

1 JULY 1975 TO 31 AUGUST 1975

BI-MONTHLY PROGRESS REPORT

T A B L E O F C O N T E N T S

1.0 INTRODUCTION AND SUMMARY

1.1 INTRODUCTION

This bi-monthly progress report covers significant activities performed or monitored by the General Electric Company on the MHW-RTG Program during the months of July and August 1975. The report includes work on both the LES 8/9 and MJS contracts in the areas of safety, design, development, integration with ERDA and associate contractors, product assurance, hardware fabrication and acceptance testing.

1.2 SUMMARY

The following summarizes some of the more significant activities for the period which are detailed in subsequent sections of this report.

A. Safety

- The final meeting of the Reentry Subpanel for LES 8/9 was held to review the results of ablation tests on the T-50 emissivity sleeve, to discuss proposed further testing and to review JPL reentry breakup analyses for MJS.

- Tests were performed in the AEDC 5-MW arc facility to determine ablation characteristics of Pyrocarb-406 material for the MJS heat source.

- The MJS Ground Safety Analysis Report, GEMS-422, was completed and submitted to ERDA for approval.

B. Systems

- The four top-level GE/MJS specifications were submitted to ERDA for review and approval

- MJS interface meetings were held on 9-10 July at JPL and 26-27 August at GE.

- The LES 8/9 Thermal Working Group Meeting was held on 9 July at TRW, and the final LES 8/9 Preparedness Review was held at Cape Canaveral on 19 August.

- A detailed evaluation was carried out to determine the effects of lower pre-launch and launch temperatures on the RTG case.

C. Isotope Heat Source

- The PMD/PRD operational demonstration test was successfully completed.

- Several methods are being investigated for sealing the plug of the GIS to prevent possible migration of Pu-bearing material.

- The new "DOP-4" Iridium material developed by HNL is being phased into PICS production.

- Two verification impact specimens from current ML/MRC "WG" PICS material failed when impact tested at GE-VF.

- Three PICS specimens made from Pt-3008 alloy survived impact testing at GE-VF.

- PISA vent testing continued at LASL.

- Gas samples from the F5 IHS and Q2 IHS have given added insight into the source of CO being produced from heat source graphitic materials.

- As a result of the new knowledge on the CO content of IHS graphitics, new high-temperature bake-out requirements are being incorporated into the processing of these materials.

- The Q2 IHS was assembled at ML/MRC.

- Stress analyses were performed on the MJS IHS End Cap during end-on reentry and on the LES 8/9 Iridium outer clad at elevated temperature and with differential pressure.

- Thermal analyses were performed to determine LES 8/9 heat source temperatures during SPC storage and LAS processing.

- Analyses were conducted to investigate the mechanisms of GIS deformation during impact.

- Materials development and testing effort continued on: Iridium clad and PICS capabilities, Ir/PuO_2 and C/PuO_2 interactions, carbon/graphite materials, fuel fabrication and fuel characterization.

D. Converter

- 18-Couple module testing results continue to show the performance benefits to be gained from the Si_3N_4 coating.

- Determination was made of the effects of heat treatment on the hardness of "C"-seal silver coatings and Inconel-X substrates.

- Structural integrity of the mounting bracket/outer shell interface was verified by a low-cycle fatigue test.

- Testing was performed to determine the size and quantity of particulate matter generated by lance penetration of the PRD rupture disk.

- The effects of reduced launch temperature on LES 8/9 RTG structure were evaluated by analyses and a review of test data and material properties.

- Analysis was made of the effects of Helium clad leakage on RTG on-pad power with Xenon cover gas.

- Analyses were performed to determine the effects of on-pad cooling on RTG internal pressure characteristics.

- Analyses were started to determine the transient power output characteristics of the MJS-RTG after lift-off.

- Converters F13 and Q2 were completed at RCA and shipped to GE.

- A SNAP-17A module at RCA passed the 10-years of operation mark and is still producing 88% of initial power.

E. Product Assurance

- 120 AN's and 17 ECN's were processed, while 3 PCP's were submitted.

- Pre-shipment buy-off reviews were completed for the F2, F4 and F5 RTGs.

- The MJS Quality Program Plan was submitted to ERDA for approval, revised as requested by SNS, and released for final distribution.

F. Hardware Fabrication

- Q2 converter hardware was processed and delivered to RCA, and Q2 IHS graphitic parts were shipped to MRC.

- Modifications continue on the Q1A and F1E converters for use on the MJS program.

G. Acceptance Testing

- The F5 ETG was converted to the RTG configuration by installation of flight cables and the IHS. Following processing in the LAS, the F5 RTG was subjected to the following tests: mass properties, pre-vibration air performance/pressure decay, OA vibration, post-vibration air performance/pressure decay, thermal vacuum performance and post-TV performance/pressure decay. The unit was put into storage to await shipment to MRC.

- The following operations were completed on the F13 unit: ETG receiving inspection, electrical checks, cold pressure decay tests, cable installation, ETG disassembly, and the start of RTG assembly.

- The F-2-RTG Gas Management Valve was reworked successfully to add an adapter to correct for damaged threads, and the following operations were then carried out on this RTG: installation of a new forward dome incorporating a PRD, pre-vibration air performance/pressure decay test, and OA vibration.

- The F3 RTG remained in storage except for gas sampling and pressure adjustment activities.

- The following operations were completed on the F4 RTG: OA vibration, post-vibration air performance/pressure decay tests, thermal vacuum testing, post-TV air performance/pressure decay tests, installation into the SC, gas sampling and finally, shipment of the unit via ERDA van to MRC for storage prior to transfer to Cape Canaveral for launch.

H. Ground Support Equipment

- Power Supply and Readout Console design modifications to meet new program requirements were finalized and documented in drawings, drawing changes and procedure revisions.
- All RTG-SC's are updated and ready for use on LES 8/9.
- Mods were completed on the first SPC for MJS, which was then shipped to MRC for Q2 use.
- The Loading and Assembly Stations functioned well except that LAS #1 had to be shut down on two occasions: once for repair of the Stokes pump, and another time for dismantling and cleaning of all valves and replacement of their O-rings.
- Updating rework continued on LAS #2 during periods when it was not being used for ETG/RTG operations.

3.0 SAFETY

3.1 SAFETY ANALYSIS

3.1.1 LES 8/9 Safety Review

The final meeting of the Re-entry Subpanel for LES 8/9 was held at GE on July 18, 1975. The purpose of the meeting was to review the results of the ablation tests on the T-50 emissivity sleeve samples for the LES 8/9 HSA. The results of these tests were reported in the May-June Bimonthly Report. Based on the test results, the Subpanel concluded that their assumption of aeroshell failure for all steep angle, high velocity re-entries was confirmed for purposes of the SER (Safety Evaluation Report) for LES 8/9.

GE's proposal for the remainder of the ablation tests was discussed. The roughness portion (wedge tests) of the T-50 material tests was to be eliminated. Both stagnation line (specimens normal to flow field) and wedge (angle) tests of the Pyrocarb 406 material for the MHW/MJS HSA ablation sleeve were to be performed pending approval from ERDA/SNS. Subsequent to this meeting, approval was received, and the tests were conducted. See Section 3.2 for a summary of the tests.

Several members of the Re-entry Subpanel indicated the desirability of obtaining additional ablation data at test facilities having higher enthalpy capability and where the specimen can be immersed in the flow. If this type of test were to be authorized, it would probably involve longer range planning since appropriate facilities might require modification to accommodate the test, and priority might need to be obtained in order to make the facility available. The possibility of using a small-scale model was also suggested in lieu of a full-scale sleeve.

As a part of this meeting, the analyses of the re-entry breakup cases performed to date by JPL for the MJS'77 mission were discussed. In the three cases analyzed (see May-June Bimonthly Report, Section 3.1.6), JPL predicted that the array of three (3) stacked RTG's will be released as a unit in an end-on orientation that will be a stable configuration (aerodynamically). GE's analysis of the RTG response in the steep angle, superorbital re-entry indicates that failure of the aeroshell (end cap) due to stress will occur for the forward RTG.

This situation was brought to the Subpanel's attention so that the situation would not exist unannounced until late in the program.

Following the regular meeting, the Subpanel held a closed session. As a result of their meeting, the following decisions and recommendations evolved:

LES Mission

1) There were no additional actions to be taken by GE for the LES mission safety evaluation.

2) The Subpanel will estimate the FSA recession assuming heat shield breakup at 10 seconds after the 400°K feet altitude for the steep angle re-entry (Case VI). The calculation will provide estimates of impact shell recession and PICS temperature using a factor of three increase for the diffusion-limited erosion.

MJS Mission

1) GE is to proceed with the AEDC arc tests of the Pyrocarb 406 sleeve samples in order to obtain an early indication of the recession capability of the sleeve.

2) A high enthalpy ablation test of the Pyrocarb sleeve with a model immersed in the flow should be pursued. Data should be obtained for the safety evaluation whether or not it is available in time to influence the design.

3) Perform an ablation test on full-scale graphite impact shells of the FSA and then conduct impact tests of FSA's with the ablated shells. Both high pressure and high enthalpy data should be obtained.

4) Perform the RTG/HSA re-entry analysis for the orbital decay case for MJS as soon as possible.

5) Perform a test to determine the contact coefficients between the ablation sleeve and the aeroshell.

Subsequent to the Re-entry Subpanel meeting, the Subpanel Chairman formally notified ERDA and JPL that the end-on analysis of the converter stack implies failure of at least the forward heat source, and both were requested to address the problem.

3.2 TESTING

A series of tests was performed during mid-August in the AEDC (Arnold Engineering Development Center) 5 MW arc facility to determine the ablation characteristics of the ablation sleeve material (Pyrocarb 406) for the MHW/MJS Heat Source. Also the roughness characteristics of the ablated specimens were to be determined. These tests are similar to those for the T-50 sleeve for MHW/LES 8, 9 reported in the May-June Bimonthly Report. Similarly, the objective of the tests was to simulate as closely as possible trajectory conditions for the high velocity, steep angle re-entry identified for MJS (36,000 fps, -45^{o}). The simulation was to include comparable stagnation pressures and best attainable values of heat transfer and stream enthalpy. As in the T-50 material tests, the ablation performance was to be compared with that of ATJ graphite and a comparison made with analytical predictions.

The specimens of the Pyrocarb 406 sleeve material used in these tests were the same size as the previous T-50 sleeve samples - 2x3 inches with the long dimension running in the circumferential direction of the sleeve. In addition to the specimens for stagnation testing, other specimens were tested in an orientation inclined to the flow in order to determine the effect of the flow shearing component. These specimens were inclined at both 45^{o} and 60^{o} angles to the midpoint of the flow at its impingement point on the sample. Stagnation pressure gages and copper block calorimeters having the same external dimensions and shape (curved) of the test specimens were used for measurement of the (arc) stream conditions. The test matrix is shown on Table 3-1.

Arc operating conditions were chosen to give as near maximum stream enthalpy as possible within the capability of the facility for the desired pressure at the test specimen position. An enthalpy level of around 2000 BTU/lb. was targeted, with the integrated heating at the higher level selected to approximate that for a 36,000 fps, -45^{o} angle re-entry, shown in Figure 3-1.

TABLE 3-1

PYROCARB 406 ABLATION PROGRAM

TEST MATRIX

ARC PRESSURE	170 ATM		
ENTHALPY	2000 BTU/LB		
MODEL DISTANCE	RUN 1	1.75 In.	
	RUN 2	1.75 In.	

Run	Sting	Material	Inclination from Vertical (Deg.)	G_L Heat Transfer (BTU/Ft^2-Sec.)	Pressure (ATM)	Test Time (Sec.)	Integrated Heating (BTU/Ft^2) Facility	Flight
1	1	Pyrocarb	0	1130	6.35	5.0	5650	9800
	2	Pyrocarb	0	1130	6.35	5.0	5650	9800
	3	Pyrocarb	0	1130	6.35	8.5	9600	9800
	4	ATJ-S	0	1130	6.35	8.5	9600	9800
	5	CAL	0	-	-	Sweep*	-	-
	6	Pressure	0	-	-	Sweep*	-	-
	7	CAL	0	-	-	Sweep*	-	-
2	1	Pyrocarb	60	565	3.17	5.0	2820	4900
	2	Pyrocarb	60	565	3.17	8.5	4800	4900
	3	Pyrocarb	45	800	4.50	5.0	4000	6940
	4	Pyrocarb	45	800	4.50	8.5	6800	6940
	5	ATJ-S	45	800	4.50	8.5	6800	6940
	6	CAL	60	-	-	Sweep*	-	
	7	CAL	45	-	-	Sweep*		

*CALS TO BE REPEATED IN REVERSE ORDER

FIGURE 3-1

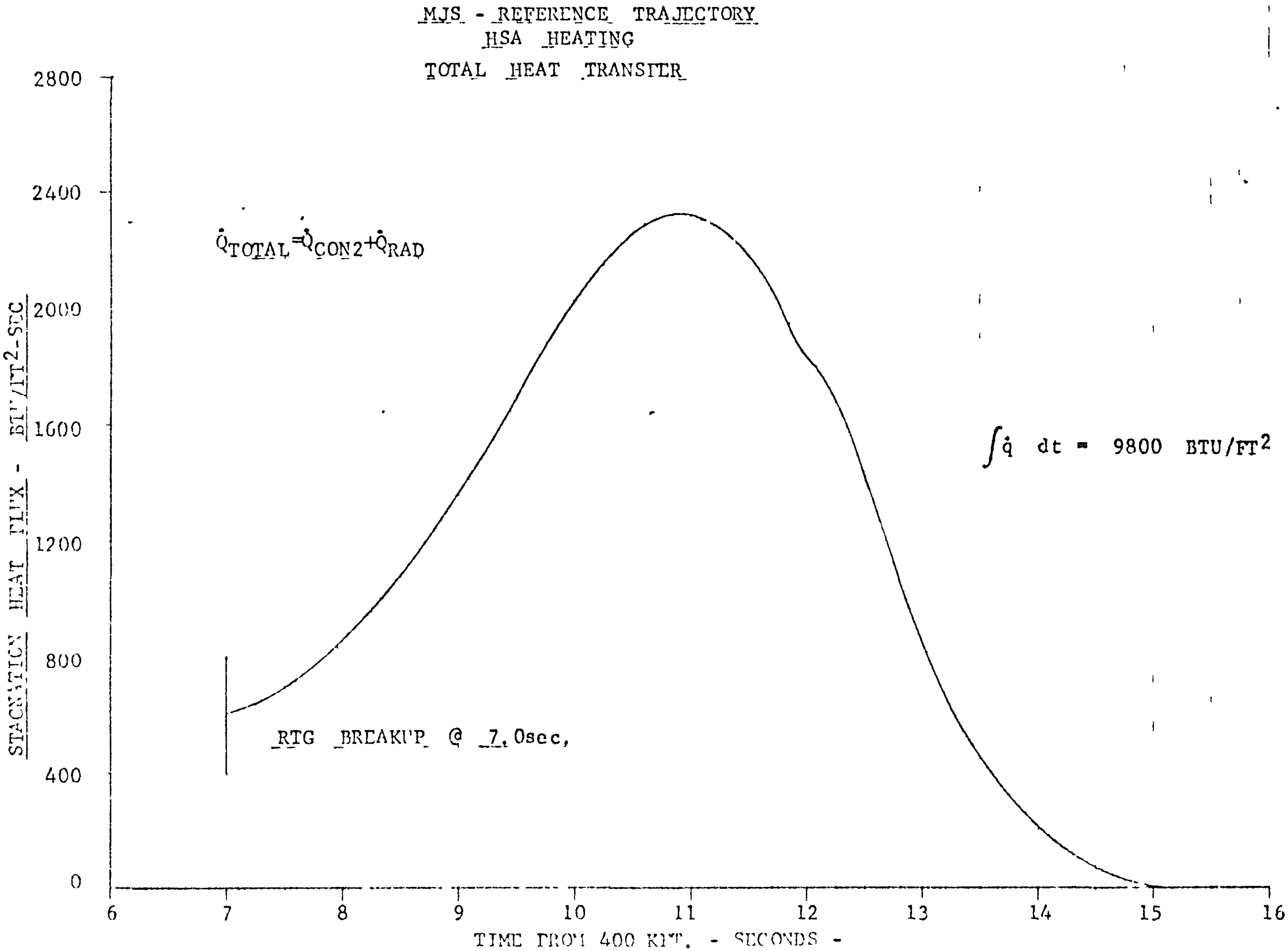
MJS - REFERENCE TRAJECTORY
HSA HEATING
TOTAL HEAT TRANSFER
$\dot{Q}_{TOTAL} = \dot{Q}_{CONV} + \dot{Q}_{RAD}$
$\int \dot{q}\ dt$ = 9800 BTU/FT²
RTG BREAKUP @ 7.0sec,
2800
2400
2000
1600
1200
800
400
0
6
7
8
9
10
11
12
13
14
15
16
STAGNATION HEAT FLUX - BTU/FT²-SEC
TIME FROM 400 KFT. - SECONDS -

Table 3-2 presents the data obtained for the first run having the test specimens normal to the flow (stagnation conditions). The results from the inclined specimens test are not yet available. An inspection of the stagnation test specimens (Pyrocarb 406) has shown that the ablation is relatively uniform around the stream centerline as contrasted with the previous T-50 specimens. No localized attack or channeling occurred in the Pyrocarb 406 specimens, and the measured recession of this material is approximately 1.2 times that of the ATJ material, the latter being comparable to the analytically-predicted value. Surface irregularities (roughness) for the ablated Pyrocarb specimens appear to be greater than one (1) mil.

3.3 OPERATIONAL SAFETY

3.3.1 MJS Ground Safety Analysis Report

The Safety Analysis Report of MHW IHS operations at GE/VFSC for the MJS Program (GSAR, GEMS-422, dated 8/29/75) was submitted to ERDA/SNS for approval. The GSAR provides a summary of the GE/VFSC plans and precautions for the safe handling of the IHS during MJS-RTG assembly and test operations. All credible accident situations are identified and analyzed with a view towards minimizing the potential consequences of such accidents. ERDA Operational Safety approval of this document is required before the Qualification Heat Source (Q-2) can be shipped from Mound Laboratory to GE.

3.3.2 MHW/MJS Radiological Protection Plan

The MHW LES 8/9 Radiological Protection Program Plan (GEMS-409) is being revised to reflect the following changes:

1. RTG/IHS modifications

2. Assembly and test operations

3. Implementation of revised ERDA Manual Chapter 0524, Standards for Radiation Protection, which reduces the allowable radiation exposures to personnel and requires that exposures are limited to the lowest levels technically and economically practicable.

TABLE 3-2

MODEL POSITION 1.75 INCHES FROM NOZZLES

Model	Material	Arc Pressure (ATM)	Model Pressure* (ATM)	Test Time (Sec)	Enthalpy (BTU/Ft^2-(Sec)	G_L Heat Transfer (BTU/Ft^2-Sec)	Integrated Heating Facility (BTU/Ft^2)	Integrated Heating+ (BTU/Ft^2)
1	Pyrocarb	16.2	7.12	4.80	2268	1200	5760	5650
2	Pyrocarb	16.2	7.12	4.95	2268	1200	5940	5650
3	Pyrocarb	16.2	7.12	8.42	2268	1200	10,100	9800
4	ATJ-S	16.2	7.12	8.37	2268	1200	10,050	9800

* Based on Preliminary Data

\+ Based on 9800 Integrated Trajectory Heating

4.0 SYSTEMS

1. The four top level GE/MJS specifications were submitted to ERDA in July for review and approval:

SS47A14617	Systems Specification, MHW Radioisotope Thermoelectric Generator for the Mariner Jupiter Saturn Spacecraft
NS-0020-05-03	Environmental Criteria and Test Requirements for the MJS Multi-Hundred Watt Program
CP47A14619	Product Specification for the MHW-RTG, MJS
CP47A14618	Product Specification for the MHW-ETG's, MJS

2. A third revision to the Lincoln Lab Source Control drawing was received on 18 July and subjected to a thorough review by the GE field team that will be working with the drawing during GE operations at the Cape. Comments and suggested additional revisions were forwarded to Lincoln Lab on 5 August.

3. MJS interface meetings were held on 9-10 July at JPL and on 26-27 August at GE. Primary topics of discussion at the first meeting were the MJS Interface Specification and Control Drawing, RTG characteristics, test and environmental interfaces and requirements and open action items.

   At the second meeting, the primary topics were the status of MJS reentry analyses, ablation test results, system safety test plans and the status of the GE transient power analysis. JPL indicated that scale model wind tunnel tests are planned for early September which, hopefully, will resolve some of the questions concerning stacked end-on reentry of the MJS RTG's. GE-proposed trim tabs will be included in the model testing.

4. GE attended and participated in a final LES 8/9 Preparedness Review at Cape Canaveral on August 19th. GE, Lincoln Lab, TRW and MMC operations at the Cape were presented and discussed.

5. GE was represented at the LES 8 & 9 Thermal Working Group meeting at TRW on July 9. The two items of particular interest to GE were the pre-launch RTG temperature predictions and their effect on the structural capability of the RTG's (cold temperature Beryllium problem), and the discovery of a new Stage-0 booster-induced loading condition. These two items triggered significant activity during the reporting period.

6. As a result of the uncertainties in the pre-launch temperatures, Lincoln Lab conducted a test of the air conditioning system using E1 and E2 ETG's in the stacked configuration. These tests were conducted with the diffuser head in both the integration and launch positions. The flow rate was 90 lbs./min. which corresponds to 180 lbs./min. for the 4 units. The ETG's were pressurized with Xenon gas. The temperatures measured on the Beryllium cases were similar to the measurements from the previous TRW air conditioning verification tests which used the aluminum RTG thermal simulators.

7. A detailed evaluation of the effects of the lower pre-launch and launch temperatures on the Beryllium RTG case was completed (see Section 6.3.2 of this report). 50°F was established as the low temperature limit. Based on fracture mechanics analyses, with suitable inspection for damage prior to assembly on the spacecraft, the structural capability of the beryllium case and stacking adapters will be adequate at the reduced temperatures.

5.0 ISOTOPE HEAT SOURCE (IHS)

During this reporting period July/August 1975, the design and development work continued with emphasis in the following areas:

- Investigation of the feasibility of sealing the GIS.
- Determination of degassing conditions for the IHS carbon components.
- A review of the outgassing from the F-4/IHS.
- A review of Ir behavior in the presence of Si.
- Calculation of the thermal behavior of the IHS during processing.

5.1 GENERAL

5.1.1 Design

Changes to specifications and drawings of the carbon/graphite components were initiated to reflect the revised requirements for high-temperature bakeout of these materials.

5.1.2 Ablation Sleeve

5.1.2.1 LES 8 & 9

The last of the T-50 composite ablation sleeves was successfully degassed in the GE-Evendale Facility.

5.1.2.2 MJS

The fabrication problems affecting the MJS Pyrocarb 406 sleeve were resolved. The sleeve for the Q-2/IHS was successfully installed at ML/MRC.

5.1.3 Gas Management System (GMS)

5.1.3.1 Function of the PMD/PRD

The PMD/PRD is a "pressure maintenance and pressure relief" device designed to manage the helium pressure of the IHS. It is attached downstream of the IHS vent valve on the converter fin. The PMD/PRD has three (3) primary functions:

1) Maintain a seal, pneumatically isolating the IHS from the air environment while on the launch pad.

2) Vent the IHS to space immediately after launch.

3) Maintain a slight helium pressure within the IHS during space operation.

The seal prior to launch is maintained by a rupture diaphragm mechanically sealed in the PMD/PRD housing.

The IHS is vented after launch by the action of a lance piercing the rupture diaphragm. This is caused by the expansion of an evacuated bellows/spring system which is activated by the reduction of atmospheric pressure subsequent to launch. This constitutes the Pressure Relief Device (PRD).

A slight helium pressure in the IHS is maintained after venting to space by the flow characteristics of a capillary tube sized to create the required back pressure at the helium generation rate of the IHS. This constitutes the Pressure Maintenance Device (PMD).

5.1.3.2 Testing of the PMD/PRD

Tests discussed in previous Bi-Monthly Reports covered operation and life testing of components. During July/August 1975, the PMD/PRD was tested as a system under operational conditions of pressure and temperature and an operational demonstration was successfully completed. After pressurizing with helium to 15 ± 0.5 psia, the leak rate was less than 1×10^{-5} scc/sec (actual leakage -- 5.0×10^{-8} scc/sec.). Subsequent to achieving operational conditions, puncture occurred and the achieved helium flow rate was 1.192×10^{-4} scc/sec (allowable range -- 1×10^{-4} to 4×10^{-4} scc/sec.). Back pressure stabilized at 1.415 psia. This successful test satisfied the operational demonstration requirements.

5.1.4 Fuel Sphere Assembly (FSA)

5.1.4.1 Graphite Impact Shell (GIS)

The possibility of providing a seal for the plug of the GIS was investigated. See Figure 5.1-1. The purpose of this sealing was to prevent the possible migration of Pu-bearing material from the inside

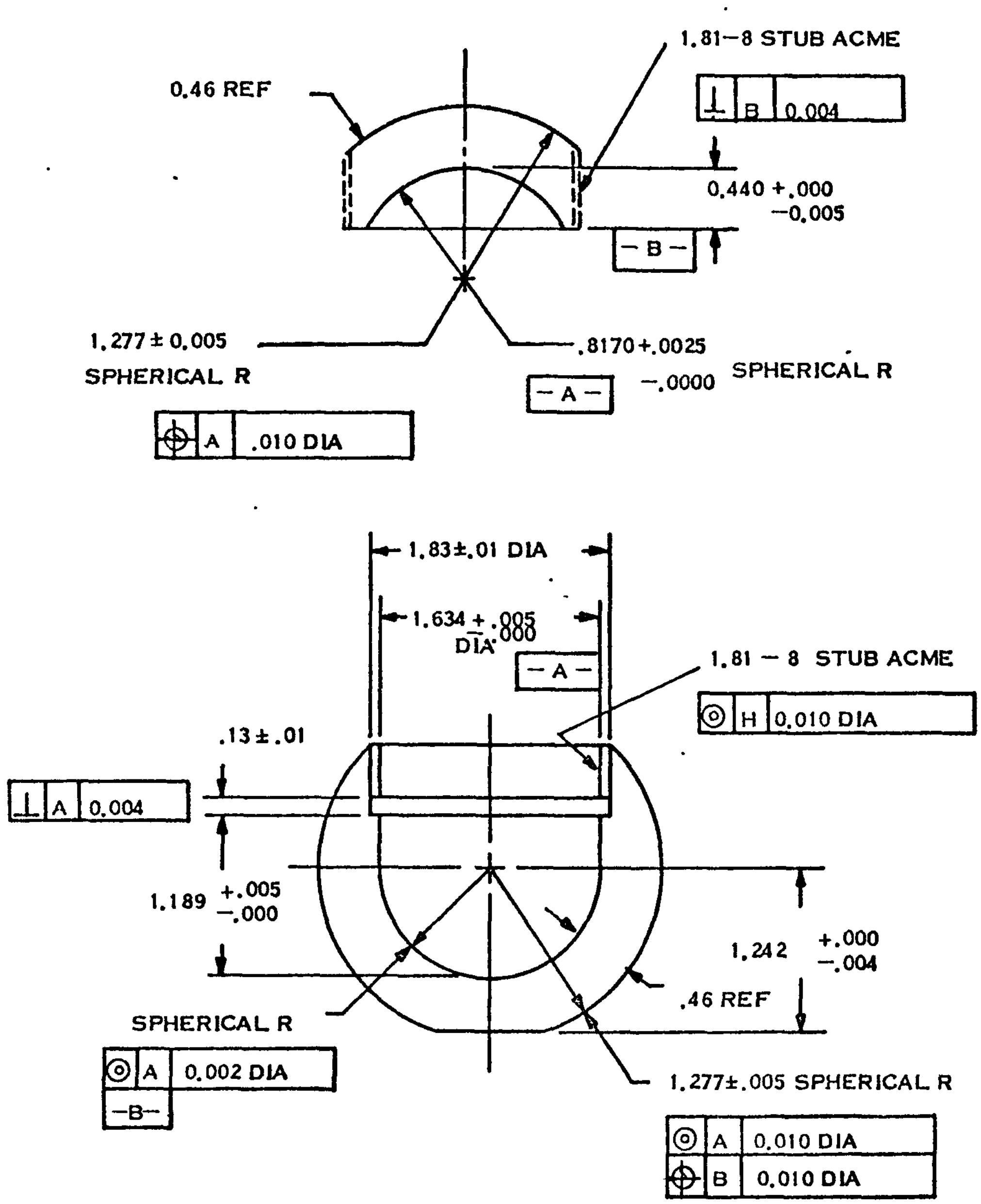

Figure 5.1-1 Graphite Impact Shell - GIS

of the GIS to the surface. (See the previous Bi-Monthly Reports for 1975 for a discussion of the anomalous behavior of MHF-13, a fueled FSA removed from the Q-1/IHS which apparently leaked Pu during storage.)

5.1.4.1.1 Sealing of the GIS Plug

Two possible methods of sealing the GIS plug were proposed:

- Use of a gasket at the base of plug.

- Use of a sealant/glue on the threads.

Both possibilities were considered and consultations were held with Oak Ridge (Y-12) and glue manufacturers. Glues having formulations containing only hydrogen and carbon were considered to minimize the possibility of constituents which could affect the integrity of the Ir PISA. Two sealant materials in the form of powders; namely: HA-43 and ITX-PITCH, and two vehicles/solvents; namely: indene and toluene, were identified as candidates. The most promising method of applying the sealant appears to be the wetting and curing of a carbon felt washer that is inserted into the body of the GIS at the base of the plug threads (see Figure 5.1-2). An alternate method consists of applying glue at the base of the threads directly as shown in Figure 5.1-3. In both cases the glue is cured in place by self-heating from the fueled PISA.

5.1.4.1.2 Problems and Proposed Testing Programs

Because of the intimate contact between the GIS and the Ir of the PISA, the materials of any seal used as well as the process of application must be shown by testing to have no adverse effects on the containment capability of the PISA. The application and curing of the seals must be carried out after assembly of the fueled PISA into the GIS in the ML/MRC "F" line. Consequently, the feasibility of performing the required operations must be demonstrated. The integrity and impermeability of the seal must also be tested. It is recognized that initiation of the sealant development program cannot be effected rapidly enough to permit use of a tested seal in the fabrication of the Q-2/IHS and the first of the MJS flight units. At the end of the July/August reporting period, no decision had been reached for implementation of the GIS sealing program.

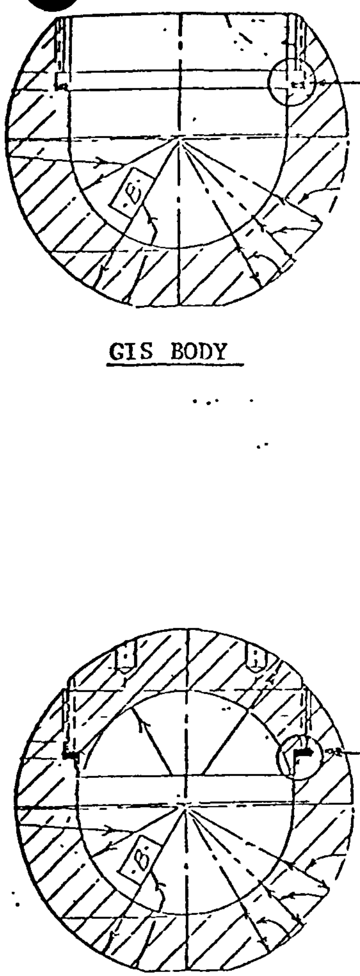

Figure 5.1-2 GIS Sealed by Carbon Felt Impregnated gasket

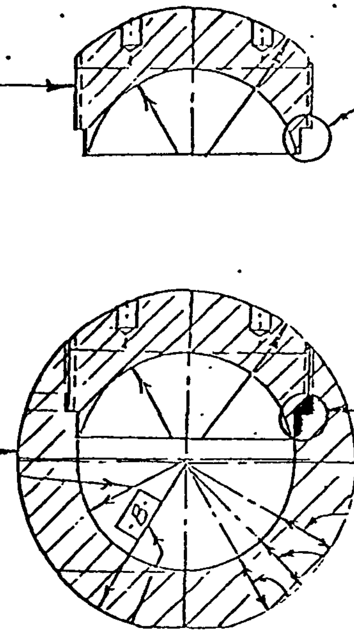

Figure 5.1-3 GIS Sealed by Glue at Base of Cap Threads

5.1.4.2 Post Impact Containment Shell (PICS)

5.1.4.2.1 Fabrication

A. Details of the production of Ir sheet and Ir hollow hemispheres are given respectively in the reports of the HNL Metallurgy and Ceramics Division and in the monthly Newsletters of ML/MRC.

B. The HNL "DOP-4" material is being phased into production for MJS. GE has recommended the establishment of a specification for the improved material which will include a determination of the mechanical response in addition to the usual requirements.

5.1.4.2.2 Impact Tests

Two additional impact tests were performed on the impact verification specimens produced by ML/MRC from the current production materials, designated WG. Both units failed on impact; see Paragraph 5.2.

5.1.4.3 PISA Venting

5.1.4.3.1 He Release

PISA vent testing continued at LASL with fueled specimens operating at temperatures simulating the operating conditions for LES 8 & 9 (on MHFT-44 in He) and for MJS (on MHFT-37 and MHF-30 in vacuum).

A. MHFT-37 is operated in vacuum at an effective fuel/Ir PICS interface temperature of $\sim$1335^{o}C. The erratic behavior of intermittent He release continued during the reporting period. The He release dropped below the detection limit and remained below this level (plugged) for $\sim$20 days after which sporadic bursts of He were observed. The effective release of He was sufficient to preclude pressurization of the PICS. This unit has been on test for 11,300 hours.

B. MHFT-44 is operated in He with the fuel/Ir PICS interface temperature at $\sim$1220^{o}C. This unit was placed on test in June 1974 and is checked once a month for He release, since continuous monitoring is precluded by the He furnace atmosphere. The He release was steady and equal to the generation rate. The erratic behavior reported in the May/June Bi-Monthly Report has apparently been cleared.

C. MHF-30, one of the FSAs removed from the Q-1/IHS is operated in vacuum with the fuel/Ir PICS interface temperature at ~1335°C. The He release from this unit has continued steadily at the generation rate during the current reporting period.

D. The vent designs are shown in Figure 5.1-4 and the performance is shown in Tables 5.1-1a and 5.1-1b.

5.1.4.3.2 Pu Release

A. The activity levels found in the GISs analyzed destructively or otherwise at ML/MRC and at LASL are shown in Table 5.1-2. A cogent explanation for the wide differences found among these units is still lacking. However, further data on the behavior of MHD-26 (discussed in the next paragraph) is suggestive.

B. The unfueled test FSA, MHD-26 has now been exposed for a total of 1535 hours at 1350°C. The data on this unit are summarized in Table 5.1-3.

The MHD-26 PISA does not contain a fuel sphere and its decon covers remain intact as shown by He leak tests. However, the quantity of Pu found in successive decontaminating washes and present on the surface as indicated by direct counting (as opposed to wipes) has continued to increase after each exposure to high temperature. These observations indicate that:

- There is virtually no useful correlation between contamination levels established by wiping and those determined by direct measurement.
- The direct measurements made immediately after PISA fabrication permit no prediction of what levels will be found after high temperature exposure.
- The very high levels found in the decontamination washes of MHD-26 after 1535 hours, $\geq 5 \times 10^7$ DPM, (~20 μCi) suggest that the current decontamination methods are not consistent.
- The wide divergence found in the amount of Pu in the GISs may result from contamination not detected by the wipe methods.

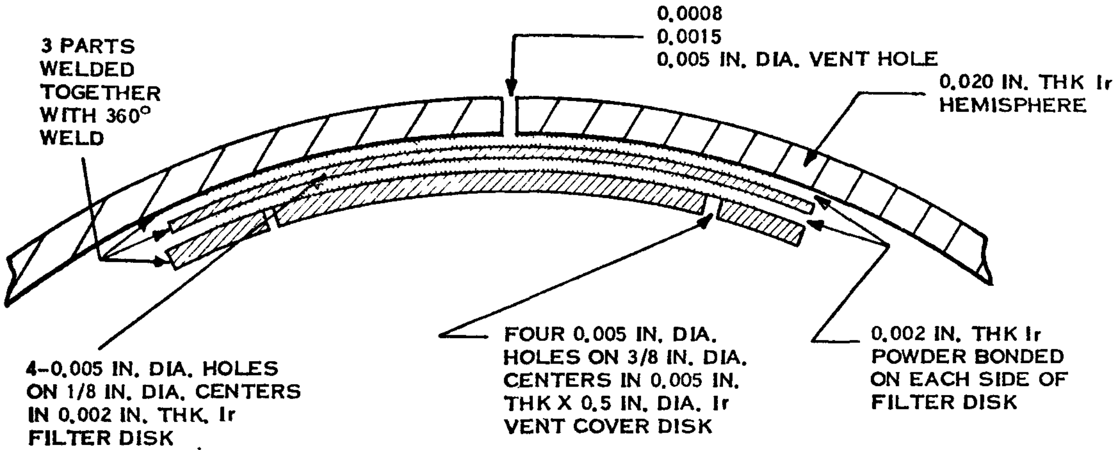

Pre-Flight MHW PISA Vent Design

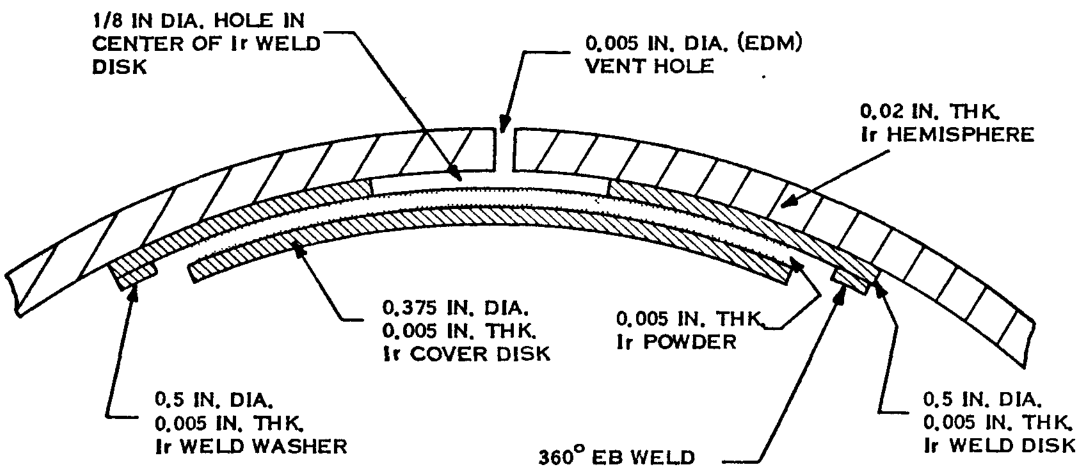

MJS & LES 8/9 Vent Design

Figure 5.1-4 MHW-IHS Vent Filter Designs

Table 5.1-1a MHW PICS Vent Test Data

(Individual Spheres)

Specimen Number	Status	Test Conditions: Temperature - °C	Exposure Time - Hours	Exposure Environment	Dimensional Change	Vent Conditions: He Mass Spec.: In Furnace (1)	In Lab (2)	Bubble Check: No. 1	No. 2	Testing Organization	Metallography/Comments
* MHFT-37	On test	1335	12000	vacuum	nyr	erra-tic	n/a	nyr	nyr	LASL	nyr; test continuing
MHFT-39	C&E	1335	2000	vacuum	none	n/a	open	nyr	nyr	LASL	Vapor deposited ceramic in vent filter: Si, Pu, Ca, O + (Mg, Al, Fe) - impacted
MHFT-40	C&E	1335	2000	vacuum	none	n/a	open	open	open	LASL	Vapor deposited ceramic in vent filter: Si, Pu, Ca, O + (Mg, Al, Fe) - impacted
MHFT-41	C&E	1335	2000	vacuum	none	n/a	closed	closed	closed	LASL	Not impacted; same as MHFT-40
* MHFT-42	C&E	1335	5400	vacuum	none	erra-tic	n/a	n/a	n/a	LASL	Vapor deposited ceramic in vent filter: O, Pu, Ca, Si, (Mg, Al, Fe) -
* MHFT-44	On test	1220	9200	Helium	nyr	n/a	open	n/a	n/a	LASL	nyr; test continuing
MHFT-45	C&E	1335	720	vacuum	none	n/a	open	open	closed	LASL	Vapor deposited ceramic in vent filter: Pu, Ca, Si, O, + (Mg, Al, Fe) - impacted
MHFT-47	C&E	1335	720	vacuum	none	n/a	open	nyr	nyr	LASL	Same as MHFT-45 - impacted
MHFT-48	C&E	1335	720	vacuum	none	n/a	open	nyr	nyr	LASL	Same as MHFT-45 - impacted
MHFT-49	C&E	1335	720	vacuum	none	n/a	open	open	closed	LASL	Same as MHFT-45 - impacted
MHFT-50	C&E	1335	720	vacuum	none	n/a	open	nyr	nyr	LASL	Same as MHFT-45 - impacted

n/a = not applicable

nyr = not yet reported

* special vent test specimens

C&E = Test complete and specimen examined

(1) Mass spec. measurement in furnace at test temperature

(2) Mass spec. measurement in lab. vac. chamber self-heat temp. ≥ 900°C

Table 5.1-1b MHW PICS Vent Test Data (Spheres from Q-1)

Specimen Number	Status	Test Conditions: Temperature °C	Exposure Time-Hours	Exposure Environment	Dimensional Change	Vent Conditions: He Mass Spec.: (1) In Furnace	(2) In Lab	Bubble Check: No. 1	No. 2	Testing Organizational	Metallography/Comments
MHF-27	C&E	~ 1220	200	He	none	N/A	open	open	open	LASL	Frit generally clean but some Pu, Ca, Si ceramic material vapor deposited
MHF-28	C&E	~ 1220	200	He	none	N/A	N/A	open	open	ML	Same as MHF-27
MHF-29	C&E	~ 1220	200	He	none	N/A	N/A	open	open	ML	Same as MHF-27
MHF-30	On test	~ 1220 1335	200 6500	He Vacuum	nyr nyr	erratic	N/A	N/A	N/A	LASL	nyr
MHF-13	C&E	~ 1200	200	He	nyr	N/A	N/A	open	open	ML	Same as MHF-27 Used old type vent filter

Note: Vent holes all .005 inch diameter.

N/A = not applicable

nyr = not yet reported

C&E = Test Complete and specimen Examined

(1) Mass spec. measurement in furnace @ test temp.

(2) Mass spec. measurement in lab vac. chamber @ self-heat temp. = 900 C.

Table 5.1-2 Plutonium Content of MHW GIS's

Sample No.	Heat Treatment			Total Pu	Comment
	Time, h	Temp.[a] °C	(°F)	μg	
MHFT-15	7395	1268	(2314)	19	vacuum
MHFT-18	1332	1180	(2156)	17	helium
MHFT-19	1100	1265	(2309)	56	vacuum
MHFT-21	4500	1180	(2156)	8	helium
MHFT-22	3400	1265	(2309)	625	vacuum, PICS cracked
MHFT-39[b,c]	2009	1207	(2205)	720	vacuum, several cracks
MHFT-40[b,c]	2009	1207	(2205)	15	vacuum, one small crack
MHFT-41[b]	2009	1207	(2205)	8	vacuum
MHFT-42	5440	1210	(2210)	1600	vacuum
MHFT-45[b,c]	720	1210	(2210)	460	vacuum, no crack
MHFT-47[b,c]	720	1210	(2210)	18700	vacuum, cracked
MHFT-48[b,c]	720	1210	(2210)	14700	vacuum, cracked
MHFT-49[b,c]	720	1210	(2210)	160	vacuum, cracked
MHF-27	200	1210	(2210)	38	Q-1 heat source
MHF-29	200	1210	(2210)	0.05	Q-1 heat source

[a] GIS exterior

[b] SVT sample

[c] Impacted

Table 5.1-3
RADIOLOGICAL CONTAMINATION DATA FOR MHD-26
(Direct Readings)

POSITION OF MEASUREMENT	CUMULATIVE EXPOSURE PERIOD AT 1350°C									
	INITIAL		100 hrs.		300 hrs		700 hrs		1535 hrs	
	CPM x 10^3	% ≥5.4 Mev	CPM x 10^3	% ≥5.4Mev	CPM x10^3	% ≥ 5.4Mev	CPM x10^3	% ≥5.4Mev	CPM	%≥5.4Mev
POLE NO.1	0.020	100 ↓	24.7	91	137.0	61	261.0	↑	↑	↑
POLE NO.2	0.002	↓	14.7	88	72.7	55	206.0	↑	↑	↑
WELD A	15.1	↓	27.6	47	70.6	51	180.0	↑	↑	↑
WELD B	4.7	↓	6.0	50	18.7	47	202.0	↑	↑	↑
WELD C	6.3	↓	9.8	45	49.2	55	97.0	~7	≥4x10^6	~27
WELD D	47.1	↓	59.3	48	119.8	53	110.0	↓	↓	↓
45° R	1.5	↓	23.1	68	134.0	59	137.0	↓	↓	↓
45° L	0.5	↓	14.9	62	81.3	53	235.0	↓	↓	↓
WIPE	300 dpm		1300 dpm		n/a		n/a		4.0 x 10^5	
DECON SOLUTION	n/a		n/a		2 x 10^6 dpm		2.3 x 10^7 dpm		5.0 x 10^7 dpm	

5.1.5 Gas Analysis on the MHW-IHS

5.1.5.1 Gas Sampling Results

Gas samples were taken on the F-5/IHS at ML/MRC and GE-VF and on the Q-2/IHS at ML/MRC. The results of the analyses are shown in Table 5.1-4a, -4b, -4c, and -4d.

5.1.5.2 Review of Gas Analyses on F-4

The apparently anomalous gas release behavior of the F-4/IHS during processing in the LAS at GE-VF is now believed to reflect the normal release of retained CO from the carbon/graphite parts which were insufficiently degassed prior to assembly; see also Paragraph 5.1.6. Under similar processing conditions the F-5/IHS behaved in a markedly similar matter. It thus appears that there was no accidental in-leakage of air into the LAS during processing and that the contributions arising from interactions with the PuO_2 fuel (see Section 5.4) were probably minimal, especially during the storage phase. However, the handling of large pieces of graphite in air, necessitated by the equipment constraints at ML/MRC, permitted resorption of O_2 and H_2O and consequent production of CO during storage and processing.

The initial proportion of CO/CO_2 observed in the F-5/IHS analyses support the supposition that a large fraction of the initial gas production occurred at the relatively low temperatures, $\sim 500^{o}C$, in the aeroshell during storage.

5.1.6 Degassing of Carbon/Graphite Components

Concern for the presence of CO/CO_2 gas in the IHS was occasioned by the adverse effect produced by CO on the Si_3N_4 coating used on the SiGe thermoelectrics to suppress volatilization of Si and SiO; see Section 6.0. In LES 8 & 9, where the Ir clad and a gas management system are used to dump gases from the IHS outboard of the RTG, the problem was less acute than for the MJS-IHS design in which the Ir clad has been eliminated. (That there was any concern at all on LES 8 & 9 arose from the difficulty of insuring the leak-tightness of the Ir can.)

Since the recognition of the CO/CO_2 generation problem in 1974, one of the more probable explanations of the source of these gases appeared to be the incomplete degassing of the carbon/graphite parts used in the IHS. For the bakeout schedules used on the LES 8 & 9 IHSs, see Table 5.1-5.

TABLE 5.1-4a GAS ANALYSES RESULTS

MBW-IHS

CONSTITUENT	VOLUME PERCENT CO	CO_2	H_2	H_2O	N_2	C_2	Ar	He	SAMPLING DATE	ANALYSIS BY
F-1/IHS										
SAMPLE NO.1	22.45	3.95	0.15	--	--	T	--	73.45	2 Jul.1974	ML/MRC
2	16.90	2.33	0.11	--	0.47	0.02	0.01	80.16	8 Aug.1974	ML/MRC
3	6.13	0.23	0.10	0.07	0.14	--	0.04	93.29	6 Sep.1974	ML/MRC
4	3.57	0.10	0.08	0.03	0.12	0.03	0.03	96.05	21 Nov.1974	ML/MRC
5	0.98	0.02	--	0.02	0.83	0.22	0.05	97.87	13 Dec.1974	ML/MRC
6	4.84	0.05	0.18	0.03	8.5	2.49	6.15	77.76	22 Jan.1975	GE
6	4.1	0.05	0.09	--	12.5	3.2	6.1	73.96	22 Jan.1975	GE/GAS (check)
7	2.1	0.02	0.09	--	0.13	0.003	8.1	89.56	22 Feb.1975	GAS
7	2.02	0.02	0.13	0.03	0.79	0.18	8.4	88.4	22 Feb.1975	ML/MRC (check)
F-2/IHS										
Sample No.1	32.60	3.46	0.06	0.01	0.39	0.01	--	63.47	25 Jul.1974	ML/MRC
2	34.42	2.86	0.07	--	0.68	0.01	--	61.96	12 Aug.1974	ML/MRC
3	6.14	0.17	--	0.03	0.24	--	--	93.42	10 Sep.1974	ML/MRC
4	3.15	0.10	0.06	--	0.34	--	--	96.35	22 Oct.1974	ML/MRC
5	2.09	0.11	0.06	0.01	0.35	0.01	--	97.37	19 Dec.1974	ML/MRC
(*) 6	0.93	--	0.01	--	25.4	7.0	0.32	66.4	13 Feb.1975	GAS
(*) 6	2.38	0.04	0.01	0.05	36.6	10.5	0.48	49.82	13 Feb.1975	ML/MRC(check)
F-3/IHS										
Sample No.1	6.47	3.40	0.07	--	1.76	--	--	88.3	12 Sep.1974	ML/MRC
2	10.24	1.31	0.06	0.07	0.16	0.01	1.21	86.94	15 Oct.1974	ML/MRC
3	4.41	0.21	0.09	--	0.97	0.02	0.09	94.21	29 Oct.1974	ML/MRC
4	3.29	0.12	0.06	--	0.24	0.01	--	96.28	17 Dec.1974	ML/MRC
5	2.5	0.03	0.02	--	0.34	--	--	97.15	6 Feb.1975	GAS
5	2.57	0.03	0.04	--	0.22	0.03	--	97.06	6 Feb.1975	ML/MRC
F-4 IHS										
Sample No.1	25.10	11.57	0.10	--	0.07	0.01	--	63.13	1 Apr. 1975	ML/MRC
2	16.87	1.23	0.02	0.01	0.22	--	0.01	81.63	30 Apr.1975	ML/MRC
(a)2	2.18	0.08	0.03	0.03	3.25	--	0.03	94.38	30 Apr.1975	ML/MRC
3	7.87	0.24	0.03	0.03	0.96	--	0.03	90.85	15 May 1975	ML/MRC
										See Table 5.1-4c for GE data

TABLE 5.1-4b GAS ANALYSES RESULTS

MBW-IHS

CONSTITUENT	VOLUME PERCENT CO	CO_2	H_2	H_2O	N_2	C_2	Ar	He	SAMPLING DATE	ANALYSIS BY
F-5 IHS										
Sample No.1	12.42	16.75	0.09	0.01	0.12	0.01	0.01	70.61	13 May 1975	ML/MRC
(a)1	1.19	0.13	0.19	--	0.02	--	--	98.47	13 May 1975	ML/MRC
2	6.25	3.46	0.06	0.01	--	--	--	90.17	20 May 1975	ML/MRC
(a)2	0.05	0.02	0.08	0.01	0.05	--	0.01	99.31	20 May 1975	ML/MRC
3	14.05	1.70	0.03	--	0.05	--	--	84.15	10 Jun.1975	ML/MRC
(a)3	2.06	0.11	0.06	--	0.01	--	--	97.75	10 Jun.1975	ML/MRC
										See Table 5.1-4d for GE data
Q-2/IHS	3.89	5.15	0.85	0.07	0.30	0.01	0.20	89.73	13 Aug.1975	ML/MRC
Sample No.1	3.89	5.15	0.25	0.07	0.30	0.01	0.20	89.73	13 Aug.1975	ML/MRC
(a)1	3.48	0.24	0.76	0.04	0.04	--	--	95.45	13 Aug.1975	ML/MRC
2	3.74	1.73	0.22	0.01	0.10	0.01	0.03	94.18	26 Aug.1975	ML/MRC
(a)2	0.87	0.15	0.16	0.01	0.16	0.03	0.01	98.62	26 Aug.1975	ML/MRC

(a) Backfill - * Sample bottle leaked

Table 5.1-4c

F-4 IHS GAS SAMPLE ANALYSES DURING LAS PROCESSING

SPECIES	TAP #1	TAP #2	TAP #3	TAP #4	TAP #5	TAP #6	TAP #7	TAP #8	TAP #9	TAP10	TAP11
CO	8.9	35.3	2.25	.61	.20	0.16	.038	.042	73.35	78.35	78.13
CO_2	.0013	.024	ND	ND	ND	ND	ND	ND	.04	.043	.044
H_2	ND	ND	ND	ND	ND	ND	ND	ND	ND	ND	.0028
N_2	.85	3.2	.065	.14	.064	.46	.06	.088	.71	.67	.68
O_2	.062	.09	.0025	.017	.014	.11	.0094	.017	.0043	ND	.12
Ar	49.0	19.1	.026	.0035	.002	.0067	.0013	.0013	.0083	.0055	.012
He	40.6	42.0	97.65	99.23	99.72	99.26	Bal	Bal	19.5	14.9	14.9
IHS Pressure (PSIA)	14.87	8.78	21.65	14.08	19.55	21.54	17.64	11.02	6.52	7.21	5.43
Grams - CO	.120	.248	3.9×10^{-2}	6.89×10^{-3}	3.13×10^{-3}	2.76×10^{-3}	5.37×10^{-4}	3.71×10^{-4}	.383	.453	.341
Rate - Grams CO/Day		9.92×10^{-1}	5.03×10^{-1}	1.79×10^{-1}	9.39×10^{-2}	3.68×10^{-2}	1.14×10^{-2}	7.88×10^{-3}	.383	.517	.355
DATE	6/1	6/2	6/2	6/2	6/3	6/3	6/4	6/5	6/6	6/7	6/8

SPECIES	TAP12	TAP13	TAP #14	TAP #15	TAP #16	TAP #17	TAP #18	TAP #18 CORRECTED	TAP #19	TAP #20	TAP #
CO	70.21	69.46	.81	.35	.18	.74	.36	.337	51.02	10.8	.83
CO_2	.042	.041	ND	ND	.0062	.0035	.015	.016	.021	.0067	.0057
H_2	.02	.013	ND	ND	ND	.0045	.0032	.0034	.019	.0055	.003
N_2	.81	4.3	.055	.025	.57 } air in sample	.42 } air in sample	5.6 } air in sample	----	2.3	.84	.61
O_2	.21	.07	.010	.001	.11 }	.09 }	1.33 }	----	.098	.09	.13
Ar	.019	.012	.0010	ND	.007	.0053	.064	----	.036	.009	.0077
He	21.4	26.1	Bal	99+	99+	98+	92+	Bal	46.5	Bal	Bal
IHS Pressure (PSIA)	3.52	2.56	25.04	16.74	1.00	1.06	1.00		.217	.348	.550
Grams - CO	.196	.1428	1.63×10^{-2}	4.69×10^{-3}	1.44×10^{-4}	5.42×10^{-4}	3.099×10^{-4}		1.03×10^{-2}	2.88×10^{-3}	6.37x10
Rate - Grams CO/Day	.207	.144	2.2×10^{-2}	3.2×10^{-2}	1.84×10^{-3}	7.147×10^{-3}	4.13×10^{-3}		2×10^{-2}	6.1×10^{-3}	8.45x10
DATE	6/9	6/10	6/11	6/12	6/13	6/13	6/14		6/15	6/16	6/17

NOTE: ALL CONCENTRATIONS SHOWN ARE CONCENTRATION % VOLUME/VOLUME.

ND = NON-DETECTABLE.

Table 5.1-4d

F-5 THS PROCESSING IN LAS

SPECIES	TAP #1	TAP #2	TAP #3	TAP #4	TAP #5	TAP #6	TAP #7	TAP #8	TAP #9	TAP #10	TAP #11	TAP #12
CO	12.7	58.28	3.8	.75	.37	.25	.044	.025	1.2	.70	4.4	8.3
CO_2	ND	.046	ND	ND	ND	ND	ND	ND	.0012	.0038	ND	.005
H_2	ND	.028	.0070	.0055	.0070	.0055	ND	ND	ND	.0045	ND	.014
N_2	<.25	ND	ND	.44	.053	.13	.25	.025	.20	1.11	.43	.49
O_2	.0068	.017	.026	.12	.0060	.013	.061	ND	.024	.22	.035	.048
Ar	34	1.83	.0095	.0048	.0008	ND	ND	ND	.012	.063	.020	.021
Xe	Bal	39.8	Bal	Bal	Bal	Bal	Bal	Bal	Bal	Bal	Bal	Bal
THS PRESSURE (PSIA)	14.8	13.48	15.21	13.63	13.2	12.87	13.39	13.29	2.07	2.31	2.059	1.83
GRAMS - CO	.1597	$5.9x10^{-1}$	$4.4x10^{-2}$	$7.7x10^{-3}$	$3.9x10^{-3}$	$2.4x10^{-3}$	$4.5x10^{-4}$	$2.5x10^{-4}$	$2.4x10^{-3}$	$1.5x10^{-3}$	$6.9x10^{-3}$	$1.1x10^{-2}$
RATE (GRAMS CO/DAY)	-----	.577	.742	.182	$7.6x10^{-2}$	$2.7x10^{-2}$	$6.8x10^{-3}$	$7.6x10^{-3}$	$6.5x10^{-3}$	$3.4x10^{-3}$	$7.2x10^{-3}$	$1.1x10^{-2}$
DATE	7/10	7/11	7/11	7/12	7/12	7/12	7/13	7/14	7/16	7/17	7/18	7/19

SPECIES	TAP #13	TAP #14	TAP #15	TAP #16	TAP #17	TAP #18	TAP #19	TAP #20	TAP #21	TAP #22	TAP #23
CO	15.8	29.0	43.0	1.3	.23	.13	.060	.055	.034	.79	2.8
CO_2	.0060	.0075	.016	ND	ND	ND	ND	ND	ND	ND	.0075
H_2	.010	.012	.026	ND	ND	ND	ND	ND	ND	ND	ND
N_2	.61	.72	.27	.20	.038	.035	.16	.04	.036	.52	.17
O_2	.033	.016	.011	.047	.0077	.0060	.033	.16	.0071	.083	.023
Ar	.014	.011	.0047	.0028	ND	ND	.0014	.0075	ND	.0060	.0030
Xe	Bal	Bal	Bal	Bal	Bal	Bal	Bal	Bal	Bal	Bal	Bal
THS PRESSURE (PSIA)	2.48	2.67	4.587	9.783	14.698	14.324	14.65	13.575	15.31	2.013	3.473
GRAMS - CO	$3.0x10^{-2}$	$5.8x10^{-2}$	$1.5x10^{-1}$	$9.6x10^{-3}$	$2.6x10^{-3}$	$1.4x10^{-3}$	$8.9x10^{-4}$	$5.7x10^{-4}$	$3.9x10^{-3}$	$1.2x10^{-3}$	$7.4x10^{-3}$
RATE (GRAMS CO/DAY)	$3.0x10^{-2}$	$6.0x10^{-2}$	$1.4x10^{-1}$	$1.0x10^{-1}$	$3.0x10^{-2}$	$1.5x10^{-2}$	$9.2x10^{-3}$	$1.1x10^{-2}$	$4.7x10^{-3}$	$1.7x10^{-3}$	$7.5x10^{-3}$
DATE	7/20	7/21	7/22	7/22	7/22	7/23	7/23	7/23	7/24	7/25	7/26

NOTE: ALL CONCENTRATIONS SHOWN ARE CONCENTRATION % VOLUME/VOLUME.

ND = NON-DETECTABLE.

At the direction of ERDA-SNS, work was initiated by BMI-CL to determine the degassing behavior of the major carbon/graphite components in the IHS. Preliminary work indicated that the quantities of CO retained by these materials was quite large even after extended bakeouts at high temperature. The T-50 composite (GIS) and the Pyrocarb 508, because of their large effective surface areas, appeared particularly difficult to degas. Later data indicated that the initial calculations were too pessimistic, but that the original, and even the revised bakeout schedules shown in Table 5.1-5, were clearly inadequate. At the end of the July/August reporting period, it had been established that the T-50 GIS material required exposure to 1500°C for 36 hours under a vacuum of $\leq 3 \times 10^{-4}$ Torr to effect degassing to acceptable levels of CO. Definition of the bakeout requirements for the POCO aeroshell and the other carbon/graphites is in progress and completion of the experiments is expected early in September 1975.

A further problem remains in defining the degree to which adequately-degassed components can resorb O_2 and H_2O from the controlled atmospheres to which they may be exposed during IHS fabrication and handling. Although the limits for the ML/MRC "F" line cells are 200 PPM for O_2 and 150 PPM for H_2O, accidental levels could rise to 5000 PPM O_2 for as long as 4 hours under correctly established procedures. In the assembly of the Q-2/IHS the O_2 rose to 2000 PPM, remained at that level for perhaps 15 minutes, and did not return below the specified normal level of 200 PPM for 2 hours.

Work at BMI-CL is in progress to define the uptake of the CO/CO_2 precursors from the controlled cell atmospheres at both the normal and impaired levels.

5.1.7 Assembly of the Q-2/IHS

A. The Q-2/IHS was assembled at ML/MRC on 6 August 1975. The complement of FSAs used and their provenance is shown in Table 5.1-6, which also shows the levels of Pu-contamination determined by wipe on the surfaces of the GIS. The total observed level is ~270 DPM as compared with 850 DPM for the Q-1/IHS.

B. During assembly a graphite tie-bolt holding the bottom 8-pack together broke and was replaced without incident.

C. The middle and bottom 8-packs used in Q-2/IHS were removed as units from the Q-1/IHS and stored for approximately 10 months in sealed storage cans. These cans were placed in a water bath to permit continous removal of the 800 $W_{(t)}$ generated by each 8-pack.

Table 5.1-5a

ORIGINAL BAKEOUT SCHEDULE FOR IHS CARBON

PART	BAKEOUT SCHEDULE TIME - Hrs	TEMP. °C	MAXIMUM PERMISSIBLE AIR EXPOSURE TIME AFTER B/O - Hrs.	BAKEOUT FACILITY LOCATION
Aeroshell	5	1200	≤ 1.0	ML/MRC
All other internal parts	1	1200	≤ 0.5	ML/MRC
Heat source supports Ablation sleeve	3	550	None (1)	GE-VF (never done)

Table 5.1-5b

MODIFIED BAKEOUT SCHEDULE FOR IHS CARBON

PART	BAKEOUT SCHEDULE TIME - Hrs	TEMP. °C	MAXIMUM PERMISSIBLE AIR EXPOSURE TIME AFTER B/O - Hrs.	BAKEOUT FACILITY LOCATION
Aeroshell	24	1500	≤ 1.0	ML/MRC
GIS	24	1350	None (2)	GE-Evendale
All other internal parts	24	1500	None (2)	GE-Evendale
Heat source supports Ablation sleeve	24 12 12	1500 1000 1500 (3)	None (1)	GE-Evendale

(1) Sealed in container pressurized with Ar (99.99%)
(2) " " " " " He "
(3) Sequential bakeout: 24 hrs @ 1500C+ 12 hrs @ 1000C + 12 hrs @ 1500C

Table 5.1-6 FSAs Used in the Q-2/IHS

	FSA Number - MHF -	Source of Ir	^{238}Pu Activity - DPM	
*Top 8-Pack (made new)	21 (old)	EI-2	10	Tray - New
	64 (new)	HNL	8	
	15 (old)	EI-2	10	
	161 (new)	HNL	24	
	162 (new)	HNL	12	
	165 (new)	HNL	22	
	166 (new)	HNL	10	
	164 (new)	HNL	24	
			120	
Middle 8-Pack (from Q-1/IHS)	22 (old)	EI-2	6	Tray - 0 DPM
	5 (old)	EI-2	8	
	17 (old)	EI-3	8	
	9 (old)	EI-2	2	
	4 (old)	EI-2	16	
	16 (old)	EI-2	14	
	11 (old)	EI-2	4	
	23 (old)	EI-2	0	
			58	
Bottom 8-Pack (all FSAs from Q-1/IHS)	26 (old)	EI-3	12	Tray-2 DPM
	24 (old)	EI-2	12	
	18 (old)	EI-3	0	
	8 (old)	EI-2	10	
	3 (old)	EI-2	6	
	10 (old)	EI-2	12	
	12 (old)	EI-2	2	
	7 (old)	EI-2	10	
			54	
			232	

Apparently due to the very high chlorine content of the water, 480 PPM, the stainless steel 8-pack containers were corrosively attacked and that which contained the middle 8-pack was penetrated at a point slightly above the water line.

When the middle 8-pack was removed from its container it was found to show a reddish coloration on the surface of the retainer ring/tray. The unit was wiped for Pu contamination measurements and the reddish material was adherent and not removed in the wipe. No specimens were taken from the 8-pack and it was assembled into the Q-2/IHS in the condition in which it was removed from the container. Analyses performed subsequently on material taken from the interior of the container showed the reddish material to contain Fe, Cr, Na, Cl, P, Mn, Ni and Cu among the more prominent constituents. The material on the inside of the container was adherent except in the bottom where it was powdery. ML/MRC concluded from the distribution of the contaminants that most of the material was transported in the vapor phase. Thus, it is inferred that a similar mix of impurities were vapor deposited on the 8-pack, although verification of this inference is not now possible without disassembly of the Q-2/IHS. Because there is no way of determining the mix of contaminants, their quantity, and their distribution in the middle 8-pack components, the Q-2/IHS was accepted only for the relatively short-term testing at GE-VF. GE has recommended disassembly of the Q-2/IHS and analysis of the contamination on the middle 8-pack before the Q-2/IHS is committed for any other operations.

5.2 IMPACT TESTS

5.2.1 Impact Testing at GE-VF

Two impact tests were carried out using the HNL-ML/MRC type WG Ir PICS and ThO_2 simulant. Both specimens failed catastrophically. MHT-94 was found to have rotated so that impact occurred at 313 FPS with the GIS plug about 70° from normal. The PICS fragmented and all the ThO_2 was dumped. MHT-95 rotated 40° and impacted at about 295 FPS. The damage to the PICS consisted of very wide hoop-stress cracks up to 0.5 inch wide and a very pronounced fingerprint on the impact face. All the ThO_2 was dumped in the impact and rebound. A summary of the tests is given in Table 5.2-1.

Table 5.2-1

FSA TEST SUMMARIES - IMPACTED AT - GE-VF - Ir PICS

DATE AND TEST NUMBER	IMPACT SPECIMEN DATA: GRAPHITE IMPACT SHELL (No.; Density = ρ - $g\text{-}cm^{-3}$; Thickness = t_c - inch; Type)	IMPACT SPECIMEN DATA: IRIDIUM CONTAINMENT (No.; Thickness; Heat treatment + date; Other; Welded by:)	IMPACT SPECIMEN DATA: SPHERE MATERIAL (Fuel: PuO_2; Simulant: ThO_2; No.; Dia.; % TD; Heat treat.; other)	IMPACT CONDITIONS: Specimen weight total - grams	IMPACT CONDITIONS: Velocity - fps	IMPACT CONDITIONS: Energy - ft-lbs	IMPACT CONDITIONS: Temperature - °C (°F)	RESULTS
30 Jul.75	903745-2 = 1.20 t_c= 0.46" T-50 compositw	WG-226-4 WG-226-3 H/T 18 hrs at 1500C before butt weld b y ML/MRC	ThO_2;#624-2 77%TD; not H/T with Ir		313		1370 (2500)	FAILED: H/D = n/a S(%) = n/a GIS rotation = 70° Catastrophic rupture and disintegration of PICS; fingerprint and hoop stress cracks; all ThO_2 dumped during impact and rebound.
27 Aug.75	931630-2 = 1.20 t_c= 0.46" T-50 Composite	WG-211-2 WG-211-3 H/T 18 hrs at 1500C before butt weld by ML/MRC	ThO_2;#625-1 77%TD; not H/T with Ir		296		1370 (2500)	FAILED: H/D = 1.185/1.868 S(%) = 13.9 GIS rotation = 40° Catastrophic failure but PICS did not breakup into fragments; deep fingerprint and hoop stress cracks; one crack = 2.5"long x 0.30" wide; all ThO_2 dumped during impact and rebound

051874

5.2.2 Impact Tests at LASL

No impact tests with fuel or simulant were done at LASL during the reporting period.

5.2.3 Multi-Sphere Tests

No multi-sphere tests were performed during the reporting period.

5.2.4 Impact Test at GE-VF with Pt-3008 Alloy PICS

Three specimens using Pt-3008 alloy made by HNL-ML/MRC for the PICS material were impacted. The results are summarized in Table 5.2-2. All units survived impact.

5.3 AEROTHERMAL AND MISCELLANEOUS ANALYSES AND TESTING

5.3.1 Reentry

The reentry data reported in the Bi-Monthly Report for May/June 1975 were used to provide input to the thermal stress analysis of the MJS end cap reported in Paragraph 5.3.2.

5.3.2 Stress Analyses

5.3.2.1 End Cap Analysis

Stress analysis of the MJS-IHS end cap were performed assuming the end-on extreme worst case but with the graphite end supports of the IHS in place as shown in Figure 5.3-1. This analysis is similar to those performed previously (Reference 1) except that in this analysis, the heat source support is assumed to remain in place during reentry. Figure 5.3-1 shows the configuration analyzed.

For the configuration shown it is assumed that the heat source support will shield the center section of the end cap during reentry and limit the interface surface temperature to approximately 4000^{o}F. The exposed area of the end cap is assumed to have a surface temperature of approximately 7000^{o}F. The temperature distribution used in the analysis was approximated by combining the temperatures derived for conditions 1 and 3 of Reference 1. The aerodynamic loading was assumed to be the

---

Ref. 1 Eardley, C. J., "Stress Analysis of the MJS Heat Source End Cap for End-On Reentry", PIR-5417, General Electric Co., Space Division, Philadelphia, Pa. (28 April 1975)

Table 5.2-2

FSA TEST SUMMARIES - IMPACTED AT - GE-VF - Pt-3008 PICS

DATE AND TEST NUMBER	IMPACT SPECIMEN DATA: GRAPHITE IMPACT SHELL No. Density = ρ - g-cm^{-3} Thickness= t_c - inch Type	IMPACT SPECIMEN DATA: Pt-3008 CONTAINMENT: No. Thickness Heat treatment + date Other; Welded by:	IMPACT SPECIMEN DATA: SPHERE MATERIAL: Fuel: PuO_2 Simulant: ThO_2 No.; Dia.; % TD; Heat treat.; other	IMPACT CONDITIONS: Specimen weight total - grams	IMPACT CONDITIONS: Velocity - fps	IMPACT CONDITIONS: Energy - ft-lbs	IMPACT CONDITIONS: Temperature - °C (°F)	RESULTS
15 Aug.75 Pt-3008-1	898760-1 p = 1.20 t_c= 0.46" T-50 Composite	Pt-3008-T1 Thk. ? No H/T before or after butt weld by ML/MRC	n/a		294		760 (1400)	PASSED: H/D = 1.184/1.766 S(%)= 10.7 GIS rotation = 65°
18 Aug.75 Pt-3008-2	903748-2 p = 1.20 t_c= 0.46" T-50 Composite	Pt-3008-T2 Thk. ? No H/T before or after butt weld by ML/MRC	n/a		290		1000 (1832)	PASSED: H/D = 1.180/1.741 S(%)= 9.1 GIS rotation = 40°
22 Aug.75 Pt-3008-3	899004-2 p = 1.20 t_c= 0.46"	Pt-3008-T3 Thk. ? No H/T before or after butt weld by ML/MRC	n/a		250		1250 (2280)	PASSED: H/D = 1.283/1.665 S(%) = 4.4 GIS rotation = 7°

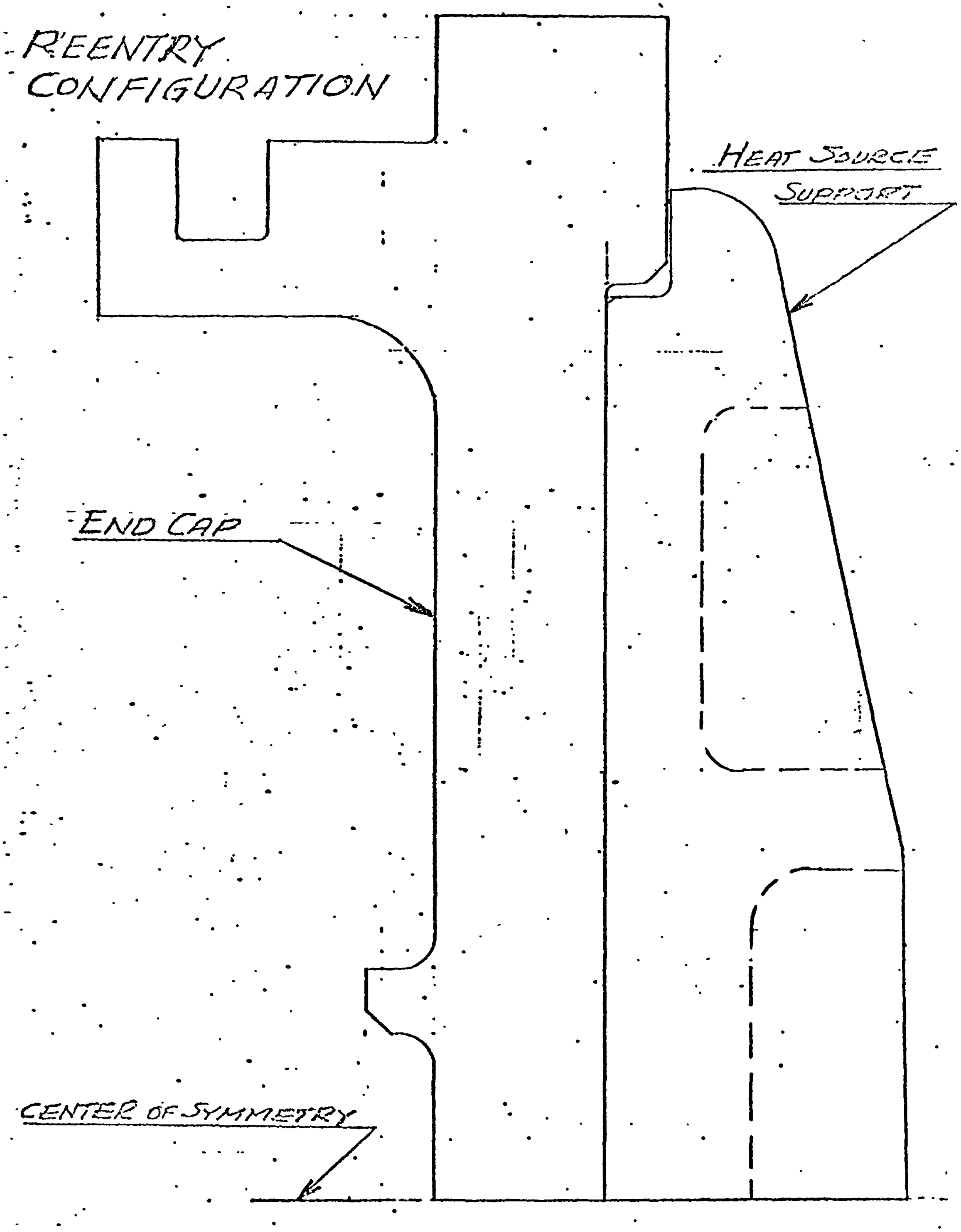

Figure 5.3-1 Reentry Configuration MJS Aeroshell End Cap

same as condition 3. The distribution of the air load across the end cap is shown on Figure 5.3-2 as a ratio of the local pressure (P) to the stagnation pressure (P_O). It is assumed that the heat source support transmits (but does not redistribute) these loads. Figure 5.3-3 shows the aerodynamic loading applied to the nodes of the finite element model.

Using these loads and the approximate temperatures, the analysis was performed using the BIG 2D machine computation program and the finite element model developed for the analyses reported in Reference 1.

The analyses of Reference 1 were performed with two different assumptions concerning the condition of support around the periphery of the end cap. The first of these assumed that the cap was simply supported (i.e., no interference between the end cap and the lock ring). The other assumed that the interference existing between the lock ring and the end cap resulted in moment restraint around the periphery.. Of these two assumptions, it was found that the simple support resulted in the lowest stresses. In order to calculate the maximum reduction in stress which could be realized due to the shielding afforded by the heat source support, this analysis was performed assuming that the end cap was simply supported. Figure 5.3-4 shows the location of the maximum calculated octahedral stress. This stress is 9671 psi and results in a negative margin of safety of 26%. The comparable analysis reported in Reference 1, showed a maximum stress of 11,665 psi, occurring at the same location and resulting in a negative margin of safety of 41%.

It is found that while the protection afforded by the heat source support substantially reduces the maximum stresses, the end cap is still not adequate to withstand the end-on reentry. The maximum temperatures and the distribution of temperatures were estimated based on previous analyses. However, since the calculated stresses far exceed the allowable tensile stress of the material, it is judged that further refinement of the temperatures would not result in acceptable stress levels. Coupling this with the uncertainty of the heat source support remaining in place during reentry, it is recommended that no additional effort be expended investigating this configuration.

5.3.2.2 Stress Analysis of the LES 8 & 9 IHS Ir Clad

The iridium clad surrounds and seals the graphite aeroshell and the IHS (Isotope Heat Source). After assembly at ambient temperatures, the IHS is inserted in the converter and reaches thermal equilibrium at an elevated temperature. During normal operation, the pressure in the converter can be as high as 25 psi while the pressure inside the heat source can be as low as 2 psi. This section presents the results

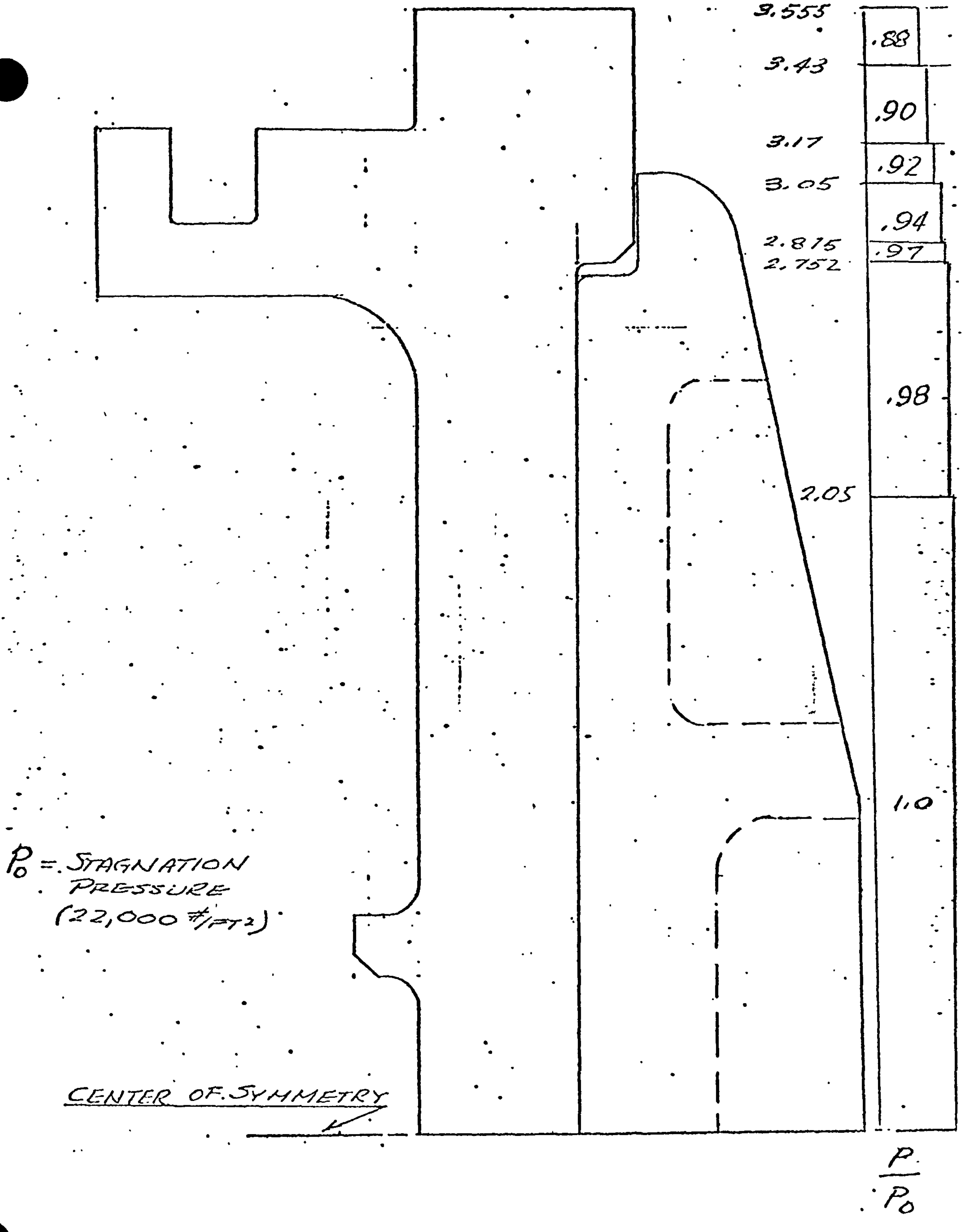

Figure 5.3-2 Aerodynamic Loading

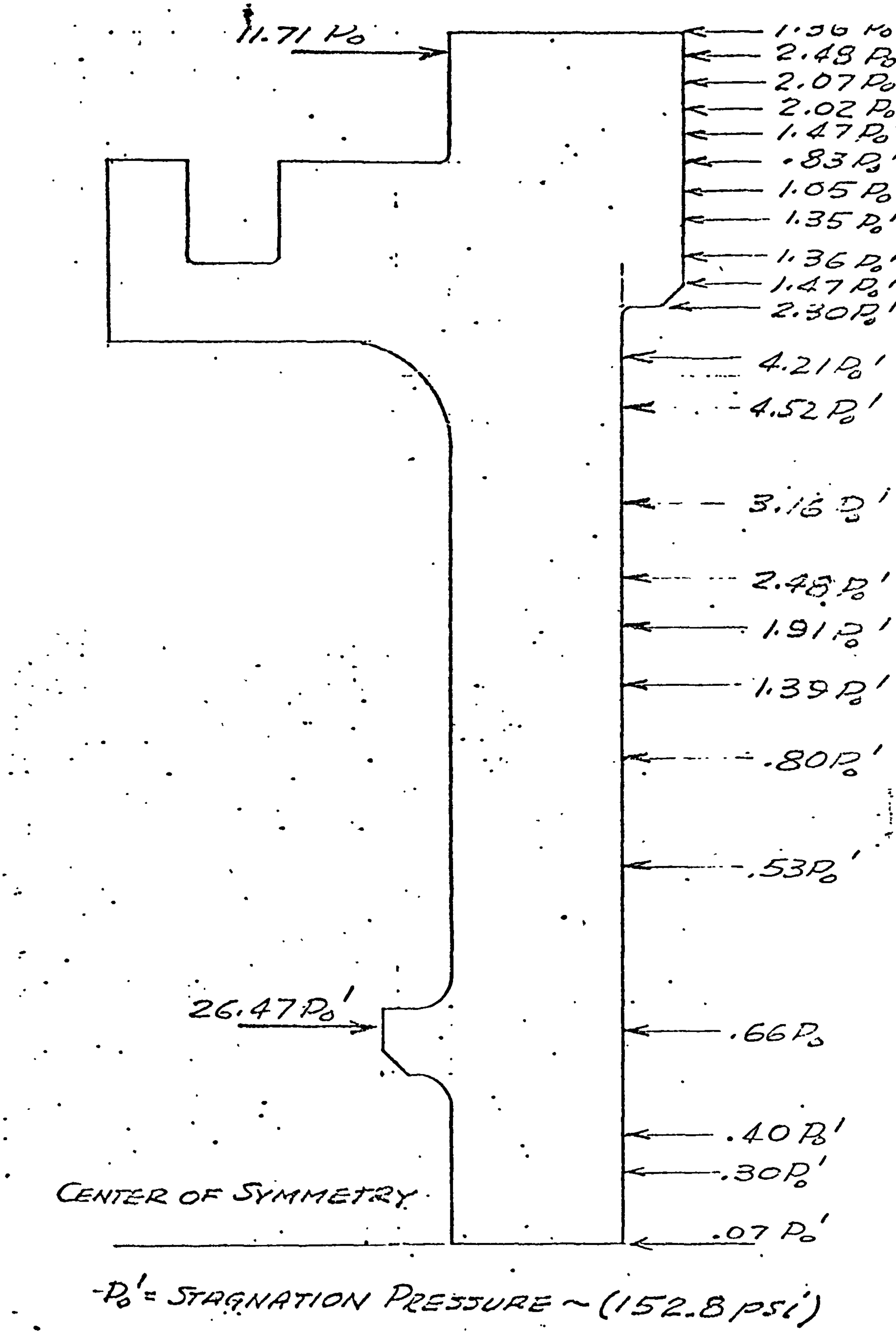

Figure 5.3-3 Aerodynamic Loads Applied to Node Points

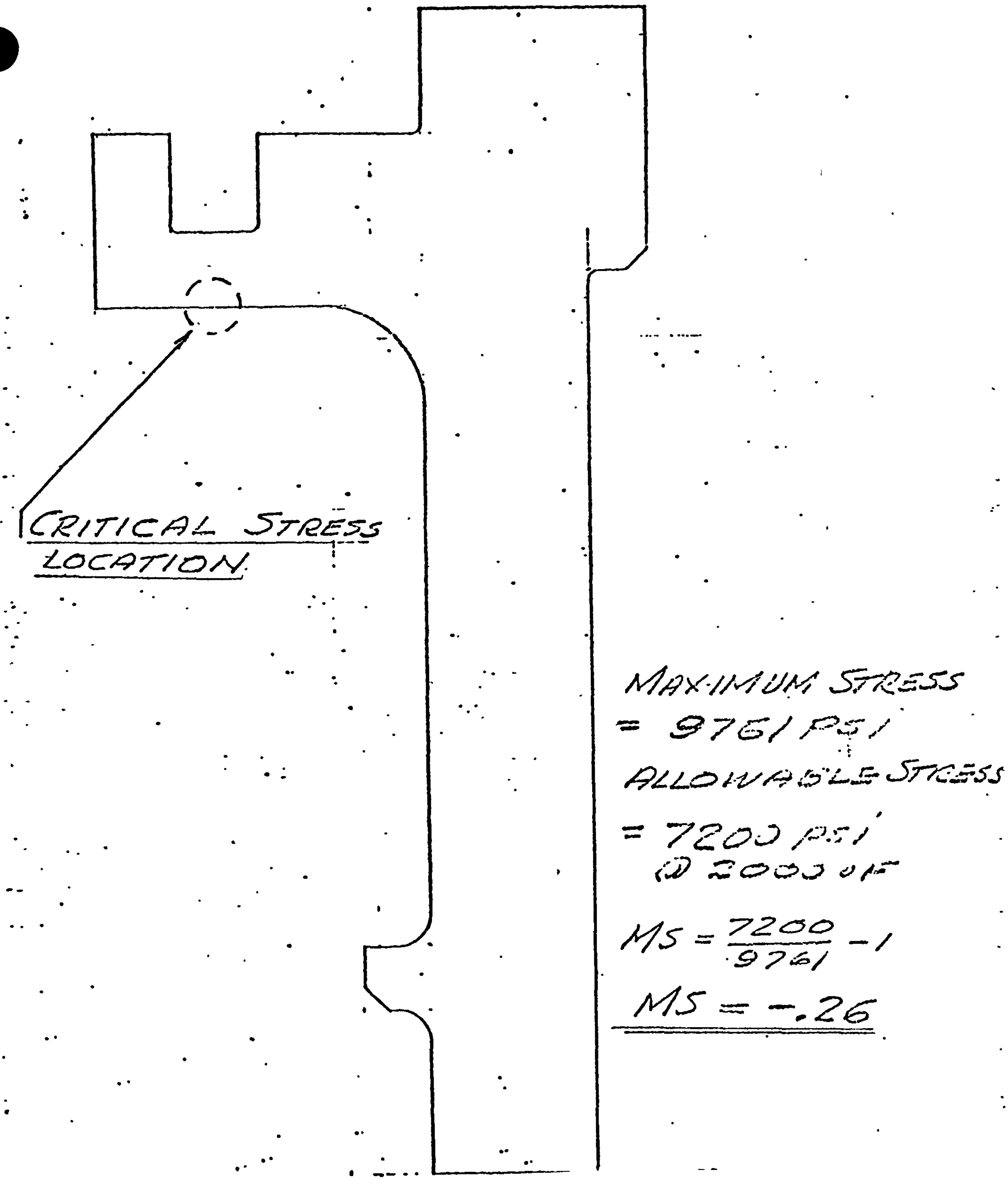

Figure 5.3-4 Location of Critical Stress in MJS End Cap - End-on Reentry

of an analysis of the effects of the elevated temperature and differential pressure on the iridium clad.

The following assumptions were made to perform the analysis.

(1) The iridium clad, graphite aeroshell and the ablation sleeve are at 1050°C (1922°F).

(2) The iridium is in the recrystallized condition. This results in the lowest compressive yield strength.

(3) The most adverse tolerances are used in the analysis. This results in: the maximum clearance between the graphite aeroshell and the iridium clad; and, the maximum interference between the clad and the ablation sleeve.

(4) The ablation sleeve is porous so that the full differential pressure is imposed on the iridium clad.

Based on the results of the analysis, it is concluded:

(1) The iridium clad cannot buckle because of the restraint of the aeroshell and sleeve.

(2) The iridium clad yields under the combined thermal and pressure loading.

(3) At temperature and with a differential pressure of 23 psi, the iridium clad will bear on the aeroshell. This results in a maximum stress of 9900 psi at a strain of .0106 in/in.

5.3.3 Thermal Analyses

A thermal analysis was performed to determine LES 8/9 heat source temperatures during SPC storage and LAS processing. The 2D 1/4-sphere model was used for the analysis.

In the SPC storage condition, the heat source gaps were filled with helium and the clad was held at 1000°F based on test results. The steady-state fuel volume average temperature was 1605°F and the PICS volume average temperature was 1458°F. The complete temperature profile for the heat source is presented in Figure 5.3-5.

For the LAS processing, the initial conditions were: evacuated LAS, evacuated converter, helium-filled heat source. The initial temperatures were the same as the operating temperatures. The processing then went as follows:

a) heat source evacuated to about 500~1000μ for 30 minutes.

b) pressurized with helium to 14.5 psia for 90 minutes.

c) evacuated again for another 30 minutes.

d) pressurized with helium to 2.5 psia for 24 hours.

There is little difference in conduction between 2.5 psia and 14.5 psia for a 40-mil gap. Both pressures result in conduction of about 90% of maximum. Pressures less than about 5000μ are essentially vacuum for conduction purposes.

Figure 5.3-6 shows fuel and PICS temperatures through the four cycles. Figure 5.3-7 shows the heat source temperature profile after 30 minutes of evacuation (a) and Figure 5.3-8 shows the heat source temperature profile after 90 minutes of helium backfill (b). It is obvious from Figure 5.3-6 that the temperatures after conditions (c) and (d) are virtually the same as those after (a) and (b), so these temperature profiles are not presented.

5.3.4 Analyses of GIS Impacts

A previous analysis of GIS impact deceleration behavior considered the as-yet uncrushed portion of the GIS body with contained PISA to be rigidly decelerated by forces present at the impacted surface. These forces were based on an estimated static crushing stress-strain relationship derived from available data. Subsequent to completing this analysis, the usefulness of a more realistic analysis based on

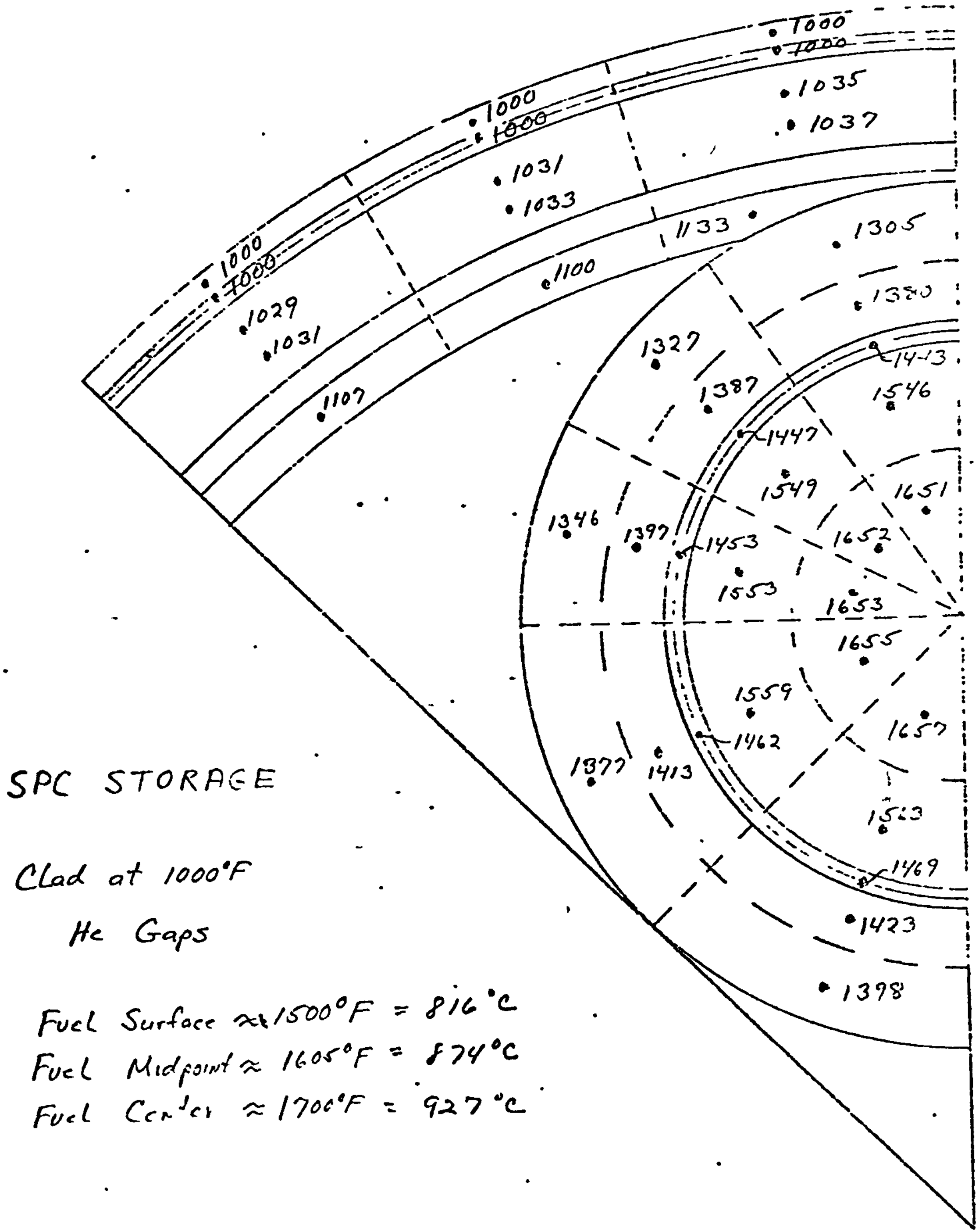

Figure 5.3-5 SPC Storage Temperatures

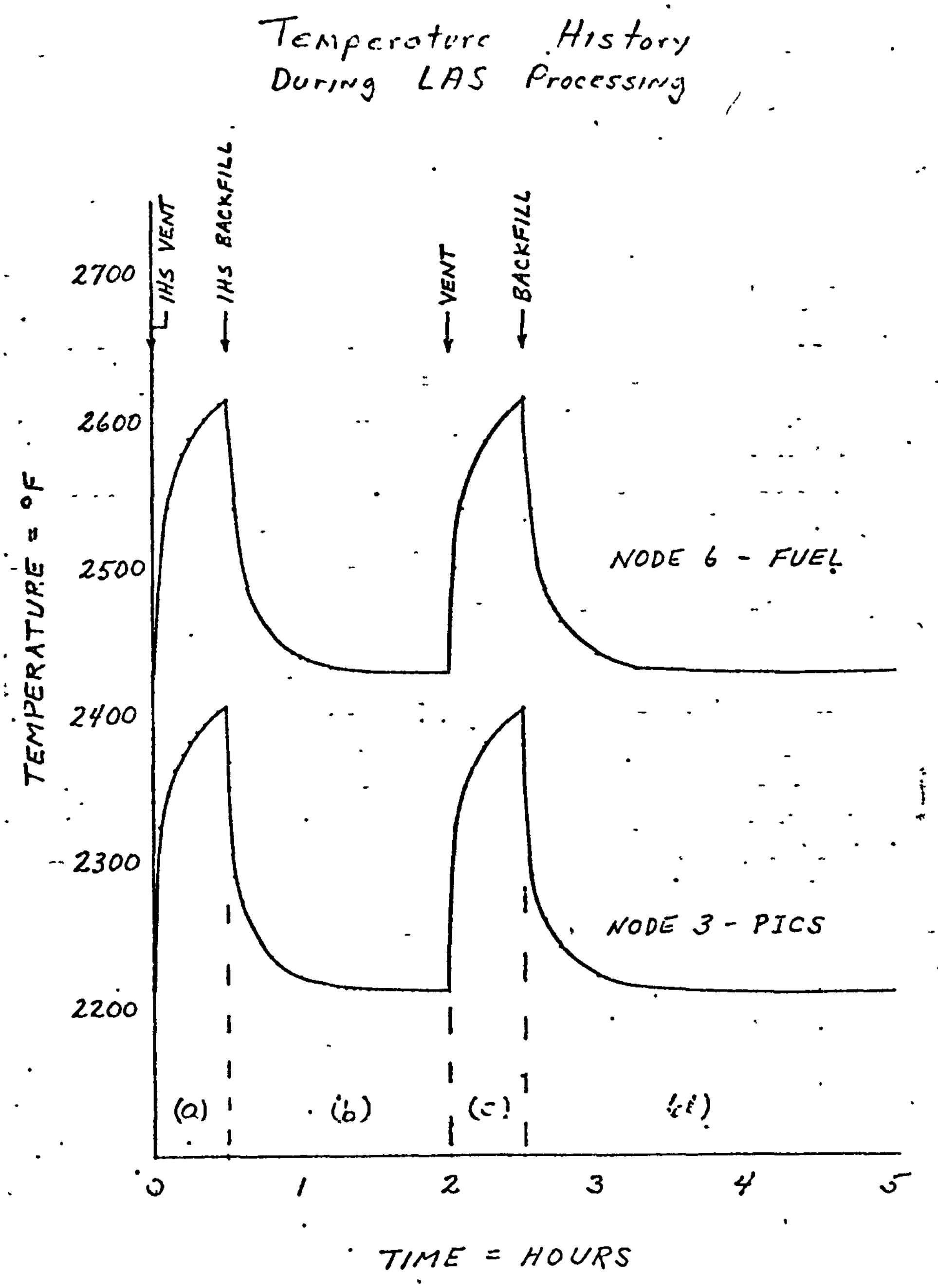

Figure 5.3-6 Temperature History during LAS Processing

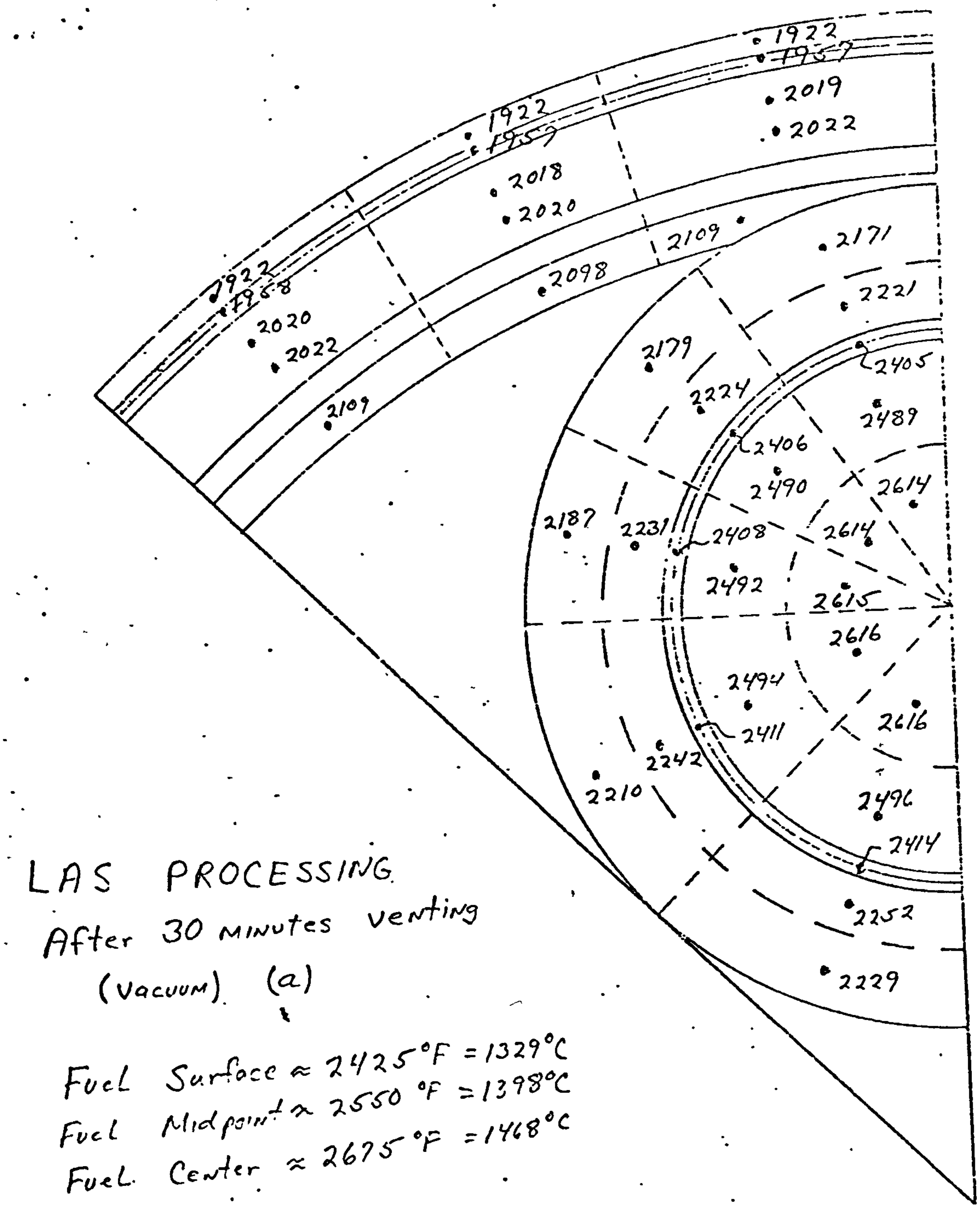

Figure 5.3-7 LAS Processing Temperatures after 30 minutes Venting

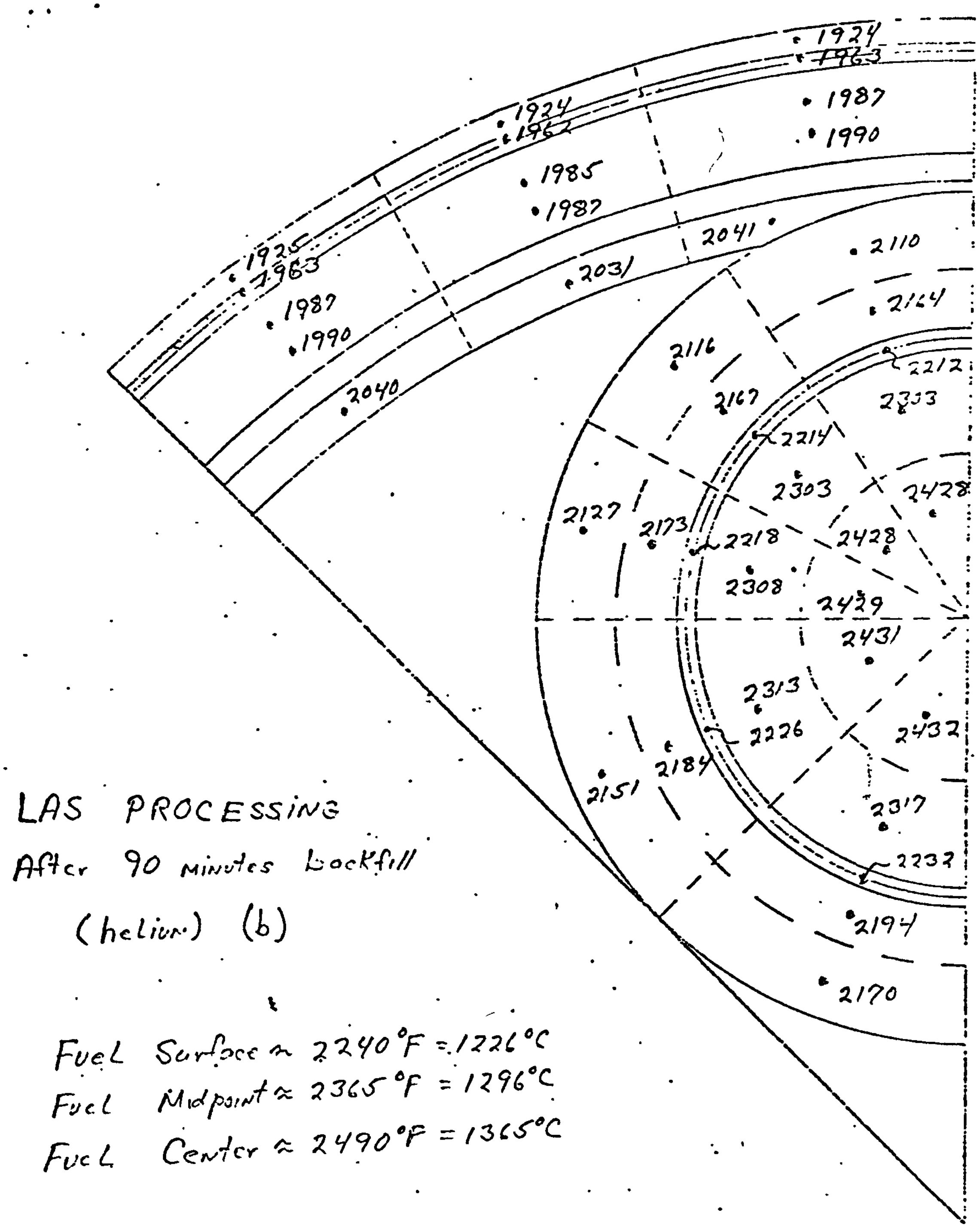

Figure 5.3-8 LAS Processing Temperatures after 90 minute Backfill

one-dimensional shock propagation theory was investigated.

The analysis is based on the following assumptions:

a) GIS material is isotropic and its response is governed by the one-dimensional mechanical shock equations

b) PISA is rigid (undeformed) and its velocity remains constant during impact. (The assessment of PISA stoppage is based on subtracting the impulse delivered to PISA from the initial momentum of the PISA and GIS end cap.

c) Interactions among the various shock fronts are ignored.

Application of the one-dimensional mechanical shock equations results in the evaluation of the shock front velocity U_n, the material velocity V_n, the shock pressure P_n, and the material density ρ_n, behind the shock front. These values satisfy the conservation of mass and momentum and the material pressure-density relations. The latter expresses the compression pressure required to produce a given amount of material compaction, ρ_n, ρ_o, ρ_o being the initial density of the GIS material.

a) <u>Development of Shock Waves</u>

The development of shock waves as the GIS interacts with the impact plane is illustrated in the sequence of Figures 5.3-9a thru 9c. The initial shock is shown in Figure 5.3-9a at the instant it arrives at the PISA surface, 24.79×10^{-6} (μ) sec, after the initiation of impact. Behind this shock, the GIS material is at rest, having been abruptly decelerated from the initial velocity of 3360 in/sec (280 fps) as the shock passed through it. A pressure of 7000 psi is present behind the shock, whose velocity is 15,194 in/sec, the reflection of this shock from the PISA (assumed rigid) subjects it to a pressure of 18,662 psi at the stagnation point (η = o) as shown in Figure 5.3-9, which incidentally depicts the reflected front (No. 2) at the moment it reaches the impact plane. The reflected pressure acting on the PISA surface decreases with increasing angles. Except for shock No. 1, all quantities vary with central position angle, as may be seen in Figure 5.3-10 plots of ρ_2/ρ_o, P_2, and U_2 vs. η. Figures 5.3-9a-9c show the development of shocks up to a time of 83.50 μ sec after impact initiation.

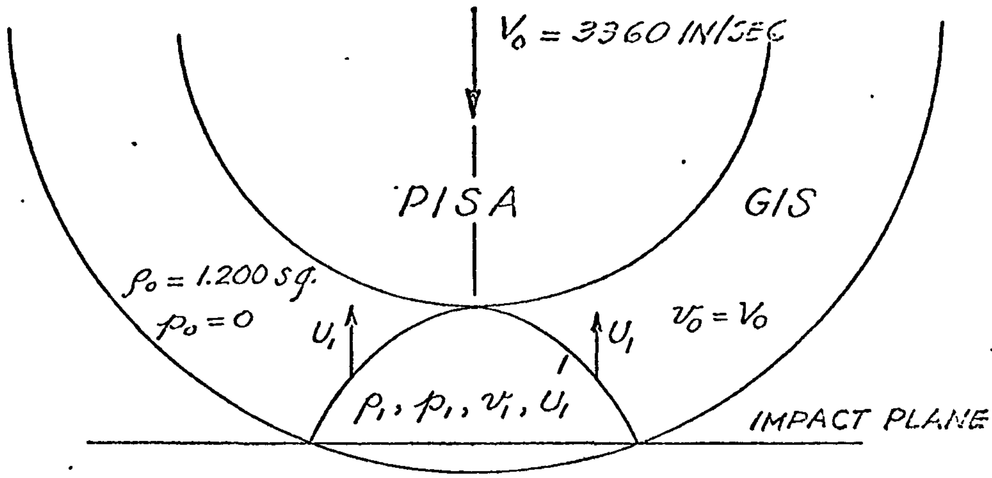

a. FRONT NO. 1 AT $t = 24.79 \mu$ SEC, $\frac{\rho_1}{\rho_0} = 1.221$, $p_1 = 7000$, $v_1 = 0$, $U_1 = +15194$

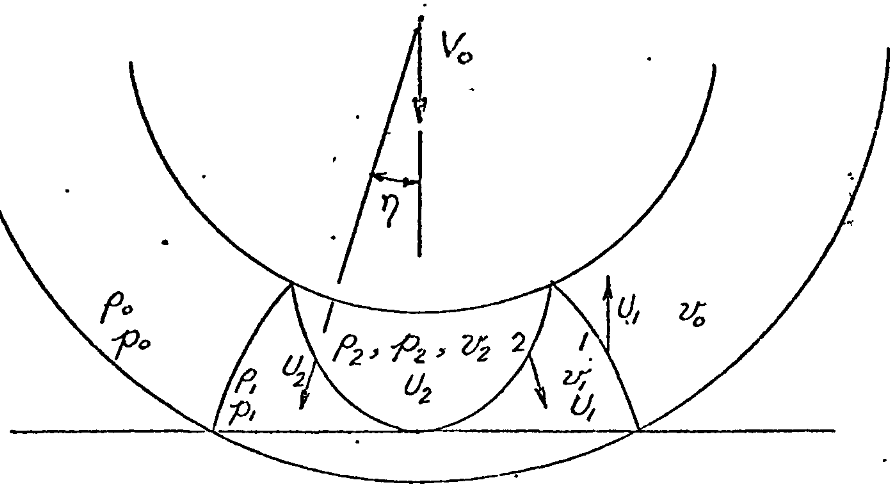

b. FRONTS NO. 1 & 2 AT $t = 39.69 \mu$ SEC., VALUES BEHIND NO. 2 FOR $\eta = 0$: $\frac{\rho_2}{\rho_0} = 1.408$, $p_2 = 18662$, $v_2 = -3360$, $U_2 = -25313$

Figure 5.3-9a SHOCK FRONTS IN GIS AT VARIOUS TIMES AFTER IMPACT INITIATION, SHOWING REPRES. VALUES OF DENSITY ρ, PRESSURE p, MATERIAL VEL. v, & SHOCK VEL. U IN LB., IN., SEC. UNITS

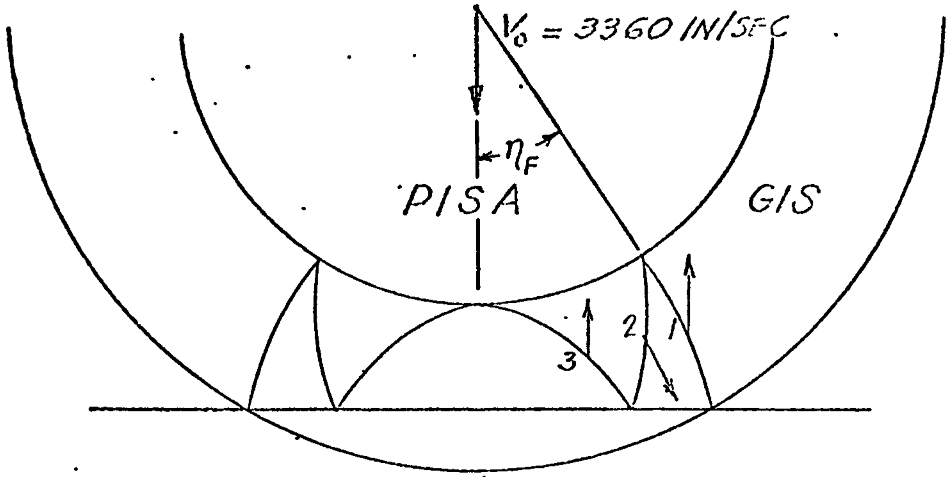

c. FRONTS NO. 1-3 AT $t = 52.29 \mu SEC$, VALUES BEHIND NO. 3 FOR $\eta = 0 : \frac{\rho_3}{\rho_0} = 1.618$, $p_3 = 32417$, $v_3 = 0$, $U_3 = 22533$

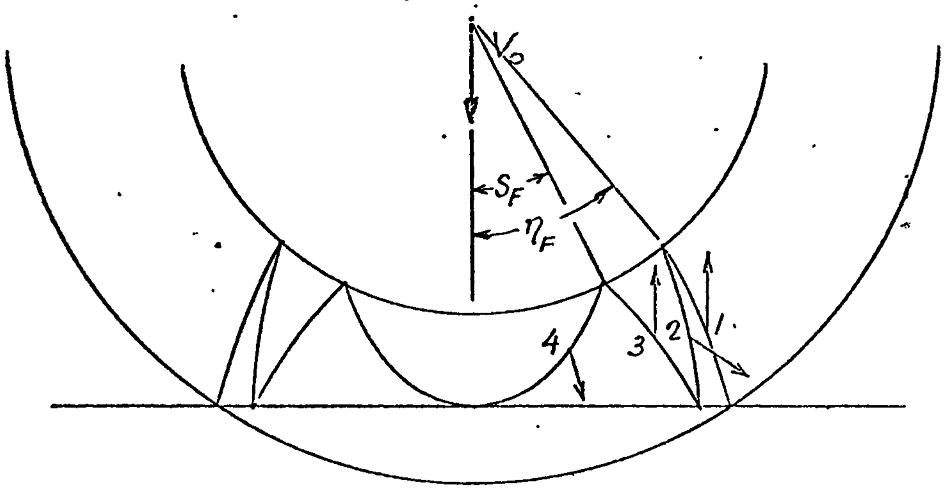

d. FRONTS NO. 1-4 AT $t = 63.53 \mu SEC$, VALUES BEHIND NO. 4 FOR $S = 0 : \frac{\rho_4}{\rho_0} = 1.866$, $p_4 = 47854$, $v_4 = -3360$, $U_4 = -25288$

Figure 5.3-9b

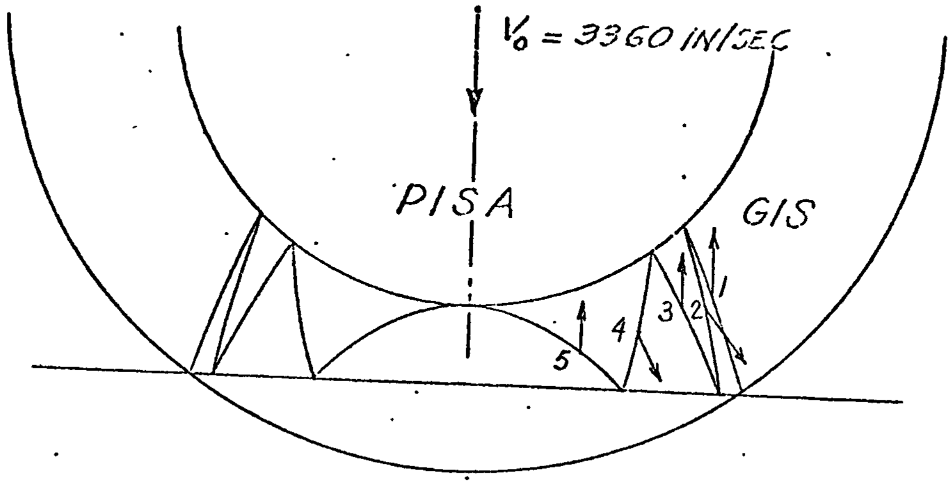

e. FRONTS NO. 1-5 AT $t = 73.86 \mu SEC$, VALUES BEHIND NO. 5 FOR $S = 0$: $\frac{\rho_5}{\rho_0} = 2.171$, $p_5 = 64668$, $v_5 = 0$, $U_5 = 20524$

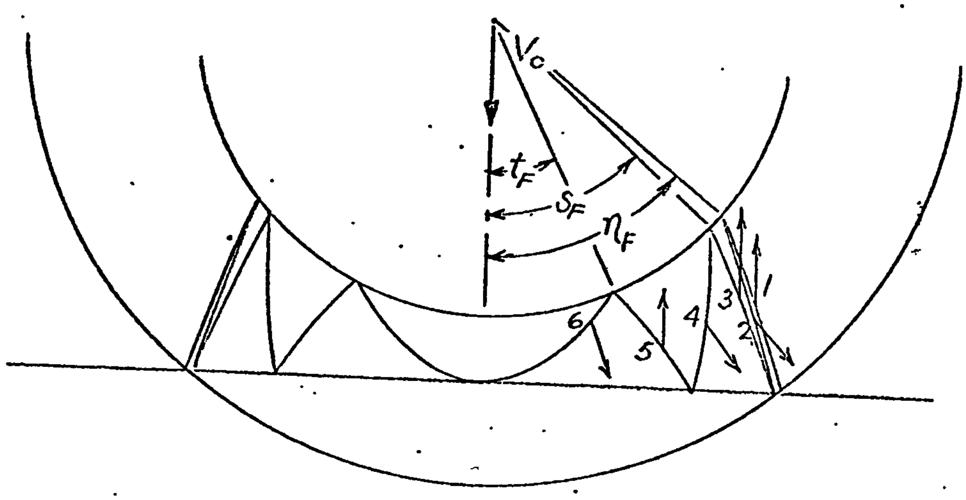

f. FRONTS NO. 1-6 AT $t = 83.50 \mu SEC$, VALUES BEHIND NO. 6 FOR ANGLE $t = 0$: $\frac{\rho_6}{\rho_0} = 2.564$, $p_6 = 82661$, $v_6 = -3360$, $U_6 = -21963$

Figure 5.3-9c

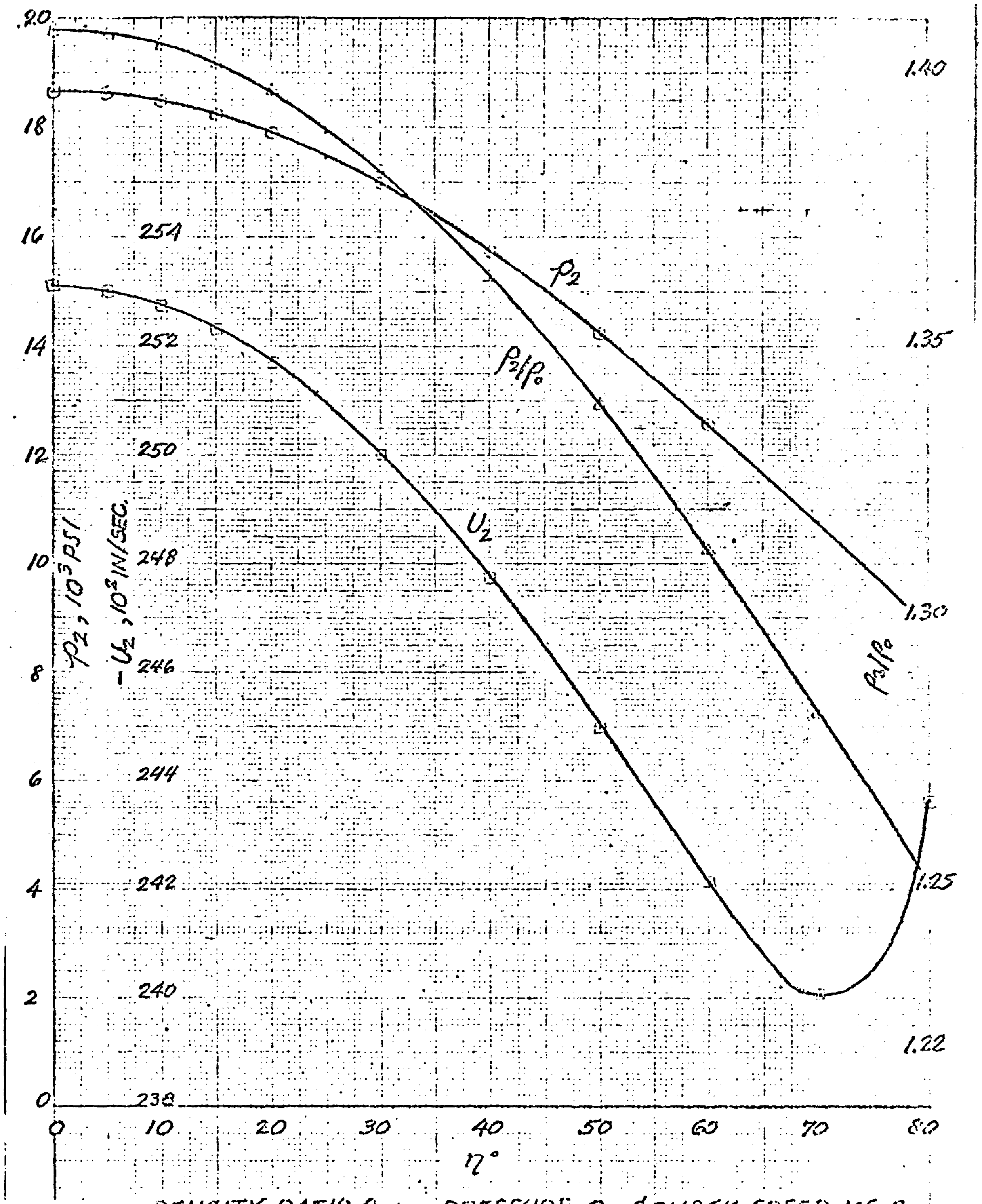

Figure 5.3-10 DENSITY RATIO ρ_2/ρ_0, PRESSURE p_2, & SHOCK SPEED VS. η

b) Pressure Loading on PISA

Behind each successive shock front the pressure and material density increase in magnitude, due to the assumption of rigid PISA and impact plane conditions. The pressure loading felt by the PISA is due to the shock waves reflected from it (ex. nos. 2, 4, 6). The pressure imposed by shock wave no. 2 spreads over the PISA surface according to angle η_F (Figure 5.3-9) by no. 4 according to angle S_F, and by no. 6 according to angle t_F. This process results in large discontinuities in pressure at the junctures of these angular regions. Within an individual angular region, however, the pressure loading varies continuously. This phenomenon is illustrated in Figure 5.3-9b for times: 73.86 and 83.50 μsec. after impact initiation respectively. Figure 5.3-11a shows two regions, one from S = 0 to 38.5° in which the pressure varies from 82.6 to 40.6 Ksi and the other from η = 38.5 to 46° with pressure ranging from 16.0 to 14.9 Ksi. This results in two pressure discontinuities at η = 38.5 and 46.0°, namely 24.6 and 14.9 Ksi respectively. In Figure 5.3-11b which pertains to a time only 9.64 μ sec later, three pressure discontinuities are present at central angles of 26.2, 48.2, and 51.5°, and are 32.5, 22.9 and 14.0 Ksi respectively. Hence, the analysis shows that concentric circular pressure discontinuities develop at the PISA surface and sweep rapidly outward. These discontinuities are larger at radial distances closer to the impact central axis and an individual one decreases with increasing time. Additionally, the discontinuities produced at earlier times tend to be overtaken by the later ones. The appropriate difference between Figures 5.3-11a and b graphically illustrated in Figure 5.3-12 in which the central angles η_F, S_F, and t_f, corresponding to the positions at the PISA of shock fronts no. 2, 4, and 6, respectively, are shown plotted against time after impact initiation. Hence front no. 2 is overtaken by fronts 4 and 6 at 89.8 and 117 μ sec respectively.

c) Possible "Fingerprint" Formation Mechanism

Such discontinuities can produce deformations in the form of circular rings in the PISA shell and are a plausible cause of the "fingerprint" deformations frequently observed in PISA shells after impact. The high magnitudes indicated for these discontinuities should be sufficient to cause circular shear or buckling failures in the PISA shell and contents. The resulting deformations, moreover, would tend to be self arresting because they would initiate an abrupt reduction of the imposed shock pressure, due to the rarefaction effect of the localized PISA wall motion. This mechanism would also account for the presence of "fingerprints" on generally spherical regions of impacted iridium shells

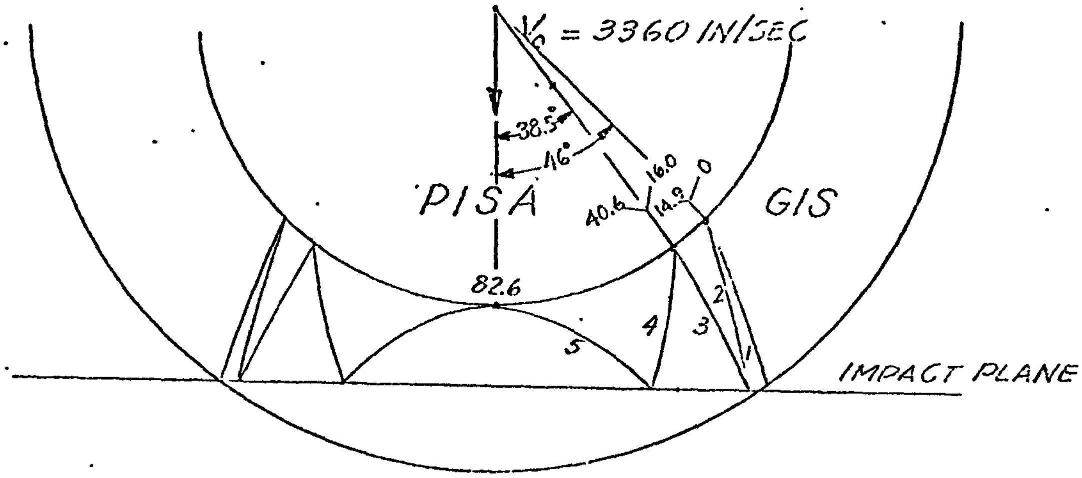

a. NORMAL PRESSURES AT SHOCK INTERSECTIONS AT
$t = 73.86\ \mu$ SEC, KSI. Δp = 24.6 KSI AT 38.5° & 14.9 AT 46°.

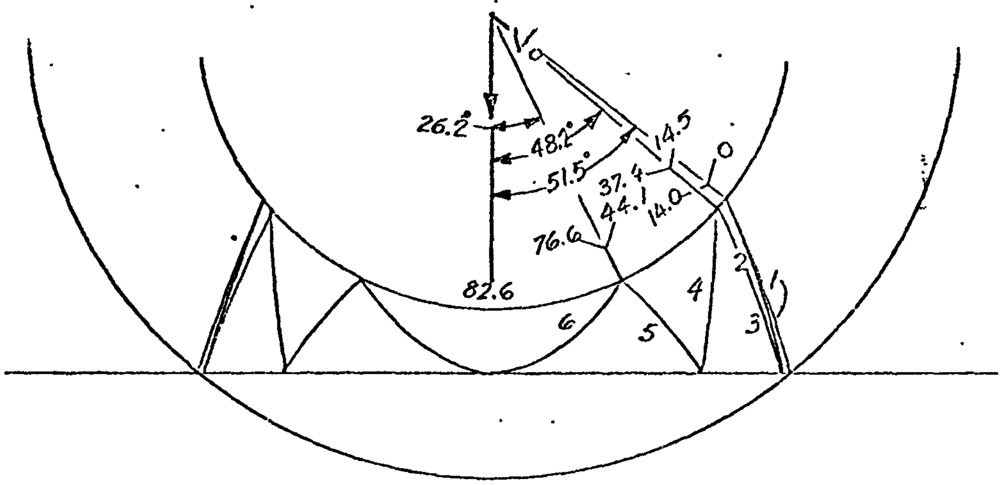

b. NORMAL PRESSURES AT SHOCK INTERSECTIONS AT
$t = 83.50\ \mu$ SEC, KSI. Δp = 32.5 KSI AT 26.2°, 22.9 AT 48.2°, & 14.0 AT 51.5°.

Figure 5.3-11
– PRESSURE LOADING DISCONTINUITIES ON PISA

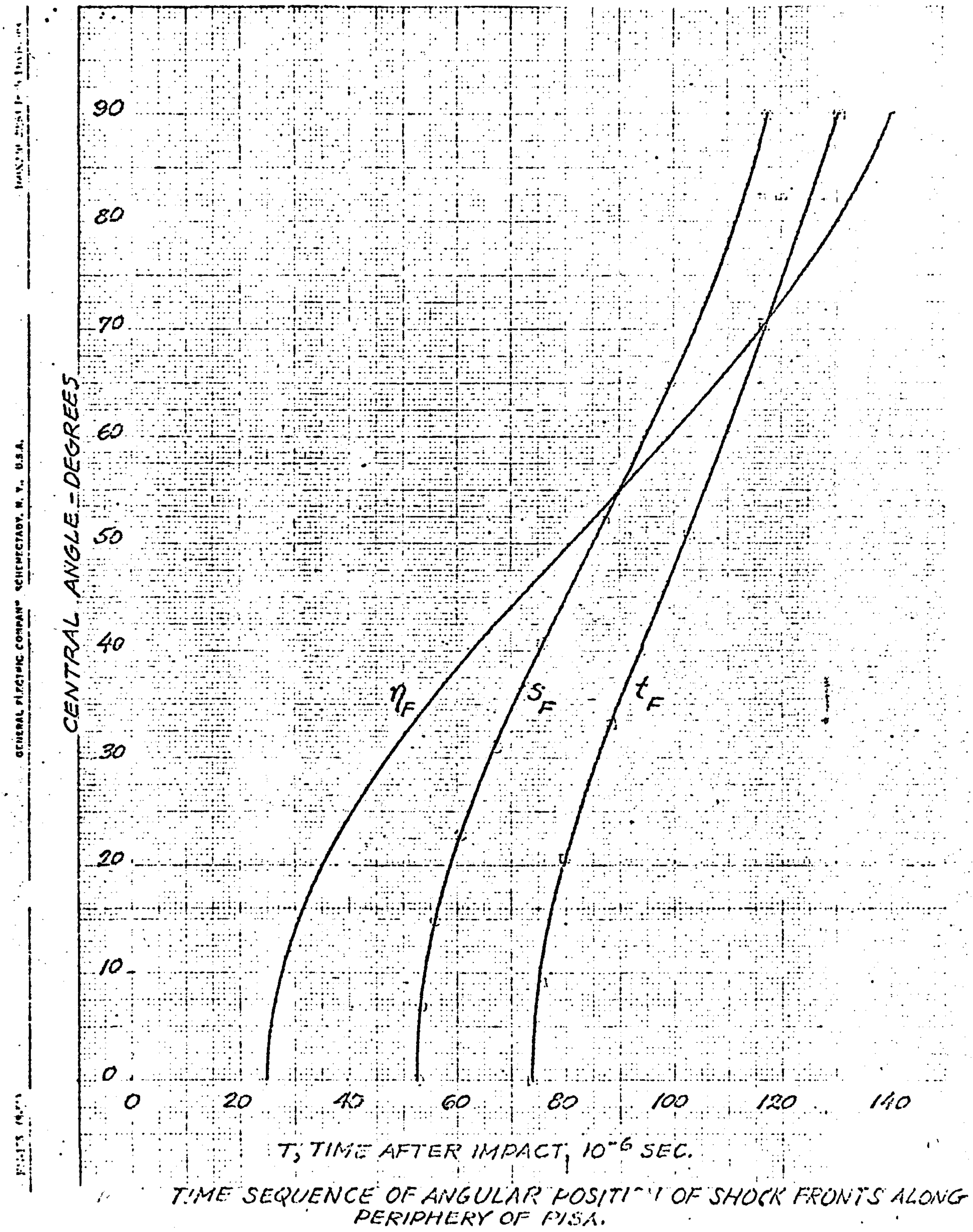

Figure 5.3-12 Time sequence of Angular Position of Schock Fronts along Periphery of PISA

Further investigation of this mechanism is needed in order to determine under what conditions "fingerprint" deformations occur and how they might be prevented.

d) Deceleration Forces Acting on PISA

The calculated normal pressures acting on the PISA surface were numerically integrated to determine the total decelerating force at various times after impact initiation. Values of force, F, impulse, I, and velocity, V, of the PISA, including the GIS end cap considered as riding with it, are listed in Table 5.3-1. Deceleration force is first imposed on the PISA at 24.79 sec. after impact initiation and rises rapidly thereafter. At the largest value of time considered, t = 117.4 μsec, the force is over 126,000 lb., a value corresponding to 170,700 g's deceleration of the PISA. Under such a deceleration level it is probable that flattening of the PISA has already occurred before this time.

A plot of PISA velocity vs. time is shown in Figure 5.3-13. For the time interval covered in the calculations, the velocity decreases from 3360 in/sec (280 fps) to 962 in/sec (80.2 fps). Calculation was not continued beyond t = 117.4 μsec because the GIS material in the vicinity of the stagnation point had already exceeded full compaction, for which a reasonable pressure-density relationship could not be assigned. The effect of this is an underestimation of the deceleration force and an overestimation of the resulting velocity. The dashed portion of the velocity curve in Figure 5.3-13 is more indicative of the correct trend.

The general levels of pressure and force calculated from this analysis are overestimated, however, because (1) they are based on a constant PISA velocity, as noted in assumption b, and (2) the pressure-density relationship assumed for the GIS material may result in overestimation of shock pressure. More realistically, the PISA can be expected to decelerate more gradually than described in Table 5.3-1 and Figure 5.3-13. Quantitative examination of x-ray photographs available from previous ball impact tests in light of the PISA behavior indicated herein will undoubtedly prove valuable for assessing the need both to modify the assumptions used and to obtain satisfactory material data.

An attempt was made to discern aspects of the impact behavior of the FSA including one dimensional shock wave effects in the GIS material. Despite the limitations to accurate prediction of real system behavior, due to the simplifying assumptions utilized, interesting phenomena such as moving pressure fronts, GIS compaction zones, and pressure

Table 5.3-1 PISA DECELERATION FORCE, IMPULSE AND VELOCITY DURING IMPACT

$\overline{T}$ μsec	F lb.	I 10^{-3} lb. sec.	V in/sec.
24.79	0	0	3360
25.44	297	.09677	3359.95
27.39	1172	1.5241	3359.20
30.59	2581	7.5309	3356.07
34.99	4460	23.0262	3347.98
40.60	6720	54.3914	3331.61
47.04	9265	105.9014	3304.72
54	13819	186.1757	3262.82
62	25202	339.3305	3182.88
70	36063	584.3903	3054.97
80	55877	1044.0937	2815.02
90	80061	1723.7852	2460.24
94.5	90920	2108.4927	2259.44
99.0	101042	2540.4072	2034.00
103	104923	2952.3385	1818.98
110	112068	3711.8103	1422.56
117.4	126235	4593.5327	962.34

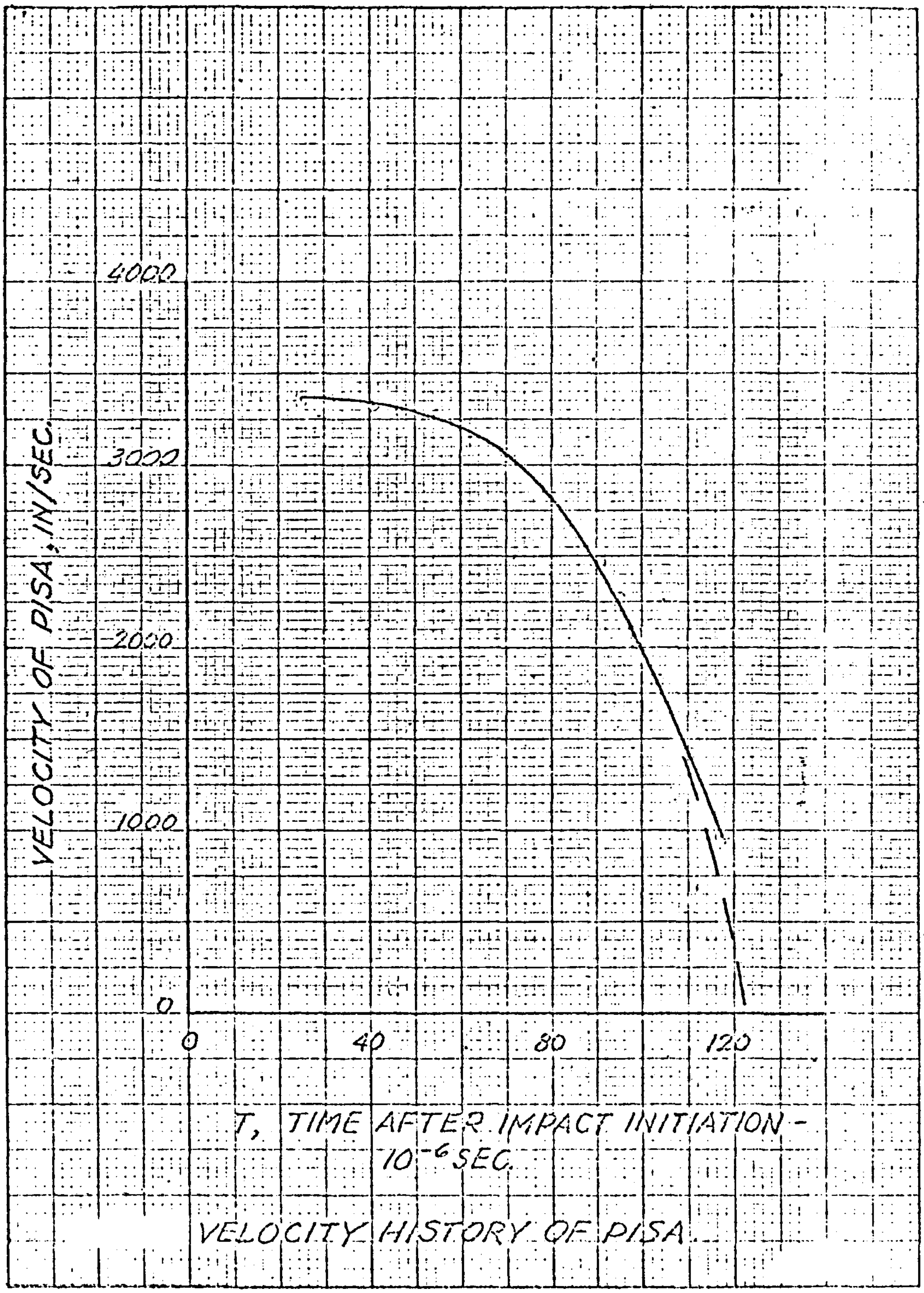

Figure 5.3-13 Velocity History of the PISA

loading discontinuities on the PISA surface have been revealed. It is believed that these phenomena are at least qualitatively correct and additionally provide useful insights about PISA overall deformation and "fingerprint" formation mechanisms. Another useful output obtained from the analysis pertains to GIS material compaction zones which, if observable in x-ray photos from FSA impact tests, may be helpful for developing improved impact absorbing materials.

Detailed study of x-ray photographic data obtained from previous FSA impact tests should be performed, and assimilated with the results obtained from present and subsequent analysis of FSA impact behavior. An additional task that should be performed without delay is GIS material compression testing, in order to determine realistic pressure-density relations.

5.4 MATERIALS DEVELOPMENT AND TESTING

5.4.1 Compatibility Tests

5.4.1.1 Unfueled Tests with Ir

A. No change in the status of the formal unfueled Ir tests occurred during this reporting period.

B. The Ir clad from the Q-1/IHS was examined after disassembly and analyzed for possible interaction with the vapors from the SiGe elements of the thermopile. Exposed regions of the Q-1 clad were determined to be free of any vapor attack resulting from tests performed on that unit; no attack was detected visually, or by electron probe examination. Regions of the Q-1 clad, shielded from direct line of sight attack by the presence of the emissivity sleeve, were also examined and found to be free of attack from converter vapors.

   Results of all experiments run to date, indicate that the MHW clad will not be degraded as a result of exposure to anticipated MHW environments.

5.4.1.2 Tests with Fuel-LASL

Details of the LASL compatibility tests on capsules and FSAs are given in the LASL monthly reports. No Ir/PuO_2 interactions have been observed in any of the test specimens examined to date.

The status of the FSA compatibility tests is shown in Table 5.4-1; see Figure 5.4-1 for the test configuration. As noted in Paragraph 5.1.4.3, the only currently observable behavior is He venting for those units continuing on test. See also Table 5.1-1a and 1b.

5.4.2 Iridium

PISA's in the first few MJS heat sources will be fabricated out of LES 8/9 type Ir but the remainder will be produced from LES 8/9 type Ir that has been doped with a few parts per million of Al, Fe, ThO_2, Ni, and Rh. The improved material, referred to as DOP-4 Ir, is currently being processed into sheet for shipment to Mound Laboratory.

Both types Ir (LES 8/9 and DOP-4) conform to current specification requirements since chemistry modification is minimal and no physical test requirements are currently written into the specification. There is general agreement that the existing specification should be revised to control the quality of the improved (DOP-4) material. To date, there are data indicating that the DOP-4 material is tougher than LES 8/9 Ir when impacted at high velocity at elevated temperature. The data are insufficient to justify meaningful changes to the existing specification, which is being used, along with ORNL process controls, to govern the flow of DOP-4 Ir at ORNL.

GE has recommended the incorporation of functional specifications governing the characteristics of the DOP-4 material. These specifications might identify requirements based on grain size, grain shape mode of fracture under high velocity impact, and ductility (elongation) in addition to chemistry. It is planned that a revised specification will be prepared by HNL for review and approval.

5.4.3 Carbon

The test program outlined in the Bi-Monthly Report for May/June 1975 was only partially completed. Difficulties in handling specimens prepared at GE-Evendale and shipped to Gollob Analytical Services, Inc. unduly biased the results. One consequence of these tests was the identification of the need to degas the shipping containers under vacuum and temperatures of at least $125^{\circ}C$. This requirement will be incorporated into the bake-out specification. See Paragraph 5.1.6 for further discussions of tests on carbon.

TABLE 5.4-1 MHW FUEL SPHERE ASSEMBLY COMPATIBILITY TESTS AT LASL

SPECIMEN NUMBER	MHW OPERATIONAL MODE - GAS IN Ir/FUEL CAP	HELIUM VENT HOLE DIAMETER - INCH	EXPOSURE TEMPERATURE - DEGREES CELSIUS		TEST START - DATE	EXPOSURE TIME - HOURS		STATUS
			O.D.GIS -MEASURED	Ir/FUEL CALCULATED		PLANNED	ACTUAL	AS OF 31 August 1975
MHFT-1	vacuum	0.0008	1340	1440	Aug. 1972	2150	2150	Exposure complete; data reported
MHFT-15	"	0.0015	"	"	25 May 1973	3300	7395	" " " "
MHFT-19	"	0.005	"	"	18 May 1973	1480	1105	" " " "
MHFT-20	"	0.005	"	"	May 1973	8760	14000	In storage; not yet examined
MHFT-22	"	0.005	"	"	15 Jun 1973	3300	3300	Exposure completed; data reported
MHFT-14	helium	0.0008	1180	1250	Mar,1973	2150	1248	Exposure complete; data reported
MHFT-18	"	0.005	"	"	21 May 1973	1460	1365	" " " "
MHFT-21	"	0.005	"	"	1 Jun.1973	8760	4500	" " " "
MHFT-10	helium	0.0008	1018	1150	Mar.1973	4380	1244	Exposure complete; data reported
MHFT-16	"	0.0015	"	"	6 Jun.1973	3300	14000	In storage; not yet examined
MHFT-17	"	0,005	"	"	7 May 1973	3300	14400	" " "
MHFT-23	"	0.005	"	"	Test not begun	--	--	Transferred to environmental test
MHFT-37	vacuum	0.005	1210	1335	24 Feb.1974	3000	12600	Test continuing
MHFT-42	"	0.005	"	"	21 Feb.1974	3000	5440	Exposure complete; data reported
MHF-30	"	0.005	"	"	Nov.1974	?3300	9200	Test continuing
MHFT-44	helium	0.005	1180	1250	3 Jun.1974	1500	6500	Test continuing

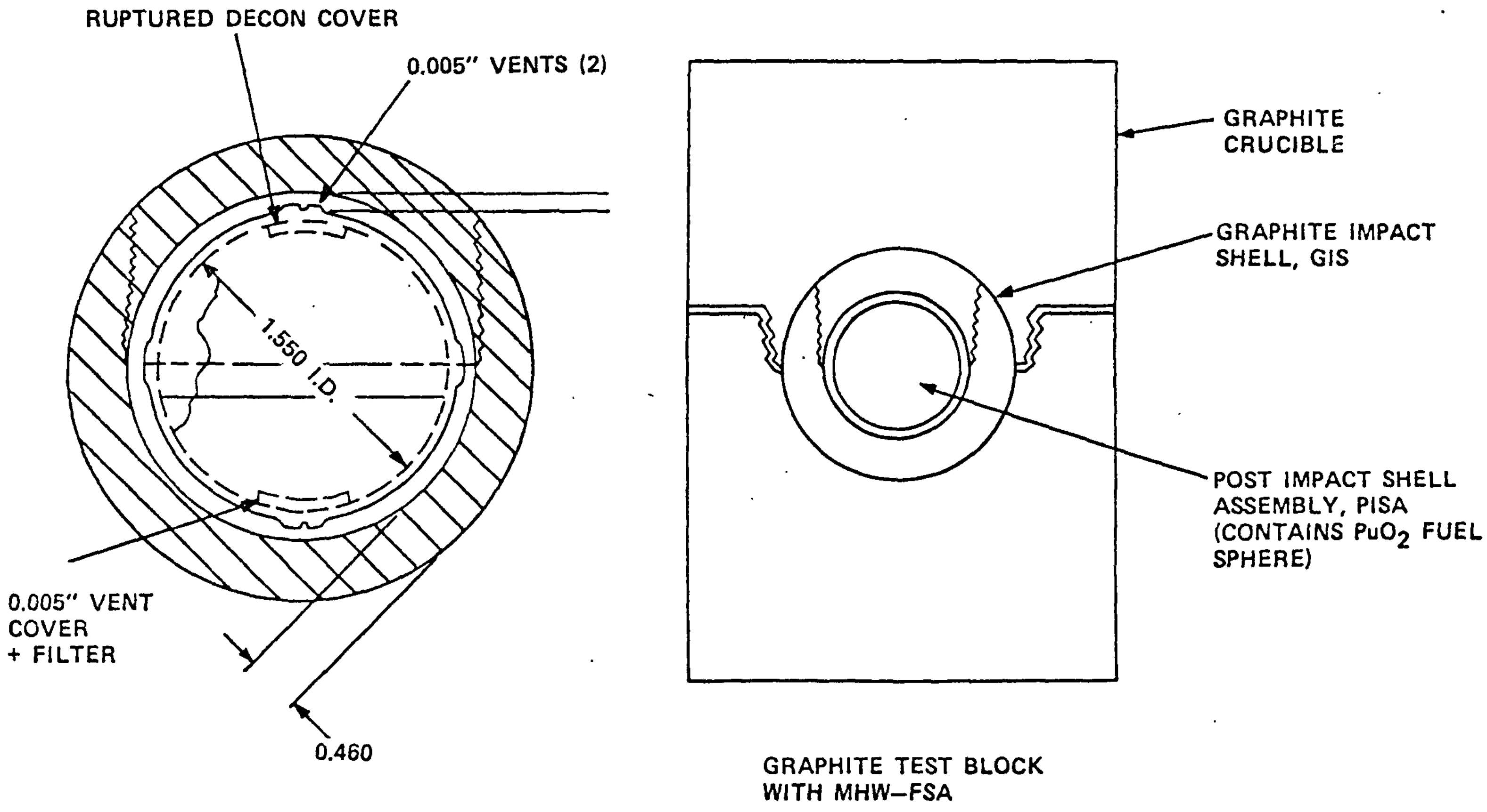

MHW-FSA

FIGURE 5.4-1 LASL FSA COMPATIBILITY CONFIGURATION

5.4.4 Fuel

5.4.4.1 Fuel Fabrication

The LASL and ML/MRC monthly reports discuss respectively the development and production fuel fabrication work.

5.4.4.2 Feed Material

Development work on feed materials is given in the SRP monthly reports. LASL has noted anomalous behavior in some of the SRP batches received over the past year. Process changes discussed in the reports already noted have been effected to restore the fabrication characteristics and to exercise more rigid control of certain impurities notably: Ca, Si and Fe.

5.4.4.3 Fuel Characterization

The status of the fuel characterization is shown in Tables 5.4-2 and 5.4-3.

5.4.4.4 Interaction Between Plutonium Dioxide Fuel and IHS Carbon Components

The possibility of generating the CO observed in the MHW-IHS by interactions between PuO_2 fuel and carbon has frequently been raised. Some of the relevant data were again reviewed.

5.4.4.4.1 Fuel Reduction

5.4.4.4.1.1 Possible Reactions

The disproportionation of $PuO_{2.00}$ at temperatures above 1200°C in vacuum, neutral and reducing environments can produce oxygen by the reaction:

$$PuO_{2.00} + (heat) \text{ ---- } PuO_{(2-x)} + x\,O_2 \qquad (1)$$

and in the IHS this would lead to

$$x\,O_2 + C \text{ ---- } x(CO/CO_2) \qquad (2)$$

TABLE 5.4-2

MHW FUELS CHARACTERIZATION - 1

(STATUS - as of 31 August 1975)

1.0 FUEL PROPERTIES

CATEGORY	STATUS	RESULTS/COMMENTS
1.1 DENSITY	CONTINUING	DIAMETRAL SECTIONING IN PROGRESS TO DEFINE POROSITY DISTRIBUTION; RANGE FOR SPHERES: 80% TD to 90% TD; NOMINAL MRC/ML 82 % TD DENSITY VARIATION WITHIN SPHERES = 15%: CENTER-TO-SURFACE
1.2 MECHANICAL	IN PROCESS	
o COMPRESSIVE	CONTINUING	ROOM TEMP. DATA ON LASL AND ML/MRC MATERIAL COMPLETED; HIGH TEMP. DATA IN PROCESS; CONTINUED TESTING SHOWS NO PLASTICITY; He INGROWTH EFFECT BEING CHECKED; TESTS WITH ^{239}Pu PLANNED
o 4-POINT BEND	" "	
o YOUNG'S MODULUS	" "	
o POISSON'S RATIO	" "	
o SHEAR	CANCELLED	NO WORK PLANNED
o HARDNESS	CANCELLED	NO WORK PLANNED
1.3 THERMAL CONDUCTIVITY	PARTIAL DATA	COMPLETE TO 1350 C; HIGH TEMPERATURE DATA, TO 2200 C, WAITING ON INSTALLATION AND CHECKOUT OF APPARATUS : DATA NEEDED NO WORK PLANNED
1.4 SPECIFIC HEAT	COMPLETE	DATA AVAILABLE FROM STUDIES ON Pu REACTOR FUELS ^{239}Pu
1.5 MELTING POINT o PURE FUEL o FUEL+Ir+CARBON	 COMPLETE COMPLETE	DATA ON PRODUCTION FUEL SHOWS EFFECTS OF IMPURITIES NEEDED TO DETERMINE SYNERGISTIC MP DEPRESSION, NO ENHANCED REACTION BELOW Ir+C EUTECTIC @ 2200 C. (DATA BY LASL)
1.6 THERMAL EXPANSION	PARTIAL DATA	COMPLETE TO 1400 C; VERIFIES PREVIOUS WORK; REQUIRES HIGH TEMPERATURE APPARATUS: DATA NEEDED NO WORK PLANNED
1.7 EMITTANCE	~~PARTIAL DATA~~ CANCELLED	LASL REPORTED DATA THROUGH 1400 C; TO 2000 C LATER; NO WORK PLANNED
1.8 SOLUBILITY	CONTINUING	SOLUBILITY IN FRESH AND SALT WATER CONTINUING UNDER STUDY; ENCAPSULATED SPHERE TEST STARTED MAR 73 (MHFT-13) SEA WATER
1.9 VAPOR PRESSURE	AVAILABLE	DATA ARE FOR "PURE" $^{239}PuO_2$; DATA CHECKS ON PRODUCTION MATERIAL ARE REQUIRED; Ca, Si, Al, Fe, Mg OXIDES FOUND IN VENT FILTERS
1.10 RADIATION	CONTINUING	DATA TO BE CHECKED ON PRODUCTION SPHERES; NEUTRON LEVELS DEPENDENT ON LIGHT ELEMENT IMPURITIES CONTENT AND EFFECTIVENESS OF ^{16}O EXCHANGE.
1.11 SINTERABILITY	IN PROCESS	SEE LASL REPORTS FOR FUEL DEVELOPMENT STUDIES; 10000 HOURS DATA REQUIRED AT OPERATIONAL TEMPERATURE

TABLE 5.4-3

MHW FUELS CHARACTERIZATION - 2

2.0 FUEL BEHAVIOR/RESPONSE

(STATUS as of 31 August 1975)

CATEGORY	STATUS	RESULTS/COMMENTS
2.1 VIBRATION o FSA @ MRC/ML	IN PROCESS	MHFT-11 VIBRATED; EXAMINED @ LASL; SPHERE BROKEN IN 5 PIECES; FINES ≈0.6% TOTAL FUEL, 7 ADDITIONAL TESTS = & BROKEN SPHERES
o HSA @ GE-ISAO	IN PROCESS	EXPOSURE OF Q-1 COMPLETE: POST MORTEM COMP'D OCT.74; NO Pu FOUND
2.2 IMPACT o PELLETS @ LASL	PARTIAL	LOW TEMPERATURE PELLET IMPACT DATA; NEED HIGH TEMPERATURE DATA
o HOT BARE SPHERES @ ML	COMPLETE	TWO SPHERES DROPPED @ 1000 C ; BROKE IN LARGE PIECES
o FSA @ LASL	IN PROCESS	10 FUELED FSAs IMPACTED; SEE IMPACT TEST Sect. 5.2) 3 WITH ORNL/ML Ir
o HSA @ SANDIA	IN PROCESS	12-PACK IMPACT No.1 GOOD RESULTS; No.2 WITH SHAVED GIS AND "BAD" Ir POOR RESULTS; 24-PACK IMPACTED; ALL Ir PISAs CRACKED; THREE BADLY
2.3 AGING EFFECTS 2.3.1 He RETENTION/RELEASE o SMALL PELLETS @ LASL	COMPLETE	DATA AVAILABLE INDICATE NO PROBLEM AT 1300 C FOR SMALL PIECES
o LARGE SAMPLES @ LASL	IN PROCESS	QUANTITATIVE RETENTION DATA @ 900, 1150, 1250, 1370, & 1450 OBTAINED
o STORED SPHERES @ LASL	IN PROCESS	ON TEST (COMPATIBILITY TEST SPHERES) SEE TABLE 5.4-1
2.3.2 RADIATION DAMAGE + He INGROWTH	IN PROCESS	CHANGE IN MECHANICAL PROPERTIES AND MICROSTRUCTURE MAY RESULT FROM He BUBBLE CONCENTRATION ALONG GRAIN BOUNDARIES ; NEW SPECIMENS BEING MADE: TESTS WITH 239 Pu PLANNED.
2.3.3 DEOXYGENATION @ LASL	IN PROCESS	LONG TERM SPHERE TESTS WITH CHANGE IN O/Pu: DIMENSIONAL CHANGES REDUCING ACTION OF CO UNDER STUDY
2.4 OXIDATION: @LASL& ML	IN PROCESS	REDUCTION AND REOXIDATION?SHOWED?SMALL DIMENSIONAL CHANGES; APPARENT REDUCTION OF FUEL IDENTIFIED AS AN ARTIFACT
2.5 Pu RELEASE o VAPOR	IN PROCESS	VAPOR TRANSPORT OF PuO_2 CAL'D FOR KNUDSEN FLOW; NEED ADDITIONAL CALC'S AT PRESSURES REACHED IN FSAs WITH INTERMITTENT VENTING
o ALPHA KNOCK-ON	CALCULATED	
o PARTICULATES	CONTINUING	LASL MAKES FINES MEASUREMENTS ON ALL IMPACTED SPHERES
2.6 ABLATION/VAPORIZATION	CANCELLED	FACILITIES PROBLEMS IN THE USE OF LIVE FUEL
2.7 COMPATIBILITY @ LASL	IN PROCESS	SEE DETAILED BREAKDOWN ON COMPLETED AND PLANNED TESTS - Sect.5.4.1.2 TESTS ON FULL-UP FSAs STARTED APR.73
@ DWDL	TEST COMPLETE	5000 HR. IN GRADIENT, ISOTHERMAL EXAMINED; TENSILE TESTS REPORTED.
2.8 THERMAL RESPONSE o REENTRY THERMAL RAMP	COMPLETE	INCLUDED IN THE SSST
o ASYMMETRICAL THERMAL RAMP	COMPLETE	SPHERES CRACKED BUT REMAINED INTEGRAL: LASL & MRC/ML SPHERES RUN
o SYMMETRICAL RAMP TO OPERATIONAL - 1450 C	COMPLETE	LASL SPHERES CHECKED AFTER 1 YEAR SHOWED NO DAMAGE OR CHANGE WHEN HEATED TO 1450 C @ MRC/ML: 1 SPHERE AFTER 6 mos STORAGE TO 1250 C OK

other reactions include:

$$PuO_{2.00} + C \text{ ---- } PuO_{(2-x)} + x\ (CO/CO_2) \qquad (3)$$

and

$$PuO_{2.00} + CO \text{ ---- } PuO_{(2-x)} + x\ (CO_2) \qquad (4)$$

followed by

$$x\ (CO_2) + C \text{ ---- } 2\ x\ (CO) \qquad (5)$$

Direct contact between the PuO_2 and C does not occur in the MHW-IHS but with the large amount of carbon present, it has been argued that the CO will have effectively the activity of C. This could occur, however, only under equilibrium conditions with the IHS not vented to vacuum. In turn, the IHS is closed off only under storage conditions at low temperature and under certain short-term test conditions.

5.4.4.4.1.2 Thermodynamic Considerations

Thermodynamic considerations based on the data shown in Tables 5.4-4 and 5.4-5 indicate that reactions reducing the fuel are marginal at the storage temperature of the MHW-IHS shown in Figure 5.4-2. At operational temperatures shown in Figure 5.4-3 reactions between PuO_2 and C do occur as indicated in Table 5.4-6 whereas the reaction with CO still appears marginal as indicated in Table 5.4-7. Table 5.4-8 summarizes the temperatures at which equilibrium values become negative for the reduction of PuO_2.

5.4.4.4.1.3 Experiments with Flowing CO

LASL has run a series of experiments with PuO_2 exposed at various temperatures to flowing Ar + CO with the partial pressure of CO at $\cong$ 76 Torr, 0.1 ATM. The fuel was found to be reduced as shown in Tables 5.4-9 and 5.4-10. The maximum reduction at 1400°C $\sim$ 1673K was to $PuO_{1.85}$. (Ref. Ke 75a)

5.4.4.4.1.4 Other LASL Data

A. FSAs

The FSAs used in the LASL compatibility test are configured as shown in Figure 5.4-1. The exposures have been at fuel/PICS interface temperatures of 1450°C, at 1225°C in He, and at the current vacuum MJS operational temperatures shown in Figure 5.4-3 for times in excess of 6000 hours. Post-test examination of these units has shown no observable

Table 5.4-4 *

REACTIONS BETWEEN $\langle PuO_2 \rangle$ and (CO) at 1300°K

Reaction				ΔG kcal/mole
$\langle PuO_2 \rangle$	+ 0.02(CO)	= $\langle PuO_{1.98} \rangle$	+ 0.02 (CO_2)	+ 0.30
$\langle PuO_2 \rangle$	+ 0.05(CO)	= $\langle PuO_{1.95} \rangle$	+ 0.05 (CO_2)	+ 0.86
$\langle PuO_2 \rangle$	+ 0.08(CO)	= $\langle PuO_{1.92} \rangle$	+ 0.08 (CO_2)	+ 1.48
$\langle PuO_2 \rangle$	+ 0.10(CO)	= $\langle PuO_{1.90} \rangle$	+ 0.10 (CO_2)	+ 1.96
$\langle PuO_2 \rangle$	+ 0.15(CO)	= $\langle PuO_{1.85} \rangle$	+ 0.15 (CO_2)	+ 3.25
$\langle PuO_2 \rangle$	+ 0.20(CO)	= $\langle PuO_{1.80} \rangle$	+ 0.20 (CO_2)	+ 4.67
$\langle PuO_2 \rangle$	+ 0.25(CO)	= $\langle PuO_{1.75} \rangle$	+ 0.25 (CO_2)	+ 6.20
$\langle PuO_2 \rangle$	+ 0.30(CO)	= $\langle PuO_{1.70} \rangle$	+ 0.30 (CO_2)	+ 7.89
$\langle PuO_2 \rangle$	+ 0.35(CO)	= $\langle PuO_{1.65} \rangle$	+ 0.35 (CO_2)	+ 9.61
$\langle PuO_2 \rangle$	+ 0.39(CO)	= $\langle PuO_{1.61} \rangle$	+ 0.39 (CO_2)	+ 11.07
$\langle PuO_2 \rangle$	+ 0.50(CO)	= $\langle PuO_{1.50} \rangle$	+ 0.50 (CO_2)	+ 15.00

Table 5.4-5 *

REACTIONS BETWEEN $\langle PuO_2 \rangle$ and $\langle C \rangle$ at 1200 °K

Reaction				ΔG kcal/mole
$\langle PuO_2 \rangle$	+ 0.02 $\langle C \rangle$	= $\langle PuO_{1.98} \rangle$	+ 0.02 (CO)	+ 0.20
$\langle PuO_2 \rangle$	+ 0.05 $\langle C \rangle$	= $\langle PuO_{1.95} \rangle$	+ 0.05 (CO)	+ 0.56
$\langle PuO_2 \rangle$	+ 0.08 $\langle C \rangle$	= $\langle PuO_{1.92} \rangle$	+ 0.08 (CO)	+ 0.96
$\langle PuO_2 \rangle$	+ 0.10 $\langle C \rangle$	= $\langle PuO_{1.90} \rangle$	+ 0.10 (CO)	+ 1.28
$\langle PuO_2 \rangle$	+ 0.15 $\langle C \rangle$	= $\langle PuO_{1.85} \rangle$	+ 0.15 (CO)	+ 2.15
$\langle PuO_2 \rangle$	+ 0.20 $\langle C \rangle$	= $\langle PuO_{1.80} \rangle$	+ 0.20 (CO)	+ 3.11
$\langle PuO_2 \rangle$	+ 0.25 $\langle C \rangle$	= $\langle PuO_{1.75} \rangle$	+ 0.25 (CO)	+ 4.15
$\langle PuO_2 \rangle$	+ 0.30 $\langle C \rangle$	= $\langle PuO_{1.70} \rangle$	+ 0.30 (CO)	+ 5.32
$\langle PuO_2 \rangle$	+ 0.35 $\langle C \rangle$	= $\langle PuO_{1.65} \rangle$	+ 0.35 (CO)	+ 6.52
$\langle PuO_2 \rangle$	+ 0.39 $\langle C \rangle$	= $\langle PuO_{1.61} \rangle$	+ 0.39 (CO)	+ 7.56
$\langle PuO_2 \rangle$	+ 0.50 $\langle C \rangle$	= $\langle PuO_{1.50} \rangle$	+ 0.50 (CO)	+ 10.34
$\langle PuO_2 \rangle$	+ 2.0 $\langle C \rangle$	= (Pu)	+ 2.0 (CO)	+ 149.8
$\langle PuO_2 \rangle$	+ 2.9 $\langle C \rangle$	= $\langle PuC_{0.9} \rangle$	+ 2.0 (CO)	+ 84.7
$\langle PuO_2 \rangle$	+ 3.5 $\langle C \rangle$	= $\langle PuC_{1.5} \rangle$	+ 2.0 (CO)	+ 80.3
$\langle PuO_2 \rangle$	+ 2.0 $\langle C \rangle$	= $\langle PuO_{0.5}C_{0.5} \rangle$	+ 1.5 (CO)	+ 71.4

(*) From Ref. Ke 73a

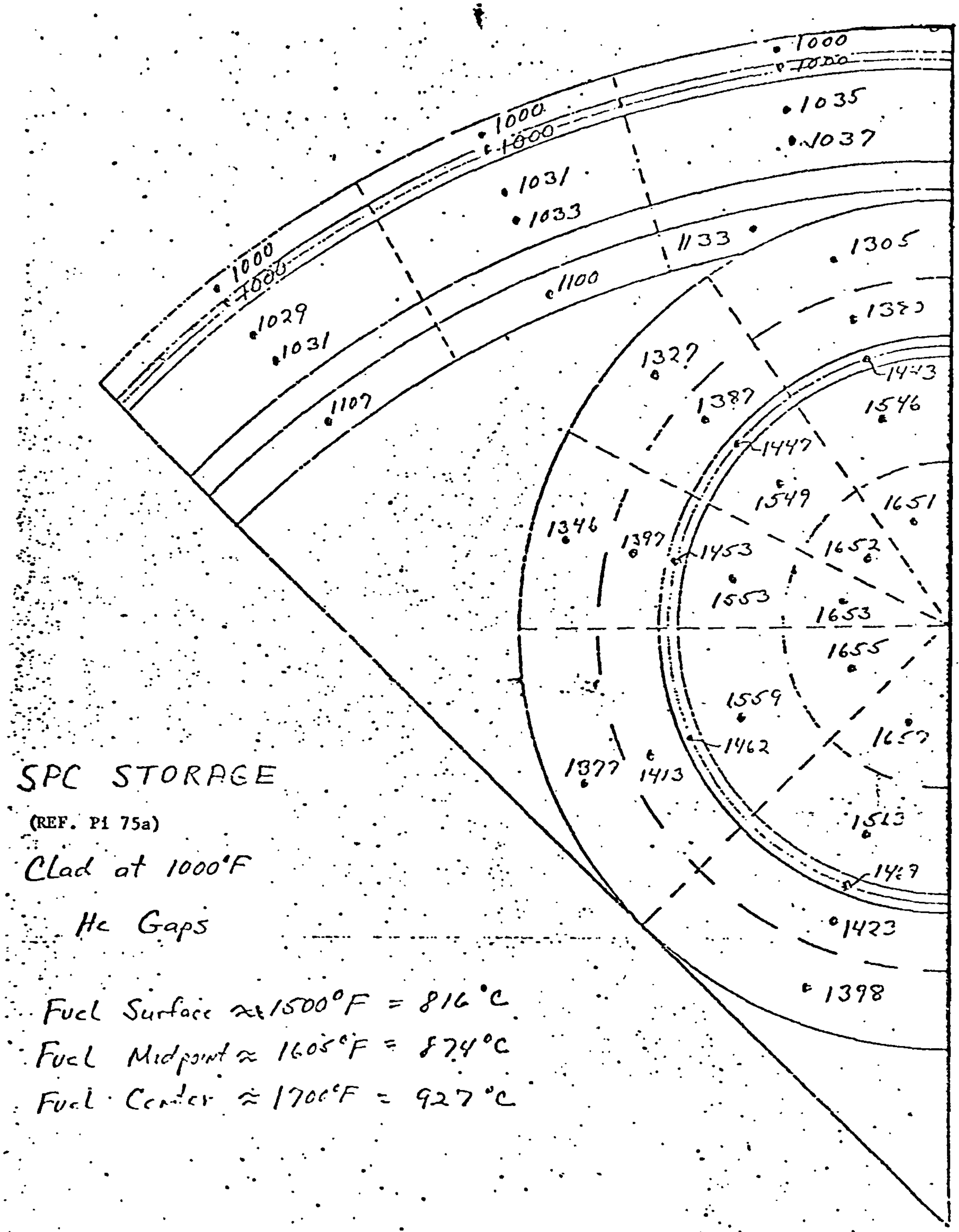

Figure 5.4-2 SPC Storage Temperatures

Table 5.4-6 *

REACTIONS BETWEEN $<PuO_2>$ and $<C>$ at 1600 °K

Reaction				ΔG kcal/mole
$<PuO_2>$	+ 0.02 $<C>$	= $<PuO_{1.98}>$	+ 0.02 (CO)	− 0.49
$<PuO_2>$	+ 0.05 $<C>$	= $<PuO_{1.95}>$	+ 0.05 (CO)	− 0.93
$<PuO_2>$	+ 0.08 $<C>$	= $<PuO_{1.92}>$	+ 0.08 (CO)	− 1.26
$<PuO_2>$	+ 0.10 $<C>$	= $<PuO_{1.90}>$	+ 0.10 (CO)	− 1.39
$<PuO_2>$	+ 0.15 $<C>$	= $<PuO_{1.85}>$	+ 0.15 (CO)	− 1.56
$<PuO_2>$	+ 0.20 $<C>$	= $<PuO_{1.80}>$	+ 0.20 (CO)	− 1.50
$<PuO_2>$	+ 0.25 $<C>$	= $<PuO_{1.75}>$	+ 0.25 (CO)	− 1.19
$<PuO_2>$	+ 0.30 $<C>$	= $<PuO_{1.70}>$	+ 0.30 (CO)	− 0.66
$<PuO_2>$	+ 0.35 $<C>$	= $<PuO_{1.65}>$	+ 0.35 (CO)	− 0.08
$<PuO_2>$	+ 0.39 $<C>$	= $<PuO_{1.61}>$	+ 0.39 (CO)	+ 0.47
$<PuO_2>$	+ 0.50 $<C>$	= $<PuO_{1.50}>$	+ 0.50 (CO)	+ 1.94
$<PuO_2>$	+ 2.0 $<C>$	= (Pu)	+ 2.0 (CO)	+ 108.3
$<PuO_2>$	+ 2.9 $<C>$	= $<PuC_{0.9}>$	+ 2.0 (CO)	+ 51.8
$<PuO_2>$	+ 3.5 $<C>$	= $<PuC_{1.5}>$	+ 2.0 (CO)	+ 46.8
$<PuO_2>$	+ 2.0 $<C>$	= $<PuO_{0.5}C_{0.5}>$	+ 1.5 (CO)	+ 47.5

Table 5.4-7 *

REACTIONS BETWEEN $<PuO_2>$ and (CO) at 1600°K

Reaction				ΔG kcal/mole
$<PuO_2>$	+ 0.02 (CO)	= $<PuO_{1.98}>$	+ 0.02 (CO_2)	+ 0.03
$<PuO_2>$	+ 0.05 (CO)	= $<PuO_{1.95}>$	+ 0.05 (CO_2)	+ 0.36
$<PuO_2>$	+ 0.08 (CO)	= $<PuO_{1.92}>$	+ 0.08 (CO_2)	+ 0.80
$<PuO_2>$	+ 0.10 (CO)	= $<PuO_{1.90}>$	+ 0.10 (CO_2)	+ 1.19
$<PuO_2>$	+ 0.15 (CO)	= $<PuO_{1.85}>$	+ 0.15 (CO_2)	+ 2.31
$<PuO_2>$	+ 0.20 (CO)	= $<PuO_{1.80}>$	+ 0.20 (CO_2)	+ 3.67
$<PuO_2>$	+ 0.25 (CO)	= $<PuO_{1.75}>$	+ 0.25 (CO_2)	+ 5.26
$<PuO_2>$	+ 0.30 (CO)	= $<PuO_{1.70}>$	+ 0.30 (CO_2)	+ 7.08
$<PuO_2>$	+ 0.35 (CO)	= $<PuO_{1.65}>$	+ 0.35 (CO_2)	+ 8.96
$<PuO_2>$	+ 0.39 (CO)	= $<PuO_{1.61}>$	+ 0.39 (CO_2)	+ 10.54
$<PuO_2>$	+ 0.50 (CO)	= $<PuO_{1.50}>$	+ 0.50 (CO_2)	+ 14.85

Table 5.4-8 *

TEMPERATURES AT WHICH EQUILIBRIUM VALUES BECOME NEGATIVE FOR THE REDUCTION OF $<PuO_2>$ TO SPECIFIC $<PuO_{2-x}>$ COMPOSITIONS

Reaction

1. $<PuO_2> + x<C> = <PuO_{2-x}> + x\,(CO)$
2. $<PuO_2> + x(CO) = <PuO_{2-x}> + x\,(CO_2)$
3. $<PuO_2> + x(H_2) = <PuO_{2-x}> + x\,(H_2O)$

$<PuO_{2-x}>$	Temperature, °C (± 20) Reaction 1	Reaction 2	Reaction 3
$<PuO_{1.98}>$	1047	1370	1290
$<PuO_{1.95}>$	1077	1540	1420
$<PuO_{1.92}>$	1100	1675	1515
$<PuO_{1.90}>$	1120	1790	1590
$<PuO_{1.85}>$	1160		1760
$<PuO_{1.80}>$	1195		1970
$<PuO_{1.75}>$	1240		
$<PuO_{1.70}>$	1282		
$<PuO_{1.65}>$	1322		
$<PuO_{1.61}>$	1357		
$<PuO_{1.50}>$	1420		

* REF. Ke 73a

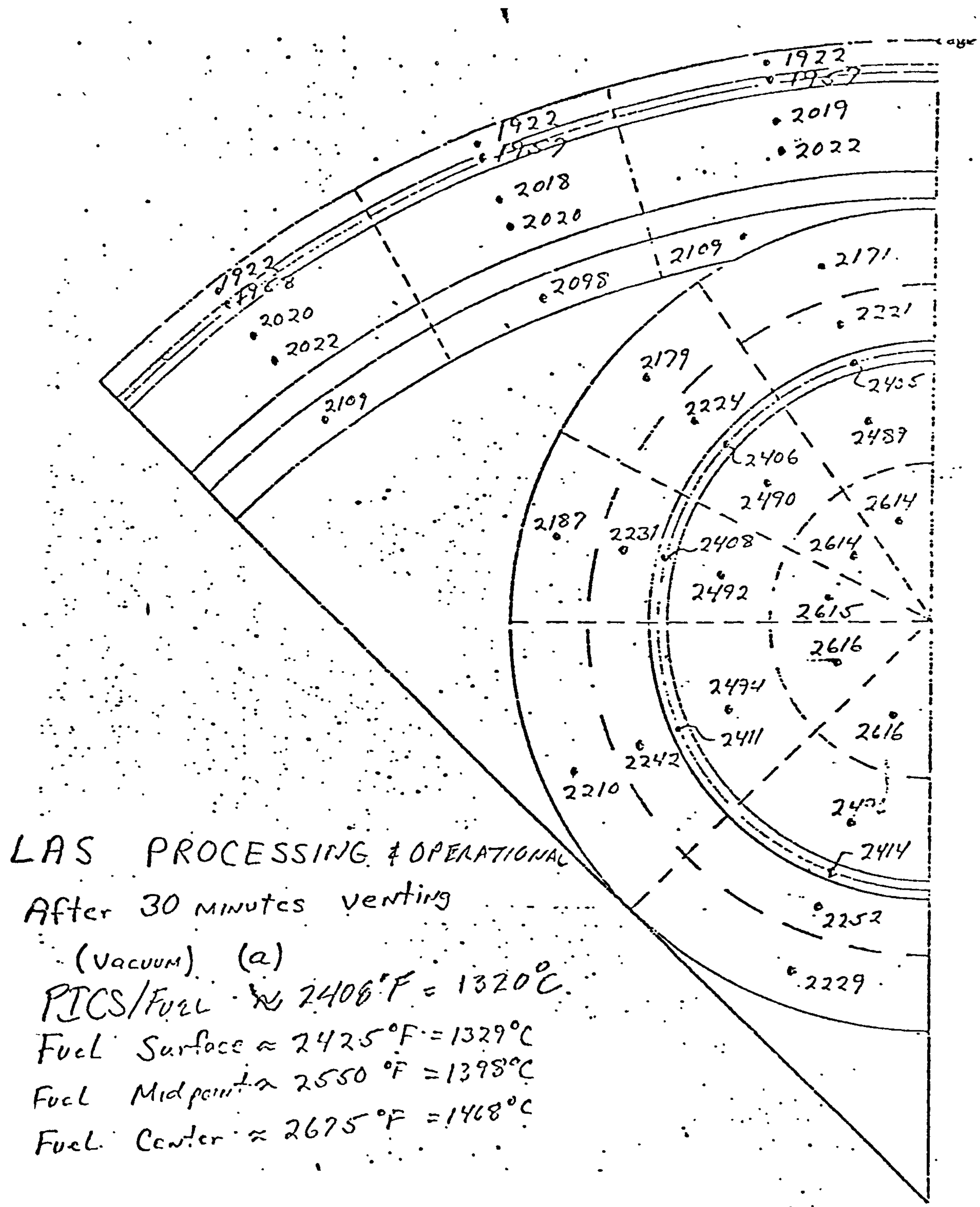

Figure 5.4-3 LAS Processing and Operational Temperatures

Table 5.4-9

EFFECTS OF TIME AND TEMPERATURE ON REDUCTION OF PuO_2 BY CO

Initial Stoichiometry $PuO_{2.00}$

Flow Gas 90 Ar-10 CO (P_{CO} = 0.1 atm)

Temp., °C	Residue O/Pu Ratio: 6 Hours	Residue O/Pu Ratio: 32 Hours
1227	1.97	1.94
1327	1.95	1.92
1427	1.94	1.89
1527	1.86	1.82

Table 5.4-10

REDUCTION OF PuO_2 BY CO AT 1400°C

P_{CO} = 0.1 atm		32 Hours Reduction	
Time, h	O/Pu	P_{CO}, atm	O/Pu
6	1.94	0.05	1.93
12	1.93	0.1	1.89
24	1.91	0.2	1.87
32	1.89	0.5	1.86
64	1.86	1.0	1.86
70	1.86	10	1.85
75	1.86	200	1.85

Conclusion: At 1400°C, CO will not reduce PuO_2 below $PuO_{1.85}$

(*) Ke 75a

reduction of the PuO_2 fuel which would have been indicated by the presence of even small amounts of the second phase α-PuO_2. If reduction did occur, it is to an O/Pu ratio $\geq$ 1.98. That some oxygen came out of the fuel, is inferred by the presence of a small crater in the inner surface of the GIS adjacent to the PICS vent. This loss of oxygen at operational temperatures is expected based on the oxygen partial pressures over PuO_2. However, a similar loss of oxygen at storage conditions appears to be unlikely (Ref. Ke 73a).

B. <u>Capsule Tests</u>

The behavior of the fuel in the capsule tests at LASL in the test configurations shown in Figures 5.4-4 and 5.4-5 does not indicate fuel reduction even after exposures at 1450°C and 11,000 hours.

5.4.4.4.1.5 Data from the Q-1/IHS Fuel

The Q-1/IHS is the most representative configuration in which fuel reduction under storage or operational conditions might have been observed. The CO problem was first found in the gas samples taken from Q-1/IHS. ML/MRC examined MHF-28 removed from Q-1 explicitly to determine whether fuel reduction had occurred during IHS fabrication, storage, shipping and testing at GE-VF. Special precautions were taken in handling the specimen to prevent its accidental re-oxidation. The results of the ML/MRC analysis on PPS-39, the fuel sphere from FSA MHF-28, showed no reduction of the fuel within the limits of accuracy of the analyses, O/Pu = 2.00 ± 0.02. It should be noted that there is currently no accepted technique for reliably analyzing the O/Pu ratio to better than ± 0.02 (Ref. WA 71a).

5.4.4.4.1.6 Evidence of Fuel Reduction

The absence of observable reduction in the fueled tests, discussed in the preceding paragraphs, at temperatures up to 120°C above the planned operational levels, does not preclude the possibility that some fuel reduction could have taken place. However, if such reduction has occurred, it has lowered the O/Pu ratio by less than 0.02 assuming that the fuel was initially at exact stoichiometry, O/Pu = 2.00. Alexander and others have suggested that some of the CO observed could be explained on the basis of a reduction of the fuel to an O/Pu ratio of $\cong$ 1.995. The loss of oxygen from PuO_2 in the amount needed to effect the reduction to $PuO_{1.995}$, could produce

PuO_2/Ir COMPATIBILITY TEST ASSEMBLY

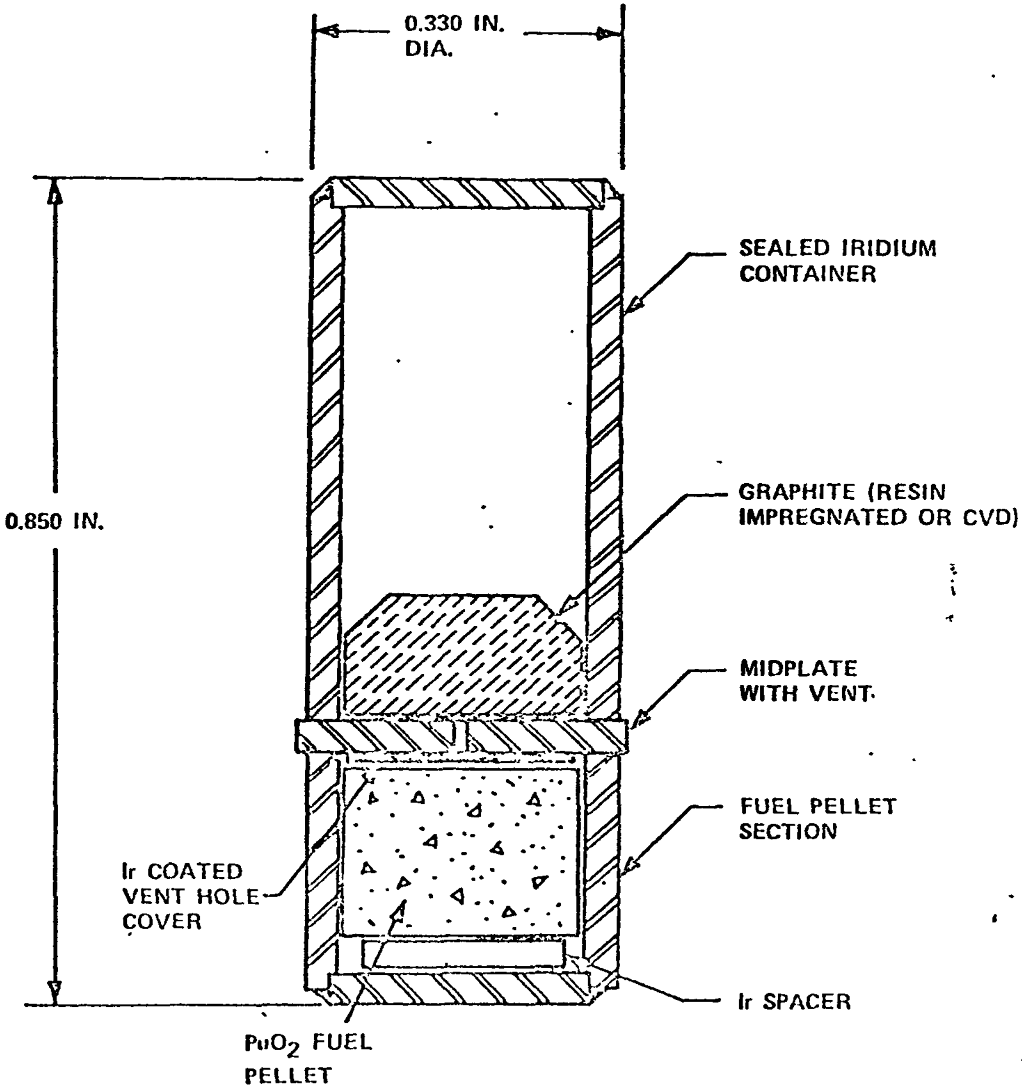

ASSEMBLY – TEST CAPSULE – UNVENTED

Figure 5.4-4

LASL–VENTED TEST CAPSULE

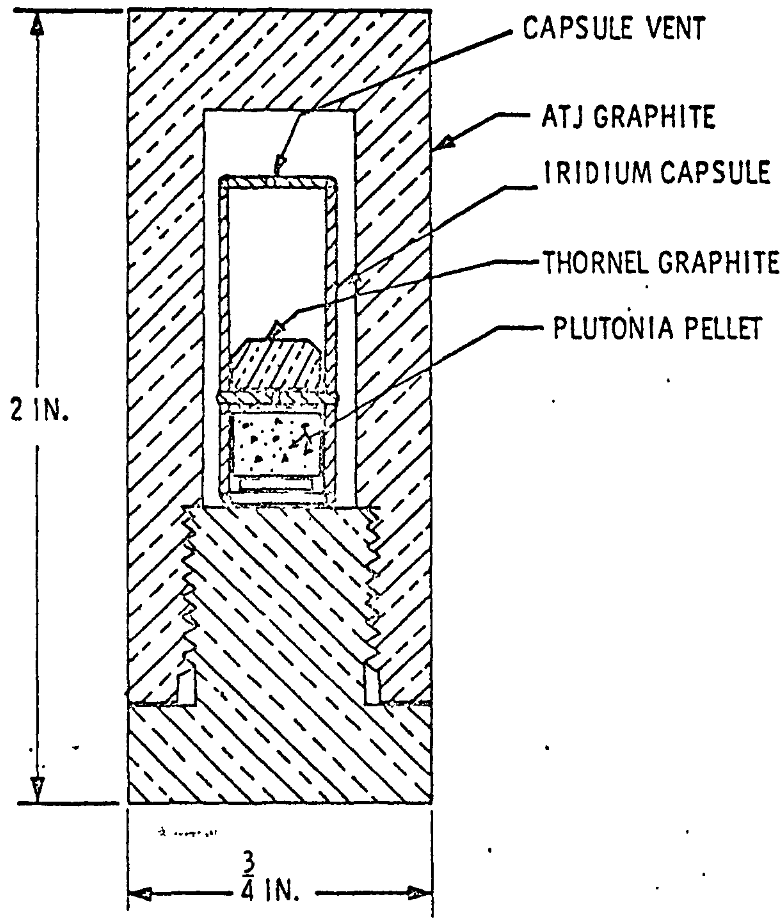

Figure 5.4-5

≅ 3.5 grams of CO, ≅ 2.8 liters. Although this quantity is not inconsistent with some of the observed CO found by sampling the IHSs, the total observed amount from F-4, for example, was over twice this amount. In addition, if the oxygen involved with the CO formation came from the fuel it would be reasonable to expect that, given the same thermal conditions, the same amount of CO would be generated in every case, since the O_2 source is fixed. This assumes that the degassing observed at GE-VF is indeed approaching an effective end point. There has been a wide variation in the amount of CO observed in the IHSs processed to date suggesting that the oxygen is coming from some source other than the fuel. The quantities of CO calculated to be left in the carbon/graphite parts by the initial and the current bakeout schedules, is sufficient to account for the observed totals without invoking the fuel reduction hypothesis.

5.4.4.4.2 Anomalies in the $^{18}O/^{16}O$ Ratio in the CO Samples

5.4.4.4.2.1 Data on Mass 28/Mass 30

In many of the gas samples analyzed at ML/MRC, LASL, GE, and GAS(*) the ratio of mass 28, $^{12}C^{16}O$, to mass 30, $^{12}C^{18}O$, was found to be significantly greater than would be expected if all the oxygen in the CO were present in its normal atmospheric isotopic concentrations. The expected ratio of 28/30 would be around 500. LASL has reported ratios from 2100 to 4300, corresponding to ^{18}O concentrations 4 to 8 times lower than the normal atmosphere. GE and GAS have reported ratios indicating ^{18}O content ranging from 2 to 12 times lower than normal (ratios of 1000 to 6000).

5.4.4.4.2.2 Oxygen-18 Content in the MHW PuO_2 Fuel

The ML/MRC oxide feed granules are subjected to an oxygen isotopic exchange process to reduce the (α, n) reaction between the fuel and 18O. The oxygen used in the exchange contains 0.005 percent of ^{18}O compared to the 0.204 percent found in air (Ref. AV 75a). The product as measured, has the ^{18}O content reduced to about 0.006 percent. Thus, the ^{18}O content in the fuel is reduced below the natural abundance by a factor of ≅ 33.

(*) Gollob Analytical Services: an independent laboratory used by GE for gas analyses.

5.4.4.4.2.3 Oxygen-18 Content in the CO from the IHSs

If all the CO observed in the mass analysis of gases from the IHSs were from the fuel via reactions (1) through (5), (see paragraph 5.4.4.4.1.1), the mass 28/30 ratio would be $\cong$ 16,600, reflecting the $\cong$ 30-fold reduction in ^{18}O in the fuel. The data given in paragraph 5.4.4.4.2.1 indicate that the fuel cannot be the sole source of oxygen in the CO analyzed. Conversely, since the ratios observed show an ^{18}O content less than atmospheric normal, some of the oxygen in the analyzed CO must have come from the fuel.

5.4.4.4.2.4 Back-Exchange of ^{18}O

PuO_2 enriched in ^{16}O (depleted in ^{17}O and ^{18}O) will more or less quickly, depending on available fuel surface area and temperature, revert to the natural O_2 isotopic concentrations (Ref. Mu 73a). LASL (Ref. Pe 74a) has calculated a time of $\cong$ 110 hours, 5 days, for a back-exchange reaction between a limited amount of CO generated from atmospheric air to exchange its ^{18}O with ^{16}O from the fuel at the SPC storage temperatures, to produce a $\sim$6-fold reduction in the ^{18}O concentration.

5.4.4.4.3 Evaluation of the CO Generation Hypotheses

5.4.4.4.3.1 Fuel Reduction

Given the current limitations on analytical techniques for determining the O/Pu ratio in the MHW PuO_2 fuel and the marginal character of the thermodynamics, it is not possible to show that the CO has or has not been produced by loss of oxygen from the fuel and reduction of the O/Pu ratio. The amount of ^{18}O found in the CO precludes the possibility that all of the CO has been generated from the fuel, but does not permit the conclusion that no interaction has occurred between CO generated from some other source and the oxygen of the fuel. The only hard data on fuel reduction from the LASL tests and from the ML/MRC examination of PPS-39 out of the Q-1/IHS, show the O/Pu ratio of the fuel to be: 2.00 ± 0.02.

5.4.4.4.3.2 CO Retained in the Carbon/Graphite Components

The data given elsewhere (see Para. 5.1.6) show that:

- parts baked out and subsequently exposed in air, will resorb significant amounts of gas/moisture, up to 50 percent of that which was removed, in $\leq$ 30 minutes;

- the initial bakeout schedule at 1200°C for 5 hours for the POCO aeroshell, and 1 hour for all the other materials, used for F-1, F-2 and F-3 IHSs was not effective.

- the current bakeout schedule at 1500°C for POCO (36 hours) and Pyrocarb (24 hours) and at 1350°C for the T-50 composite-GIS (24 hours) is also ineffective; the calculated amounts of CO remaining after bakeout for the whole IHS are: 3 grams in the POCO, 3 grams in the Pyrocarb, and 12 grams in the T-50 composite.

On the basis of these data, it is unnecessary to postulate any source of CO other than inadequately baked-out parts.

5.4.4.4.3.3 Oxygen-18 Anomaly

The concentrations of ^{18}O found in the CO by various analyses show that some of the oxygen must have come from the fuel. A cyclic reaction starting with some CO deriving initially from poorly degassed carbon which could initiate the reactions (4) and (5) shown in Paragraph 5.4.4.4.1.1, cannot be precluded but as noted in 5.4.4.4.1.5, analytical data available provide no support for this hypothesis. The hypothesis of back-exchange of CO produced from normal oxygen concentrations with the ^{18}O depleted oxygen of the fuel, explains the observed data, but is not necessarily correct.

5.4.4.4.4 Conclusion

A reasonable conclusion from the available data and calculations is that the CO, observed in the IHS gas samples thus far analyzed, came from inadequately baked-out carbon/graphite parts and that oxygen from the CO thus produced back-exchanged with the ^{18}O depleted fuel.

5.4.4.4.5 References

Al 75a Alexander, C. A., (BMI): Private Communication, June 1975 (Reduction of Fuel $PuO_2 \leq 0.005$)

Av 75a Avona, V. (ML/MRC): Private Communication, July 1975 (^{16}O Content of ^{16}O used for fuel exchange at ML/MRC)

Ke 73a Kent, R. A.: "Thermodynamic Analysis of MHW Space Electric Power Generator". LASL Informal Report: LA-5202-MS; Los Alamos Scientific Laboratory, Los Alamos, New Mexico, March 1973.

Ke 75a Kent, R. A.: "LASL Fuels Development Program" presented at Technology Information Exchange, Isotope Technology Branch, SNS/ERDA, Germantown, MD, 14 May 1975.

Ko 74a Kokenge, B. R. (ML/MRC): Private Communication June 1974 (^{18}O Content in ML/MRC ^{16}O Exchanged PuO_2)

Mu 73a Mullins, L. H. (LASL): Private Communication June 1973 (Back Exchange of Oxygen from Air with ^{16}O Enriched $^{238}PuO_2$- Medical Grade)

Pa 62a Paprocki, S. J., Keller, D. L., Alexander, C. A., and Pardue, W. M.: "The Volatility of PuO_2 in Nonreducing Atmospheres", USAEC Report BMI-1591, Battelle Memorial Institute, Columbus, Ohio, 16 August 1962.

Pe 74a Petersen, D. E.: "Theoretical Examination of Isotopic Exchange Between CO (30) and Fuel Oxygen (16) via the Frit/Vent Orifice" LASL CMB-5-C-575, Los Alamos Scientific Laboratory, Los Alamos, New Mexico, 3 September 1974.

Pi 75a Pigeon, J.: "LES 8 & 9 Heat Source Temperatures During SPC Storage and LAS Processing"; PIR-MHW-5530, General Electric Co., Space Division, Philadelphia, Pa., 22 July 1975.

Wa 71a Waterbury, G. R., Dahlby, J. W., and Metz, C. F.: "The Measurement of Oxygen to Heavy Metal Ratio in Unirradiated Mixed Oxide Fuels"; IAEA/SM-149/33 Presented at the Symposium on Analytical Methods in the Nuclear Fuel Cycle, Vienna, 29 November - 3 December 1971.

6.0 CONVERTER

6.1 MODULE ANALYSIS

6.1.1 18-Couple Module Testing

6.1.1.1 Resistance from Module to Foil

Table 6.1.1-1 summarizes the nominal operating temperatures and times of the Si_3N_4-coated couples in Modules 18Φ and SN-1 through SN-6. Module 18Φ was the first module to incorporate the Si_3N_4 coating on the hot shoes and legs.

Figure 6.1.1-1 shows the performance of the 1135°C modules. It is seen from a comparison of 18Φ with 18K (which does not contain Si_3N_4 couples) that the coating increases the time to reach a given resistance level by a factor of from 15 to 20.

Module SN-1 was showing performance similar to 18Φ up to 5,000 hours, whereas from 5,000 to 9,600 hours the resistance has remained relatively constant at ~2,000 ohms. It is postulated that the plateauing of the resistance may be due to the resistance afforded by the 12,000 Å Si_3N_4 coating. That a similar plateau was not observed in Module 18Φ may be attributed to a less uniform thickness of the coating in 18Φ, particularly in the region between the N & P legs which is most difficult to coat uniformly.

Figure 6.1.1-2 shows the performance of SN-1, -2 and -3, along with 18D, uncoated and operating at 1035°C. A comparison of 18D and SN-3 shows that after ~ 1 year of testing, the resistance of the Si_3N_4-coated module is a factor of 50 greater than the uncoated module.

Module SN-2 operating at 1085°C shows a rather abrupt drop in resistance at ~6,000 hours. However, the last few data points show a slope similar to SN-1. The reason for the abrupt drop is not known at the present time.

The results to date of the Si_3N_4-coated modules indicate that there will not be a significant power loss due to shorting to foils. Based on the $Si + SiO_2 \longrightarrow 2\ SiO$ model, 5 years at a constant temperature of 1035°C is equivalent to 2,700 hours at 1135°C. From 18Φ and SN-1, the resistance is 7,000 to 10,000 ohms, which is equivalent to over 400 ohms in a full scale converter.

TABLE 6.1.1-1

18-Couple Module Performance

MODULE	TIME, HOURS AS OF 8-31-75	RESISTANCE TO FOIL	NOMINAL TEMPERATURE, °C
18 Ø	12,000	220	1135
SN-1	9,600	2,000	1135
SN-2	6,000	42,000	1085
SN-3	6,900	100,000	1035
SN-4	-----	---------	1135
SN-5	78	19,800	1085
SN-6	333	18,100	1035

FIGURE 6.1.1-1

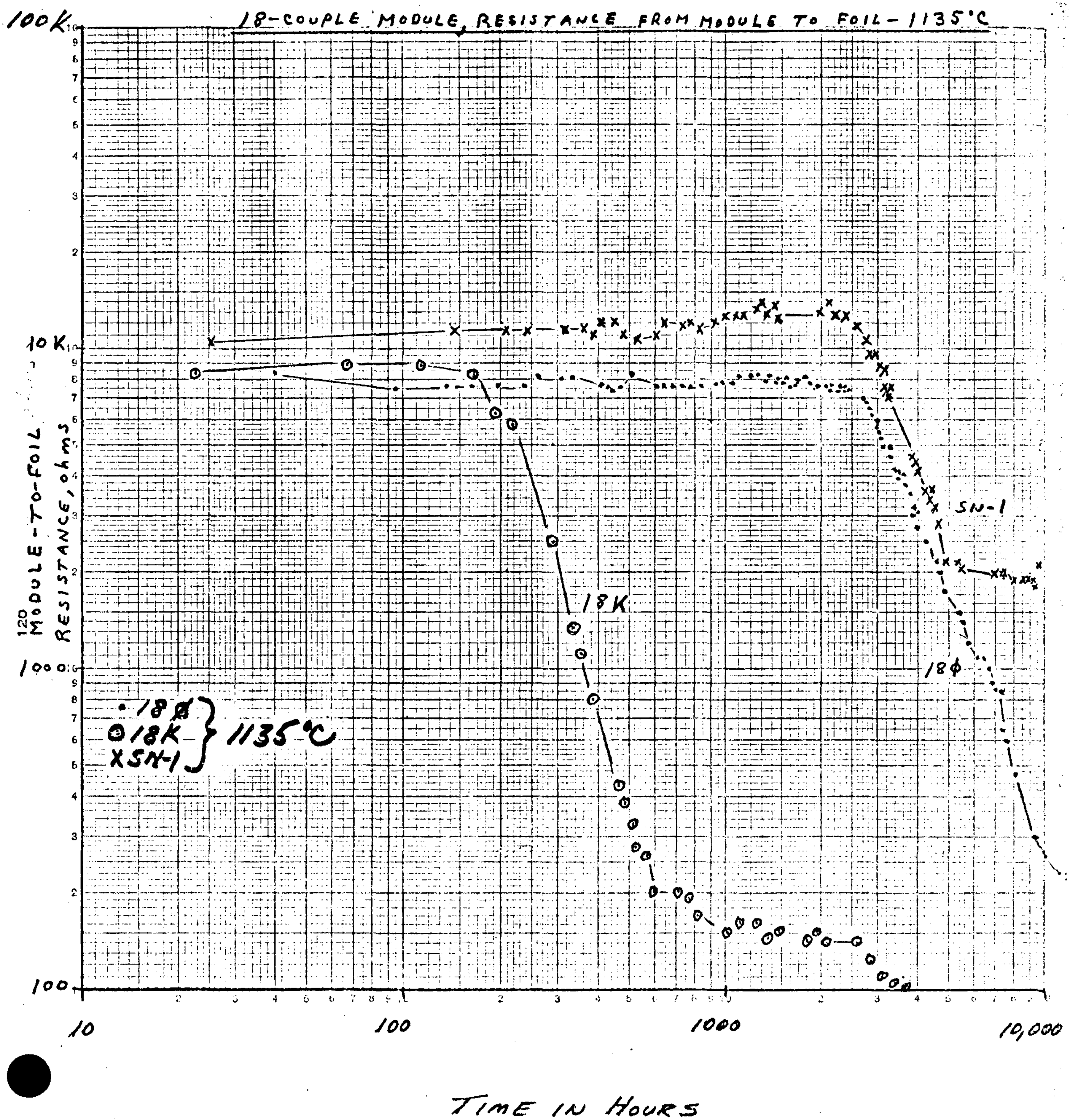

18-COUPLE MODULE, RESISTANCE FROM MODULE TO FOIL - 1135°C
100K
10K
1000
100
MODULE-TO-FOIL RESISTANCE, ohms
10
100
1000
10,000
TIME IN HOURS
18K
SN-1
18Ø
• 18Ø
ʘ 18K
X SN-1
1135°C

FIGURE 6.1.1-2

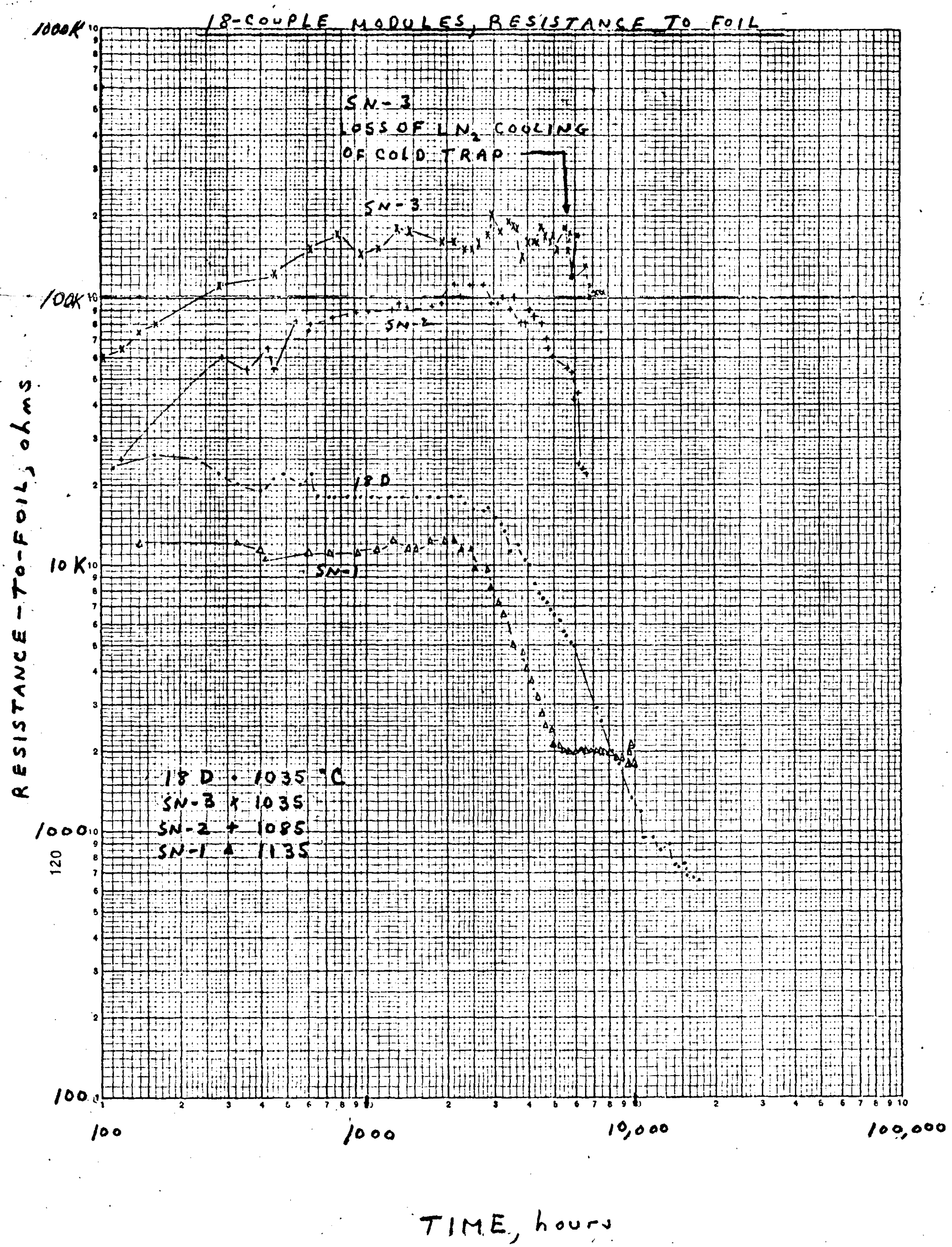

18-COUPLE MODULES, RESISTANCE TO FOIL
SN-3
LOSS OF LN_2 COOLING
OF COLD TRAP
SN-3
SN-2
18 D
SN-1
18 D • 1035 °C
SN-3 x 1035
SN-2 + 1085
SN-1 ▲ 1135
1000K
100K
10 K
1000
100
100
1000
10,000
100,000
RESISTANCE-TO-FOIL, ohms
TIME, hours

6.1.1.2 T/E Performance 1135°C Modules

Figure 6.1.1-3 shows the ratio of the power, open circuit voltage and internal resistance to the theoretical values as predicted by the N & P dopant precipitation model developed by RAAG of Syncal. Multipliers of 1.075 and .969 are applied to the basic resistivity and Seebeck coefficient as reported by RAAG. These factors were determined from the 1,500-hour data of the TBC-4 converter. The most significant point to be made concerns the slopes of the data rather than the absolute values. Comparison of the 18K uncoated couples with SN-1 shows that the Si_3N_4 coating results in a slower rate of increase in internal resistance. This indicates that the coating is also improving the T/E performance by suppressing the loss of leg dopants as well as suppressing Si and Ge loss near the hot junction which normally results in a geometric necking down and a subsequent increase in internal resistance. Consequently, it is to be expected that the coating will not only provide suppression of shorts to foils but also will provide improved T/E performance. This is clearly indicated by the relative slopes of the 18K and and SN-1 data. 18ϕ total module data is not comparable since it contains three types of hot shoe designs. Individual performance of the three designs will be reported later.

FIGURE 6.1.1-3

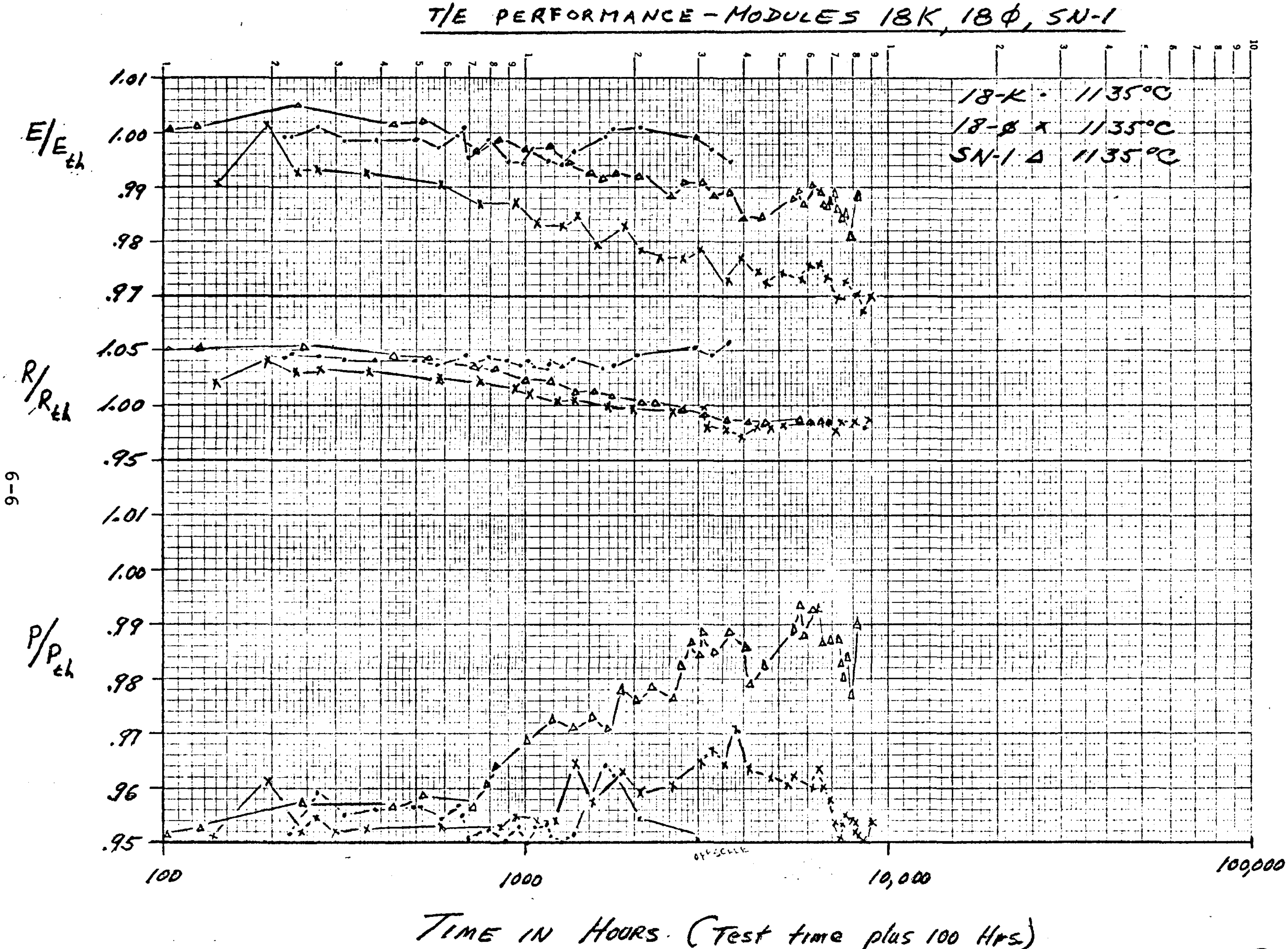
T/E PERFORMANCE - MODULES 18K, 18Φ, SN-1
18-K • 1135°C
18-Φ x 1135°C
SN-1 Δ 1135°C
E/E_th
R/R_th
P/P_th
1.01
1.00
.99
.98
.97
1.05
1.00
.95
1.01
1.00
.99
.98
.97
.96
.95
100
1000
10,000
100,000
TIME IN HOURS (Test time plus 100 Hrs)

6.2 MATERIAL ANALYSES

6.2.1 Determination of "C" Seal Hardness Vs. Heat Treatment

During the reporting period, determination was made of the Knoop hardness of the silver coating and Inconel-X substrate of a P1 C seal in response to heat treatment. The results are shown in Table 6.2.1-1.

The hardness of the silver drops to half its initial hardness after only a few hours exposure to storage temperature; doubling the heat treat temperature, to 1000°F, further reduces the hardness of the silver. These data indicate that the silver on "C" seals will continue to soften with time at 500°F.

The Inconel-X used in P1 "C" seals is not aged upon receipt (probably in the solution annealed, cold worked condition). A 500°F exposure does not change the as-received hardness but exposure to 1000°F does age harden the material significantly.

These data indicate that the present plan of using un-heat-treated P1 "C" seals should be continued but that a change should be made to the existing specification. That is, a specimen should not be heat treated to 1000°F prior to the measurement for hardness of the silver coating. The hardness of the as-plated "C" seal is of interest since this is the hardness of the material at the time of assembly. The acceptable hardness limit should be raised to 100 max. (average), KNOOP from the current 75 max. It has been demonstrated that a seal can be made with coating as hard as 100 max. and that sealing will improve as temperature rises to storage and operation conditions.

6.2.2 Evaluation of a Fatigue Test of the Mounting Bracket Attachment

The structural integrity of the interface between the titanium mounting brackets and the beryllium outer shell was substantiated by a low-cycle fatigue component test conducted at room temperature.

6.2.2.1 Test Specimens

1) Per Drawing No. 47C301426G1

2) Per Drawing No. 47C301426G2

The test configuration with the test specimen is shown in Figure 6.2.2-1.

TABLE 6.2.1-1

P1 "C" Seal - Ag Coating & Inconel Hardness

Vs. Heat Treatment

Heat Treatment	Avg. KHN Hardness (Knoop)	
	Ag Coating	Inconel
None (1)	92.3 81.8	330 365
500°F (2) 4-Hr.	48.5 41.0 47.5	377 362 358
1000°F (3) 1/2 Hr.	34.8 33.6 35.0	478 484 473

Notes:

(1) Hardness of the material in the as-received condition.

(2) After the "C" Seals are assembled on the converter, they reach 465°F in the RTG (storage), 356°F at launch, and 518°F in vacuum.

(3) The present specification requires a 1/2 hr. treatment of one specimen prior to hardness determination; flight seals are not heat treated.

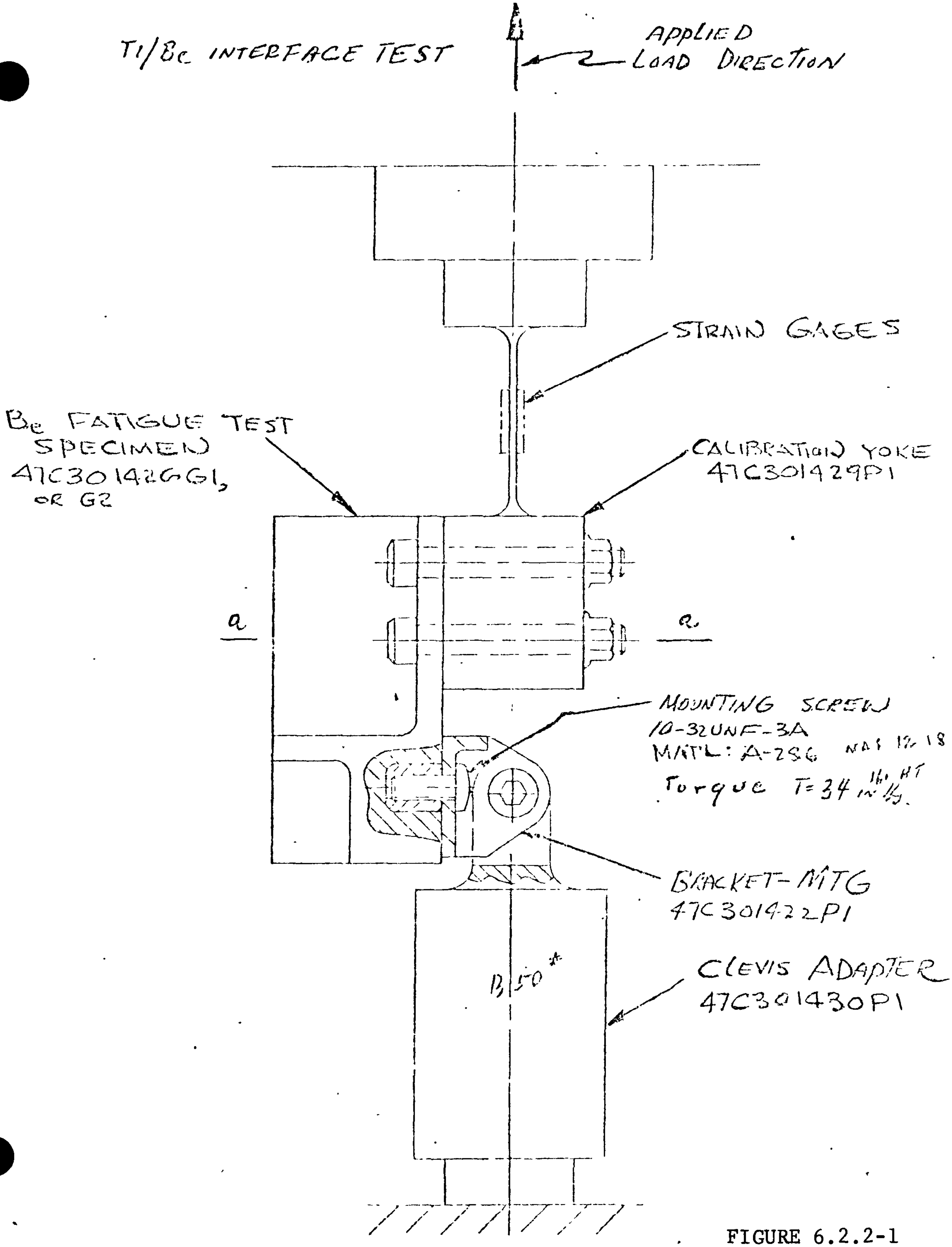
Ti/Be INTERFACE TEST
APPLIED LOAD DIRECTION
STRAIN GAGES
Be FATIGUE TEST SPECIMEN 47C301426G1, or G2
CALIBRATION YOKE 47C301429P1
a
a
MOUNTING SCREW 10-32UNF-3A MATL: A-286 NAS 1218
Torque T=34 in lb.
BRACKET-MTG 47C301422P1
CLEVIS ADAPTER 47C301430P1

FIGURE 6.2.2-1

6.2.2.2 Load Condition

The maximum design load for one mounting bracket is 600 lbs.

6.2.2.3 Test Results

Each of the two configurations was subjected to the loads as shown in Table 6.2.2-1. A static tension load was applied and the load alternated from a maximum tension load to the static preload.

A maximum of P = 1350 lbs. was obtained giving a margin of MS = 1.25 against the design load.

The total number of cycles for each configuration was 21,000 cycles. (See Table 6.2.2-1). No failure occurred and no permanent deformation could be determined. Configuration G-1 was selected for the final design. The maximum stress level through the bolt holes of the beryllium component was f = 10430 psi in section a - a of Figure 6.2.2-1. This represents a margin against the yield allowable of MS = 1.39.

6.3 CONVERTER SYSTEMS AND DESIGN

6.3.1 Particulate Matter Generated by Penetration of the PRD Rupture Diaphragm

6.3.1.1 Introduction

Testing was performed to determine the size and quantity of particulate matter generated by a lance penetrating a PRD rupture disk. The testing is conservative and includes many worst case conditions as follows:

a) The lance utilized was Engineering test hardware that has been used many times. The point and edges are ragged and dull compared to prime unused hardware.

b) The lance was hand-held during puncher tests. This results in unequal and uneven loads being applied to the disk at the lance edges. This probably resulted in a more ragged cutting action by the lance.

TABLE 6.2.2-1

Test	Specimen	Static Load lbs	Alternate Load lbs	Max Load lbs	Min Load lbs	Total Cycles
1 - 3	G 1	280	360	640	280	9000
7	↑	480	280	760	400	3000
9	|	540	300	840	540	3000
13	↓	800	320	1120	800	3000
15	G 1	1040	300	1340	1040	3000
				G 1 -- TOTAL CYCLES:		21000
4 - 5	G 2	360	280	640	360	9000
8	↑	400	340	740	400	3000
10	|	520	300	820	520	3000
14	↓	820	300	1120	820	3000
16	G 2	1050	350	1350	1050	3000
				G 2 -- TOTAL CYCLES:		21000

c) The cleanliness was difficult to maintain during testing. Some of the particulate appeared to be foreign to the hardware (i.e. dull dark grains).

6.3.1.2 Test Procedure

The test procedure was kept as simple as possible to avoid possible contamination. The holding fixtures were made of plastic to aid in identifying contamination from them. This eliminated 4 or 5 particles from consideration. The testing was done as follows:

- Parts and assemblies were ultrasonic cleaned for 15 min. in deionized water (DW).
- The disk was penetrated over a beaker filled with DW. The disk, holder, and lance were immediately placed in the beaker and covered with clean filter paper.
- Parts were ultrasonic cleaned for 15 min.
- The D.W. was filtered through filter paper, parts were rinsed with D.W. and rinse D.W. was filtered.
- Parts and filter paper were examined at 30 X for particulate.

6.3.1.3 Results

The results are presented in the following two tables. Table 6.3.1-1 presents them for the individual disk in order of size and Table 6.3.1-2 presents them by combining the three test results in order of size.

TABLE 6.3.1-1

INDIVIDUAL RESULTS OF TESTS

TEST NO.	QTY	SIZE MILS	APPEARANCE OR SHAPE
1	1	7 x 1	Metallic Sliver
1	1	5 x 4	Metallic
1	1	4 x 2	Met.
1	7	4 x 1	Met.
1	2	3 x 2	Met.
1	7	2 x 1	Met.
1 Tot.	19		
2	1	5 x 2	Met., Shiny
2	1	5 x 1	Met., Shiny
2	1	2.5 x 2.5	Met., Shiny
2	2	2 x 2	Met., Shiny
2	3	2 x 2	Dull, Black Grain
2	2	2 x 1	Met., Shiny
2	4	<2	Varied
2 Tot.	14		
3	1	10 x 1.5	Met., Shiny
3	1	5 x 5	Met., Dull
3	1	3 x 2	Met., Dull
3	1	1 x 1	Met., Shiny
3	4	<3	Dull, Dark Grain
3 Tot.	8		

TABLE 6.3.1-2

COMBINED RESULTS OF THREE TESTS

Largest Particle Observed

	10 x 1.5 mil	Bright Metallic Sliver

Particles between 5 and 10 Mils, Total 5

	7 x 1 Mil	Bright Metallic Sliver
	5 x 5 Mil	Dull Metallic
	5 x 4 Mil	Bright Metallic
	5 x 2 Mil	Bright Metallic
	5 x 1 Mil	Bright Metallic

Particles between 2.5 and 5 Mils, Total 6

	4 x 2 Mil	Metallic
7,	4 x 1 Mil	Metallic
2,	3 x 2 Mil	Metallic
	3 x 2 Mil	Dull Black Grain
	2.5 x 2.5 Mil	Bright Metallic
4,	$<$3 Mil	Dull Black Grains

Particles Less than 2.5 Mils in any Dimension, Total 19

9,	2 x 1 Mil	Metallic
2,	2 x 2 Mil	Bright Metallic
3,	2 x 2 Mil	Dull Black Grains
5,	Less than 2 Mil	

6.3.2 Evaluation of Effects of Reduced Launch Temperature on LES 8 and 9 RTG Structure

6.3.2.1 Introduction

The design of the MHW RTG was based on an average outer case temperature of 350°F during launch. The corresponding temperature in the regions of the stacking adapters and uniball mounts is approximately 280°F. The results of TRW system thermal analyses performed prior to the air conditioning tests predicted similar temperatures for the RTGs at liftoff (380°F average case temperature) and suitable cooling of other payload components with an air flow rate of 225 pounds per minute.

The results of a preliminary parametric air conditioning test performed by Martin-Marietta in April, 1974 indicated that the air conditioning system could be more effective than anticipated and could result in lower temperatures of the RTGs for an air flow of 225 pounds per minute. However, since this test did not include a shroud simulation or a "full-up" spacecraft simulation, the results were not considered representative.

A "full-up" air conditioning test, including a shroud and an essentially complete spacecraft simulation, was subsequently performed at TRW for several flow rates. The results, received by GE in March, 1975, were parametric in nature, but indicated a significant potential reduction in RTG case temperatures. Based on the results of this test, Lincoln Laboratories selected an air flow rate of 225 pounds per minute to meet on-pad cooling requirements, resulting in the following predicted temperatures for the LES 8 RTGs at liftoff:

Average Case Temperature	$\approx$ 125°F
Stacking Adapter Region	$\approx$ 90°F
Uniball Mount	$\approx$ 97°F

This reduction in RTG temperatures required a reassessment of the structural capability of the RTGs with emphasis on the following areas of concern:

- The ductility of the beryllium outer case and stacking adapters decreases with decreasing temperature, raising the question of sensitivity to any flaws or cracks which might be present.

- The thermopile assembly has been designed and tested at an average case temperature of 350°F at launch. The reduced temperature will change clearances and affect material properties and residual stresses in the unicouples.

- All ETG and RTG development, acceptance and qualification structural tests have been performed at an average case temperature of approximately 350°F.

6.3.2.2 Conclusions and Recommendations

- Some additional risk exists due to the limited test data on the low temperature capability of the thermopile. However, since it is believed that a large share of the thermopile load is supported by the heat source support system, and component tests of unicouples indicate considerable strength at room temperature, this risk is believed to be low.

- The ductility and fracture toughness of beryllium is lower at the reduced temperatures, making it more susceptible to flaws and cracks. However, based on fracture mechanic analyses, the yield strength remains limiting and the theoretical margins of safety increase slightly at the reduced temperature. Therefore, with suitable inspection for damage prior to assembly on the spacecraft, the structural capability of the beryllium case and stacking adapters will be adequate at the reduced temperatures.

- No additional structural tests are recommended.

- The present on-pad air conditioning plans should be continued. However, the RTG temperatures should be maintained as high as mission constraints will allow (avg. case temperature $\leq$ 350°F) to more nearly approach the dynamic test conditions and minimize risks.

6.3.2.3 Evaluation

To evaluate the significance of the reduced temperatures as related to the structural capability of the RTGs, all previous component and system level RTG structural tests were reviewed. In addition, the material property data for beryllium were supplemented with the results of additional tests and fracture toughness data published by others. Fracture mechanics analyses were performed to evaluate the effects of flaws at the reduced temperature. Finally, potential verification tests were investigated.

6.3.2.3.1 Review of Previous Tests

All ETG and RTG structural tests have been performed with an average case temperature of approximately 350°F and mounting point (uniball or stacking adapter) temperatures of 250°F to 280°F. A summary of these tests is given in Table 6.3.2-1.

TABLE 6.3.2-1

ETG and RTG STRUCTURAL TESTS

UNIT	TYPE*	TYPE OF TEST	
TBC #3	ETG	Acoustic Acceleration Vibration Shock	LES 8/9 Qualification (Acoustic, Acceleration)
Q - 1	RTG	Vibration Shock	LES 8/9 Qualification
Q - 1A	ETG	Static Load Vibration	LES 8/9 Qualification (Static Load)
F-4; F-5	RTG	Vibration	

*ETG --- Electrically Heated Thermoelectric Generator

RTG --- Radioisotope Thermoelectric Generator

TBC #3 was essentially a flight-type generator except for the simulation of the nuclear heat source by a mass-simulated electrical heat source. The unit was subjected to qualification level structural tests at 350°F average while mounted on the three uniballs. The acoustic and acceleration tests provided the basis for qualification of the design.

Q-1 was the flight-type qualification unit for the LES 8 and 9 Mission and included a nuclear heat source. The unit was subjected to the shock and vibration qualification tests at 350°F average case temperature while mounted on the three uniballs.

Q-1A was a flight-type generator except for minor changes in the thermopile and the use of an electric heat source in place of a nuclear heat source.

The static load test assembly consisted of Q-1A mounted on a LES 9 truss and a loading fixture joined to the top of Q-1A using three flight-type stacking adapters. The loading fixture was designed to provide flexibility at the stacking adapter interface similar to an RTG. A strap heater attached to the loading fixture maintained the stacking adapters at approximately 250°F, while the average case temperature of Q-1A was maintained at approximately 350°F. The assembly was subjected to increasing increments of simultaneously applied longitudinal and lateral loads until 125% of the 8g longitudinal and 5g lateral design loads were reached.

The Q-1A vibration test was performed at the MJS mission qualification levels at an average case temperature of approximately 350°F with the unit mounted in the uniballs.

F-4 and F-5 are flight units. These units were subjected to acceptance vibration tests while mounted in the uniballs and at an average case temperature of 350°F.

All of the above tests were completed without the occurrence of any structural failure.

Although no ETG or RTG structural tests have been performed at low temperatures, several component level tests performed at room temperature provide an indication of the structural capability of the RTGs at the reduced launch temperature. A summary of these tests is shown in Table 6.3.2-2.

TABLE 6.3.2-2

ROOM TEMPERATURE COMPONENT TESTS

ITEM	TYPE OF TEST	LEVEL
Heat Source Support Fitting Attachment to Be Case.	Alternating & Static Load	225% of Design Load
Uniball Mount	Alternating	230% of Design Load
Stacking Adapter	Vibration	S/C System Qualification
Thermopile	Vibration Shock	$\approx$200% Qual Vibration Level 100% Qual Shock Level
Unicouple	Static Load	See Text

The heat source loads are transmitted to the beryllium case through fittings which are attached to the case by Number 10 screws which mate with helicoils inserted into the case. A combined static plus alternating load test was performed at room temperature on this attachment area with progressively increasing loads up to 225% of design load. No failure occurred.

The uniball/mount test was performed using a flight-type uniball and a representative beryllium section of the lower case mount area. Progressively increasing alternating loads were applied to the assembly at room temperature until 230% of design load and an accumulation of 39,000 cycles were reached. No failure occurred.

Room temperature testing of the stacking adapters was limited to vibration tests performed by Lincoln Laboratory. Three flight-type beryllium stacking adapters were used to join two dynamically-simulated RTGs in the LES 9 system level vibration qualification test at TRW. The spacecraft assembly was subjected to qualification level testing along three axes at room temperature. No failures of the stacking adapters occurred. Numerous engineering vibration tests have since been performed by Lincoln Laboratory using the same stacking adapters at room temperature without experiencing failure of the adapters. Since the calculated margins of safety for the stacking adapters and the mating regions of the case are nearly equal, this can be considered as equal evidence of the structural capability of the case in this region.

No structural tests have been performed at reduced temperatures for a complete thermopile assembly. However, a significant amount of vibration testing has been performed at room temperature using small modules consisting of several unicouples supporting a representative weight of foil insulation. The results indicate that the unicouples have significant strength at room temperature. Figure 6.3.2-1 shows the results of a vibration test performed at room temperature using two flight-type unicouples supporting a representative weight of foil insulation. The assembly was initially subjected to qualification shock testing along each of three axes and qualification level vibration for three minutes along each of three axes. The duration and amplitude of the qualification level testing for the longitudinal axis is shown in the shaded block of Figure 6.3.2-1. The unit was then subjected to increasing increments of vibration amplitude until a failure occurred at approximately 200% of the qualification level. The accumulated test time along this axis at the time of failure was 17 minutes.

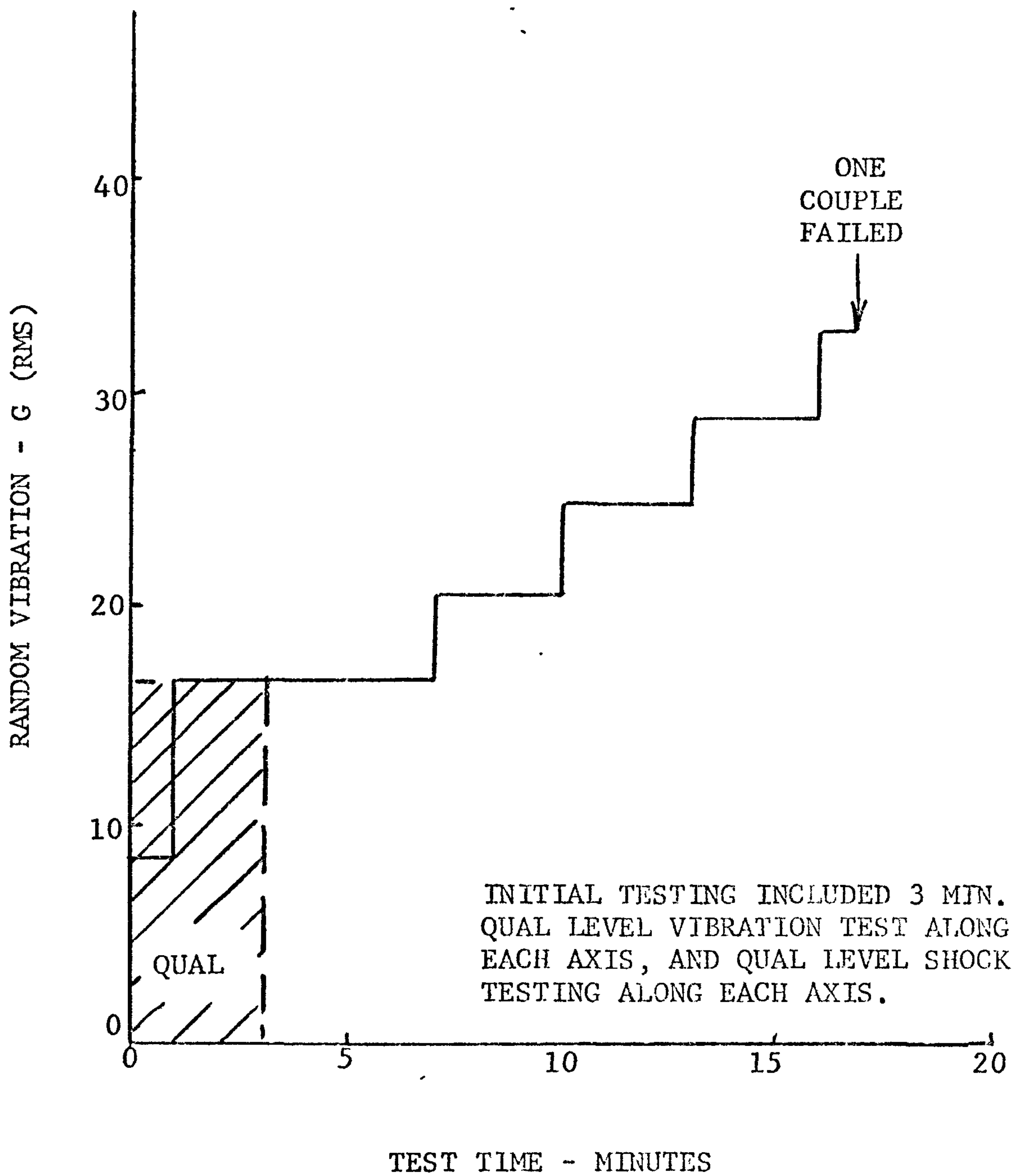

FIGURE 6.3.2-1

UNICOUPLE DEVELOPMENT TEST

A static load test of individual unicouples was performed at room temperature and at operating temperature. The unicouples were loaded as cantilevers in the longitudinal direction of the RTGs as shown in Figure 6.3.2-2. The results show that the unicouple static load capability is generally higher at elevated temperatures than at room temperature.

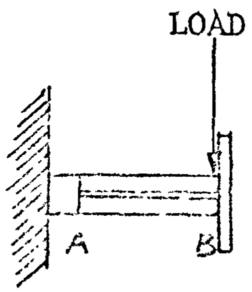

Temperature °F		Failure Loads Pounds
A	B	
70	70	15-18
390	1600	18-20

UNICOUPLE STATIC LOAD TEST

FIGURE 6.3.2-2

The dynamic loads of the thermopile are shared between the unicouples and the heat source support system. The actual load carried by each unicouple can not be determined analytically due to the redundancy and non-linearities in the assembly. However, due to the high flexibility of the heat shunts at the base of the unicouples, it is believed that a large portion of the load in the longitudinal direction is carried by the heat source support system.

6.3.2.3.2 Analyses

6.3.2.3.2.1 Material Properties Data

Material properties for beryllium HP-10 are shown in Figure 6.3.2-3. The specification values for ultimate and yield tensile strength increase with decreasing temperature. The tensile tests results for all accepted billets exceed these requirements. The curve of the 1σ yield strength was based on the results of tensile tests for 11 billets used for the LES 8/9 Mission. The margins of safety were based on this 1σ curve. As shown, the ductility of the material exhibits a decrease with decreasing temperature. In the low temperature region, the elongation in the longitudinal direction is approximately one-half the elongation in the transverse direction. The scatter in test data is shown by the bars on the curve of longitudinal elongation.

6.3.2.3.2.2 Stress Analysis of the Beryllium Case

The locations of the minimum margins of safety for the beryllium structure are in the stacking adapters and in the mating regions at the top of the case where the calculated margins of safety for the stacking adapters and case structure are nearly equal. Table 6.3.2-3 summarizes some of the significant parameters associated with the RTG and the stacking adapters. The margins of safety shown are based on the design load factors, 5g lateral and 8g longitudinal simultaneously applied. The critical locations for this region are shown in Figure 6.3.2-4. The locations of the significant stresses in the lower part of the case are also shown in Figure 6.3.2-4 and the corresponding margins of safety are included in Table 6.3.2-3.

Fortunately, the minimum margins of safety are associated with stress primarily in the transverse directions which exhibit greater ductility than the longitudinal direction. Note that the tensile strength increases slightly with decreased temperature, resulting in an apparent increase in load capability. However, the ductility decrease with decreased temperature reduces the fracture toughness and makes the structure more susceptible to failures due to flaw and stress concentrations.

Table 6.3.2-4 shows a correlation of the predicted temperatures of the stacking adapters with the significant launch events and associated critical stress levels. The design temperature and associated stress level for 5g lateral and 8g longitudinal are shown for comparison.

FIGURE 6.3.2-3

MATERIAL PROPERTIES

BERYLLIUM BLOCK HP-10

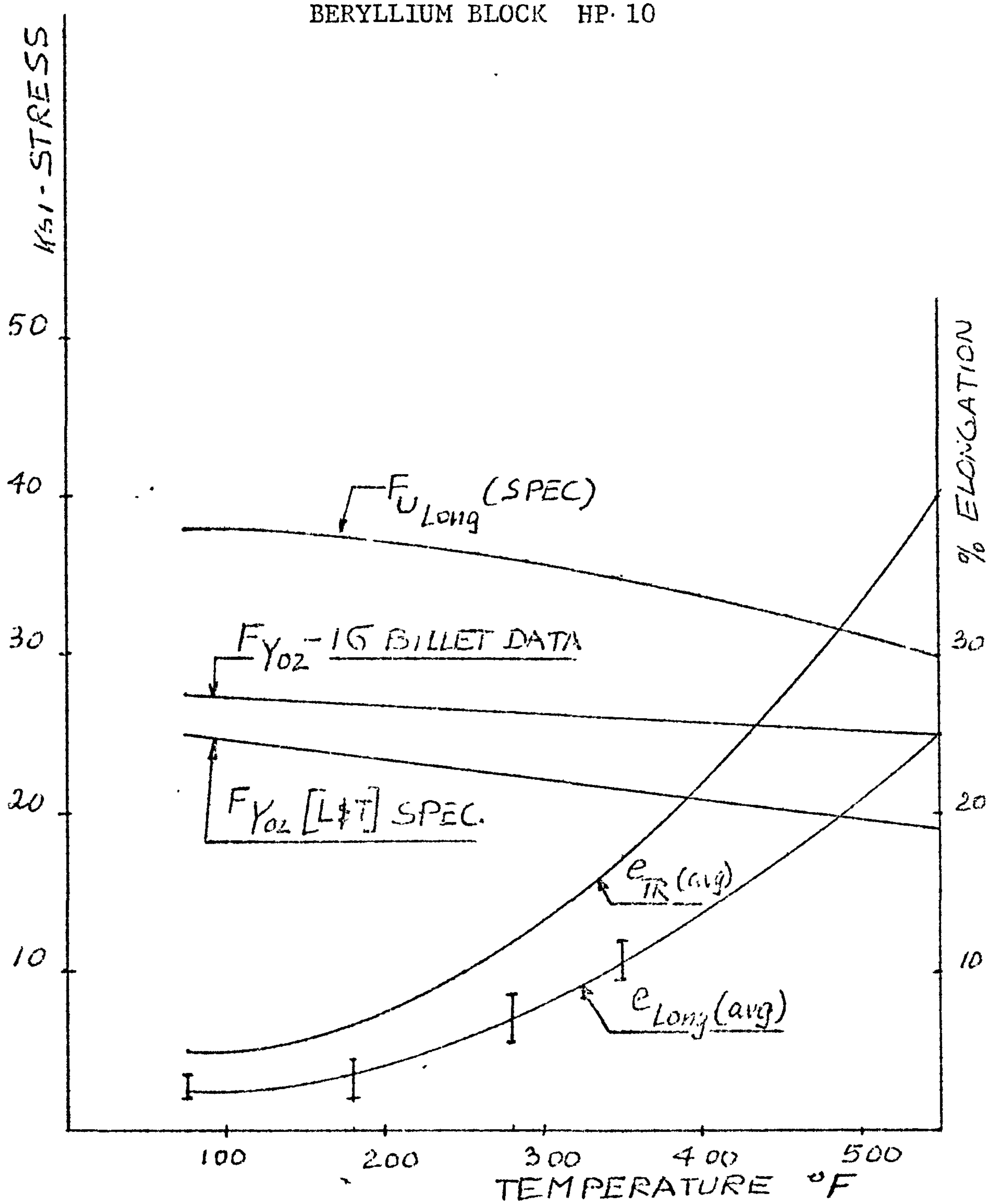

TABLE 6.3.2-3

STRUCTURAL MARGINS IN CRITICAL AREAS OF BERYLLIUM CASE

LOCATION	DIRECTION	DESIGN TEMPERATURE TEMP. °F	DUCTILITY %	M. S.	LOW TEMPERATURE TEMP. °F	DUCTILITY %	M. S.
1. Stacking Adapter	Transverse	280	12%	.62	90	5.0%	.70
2. Stacking Adapter	Longitudinal	↓	2.8%	2.89	↓	2.2%	2.11
3. Top of Case	Transverse	↓	12%	.83	↓	5.0%	.95
4. Top of Case	Longitudinal	↓	2.8%	2.2	↓	2.2%	2.44
5. Bottom of Case	Longitudinal	↓	2.8%	2.71	↓	2.2%	2.48
6. Bottom	Longitudinal	↓	2.8%	1.26	↓	2.2%	1.42

- Transverse ductility based on design material properties.
- Longitudinal ductility based on minimum test specimen results.

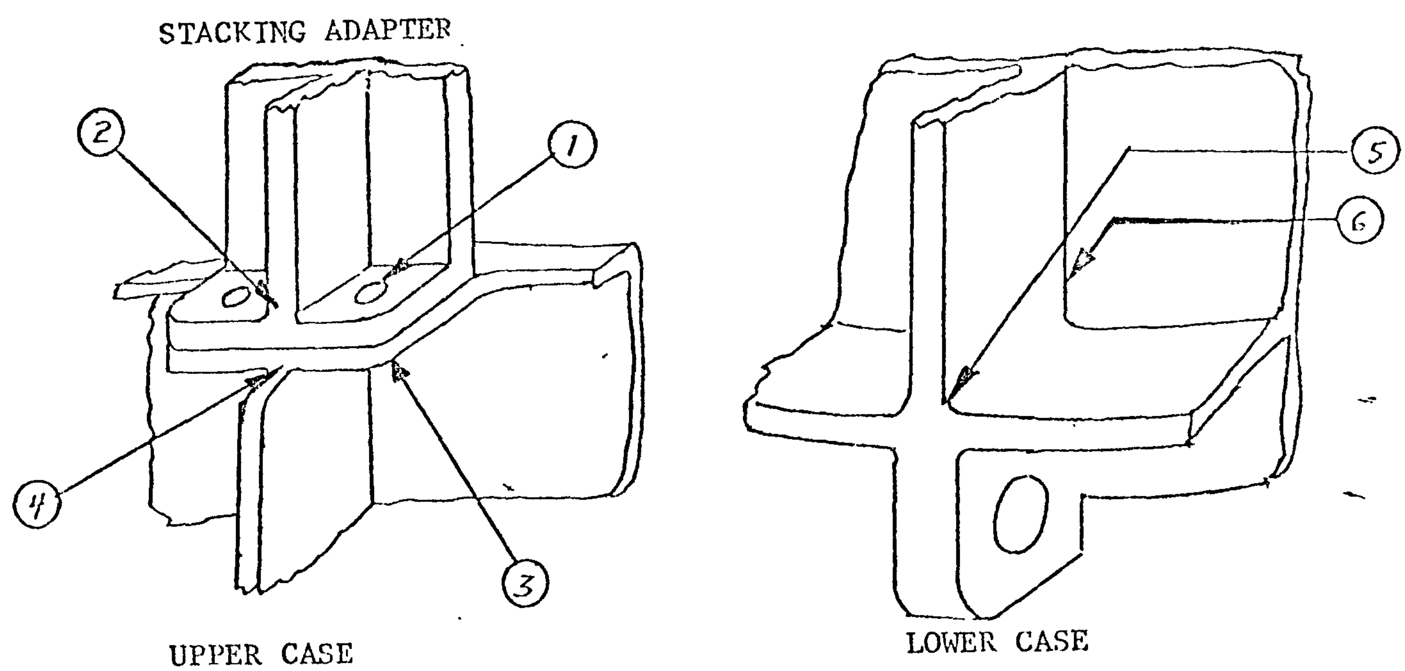

LOCATIONS OF CRITICAL STRESSES

FIGURE 6.3.2-4

TABLE 6.3.2-4

CORRELATION OF TEMPERATURE WITH LAUNCH EVENTS AND STRESSES

TIME (SECONDS)	EVENT	STACKING ADAPTER TEMPERATURE (°F)	STRESS* (PSI)
-----	DESIGN	280°F	16,395
0	STAGE 0 IGNITION	90°F	8,526
256	STAGE I BURNOUT	140°F	9,800
4346	STAGE III IGNITION (1)	400°F	6,800
4657	STAGE III SHUTDOWN (1)	400°F	9,400
23736	STAGE III IGNITION (2)	400°F	10,800
23836	STAGE III SHUTDOWN (2)	400°F	5,400

CRITICAL EVENTS ARE:

STAGE 0 IGNITION }
STAGE I BURNOUT } LOW TEMPERATURE

*Maximum stress in stacking adapter and mating pad of case.

The temperatures shown for the launch events are based on an on-pad cooling air flow rate of 225 pounds per minute. The critical events are Stage 0 ignition and Stage I burnout which occur while the temperatures are below the design temperature. A comparison between the stresses associated with the launch events and the stress based on the design load factors shows that the design is conservative for the anticipated launch loads.

6.3.2.3.2.3 Fracture Mechanics Analysis*

The reduced temperatures predicted for the RTGs during the vibratory launch environment requires a closer look at the beryllium properties and the behavior of beryllium in this more brittle condition. The concepts and methods of linear elastic fracture mechanics have been used to assess the brittleness problem.

To apply fracture mechanics concepts it is necessary to know the fracture toughness, K_{IC}, of the material. This is the critical value of the stress intensity where a crack becomes unstable and fracture occurs. Fracture toughness must be determined experimentally. Table 6.3.2-5 shows the result of a literature search of fracture toughness values determined for beryllium by various laboratories. The chemical composition is listed for each specimen because the BeO content and the ratio of Fe/Al have an important influence on ductility and fracture toughness. A fracture toughness value of $K_{IC} = 10$ Ksi $\sqrt{in}$ has been selected as a conservative number for use at room temperature in the analysis.

---

*NOTE: Professor George R. Irwin, of the University of Maryland, consulted as an expert on fracture mechanics, agreed with the results of this analysis. He pointed out that with the conservative selection of the low fracture toughness value, the result of the analysis indicates no fracture mechanics problems with the beryllium.

TABLE 6.3.2-5

BERYLLIUM FRACTURE TOUGHNESS VALUES

Reference	B	BeO	C	Fe	Al	Mg	Si	Other	Fe/Al	e %	K_{IC} Ksi $\sqrt{in}$	Remarks
GE Spec HP10 Hot Pressed Block	98.5	1.0	.15	.15	.1	.08	.08	.04	2	2.2	10.5 * 11.4**	Ref.Beryllco Mr. Filer * HP Block **Aged Matl.
*L. L. L. 1972 (1)	98.48	1.72	.065	.12	.02	.003	.036	.05	6	1.74	10	Hot Pressed Block Fe/Al = 6
UCID 15970 Rev. 1 (2)	98.47	1.7	.096	.11	.047	.008	.042	.05	2.3	2.0	14	Hot Pressed Block Fe/Al = 2.3
1968 Symposium Harrod, H & M	98.2	1.7	.12	.14	.08	.005	.03	.01	1.75	2.5	21	S 200
ASTM 1968 Journal of Materials	99.3	.9	.032	.048	.018	.003	.005	.04	2.72	2.6	18.0 20.2	N50A II
Vol. 3 No. 1	98.34	1.97	.117	.136	.045	.037	.043	.04	3.03	1.84	19.8 26.0	S200 II
Journal of Testing and Evaluation - Vol. 1 No. 2 March, 1973 Jones, Bubsey & Brown	98.1	1.67	.11	.107	.07	.004	.025	.04	1.53	1.2	10	H Block (S 200)
	97.9	1.71	.128	.13	.04	.011	.026	.04	3.25	11	> 10	Forged Disk
	98.9	.76	.040	.104	.045	.004	.03	.04	2.3	23.2	16.5	Rolled Sheet From Block
	96.9	2.76	.07	.13	.05	.01	.03	.03	2.6	39 -	39 -	Rolled Sheet From Block

* L.L.L. -- LAWRENCE LIVERMORE LABORATORY

The variation of fracture toughness of beryllium S200 hot pressed block with temperature is shown in Figure 6.3.2-5 for unheat-treated and heat-treated conditions. It is reasonable to assume that the curves for HP 10 would have similar characteristics. Therefore, an estimated curve for HP 10, passing through K_{IC} = 10.5 Ksi $\sqrt{in}$ at 70°F (as reported by Kawecki Berylco Company) has been superimposed. From the estimated curve, it can be concluded that the fracture toughness at 90°F is approximately 70% of the fracture toughness at 280°F.

6.3.2.3.2.4 Static Failure Analysis

The critical design stress (based on load factors of 5g lateral and 8g longitudinal) and the yield stress at room temperature are:

Design Stress σ = 16,400 psi

Yield Stress σ = 27,500 psi

The maximum flaw size permitted by the billet specification is 0.03 inches. Assume for a worst case that the flaw is at or very near an edge. Then the allowable failure stress can be expressed:

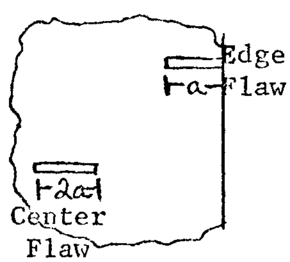

$$\sigma_{allowable} = K_{IC}/\sqrt{\pi a}$$
$$= 10/\sqrt{\pi \times .03}$$
$$= 32,575 \text{ psi}$$

Since this value is above the allowable yield stress, it is not controlling and does not affect the margins of safety shown in Table 6.3.2-3.

For the design stress, 16,400 psi, the critical edge flaw size can be determined as follows:

$$a = \frac{1}{\pi}\left(\frac{K_{IC}}{\sigma}\right)^2$$
$$= \frac{1}{\pi}\left(\frac{10}{16.4}\right)^2$$
$$= 0.118 \text{ inches} > .03 \text{ inches}$$

FIGURE 6.3.2-5

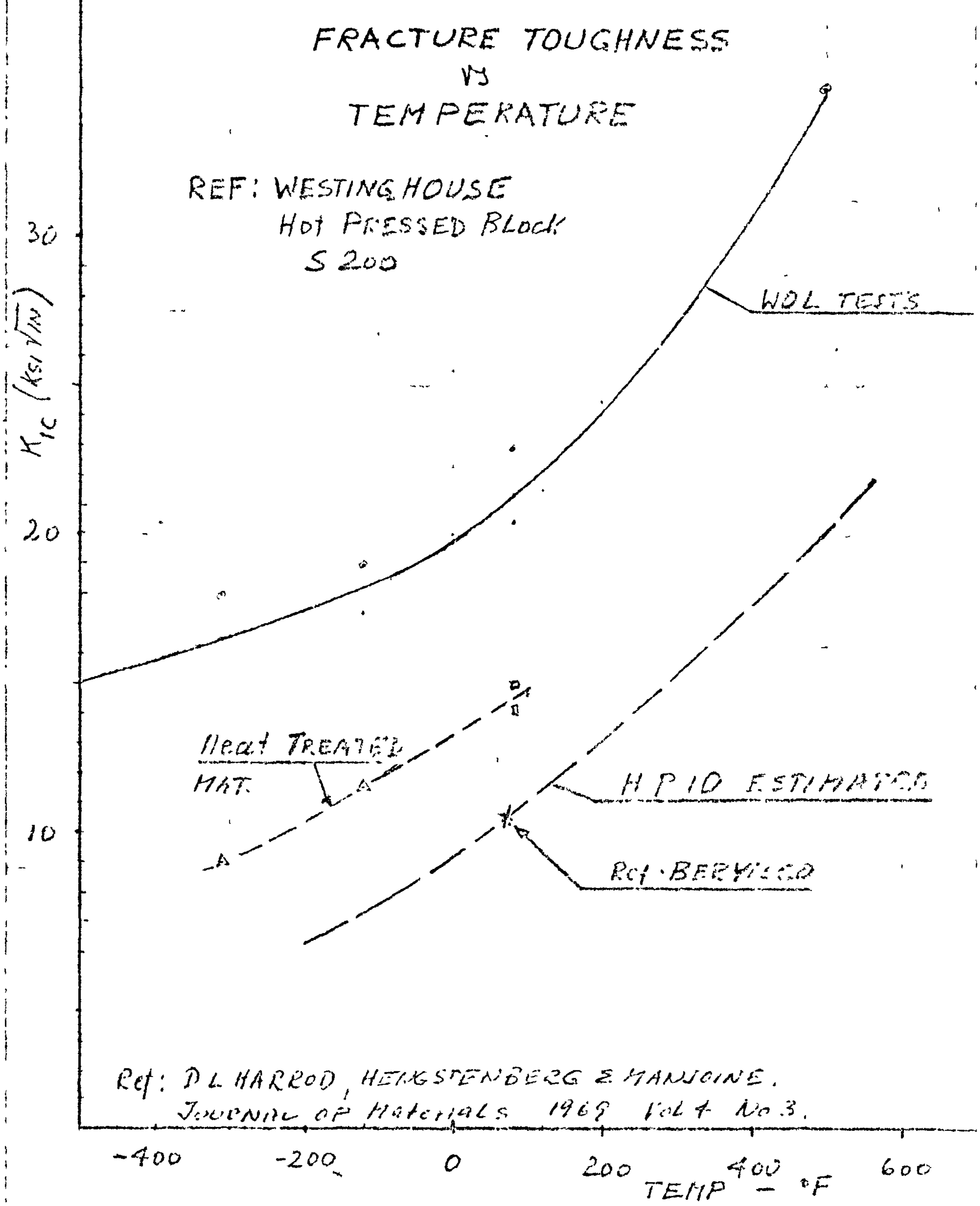
FRACTURE TOUGHNESS
vs
TEMPERATURE
REF: WESTINGHOUSE
Hot PRESSED Block
S 200
WOL TESTS
Heat TREATED
MAT.
H P 10
30
20
10
K_{IC} (KSI √IN)
-400
-200
0
200
400
600
TEMP - °F
Ref: D L HARROD, HENGSTENBERG & MANJOINE.
Journal of Materials 1969 Vol 4 No 3.

This allowable flaw size provides a considerable margin over the size permitted by the billet specification; 0.03 inches.

6.3.2.3.2.5 Evaluation of the Crack Growth Rate During Cyclic Loading

The crack growth rate during cyclic loading for a working stress of 16,400 psi and a conservative flaw size of .050 inch can be evaluated as follows:

The stress intensity factor can be calculated from:

$$K_{TH} = \sigma \sqrt{\pi a}$$

$$= 16.4 \sqrt{\pi \times .05}$$

$$= 6.50 \text{ Ksi} \sqrt{in}$$

Figure 6.3.2-6 shows the relationship between stress integrity and crack growth rate for several materials including S-200 hot pressed block beryllium which is similar to HP-10. For $K_{TH} = 6.5$ Ksi $\sqrt{in}$, Figure VI yields $\frac{da}{dN} = 10^{-7}$ in/cycle.

Assuming the number of cycles N = 1000 cycles, the resulting crack growth is 0.0001 inches which is insignificant.

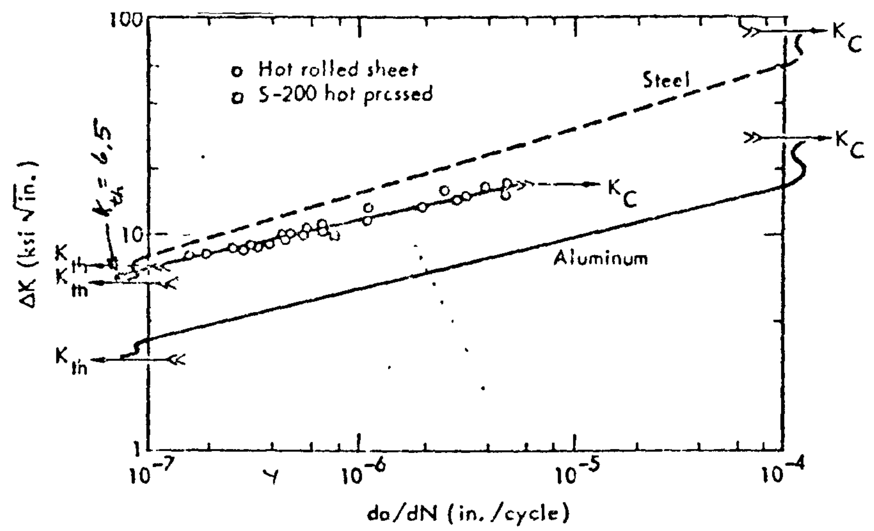

FIGURE 6.3.2-6. Fatigue crack growth rate in beryllium, along with typical results for steel and aluminum alloys.

6.3.2.3.2.6 Fatigue Properties

Data on the fatigue performance of beryllium was obtained at the Lawrence Radiation Laboratory, Livermore, California. The data is shown in Figure 6.3.2-7 with K_{Ii}/K_{IC} vs. cycles to failure.

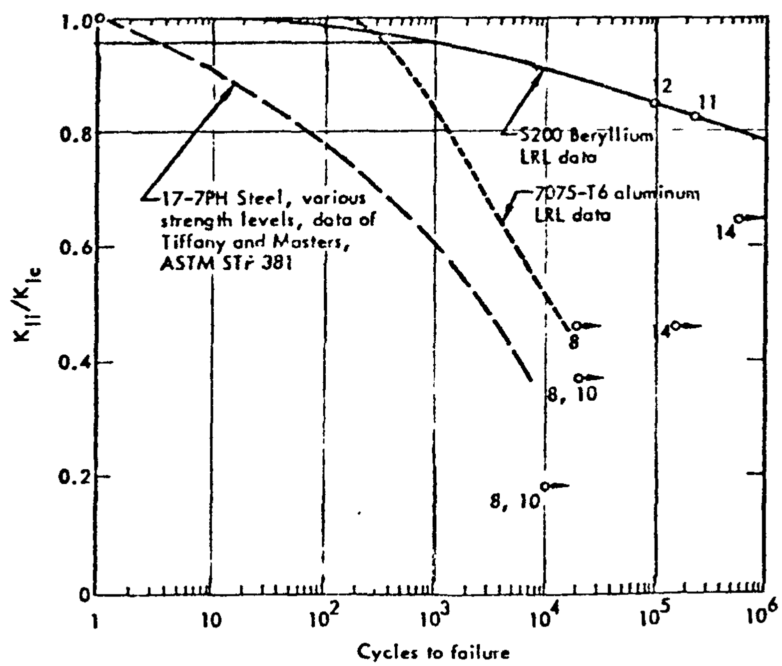

FIGURE 6.3.2-7. K_{Ii}/K_{IC} vs. cycles to failure for various materials. Specimen number indicated by data points.

K_{Ii} is the initial maximum stress intensity factor applied during the fatigue cycling. These results show that the strength of beryllium is degraded only a relatively small amount by fatigue loading and that this material is well suited for fatigue applications.

The data of the above figure can be used to derive an allowable for fatigue loading as follows:

Assume: Edge Flaw Size $a = .030$ in.

Number of Cycles $N = 10^3$

The initial stress intensity factor K_{Ii} can be derived as follows:

$$K_{Ii} = \sigma (\pi a)^{\frac{1}{2}}$$

$$= \sigma (.03\pi)^{\frac{1}{2}}$$

$$= .307 \sigma$$

From Figure 6.3.2-7 for 10^3 cycles:

$$K = \frac{K_{Ii}}{K_{IC}} = .95$$

Using a room temperature fracture toughness number of $K_{IC} = 10$ Ksi $\sqrt{in}$, the allowable stress for fatigue loading is:

$$\sigma = \frac{K_{IC}}{.307} K$$

$$= \frac{10}{.307} \times .95$$

$$= 31{,}000 \text{ psi}$$

This value is greater than the yield allowable which was used to derive the margins of safety. Therefore, the yield stress can be used as the allowable for 1000 cycles of loading.

The fracture toughness of the beryllium material is lower at the reduced temperature. However, the results of this fracture mechanics analysis indicates that flaws not in excess of those permitted by the material specification do not reduce the margins of safety based on the allowable yield stress.

6.3.2.3.3 Fabrication and Inspection

Particular care is exercised throughout the manufacturing cycle for the beryllium outer case and stacking adapters to avoid flaws and machining cracks.

The beryllium billets, which have a wall thickness of approximately 2.4 inches, are subjected to radiographic inspection and the maximum permissible flaw dimension is limited to 0.030 inches. No cracks are permitted in the billet. Stringering restrictions prevent a local concentration of small flaws which could weaken the material. Grain size is limited to 25 microns. In addition, the BeO content is limited to a maximum of 1% and the ratio of Fe/Al is limited to 2% to control ductility.

All machined surfaces are chem-etched .001-.002 inches except where not permissible due to surface finish or tolerances. Final machining passes in areas not to be etched are limited to .001 inches in depth.

Following rough machining, the case is stress relieved and subjected to a fluorescent inspection. No cracks are permitted.

A final visual inspection of critical areas will be made prior to assembling of the RTGs on the spacecraft.

6.3.2.3.4 Verification Tests Considered

As a part of this assessment, the following tests were considered for verifying the capability of the RTGs to survive the launch environment at the reduced temperature.

<u>Room Temperature Toughness Tests for Beryllium</u>

These tests would provide toughness data for the actual billets used in the manufacture of the RTG cases. However, based on existing toughness test data for similar materials, the results of fracture mechanics analyses show that the design is sufficiently conservative to require no additional test data. Therefore, no toughness tests are recommended.

Stacking Adapter Static Load or Low Cycle Fatigue Test

The margins of safety for the stacking adapters and the mating flange area of the RTG cases are nearly equal. Therefore, a stacking adapter structural test at room temperature would verify analytically derived margins of safety for both the case and the stacking adapters if no flaws or cracks were present. Since the tensile strength properties of the beryllium are higher at the reduced temperature, the margins of safety should be higher at the reduced temperature. However, this test would not address the basic question of the effects of flaws and cracks on structural capability. Therefore, this test is not recommended.

ETG Low Temperature Vibration Test

This test was considered as a means of evaluation of the structural capability of the thermopile at the reduced temperature. To perform this test the ETG would be energized by applying approximately 2400 watts to the electric heat source and the outer case would be cooled by an air circulation system to the reduced temperatures predicted for liftoff. Only two ETGs are available for this test; E-1 (formerly TBC #3), and E-2 (formerly TBC #4). E-1 has been subjected to qualification shock, vibration and acoustic testing. E-2 has been aged for over 10,000 hours. Based on the previous history of these units, a failure of the thermopile during a reduced temperature dynamic test could not be reliably attributed to the effects of temperature. As a result, a low-temperature ETG test is not recommended.

6.4 CONVERTER PERFORMANCE AND ANALYSIS

6.4.1 RTG On-Pad Power with I.H.S. Clad Leakage

Because of a request from Lincoln Laboratory to have additional preorbit power for the LES 8/9 mission, Xenon gas will be required instead of the Argon cover gas. Since the preorbit power is at a premium, a sensitivity analysis was made to determine the Helium clad leakage effects on RTG on-pad power with the RTG filled with Xenon gas.

As shown in Figure 6.4.1-1, the Helium effects are severe and the present clad leak rates may not be compatible with the revised power requirements. To date, obtaining accurate clad leak rates has been difficult due to the large temperature gradients between the heat source and pressure measuring gauges. However, all data obtained indicates the clad leakage for some RTG's to be $>3 \times 10^{-4}$ scc/sec.-He.

It must be emphasized that the power levels are based on 30 days from the time the RTG gas exchange was performed.

Based on both the on-pad time uncertainty and the clad leakage, it was decided that the Helium in the IHS will be replaced with Xenon at the same time as the RTG gas exchange is made. This will limit the effects to $< 1 \times 10^{-4}$ scc/sec. (He generation rate with Xe cover gas) and therefore provide maximum on-pad power.

6.4.2 RTG Pressure Decay Response to On-Pad Cooling

6.4.2.1 Introduction

Analyses were performed to determine the effect of continuous on-pad cooling with respect to RTG internal pressure characteristics. Of specific interest was the impact of such cooling on the requirement that the RTG be capable of maintaining a minimum positive pressure of 0.5 PSI with respect to the atmosphere at the end of an unattended 30-day hold period prior to launch. The analyses considered the use of both Xenon and Argon as the RTG cover gas.

The results of this analysis show that on-pad cooling will not prevent the RTG from meeting its 30-day pressurization requirements (See Figure 6.4.2-1).

RTG POWER VS CLAD LEAK RATE

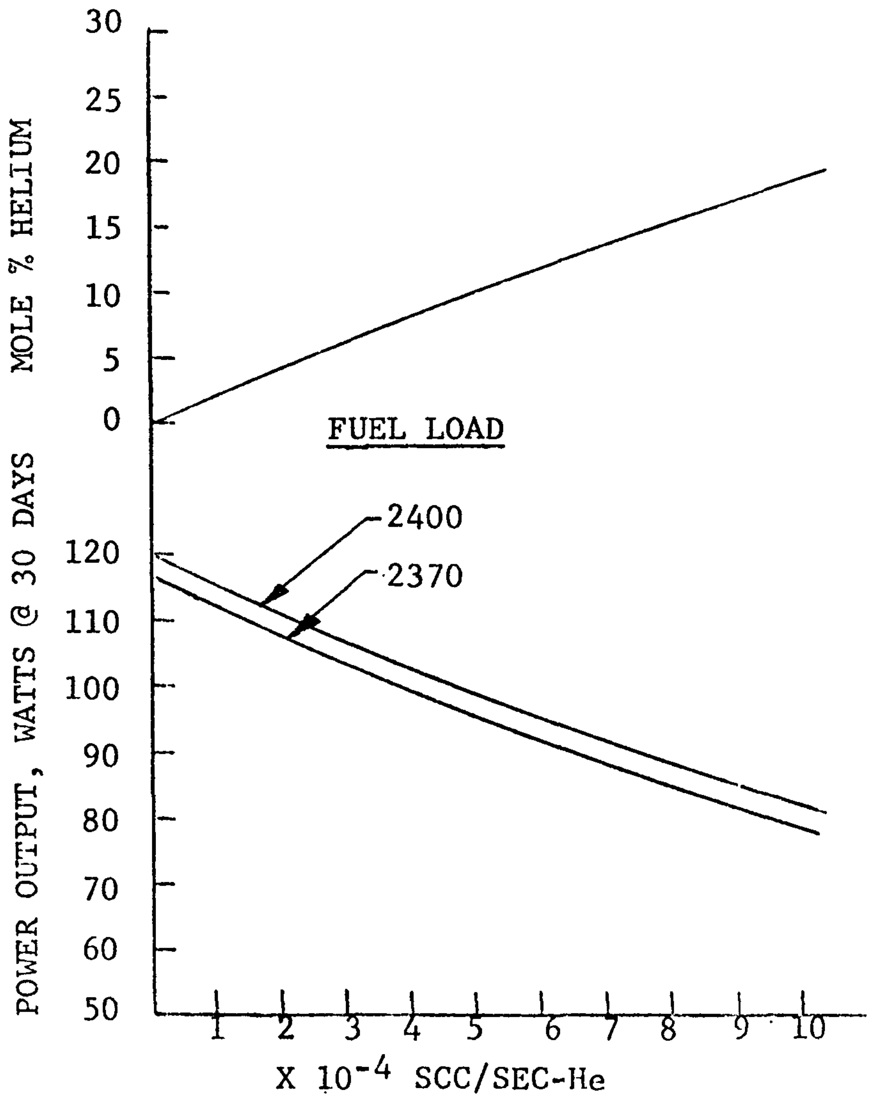

CLAD LEAK RATE

NOTE - POWER OUTPUT IS BASED ON 30 DAYS FROM THE TIME OF THE ARGON/XENON GAS EXCHANGE

FIGURE 6.4.1-1

6.4.2.2 Analysis of Effects with Xenon Cover Gas

The effect of continuous cooling on a Xenon-filled RTG was examined for the following case temperatures: 300°F, 350°F, and 400°F. Several basic assumptions were made in performing this analysis. They are as follows:

1. Prior to removal of the RTG from the RTG-SC, the RTG is purged with argon to remove helium accumulated during storage and is then backfilled with Xenon to a pressure of 25 PSIA.

2. After removal from the RTG-SC the RTG is allowed to stabilize at ambient conditions and is then again charged with Xenon to achieve an internal pressure of 25 PSIA.

3. Prior to initiation of cooling, the RTG is then subjected to a two-day period in an atmospheric environment during which RTG mating and integration activity is performed.

4. RTG cover gas temperature response to changes in RTG operational conditions is small (2-3 hours) and is therefore neglected.

5. The RTG overall leak rate is assumed to remain constant despite changes in RTG case temperatures. The leak rate used is that defined in the RTG Specification (See Figure 6.4.2-1).

6. To factor in the effect of helium generation over the 30-day hold period the two worst case conditions were considered:

    1) Helium generation has no effect on overall RTG internal pressure.

    2) The 15°C drop in heat source temperature at the end of the 30-day hold period due to the presence of helium was assumed to be constant for the entire period.

The analysis was divided into two segments or events corresponding to a particular set of operational conditions. The events and their associated conditions are as follows:

FIGURE 6.4.2-1

RTG/ETG ALLOWABLE PRESSURE DECAY

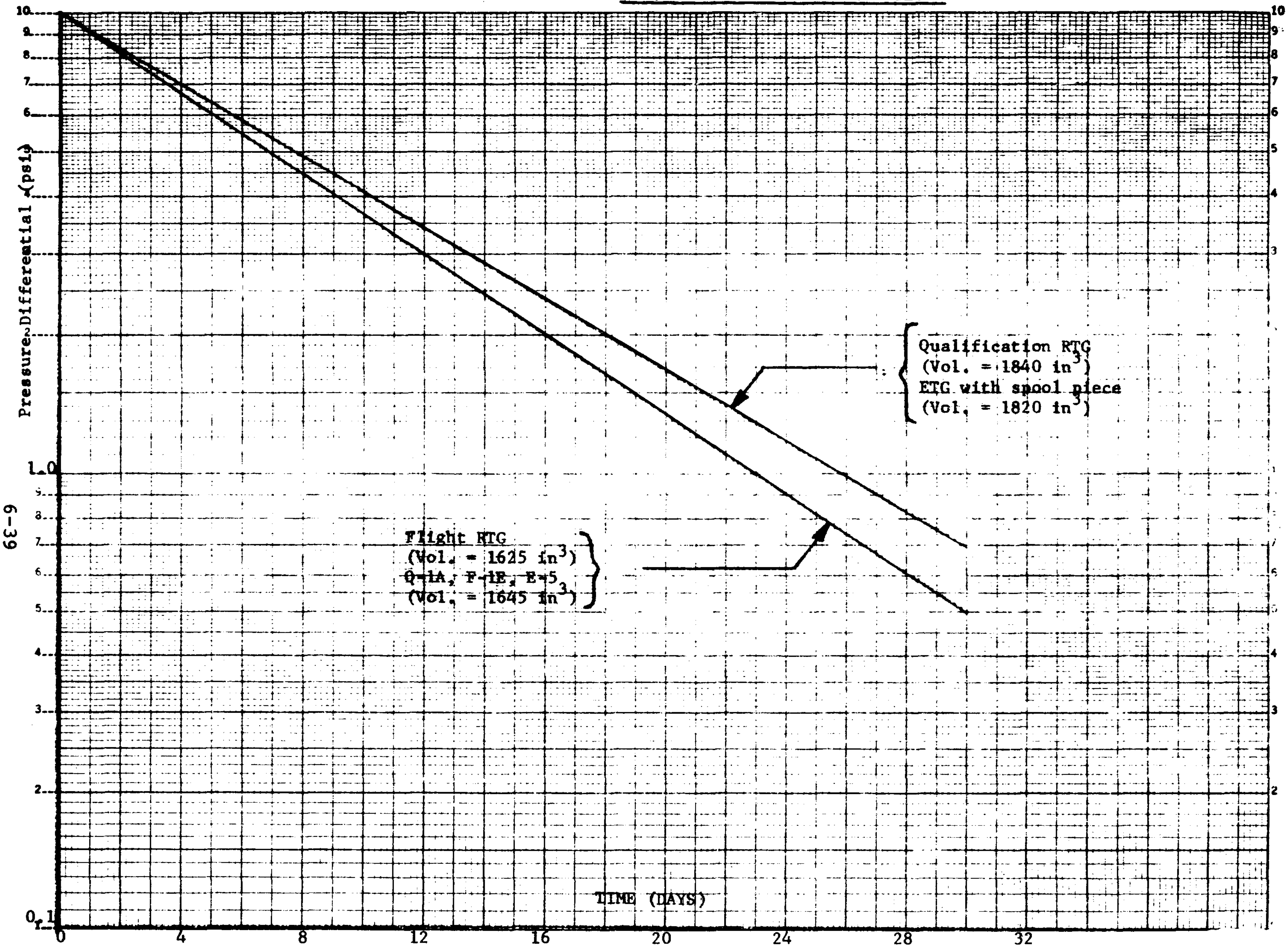

Event 1: Final Pressurization of the RTG

a) RTG stabilized in ambient air.

b) RTG in short circuit mode.

c) Case Temperature (T_C) = 828.6°R (368°F);
Heat Source Temperature = 2021.6°R (1562°F)

Event 2: On-Pad Cooling Phase

a) RTG in cooled air environment.

b) RTG carrying a 30-volt load.

Beginning with Event 1 the initial pressurization condition of P = 25 PSIA was considered. This value for P was then used in conjunction with the Gas Equation of State

$$PV = mRT_{BG} \tag{1}$$

where

P	=	pressure
V	=	RTG volume
m	=	mass of cover gas
R	=	gas constant for xenon
T_{BG}	=	cover gas bulk temperature

to assess the available mass within the converter. The values for T_{BG} are obtained from the relationship

$$T_{BG} = .5\ (T_C + T_{HS}) \tag{2}$$

where

T_{BG}	=	cover gas bulk temperature
T_C	=	RTG case temperature
T_{HS}	=	Heat Source temperature

This relationship was derived from previous RTG operational data.

The RTG pressure differential was found by

$$\Delta P = P_C - P_A \tag{3}$$

where ΔP = RTG pressure differential
P_C = Absolute converter pressure
P_A = Atmospheric pressure = 14.7 lbf/in^2

The maximum allowable leak rate is defined by the equation

$$y(t) = \Delta P e^{-zt} \qquad (4)$$

where $y(t)$ = RTG pressure differential at t days

ΔP = RTG pressure differential at time t = 0

z = constant = .09986
t = time in days

This relationship was used to establish the RTG pressure differential at the end of Event 1.

Event 2 was broken down into three cases with continuous cooling of the RTG outer shell to 300^oF, 350^oF, and 400^oF respectively. For Event 2 calculation the relation

$$\Delta T_{HS} = .8 \Delta T_C \qquad (5)$$

where ΔT_{HS} = change in Heat Source temperature

ΔT_C = change in RTG case temperature

was used to determine the Heat Source temperature with respect to RTG case temperature. Equations (1), (2), (3), (4), and (5) were then used to determine Event 2 initial pressure conditions and then to establish the time required for the RTG pressure differential to decay to 0.5 PSI from the start of Event 2.

The time to decay to a 0.5 PSI differential from the beginning of Event 2 was then added to the two-day period in Event 1 to obtain the total time required for the RTG to decay to a 0.5 PSI differential after final RTG charging. Analysis shows that for maximum anticipated cooling, case temperature of 300°F, the RTG pressure differential will decay to 0.5 PSI differential in 30.25 days after final pressurization, slightly exceeding specification requirements. Cooling temperatures above 300°F present no problem with respect to RTG pressure decay requirements.

The results of the analysis, as shown in Figure 6.4.2-2, indicate that on-pad cooling will not prevent the RTG from meeting its 30-day pressurization requirements with Xenon used as the cover gas.

6.4.2.3 Analysis of Effect with Argon Cover Gas and Maximum Allowable Leak Rate

Several basic assumptions were made in performing this analysis. They are as follows:

1. Argon is assumed to be the RTG cover gas.

2. RTG cover gas temperature response to changes in RTG operational conditions is small (2-3 hours) and is therefore neglected.

3. The RTG overall leak rate is assumed to remain constant despite changes in RTG case temperatures. The leak rate used is that defined in the RTG Specification (See Figure 6.4.2-1).

4. The RTG pre-launch case temperature profile is based on the AFETR Cooling Airflow History as provided by TRW (See Figure 6.4.2-3).

The analysis was divided into three segments or events corresponding to a particular set of RTG operational conditions. These events and their associated operational conditions are as follows:

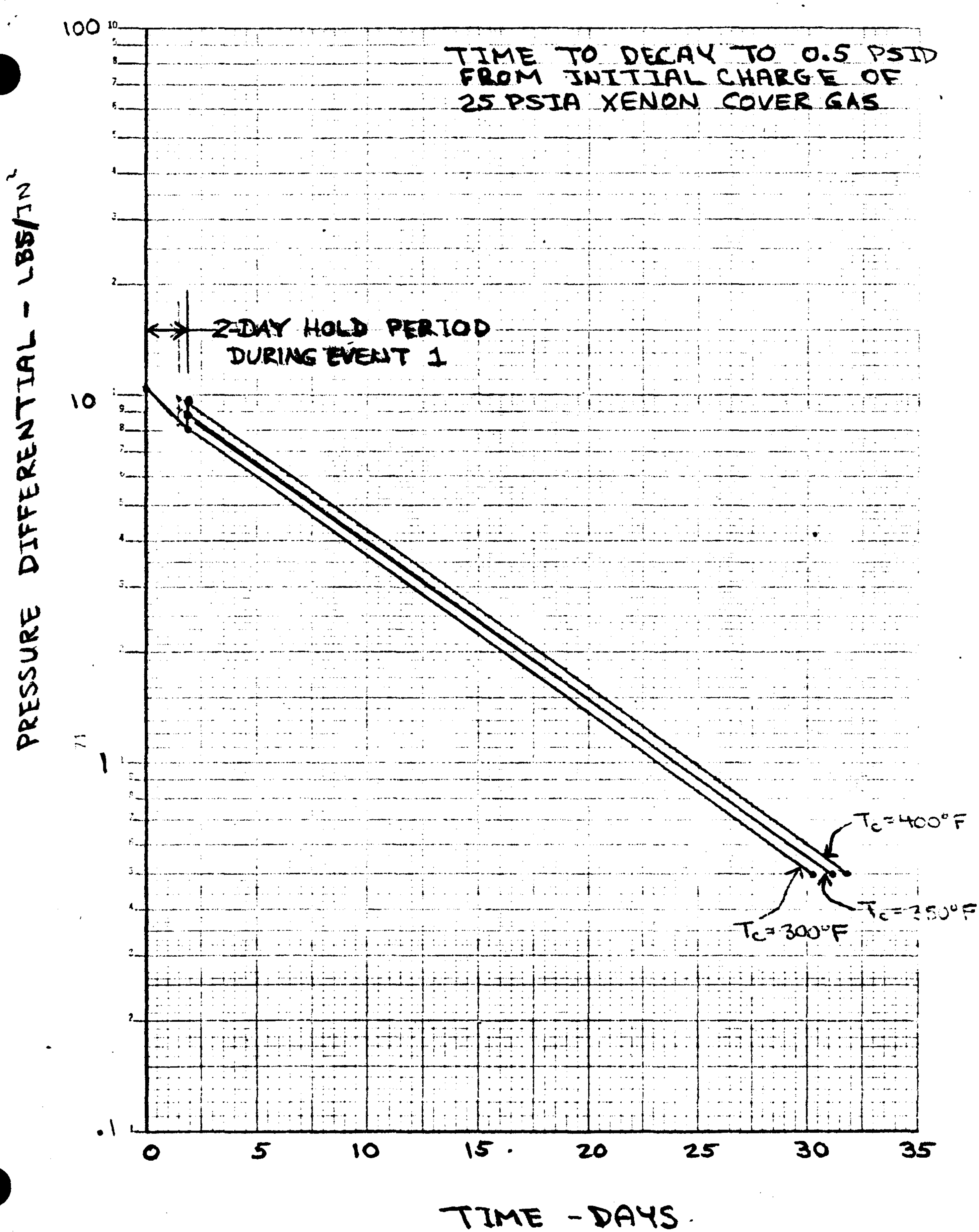
TIME TO DECAY TO 0.5 PSID
FROM INITIAL CHARGE OF
25 PSIA XENON COVER GAS
2-DAY HOLD PERIOD
DURING EVENT 1
PRESSURE DIFFERENTIAL - LBS/IN²
TIME - DAYS
Tc = 400°F
Tc = 350°F
Tc = 300°F
100
10
1
.1
0
5
10
15
20
25
30
35

FIGURE 6.4.2-2

AFETR COOLING AIRFLOW HISTORY

SUPPLY AIR TEMPERATURE AT HEPA FILTER = 55°F TO 65°F

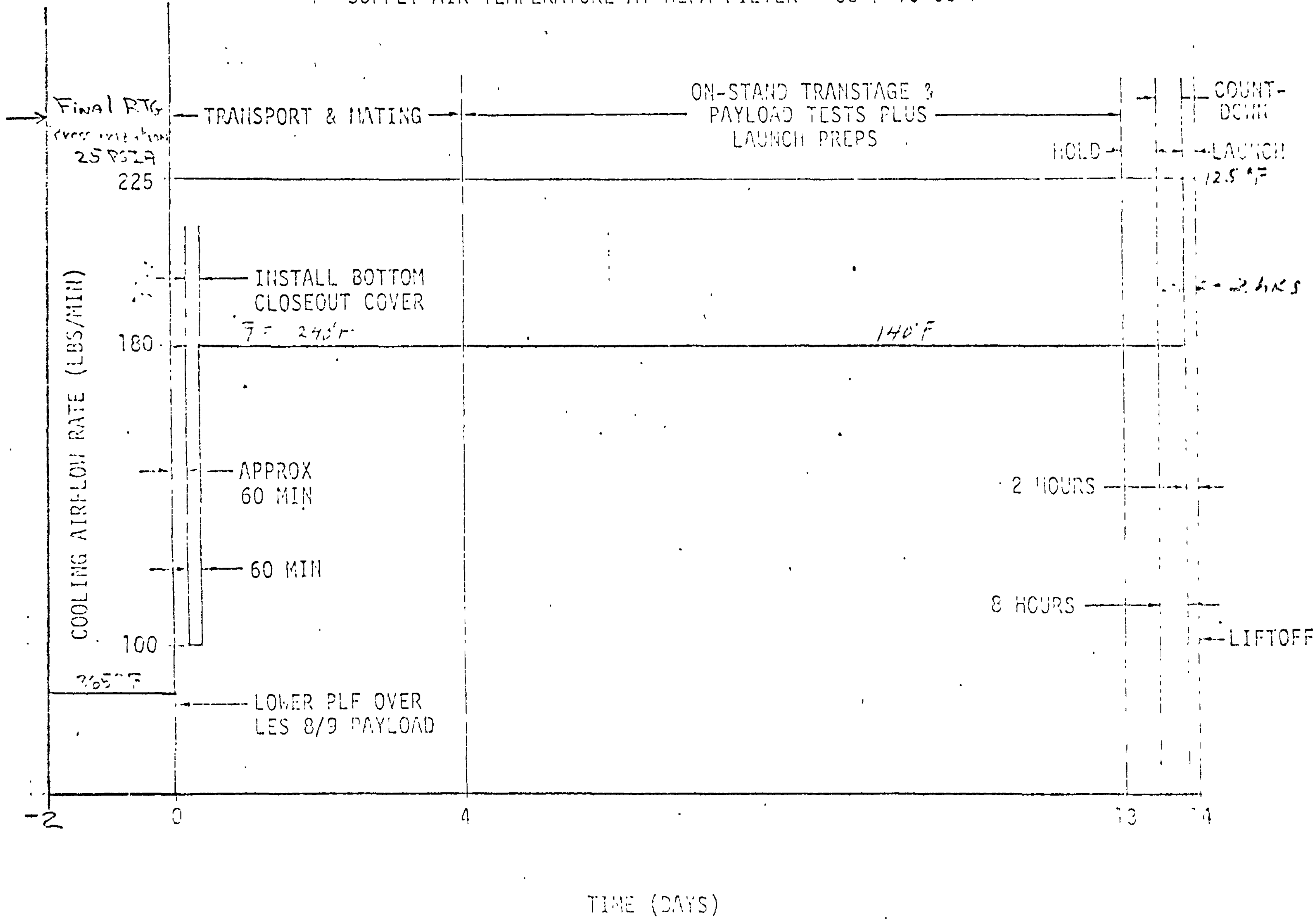

FIGURE 6.4.2-3

EVENT 1: Final Pressurization of the RTG

a. RTG in ambient air
b. RTG in short circuit mode
c. RTG pressurized with argon to 25 psia
d. Case temperature (T_C) = 824.67°R (365°F); Heat Source Temperature (T_{HS}) = 1931.67°R (1472°F)
e. Event 1 covers a period of two days

EVENT 2: Transport and Mating

a. RTG in cooled air environment
b. T_C = 699.67 R (240°F)
c. RTG carrying a 30-volt load
d. Event 2 covers a period of four days

EVENT 3: On Stand Transtage & Payload Test Plus Launch Preps

a. RTG in cooled air environment
b. T_C = 599.67°R (140°F)
c. RTG carrying a 30-volt load
d. Event 3 covers a period of 10 days

EVENT 4: Immediate Pre-Launch Cooling

a. RTG in cooled air environment
b. T_C = 584.67°R (125°F)
c. RTG carrying a 30-volt load
d. Event 4 covers a period of two hours

Beginning with Event 1 the initial pressurization condition of P = 25 psia in ambient air was considered. This value of P was then used in conjunction with the Gas Equation of State:

$$PV = m R T_{BG} \qquad (1)$$

where:
- P = pressure
- V = RTG volume
- m = mass of cover gas
- R = gas constant for argon
- T_{BG} = cover gas bulk temperature

to assess the mass available within the converter. The value for T_{BG} is obtained from the relationship:

$$T_{BG} = .5\ (T_C + T_{HS}) \qquad (2)$$

where: T_{BG} = cover gas bulk temperature
T_C = RTG case temperature
T_{HS} = heat source temperature

This relationship was derived from previous RTG operational data.

The RTG pressure differential was found by:

$$\Delta P = P_C - P_A \qquad (3)$$

where: ΔP = RTG pressure differential
P_C = absolute converter pressure
P_A = atmospheric pressure = 14.7 lbf/in^2

The maximum allowable leak rate (see Figure 6.4.2-1) is defined by the equation:

$$y(t) = \Delta P e^{-zt} \qquad (4)$$

where: $y(t)$ = RTG pressure differential at t days
ΔP = RTG pressure differential at time t = 0
Z = constant = 0.09986
t = time in days

This relationship was used to establish the RTG pressure differential at the end of Event 1.

Events 2, 3 and 4 were analyzed in the same manner as Event 1, making use of an additional relationship

$$\Delta T_{HS} = .85\ \Delta T_C \qquad (5)$$

where: ΔT_{HS} = change in heat source temperature
ΔT_C = change in RTG case temperature

which was used to determine the change in heat source temperature with respect to change in RTG case temperature.

As shown in Figure 6.4.2-4, it was determined that the RTG pressure differential at the time of launch will be 1.1 psid with respect to the atmosphere. This value is more than adequate to meet the required RTG pressurization requirements.

Additionally, the time required for the RTG to attain a minimal differential pressure of 0.5 psid from the end of Event 3 was determined. Assuming continued cooling at a case temperature of 140°F, the calculated time is 9 days. With immediate pre-launch cooling at a case temperature of 125°F, the time to decay to 0.5 psid is 8.3 days (as opposed to the planned two-hour period for Event 4). These values are significant in that they provide a comfortable margin of safety to allow for unexpected on-pad hold time.

6.4.2.4 Analysis of Effect with Argon Cover Gas and Measured Leak Rates

This analysis differs from that of Paragraph 6.4.2.3 in that the flight units are treated individually and measured leak rates are used rather than the maximum allowable leak rate referred to in the RTG specifications. Within the context of the on-pad cooling profile, two RTG pressurization techniques were considered:

Case 1:

The RTG's receive final pressurization to 25 psia before removal from the RTG-SC and are not repressurized prior to launch. (Figure 6.4.2-5).

Case 2:

The RTG's are repressurized to 25 psia after removal from the RTG-SC but prior to the commencement of the cooling sequence. (Figure 6.4.2-6).

Table 6.4.2-1 gives the results of the analysis for the individual RTG's and the LES 9 RTG stack (details of the analysis are similar to those described in Para. 6.4.2.3 above, and were omitted here for the sake of brevity).

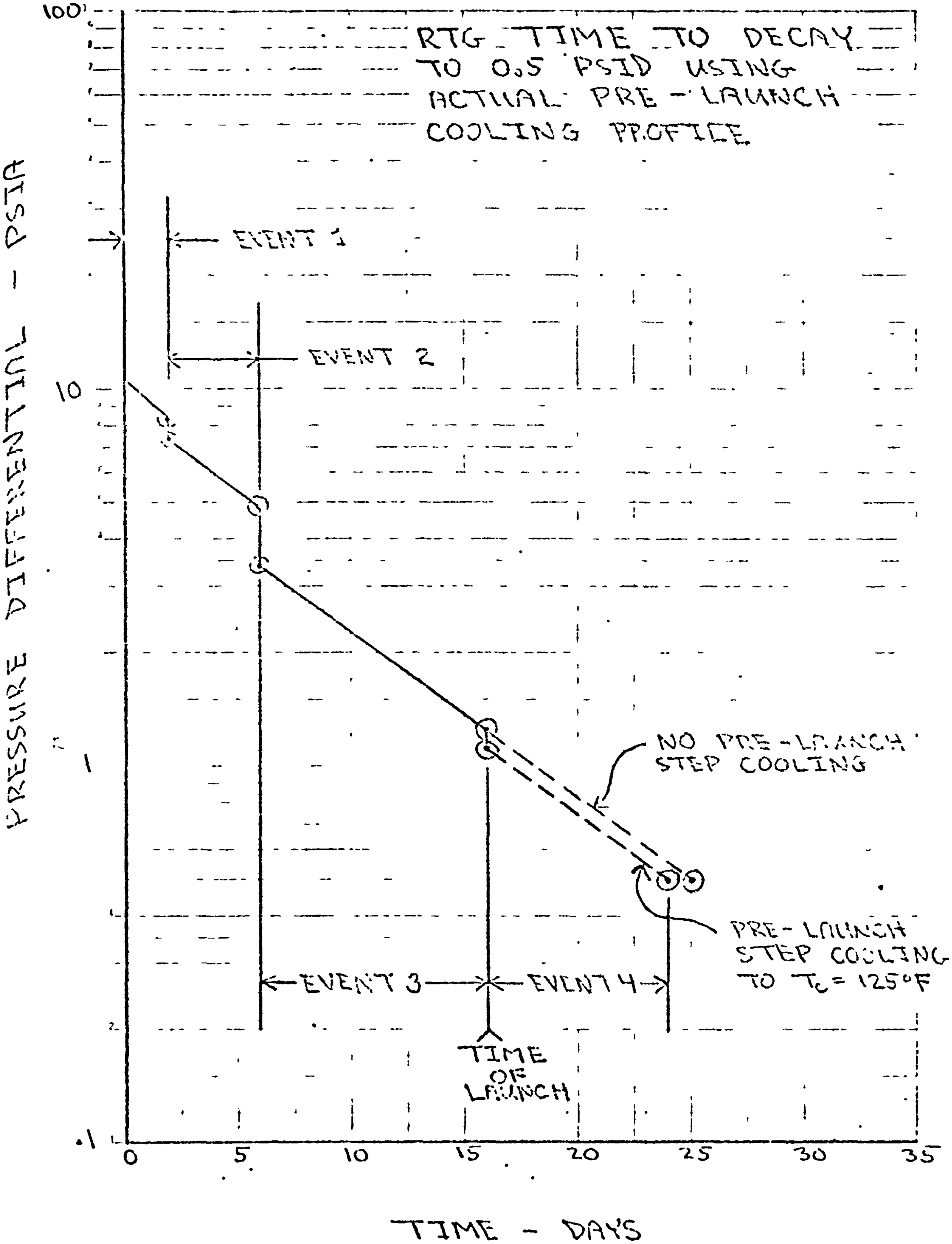
RTG TIME TO DECAY TO 0.5 PSID USING ACTUAL PRE-LAUNCH COOLING PROFILE
PRESSURE DIFFERENTIAL - PSIA
100
10
1
.1
EVENT 1
EVENT 2
EVENT 3
EVENT 4
NO PRE-LAUNCH STEP COOLING
PRE-LAUNCH STEP COOLING TO T_c = 125°F
TIME OF LAUNCH
0
5
10
15
20
25
30
35
TIME - DAYS

FIGURE 6.4.2-4

FIGURE 6.4.2-5

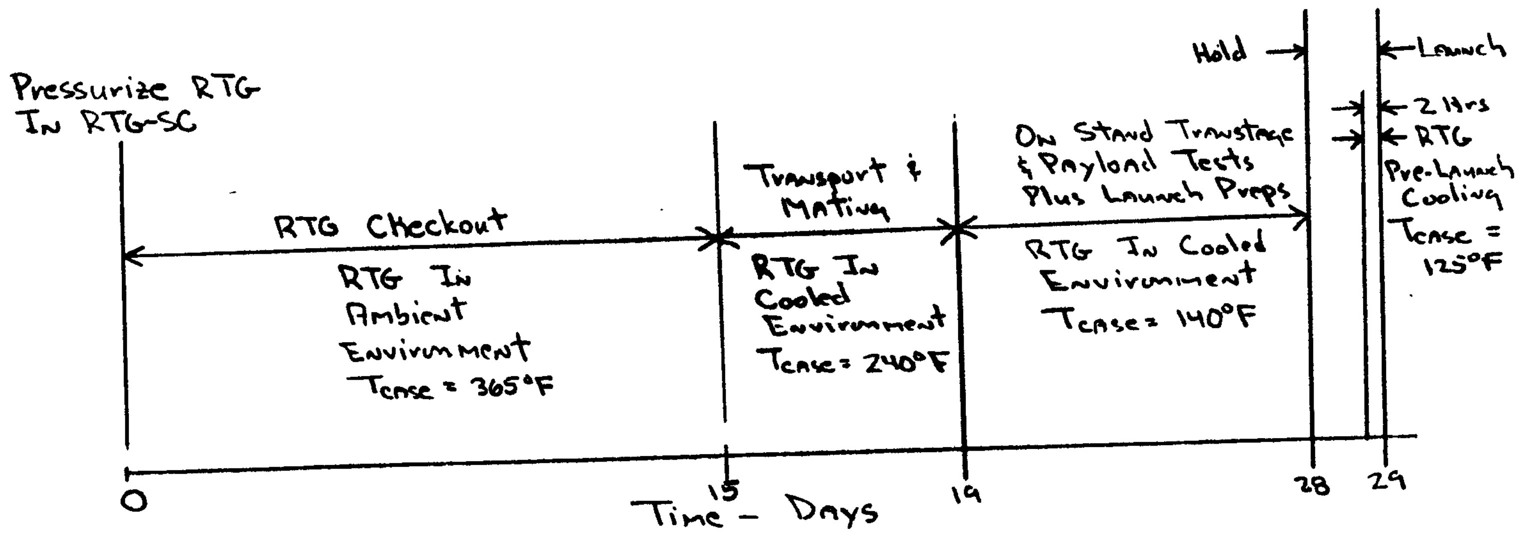

CASE 1 – RTG PRESSURIZATION IN RTG-SC

FIGURE 6.4.2-6

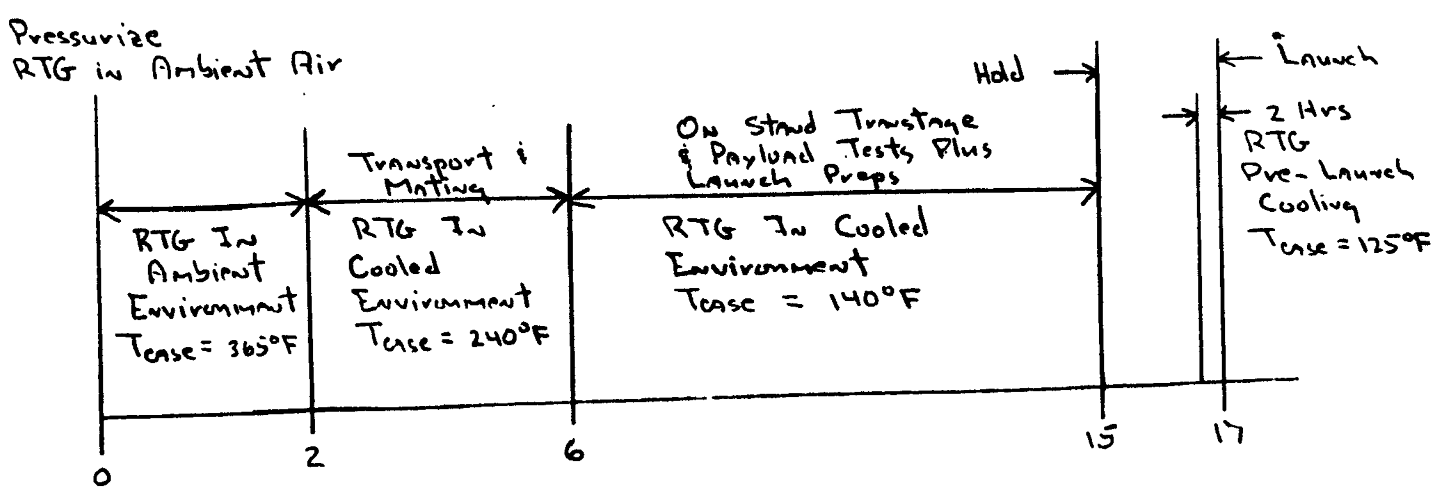

CASE 2 - RTG PRESSURIZATION PRIOR TO COOLING

TABLE 6.4.2-1

ARGON COVER GAS

UNIT	LEAK RATE	CASE 1 PRESSURE AT LAUNCH (lbs/in^2)	CASE 1 TIME TO DECAY TO .5 PSIA (days)	CASE 2 PRESSURE AT LAUNCH (lbs/in^2)	CASE 2 TIME TO DECAY TO .5 PSIA (days)
F-2	.07 psia/48 hrs.	5.43	699	6.74	762
F-4	.86 psia/48 hrs.	1.05	16	3.26	42
F-5	.56 psia/48 hrs.	2.22	54	4.41	79
F-4/F-5	.71 psia/48 hrs.	1.55	31	3.78	56

The results of the analysis show that the RTG's, both as individual units and in the stacked flight configuration, are more than capable of maintaining a minimum positive pressure differential of 0.5 psid with respect to the atmosphere at the time of launch. This result is valid irrespective of choice of RTG pressurization technique.

6.4.3 M.J.S. Launch Power Transient Analysis

Analyses are being performed to determine the transient power output characteristics of the MHW converter after liftoff during the MJS mission. The converter power output will decrease below the launch pad power output after launch because of a more rapid increase in cold than hot junction temperature.

To determine the transient hot and cold junction temperatures, a digital computer model is being used. The model consists of the ¼-sphere 63-node heat source model and a 14-node model of the thermopile. Included in the model are the changes in convection heat transfer as a function of altitude (air pressure), changes in the sink temperature and the blockage of the RTG radiation exchange factor by the spacecraft. The range of parameters used is given in Table 6.4.3-1.

Power output levels for the nominal launch outer case temperature of 350°F and no spacecraft blockage are shown in Figure 6.4.3-1. Results for the nominal 350°F temperature and 10, 20 and 30% blockage are shown in Figures 6.4.3-2 through 6.4.3-4. Results for launch pad outer case temperatures 50°F below the nominal are given in Figures 6.4.3-5 through 6.4.3-8.

Two power curves are shown on each plot. The lower curve represents the power profile resulting from the calculated hot and cold junction temperatures by using the 2-year thermoelectric property data. The upper curve is calculated from 3,900-hour property data. The 3,900 hour property data is taken to be the equivalent age time of the couples after 2 years of storage at lower temperature than operation under vacuum conditions. (Storage temperatures are TH/TC = 760°C/260°C). For short times, up to about one hour, the lower curve is followed. For longer times the power is intermediate, probably closer to the 3,900 hour curve by 6 hours although the exact kinetics of the transition are not known.[1]

The initial power levels shown on the plots do not include the effect of 30 days helium buildup in the converter. This effect reduced the initial power output by 2 watts. The present best estimate of the initial pad power for the nominal 350°F case after 2 years of storage and 30 days of helium buildup is 113 watts. This value is 2 watts

---

(1) "Effects of Low Temperature Storage on the Performance Characteristics of the MHW RTG"; V. Raag, Syncal Corporation; Dec. 13, 1974.

TABLE 6.4.3-1

- CONVECTION COEFFICIENT VARIATION

TIME SECONDS	h/ho
0	1.0
10	.983
20	.92
30	.829
40	.67
50	.53
60	.40
70	.29
80	.188
90	.112
100	.053
120	.020
140	.009

- SINK TEMPERATURE VARIATION

SINK = 100^{o}F UP TO 50 MIN.

= -86^{o}F 50 TO 67 MIN.

= 100^{o}F BEYOND 67 MIN.

- BLOCKAGE BY SPACECRAFT

0, 10, 20, 30%

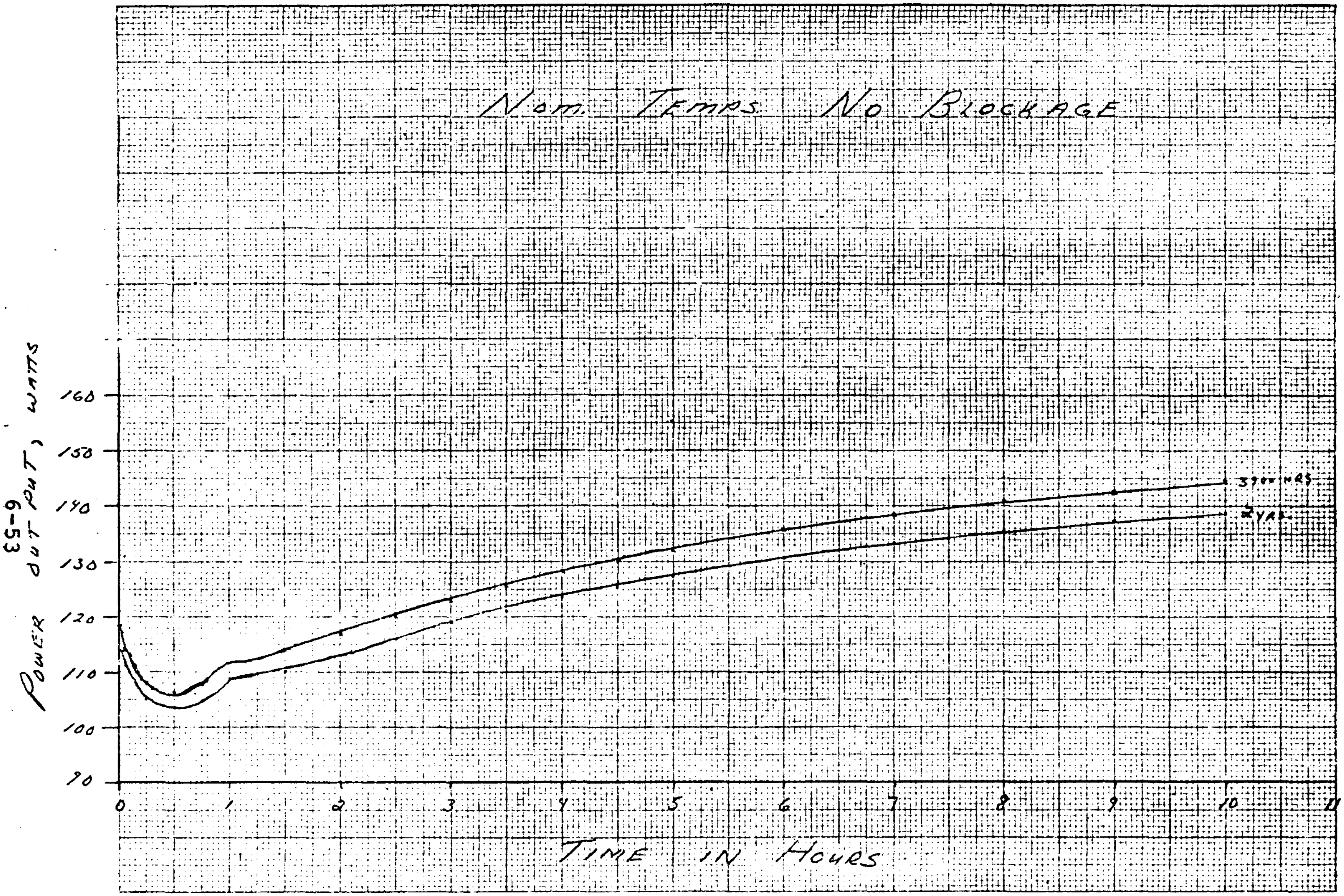
Nom. Temps No Blockage
Power output, watts
90
100
110
120
130
140
150
160
0
1
2
3
4
5
6
7
8
9
10
11
Time in Hours
2 YRS.

FIGURE 6.4.3-1

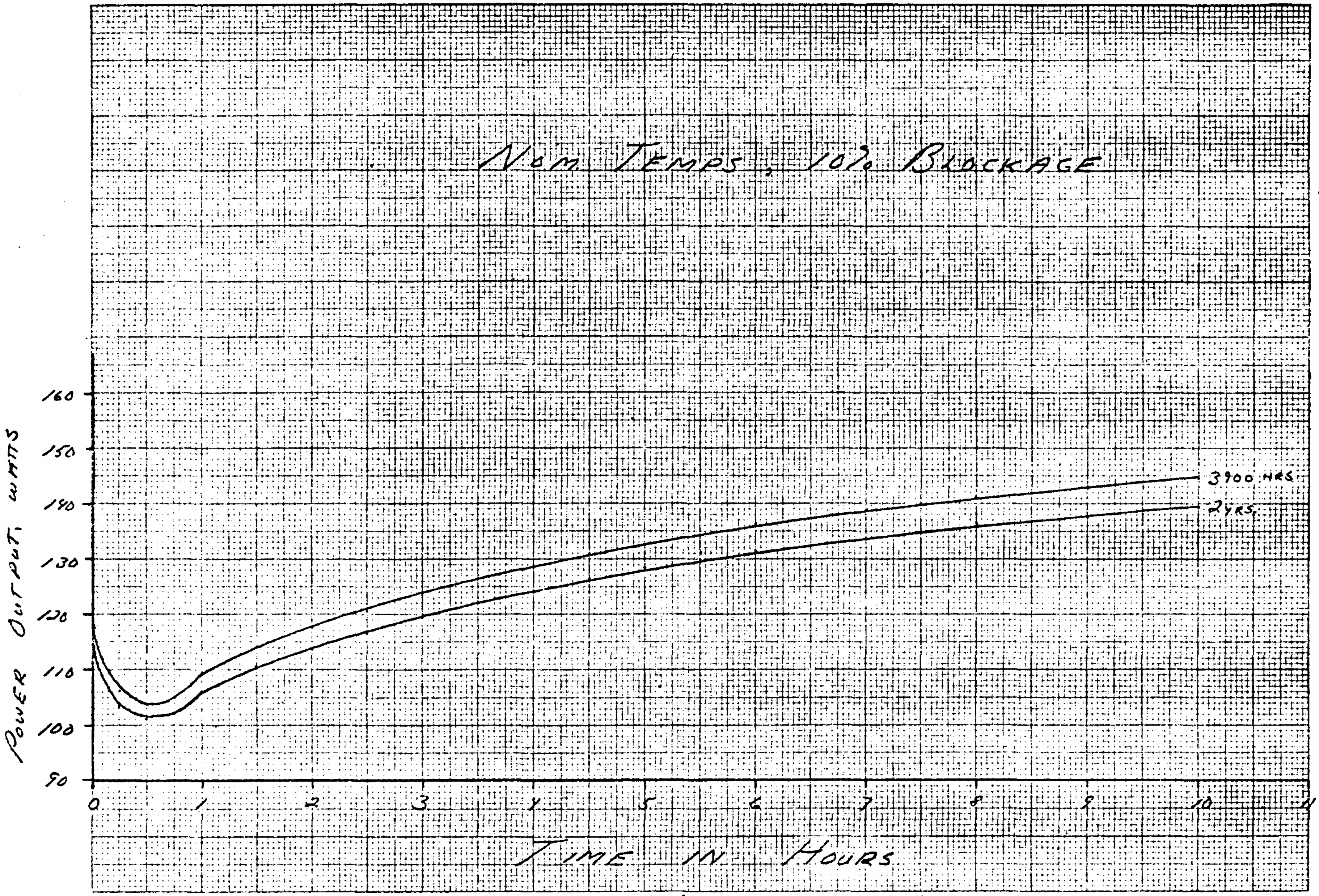
NOM TEMPS, 10% BLOCKAGE
160
150
140
130
120
110
100
90
POWER OUTPUT WATTS
0
1
2
3
4
5
6
7
8
9
10
11
TIME IN HOURS
3900 HRS
2 YRS

FIGURE 6.4.3-2

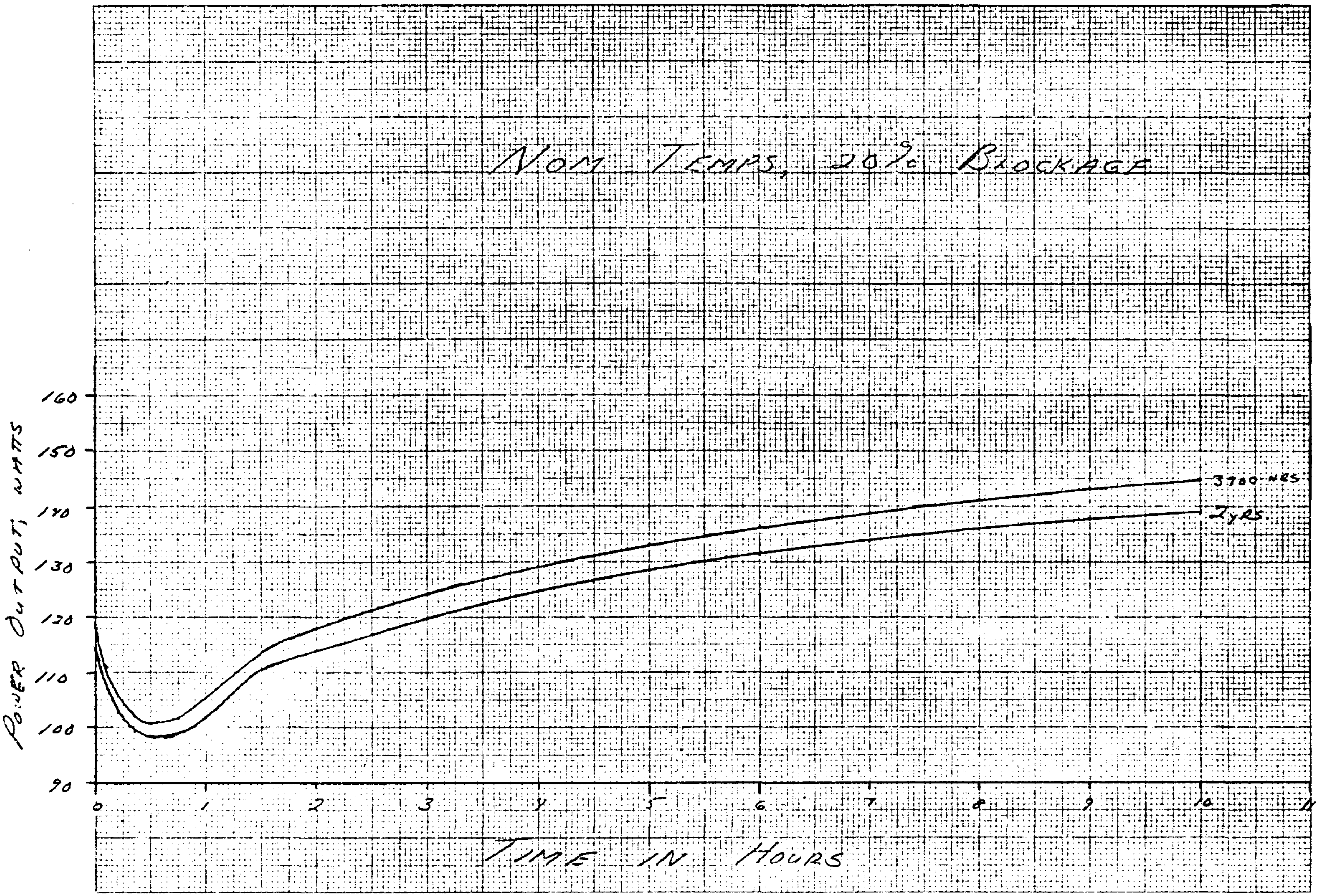
NOM TEMPS, 20% BLOCKAGE
POWER OUTPUT, WATTS
160
150
140
130
120
110
100
90
0
1
2
3
4
5
6
7
8
9
10
11
TIME IN HOURS
3700 HRS
2 YRS

FIGURE 6.4.3-3

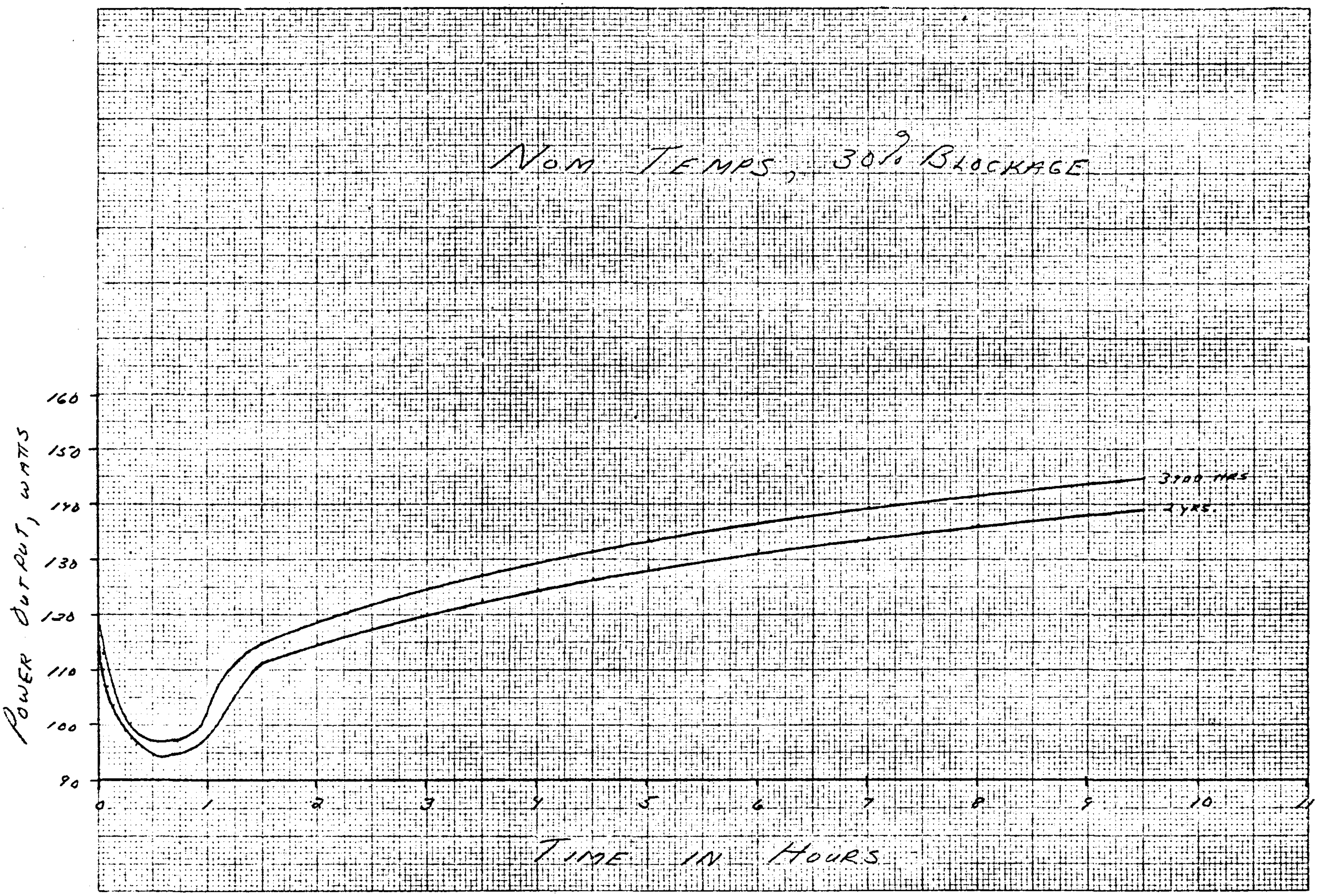
NOM TEMPS, 30% BLOCKAGE
POWER OUTPUT, WATTS
160
150
140
130
120
110
100
90
0
1
2
3
4
5
6
7
8
9
10
11
TIME IN HOURS
3900 HRS
2 YRS.

FIGURE 6.4.3-4

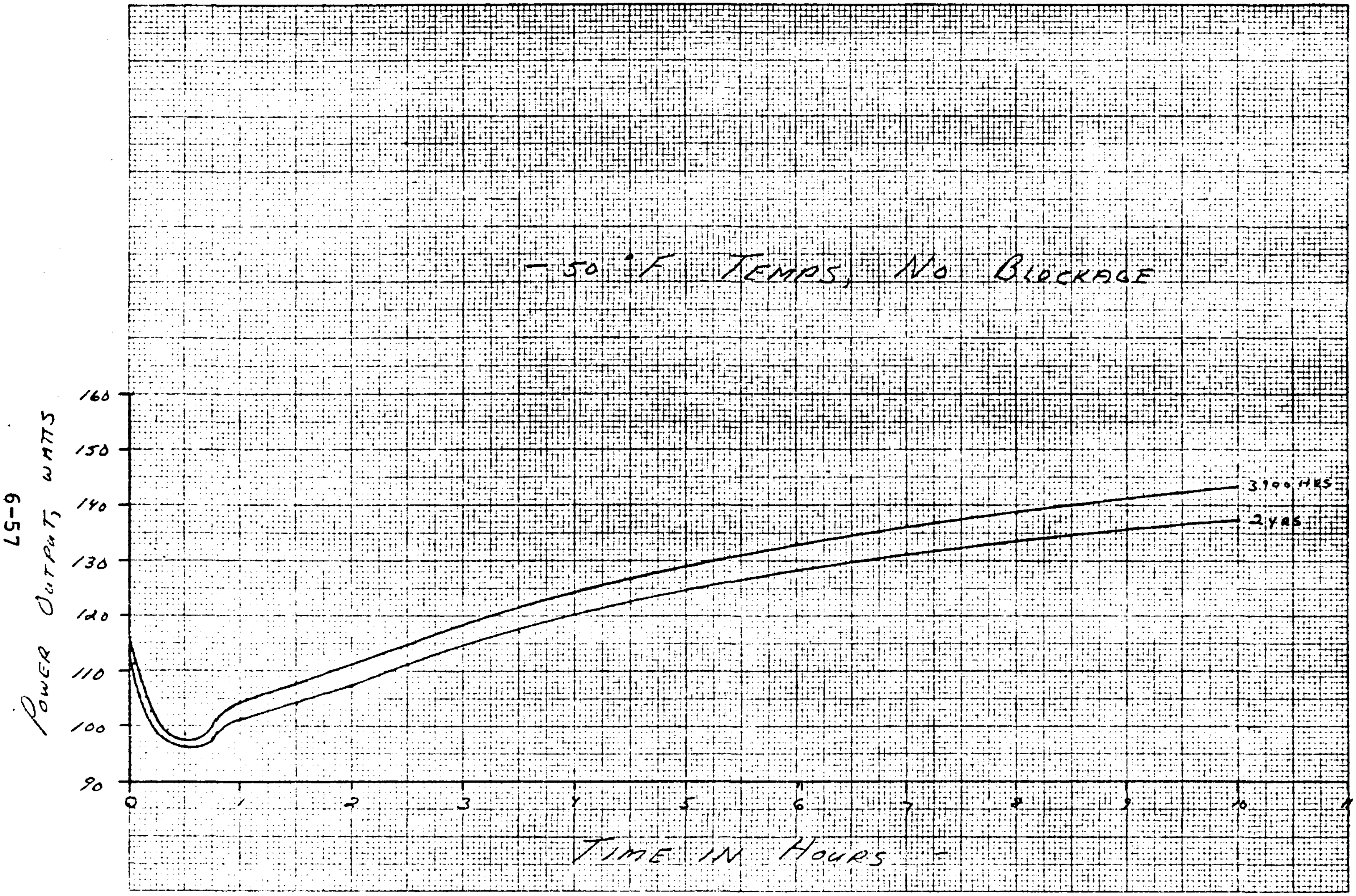
-50 °F Temps, No Blockage
Power Output, Watts
160
150
140
130
120
110
100
90
0
1
2
3
4
5
6
7
8
9
10
11
Time in Hours
3,100 HRS
2 YRS

FIGURE 6.4.3-5

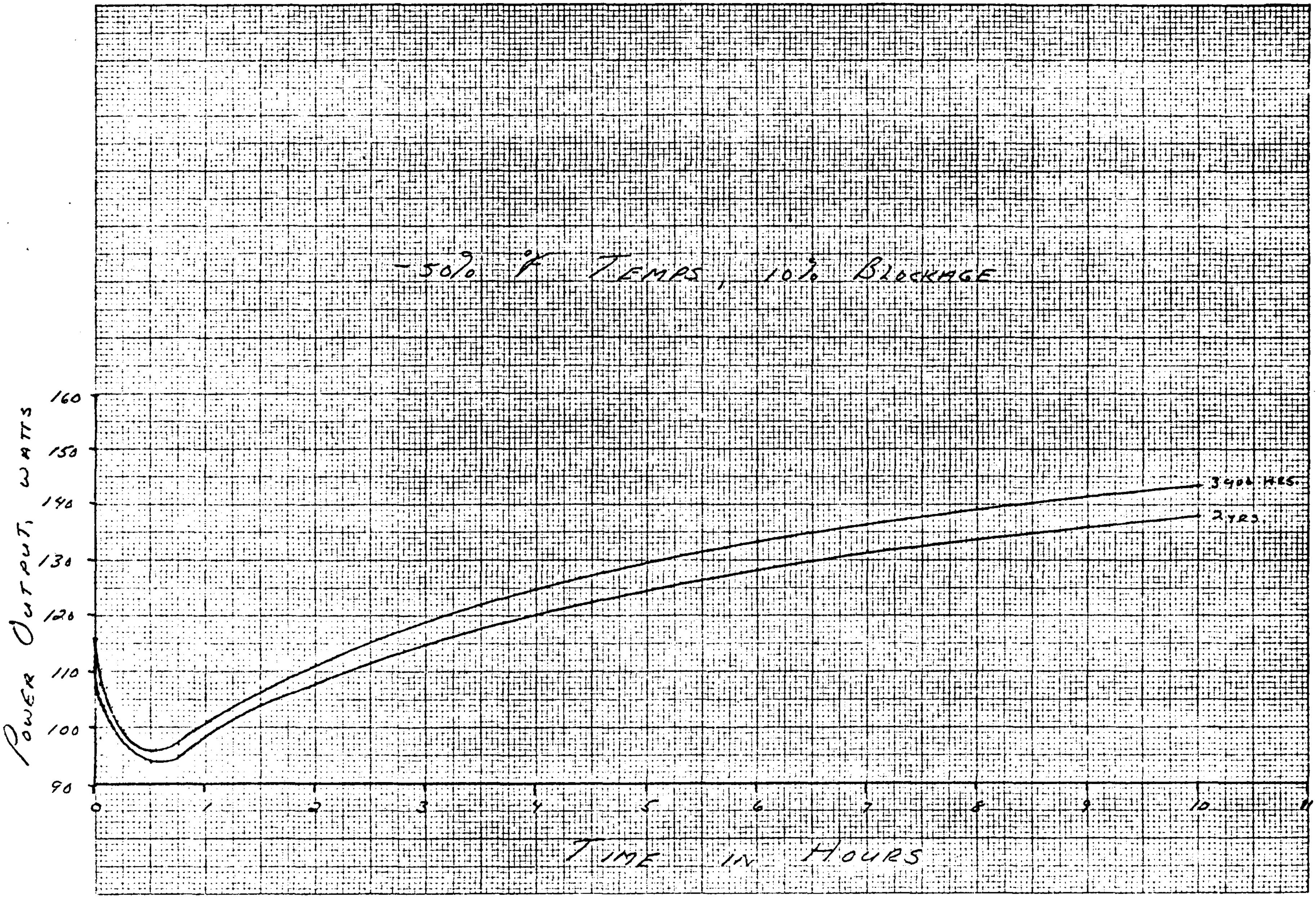

-50°F TEMPS, 10% BLOCKAGE
POWER OUTPUT, WATTS
160
150
140
130
120
110
100
90
0
1
2
3
4
5
6
7
8
9
10
11
TIME IN HOURS
3400 HRS.
2 YRS

FIGURE 6.4.3-6

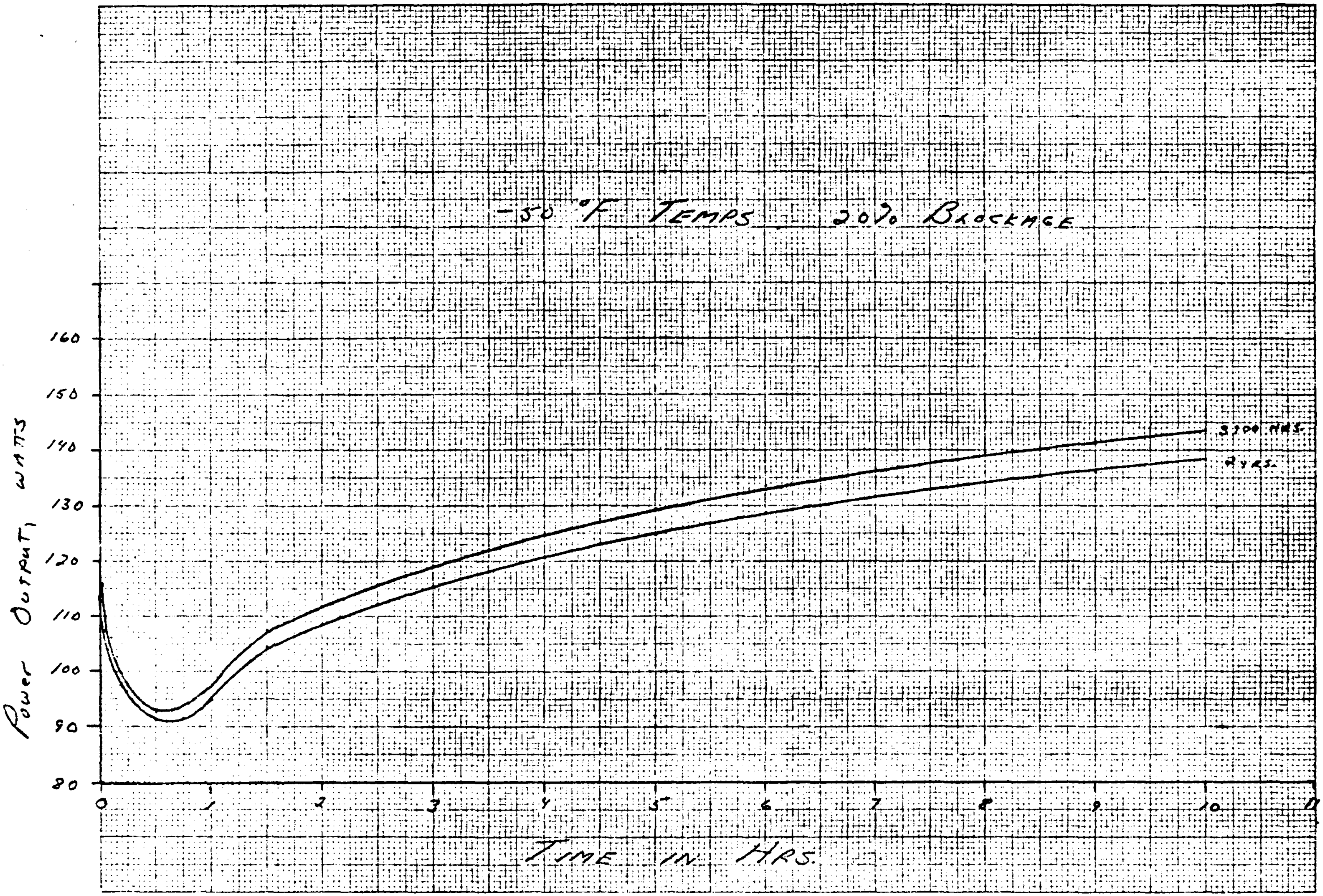
-50 °F TEMPS 20% BLOCKAGE
POWER OUTPUT, WATTS
160
150
140
130
120
110
100
90
80
0
1
2
3
4
5
6
7
8
9
10
11
TIME IN HRS.
3700 HRS.
2 YRS.

FIGURE 6.4.3-7

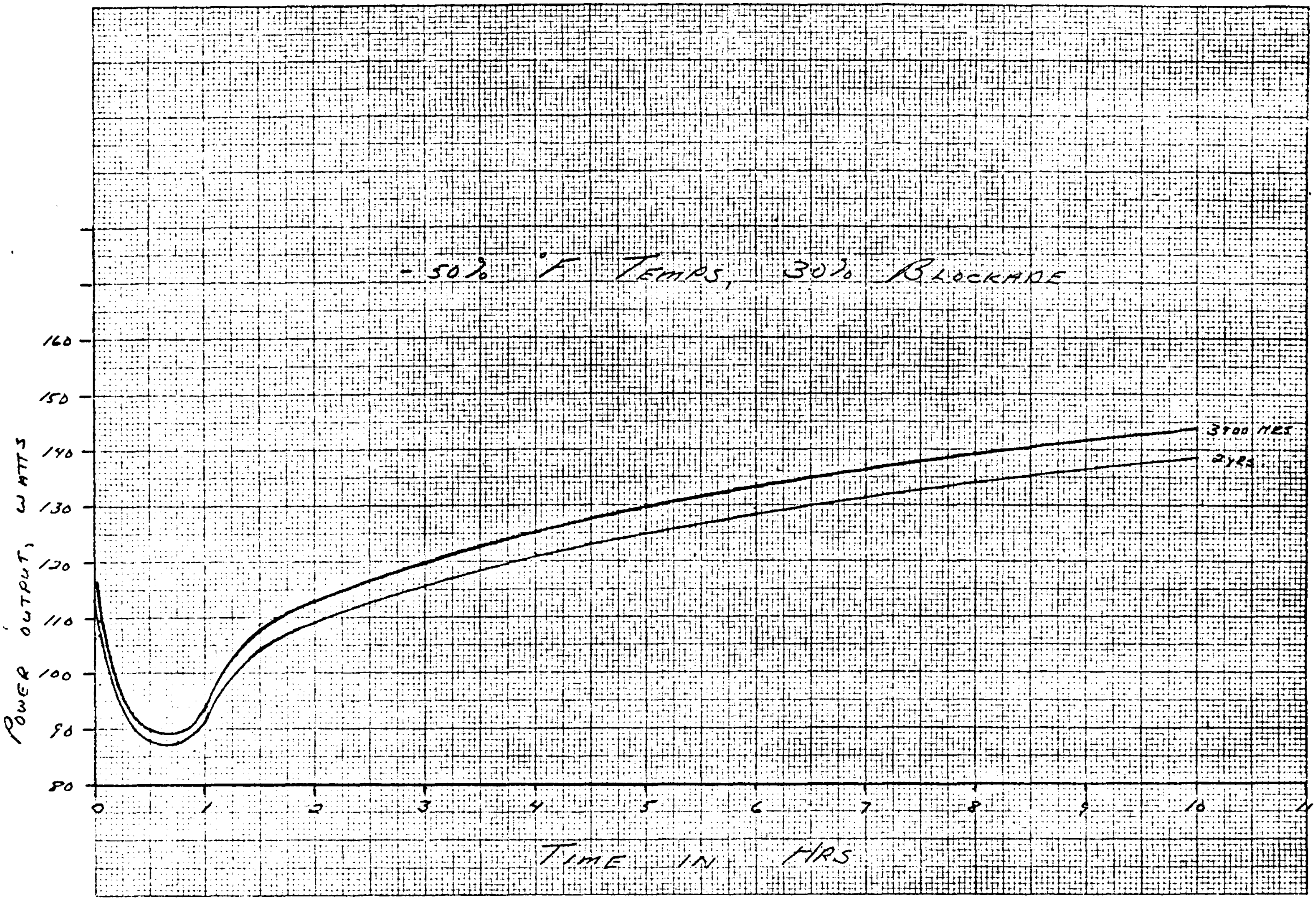
-50% °F TEMPS, 30% BLOCKADE
POWER OUTPUT, WATTS
80
90
100
110
120
130
140
150
160
0
1
2
3
4
5
6
7
8
9
10
11
TIME IN HRS
3900 HRS
2 YRS

FIGURE 6.4.3-8

higher than determined by a detailed review of the TBC-3 converter performance with Xenon. The vacuum stabilized power after 2 years storage is calculated to be 150 watts.

Table 6.4.3-2 shows the initial power, the minimum power and the six and ten hour power for all cases considered thus far.

These results are based on maintaining a gas conductance in the internal heat source gaps between surfaces outside the Iridium PICS. Runs are in progress to determine the effect of changing the gap heat transfer from gas conduction plus radiation to radiation only. It is expected that this effect will cause a further decrease in minimum power point since the reduced heat transfer rate within the heat source will cause a transient drop in the hot junction temperature. The dynamics of the heat source gas evaluation are not known and the initial run will be made with a step function change to obtain worst case results.

In order to increase the confidence in the transient power predictions, two additional analyses are in progress. A thermal model of the electric heat source is being modified to be compatible with the present converter model to compare with the Q1A EHS converter vent test data, and the IHS model is being run with converter venting of Argon at 2.3 hours after chamber venting to compare with the measured power transient of the fueled F-5 flight converter.

TABLE 6.4.3-2

TRANSIENT ANALYSIS RESULTS

	INITIAL POWER	MINIMUM POWER	P 6 HOURS	P 10 HOURS
350°F	114.7	103.7	130.7 - 135.8 (87 TO 91%)	138.9 - 144.5
BLOCKAGE				
10%		101.1	131.2 - 136.3	138.8 - 144.5
20%		98.1	131.2 - 136.3	138.8 - 144.5
30%		94.6	131.4 - 136.5	139.1 - 144.8
400°F	115.7	110.7	133.3 - 138.6 (89 TO 92%)	139.9 - 145.6
10%		108.1	133.6 - 138.9	140.1 - 145.8
20%		104.8	133.9 - 139.2	140.1 - 145.8
30%		101.4	134.1 - 139.4	140.4 - 146.1
300°F	113.6	96.3	128.2 - 133.1 (85 TO 89%)	137.6 - 143.2
10%		93.7	128.5 - 133.4	137.9 - 143.4
20%		91.0	128.7 - 133.6	137.9 - 143.4
30%		87.5	128.9 - 133.9	138.1 - 143.7

6.5 RCA ACTIVITIES

Converter F-13 completed its processing on July 3, 1975 and was shipped to GE on July 8, 1975.

The converter assembly and processing of Converter Q-2 were completed, and the unit was shipped to G.E. on August 22, 1975. The highest initial shunt resistances (after processing at temperature) ever realized were achieved with Converter Q-2; 12.3 $K\Omega$ for Thermopile-to-Foil and 19.7 $K\Omega$ for Thermopile-to-Shell. This is believed due to the additional room temperature outgassing given Q-2 prior to its thermal processing.

Thermopile assembly of Converter E-5 continued during the reporting period. Fabrication in all other areas proceeded at normal yields. The delivery schedule for the next four converters is as follows:

E-5 - 10/17/75
F-6 - 11/25/75
F-7 - 1/8/76
F-8 - 2/4/76

An event of special note is that SNAP-17A Module MTA8A-9 passed the ten year point, more than 87,800 hours of operation at 1050^{o}C hot shoe temperature in vacuum. While the cold side bonds of this device are different from those used on current MHW hardware, the basic SiGe/SiMo Air-Vac structure is similar, and the ten year performance of MTA8A-9 demonstrates in real time the long life capability of the materials. The power output of the device is still over 88% of the output at 500 hours.

Eleven Si_3N_4 first bond coating runs were found to exceed the maximum chlorine content limit. The difficulty was traced to an equipment defect, which was corrected and coating was resumed. Steps were taken to prevent a recurrence of the problem. An NR was submitted to MRB and approved to have the higher chlorine content product used as is and distributed over the remaining seven MJS converters to be fabricated. There would be an approximate increase of 4% in the chlorine level in accordance with this approach, which is considered to have a negligible affect on converter performance.

6.5.1 Thermoelectric Materials Fabrication and Thermocouple Bonding & Unicouple Fabrication

During the reporting period, fabrication proceeded normally in all areas. The problem, previously reported, of inadvertent introduction of unacceptable cold stack ceramic body material by the vendor into some recently shipped lots was resolved by X-ray examination of all cold stack ceramics, cold stack assemblies, and unicouple assemblies made using material from the affected lots. All unacceptable pieces were identified and scrapped from prime inventory. The reject rate for all parts and assemblies was approximately 3 percent.

Table 6.5.1-1 shows the status of the thermoelectric materials fabrication, thermocouple bonding, and unicouple fabrication for each converter.

6.5.2 Foil Insulation Assembly and Thermopile & Converter Assembly

Delineated below is the status as of 8/31/75 of the foil insulation assemblies and thermopile and converter assembly for each converter worked on during the reporting period.

	Inner Moly Frame	T/P Foil Ins. Ass'y	Foil End Cap Assy's	T/P Ass'y	Conv. Ass'y
F-13 (shipped)	C	C	C	C	C
Q-2	C	C	C	C	C
E-5	C	C	C	In Pro	-
F-6	C	In Pro	C	-	-
F-7	In Pro	-	-	-	-

LEGEND: C - Sub-Assembly Completed for that Converter
In Pro - Fabrication of that Assembly is in Progress
\- - Fabrication Has Not Commenced

6.5.3 Testing

6.5.3.1 Module Testing

All modules operated normally during the reporting period, with the exceptions listed in the following paragraphs. Tables 6.5.3-1 through 6.5.3-3 show the status of all units. The performance curves for all devices on test are shown in Figures 6.5.3-1 through 6.5.3-27.

TABLE 6.5.1-1

UNICOUPLE PARTS AND MATERIAL STATUS

(as of 8-31-75)

	T/E Mat'ls.	1st Bond	Si_3N_4 Coating	2nd Bond	Mach. Couple Preass'y.	Cold Stack Ass'y.	Unicouple Ass'y.	Wrapped U/C Ass'y.
Good Req'd./Conv't.	478	421	408	342	335	335	323	320
Fabrication Status:								
F-5	C	C	C	C	C	C	C	C
F-6	C	C	C	C	C	200	35	35
F-7	C	C	C	C	294	-	-	-
F-8	C	C	65	61	-	-	-	-
F-9	C	1	-	-	-	-	-	-
F-10	In Pro	-	-	-	-	-	-	-
Yield History:								
MJS:								
Planned:		88.1%	96.0%	83.9%	97.9%	95.0%	96.4%	99.3%
Actual:								
E-5		87.2	98.8	94.7	99.1	100.0	95.8	98.7
F-6		88.2	98.4	97.4	98.8	98.0*	100.0*	100.0*
F-7		79.6	99.2	95.2	95.5*	-	-	-
F-8		90.3	100.0*	98.4*	-	-	-	-
F-9		100.0*	-	-	-	-	-	-
Overall Inception To Date Yields: (Includes LES 8/9)		84.2%	97.6%	81.3%	95.1%	98.9%	94.2%	99.2%

Legend:

C - Complete Complement of Assemblies Has Been Fabricated

In Pro - Fabrication In Progress

— - Fabrication Has Not Commenced

* - Complement Not Completed, Yields To Date Given

TABLE 6.5.3-1

AIR VAC LIFE TEST STATUS - 18 COUPLE CONVERTERS

Device	Device Description	Type of Test	Average Hours Operation	Average Hot Shoe Temp, °C	Average Cold Shoe Temp. °C	P_{in}	P_o	EL	IL	E_{oc}	Status
18-C	18 TBC Design Couples Moly/Astro Foil	Long Life Vac	19,457	1026	307	156.78	7.896	3.463	2.280	6.868	At Operating Temp.
18-D	18 TBC-3 Design Cpls.-Moly/Astro (Ionization Gauge on Shell) Al_2O_3 Barrier (slip-on)	Long Life Vac (Turbo Stat.)	17,981	1019	303	152.73	7.955	3.548	2.242	6.762	At Operating Temp.
18-E	18 TBC-4 Design Cpls.-Moly/Astro Foil; Al_2O_3 Barrier (slip-on) Iridium Heater Sleeve	Long Life Vac	17,893	1028	306	157.88	7.943	3.496	2.272	6.816	At Operating Temp.
18-G	18 TBC-4 Design Cpls.-Moly/Astro Foil; Al_2O_3 Barrier; Iridium Heater Sleeve removed at 4227 Hrs.	Long Life Vac (Turbo Stat.)	18,607	1027	306	154.20	8.029	3.517	2.283	6.794	At Operating Temp.
18-H	18 TBC-4 Design Cpls.-Moly/Astro Foil	Long Life Vac	18,902	979	299	140.35	7.172	3.495	2.052	6.379	At Operating Temp.
18-O	Si_3N_4 Coated SiMo H.S. (N-P W/Ti, N-P W/O Ti, all P).	Long Life Vac	11,623	1129	305	188.86	10.297	3.500	2.942	7.508	At Operating Temp.

TABLE 6.5.3-1 (CONTINUED)

Device	Device Description	Type of Test	Average Hours Operation	Average Hot Shoe Temp. °C	Average Cold Shoe Temp. °C	P_{in}	P_o	EL	IL	E_{oc}	Status
DC-12A	3 Separate Circuits of 6 Cpls. ea (1-DC-9 type (2-DC-9 type (3-DC-9 type with 28 mil wrap Isothermally Processed to 315°C	Long Life Vac	7,326	1135 (nominal)	287	191.54	9.807	3.441	2.850	7.495	Test terminated because of erratic heater operation. To be shipped to G.E. for post test analysis.
DC-13	.450" SiO_2 Barriers	Long Life Vac	10,228	1035 (nominal)	290	160.83	8.858	3.489	2.539	6.895	At Operating Temp.
SN-1	Like 18-0, except all LES 8/9 Hot Shoes (Si_3N_4 Coated 1st Bonds)	Long Life Vac	9,207	1135 (nominal)*	300	191.22	10.444	3.514	2.972	7.503	At Operating Temp.
SN-2	Like 18-0, except all LES 8/9 Hot Shoes (Si_3N_4 Coated 1st Bonds) Includes provision for sampling residual gas.	Long Life Vac	5,613	1092	304	187.69	10.089	3.513	2.872	7.216	At Operating Temp.
SN-3	Like 18-0, except all LES 8/9 Hot Shoes (Si_3N_4 Coated 1st Bonds) Includes provision for sampling residual gas.	Long Life Vac	6,581	1040	300	167.83	8.796	3.506	2.509	6.811	At Operating Temp.
SN-5	Like SN-1, except one-half of couples have plasma sprayed Al_2O_3 on Heat Shunts.	Long Life Vac	In Proc.	1085 (nominal)	-	-	-	-	-	-	In Processing
		Long Life Vac	21	1038	295	160.96	9.09	3.56	2.55	6.38	At Operating Temp.
SN-6	Like SN-5										

NOTE: Nominal temperature shown where converter has no hot shoe instrumentation

* All hot shoe instrumentation deteriorating. Nominal temperature determined from open circuit voltage.

TABLE 6.5.3-2

AIR-VAC LIFE TEST STATUS

4-COUPLE PCMS

Device Designation	Principle Feature	Test Temp. Hot Shoe	Hours	Status (8/18/75)
PCM 1	Q1 Unicouple Design-Control	1035°C	11,160	At Temp.
2	Q1 Unicouple Design-Control	1085	11,160	At Temp.
3	Q1 Unicouple Design-Control	1135	11,160	At Temp.
4	Q1A Unicouple Design-Control	1135	11,160	At Temp.
5	Simulated Unicouple	1135	10,952	At Temp.
6	JB-40 and UT6-ST-Graphite H.S.	1015	11,669	At Temp.
7	JB-40 and UT6-ST-Graphite H.S.	1115	10,952	At Temp.
8	JB-40 and UT6-ST-Graphite H.S. Si_3N_4 Coated	1115	10,952	At Temp.
9	Si_3N_4 Coated N-P W/Ti & W/O Ti SiMo H.S.	1035	11,670	At Temp.
10	Si_3N_4 Coated N-P W/Ti & W/O Ti SiMo H.S.	1085	11,669	At Temp.
14	Same as PCM's 9-10 plus Si_3N_4 Coated Al_2O_3	1135	9,789	At Temp.
15	Si_3N_4 Coated Hot Shoes Only	1135	7,735	At Temp.
16	Si_3N_4 Coated Legs Only	1135	7,737	At Temp.
17(R)	Special Construction to determine Location of Leakage	1135	8,973	At Temp.
18	Si_3N_4 Coated (Interim Facility)	1135	5,275	At Temp.
PD-2	1 Cpl. N-P W/Ti; 3 Cpls. N-P W/O Ti	1035	17,496	At Temp.
PD-3	All P SiMo H.S.	1035	12,604	At Temp.

TABLE 6.5.3-3

RCA SiGe THERMOELECTRIC MODULE LIFE TESTS - SNAP 17A MODULES

DATE 8/19/75

Module Number	Module Hours Total	Number of Couples	Leg Dia. Inches	Vac. Torr	Nominal T_h °C	Measured T_h °C	Measured T_c °C	Measured ΔT °C	Normalizing ΔT °C	R mΩ per cpl	E_{oc} Mv Per Couple Normalized	P_o mw Per Couple Normalized	% of 500 Hour Po	Couple Hours
MTA4-5	91,136	6	.230	$1x10^{-6}$	850	854	251	603	606	84.0	262	204	75.6	546,816
MTA7-10	88,005	6	.275	$1x10^{-6}$	850	851	295	556	606	84.3	347	357	95.7	528,030
MTA8A-9	87,838	4	.275	$1x10^{-6}$	1050	1049	373	676	606	78.0	334	358	88.2*	430,332
MTA8A-18	87,448	6	.275	$1x10^{-6}$	825	825	275	550	612	76.0	331	360	88.9	524,688
MTA9-1	88,633	14	.275	Air	325	846	190	656	612	73.1	273	255	75.9	1,240,862

*Adjusted for removal of 2 couples at 39,210 hours.
See May 69 report for details.

TOTAL COUPLE HOURS 3,270,728

REMARKS: Air Module MTA9-1 cycled to room temperature after test on 8-19-75. To replace defective furnace heaters.

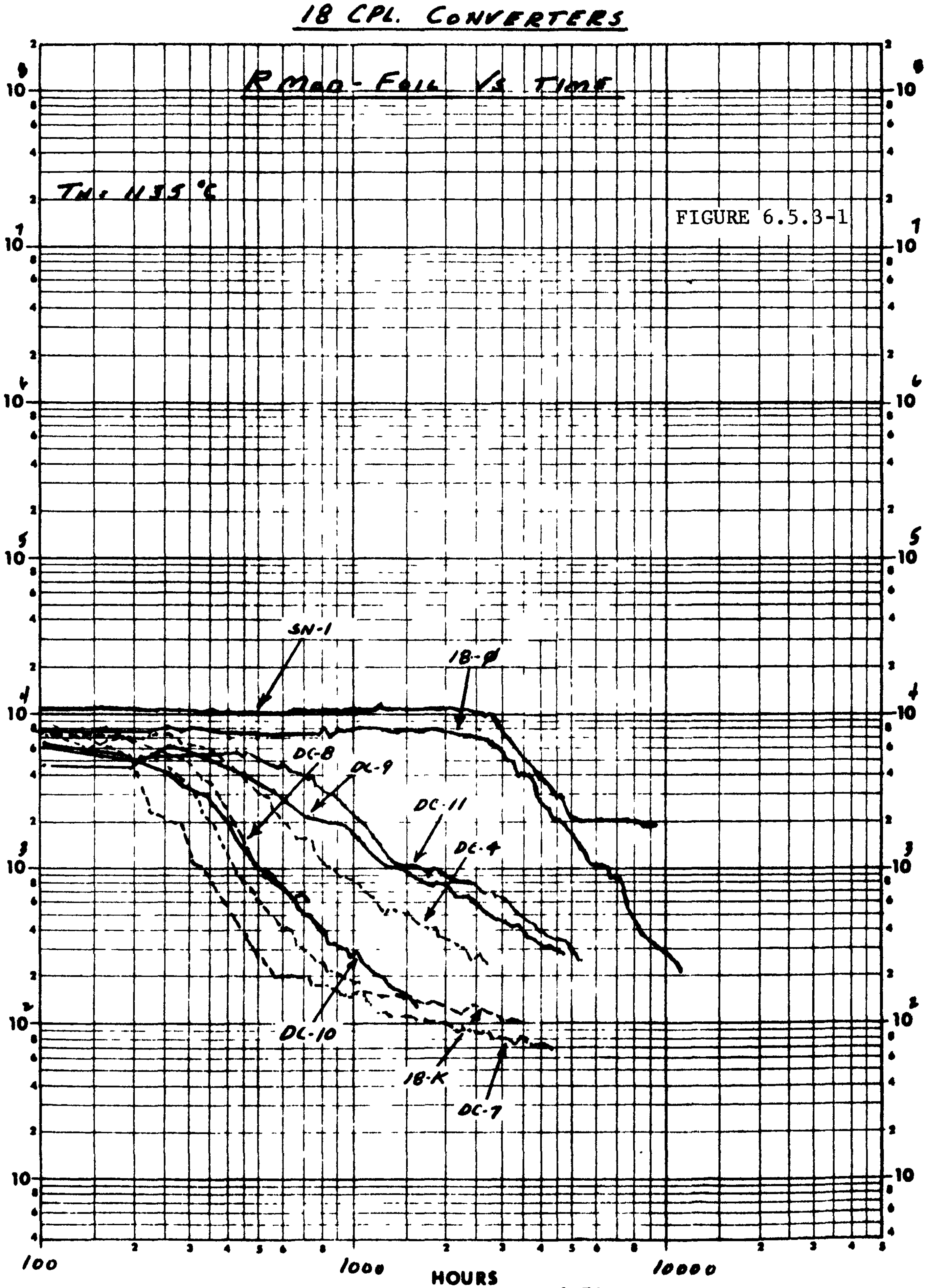
18 CPL. CONVERTERS
R MOD-FOIL VS TIME
TH = 1135 °C
FIGURE 6.5.3-1
SN-1
18-Ø
DC-8
DC-9
DC-11
DC-4
DC-10
18-K
DC-7
100
1000
10000
HOURS

18 CPL CONVERTERS
RMOD-SHELL AND RSHELL-FOIL VS TIME

FIGURE 6.5.3-2

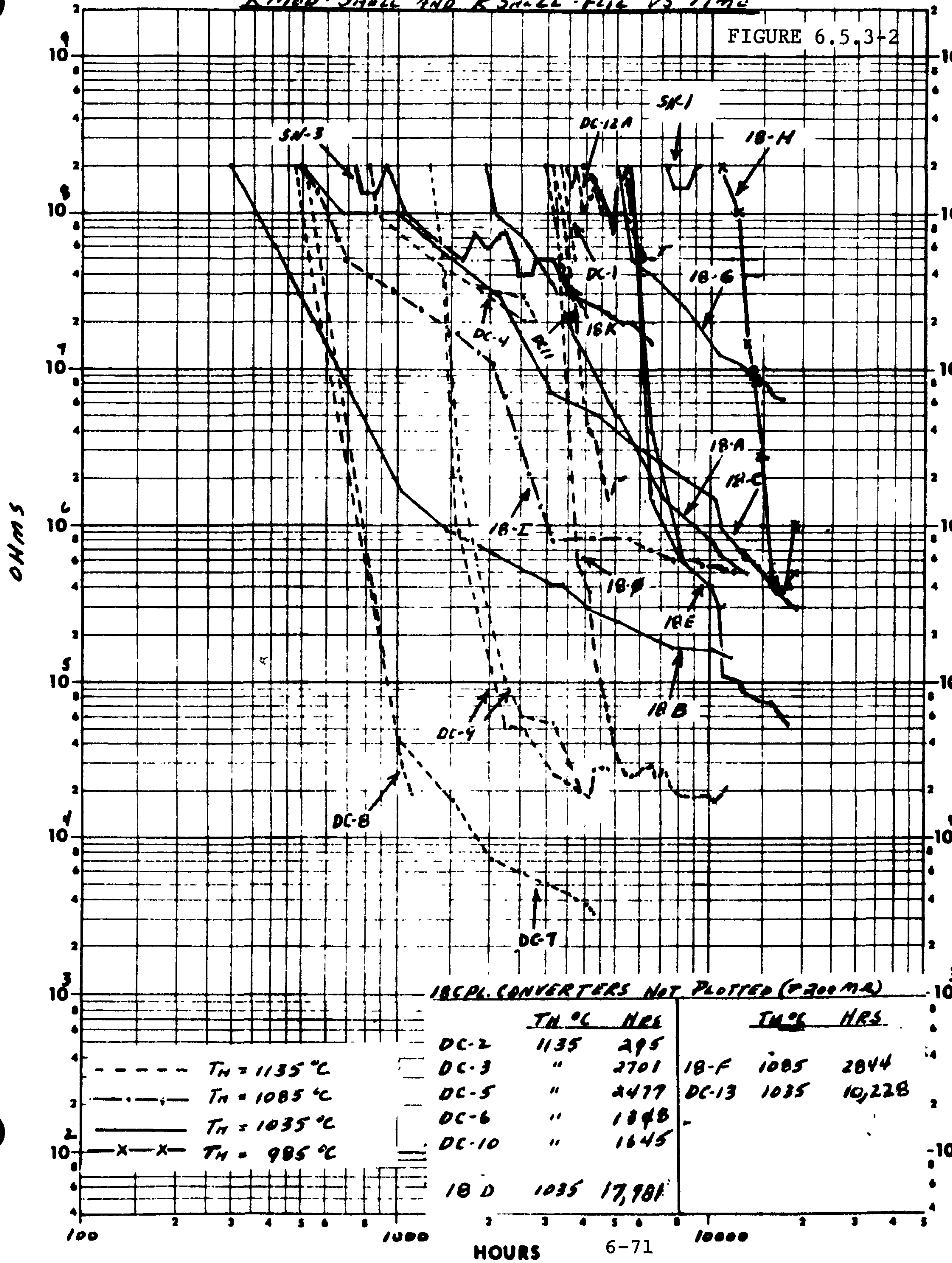

18CPL CONVERTERS NOT PLOTTED (>200 MA)

	T_H °C	HRS
DC-2	1135	295
DC-3	"	2701
DC-5	"	2477
DC-6	"	1848
DC-10	"	1645
18 D	1035	17,981
18-F	1085	2844
DC-13	1035	10,228

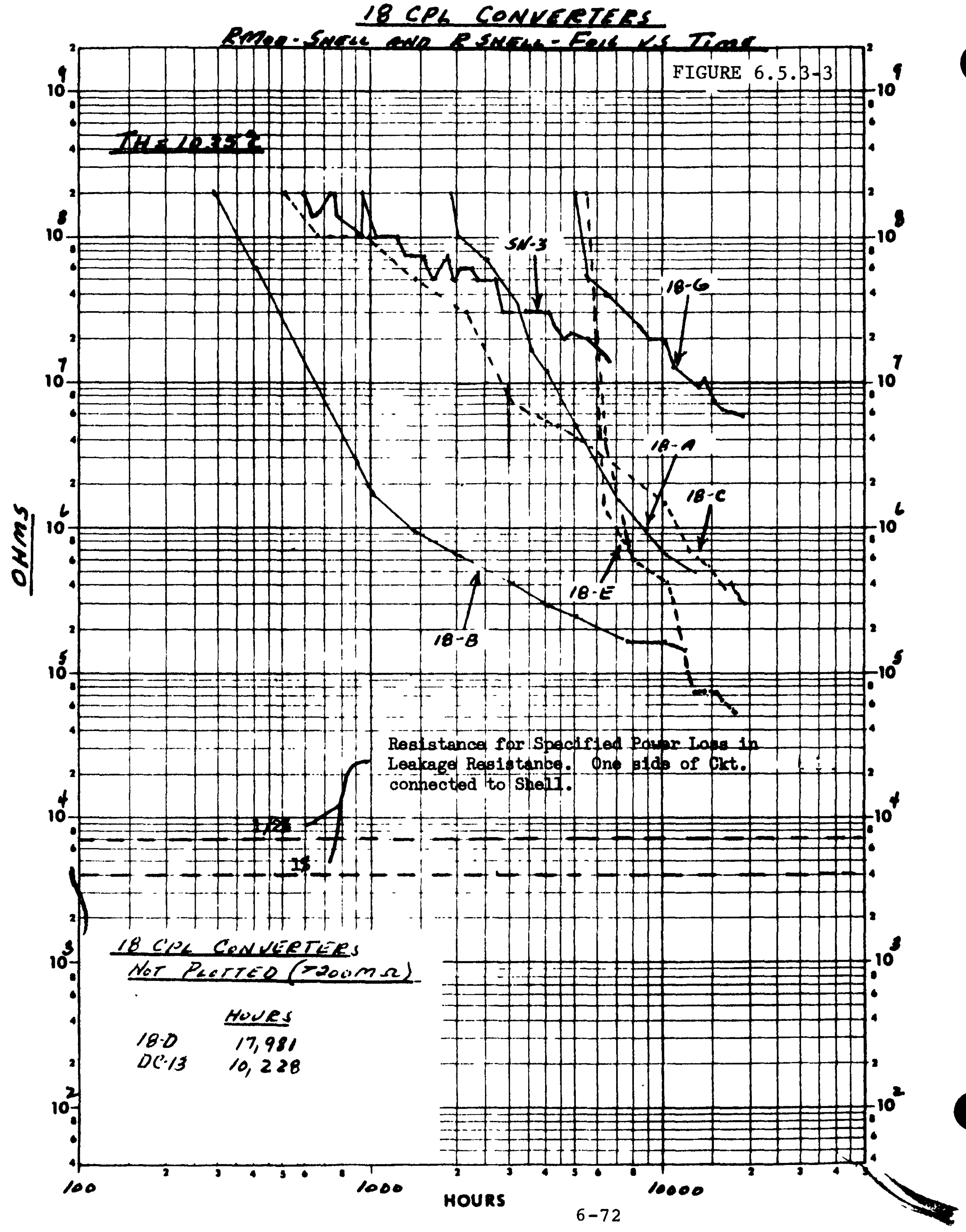
18 CPL CONVERTERS
RMOD-SHELL AND RSHELL-FOIL VS TIME
FIGURE 6.5.3-3
TH=1035°C
OHMS
HOURS
SN-3
18-G
18-A
18-C
18-E
18-B
Resistance for Specified Power Loss in Leakage Resistance. One side of Ckt. connected to Shell.
1/2%
1%
18 CPL CONVERTERS
NOT PLOTTED (>200 MΩ)
HOURS
18-D 17,981
DC-13 10,228

18 CPL CONVERTERS
RMOD-SHELL AND RSHELL-FOIL VS TIME

FIGURE 6.5.3-4

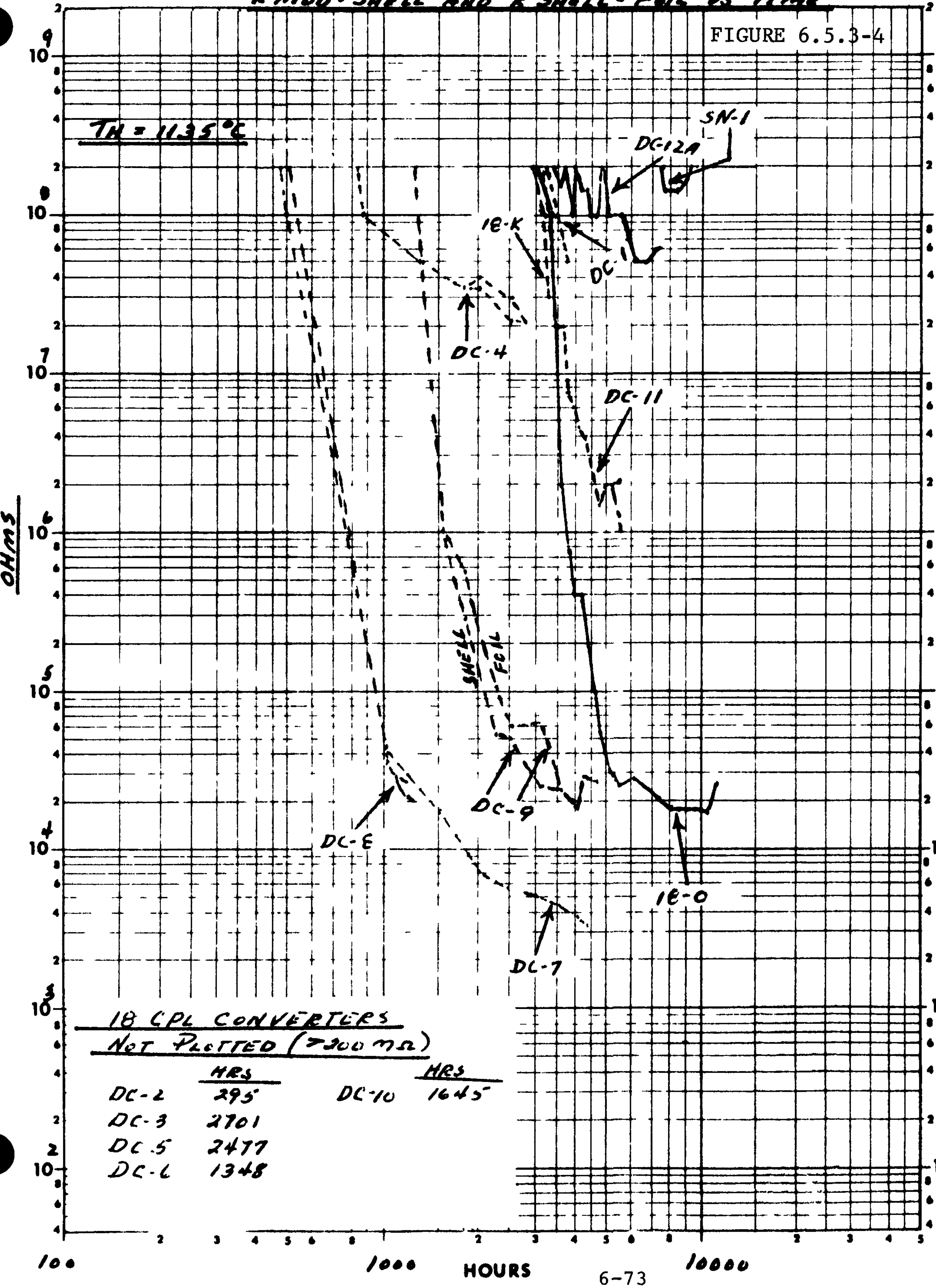

18 CPL CONVERTERS
RMOD-SHELL AND R SHELL-FOIL VS TIME

FIGURE 6.5.3-5

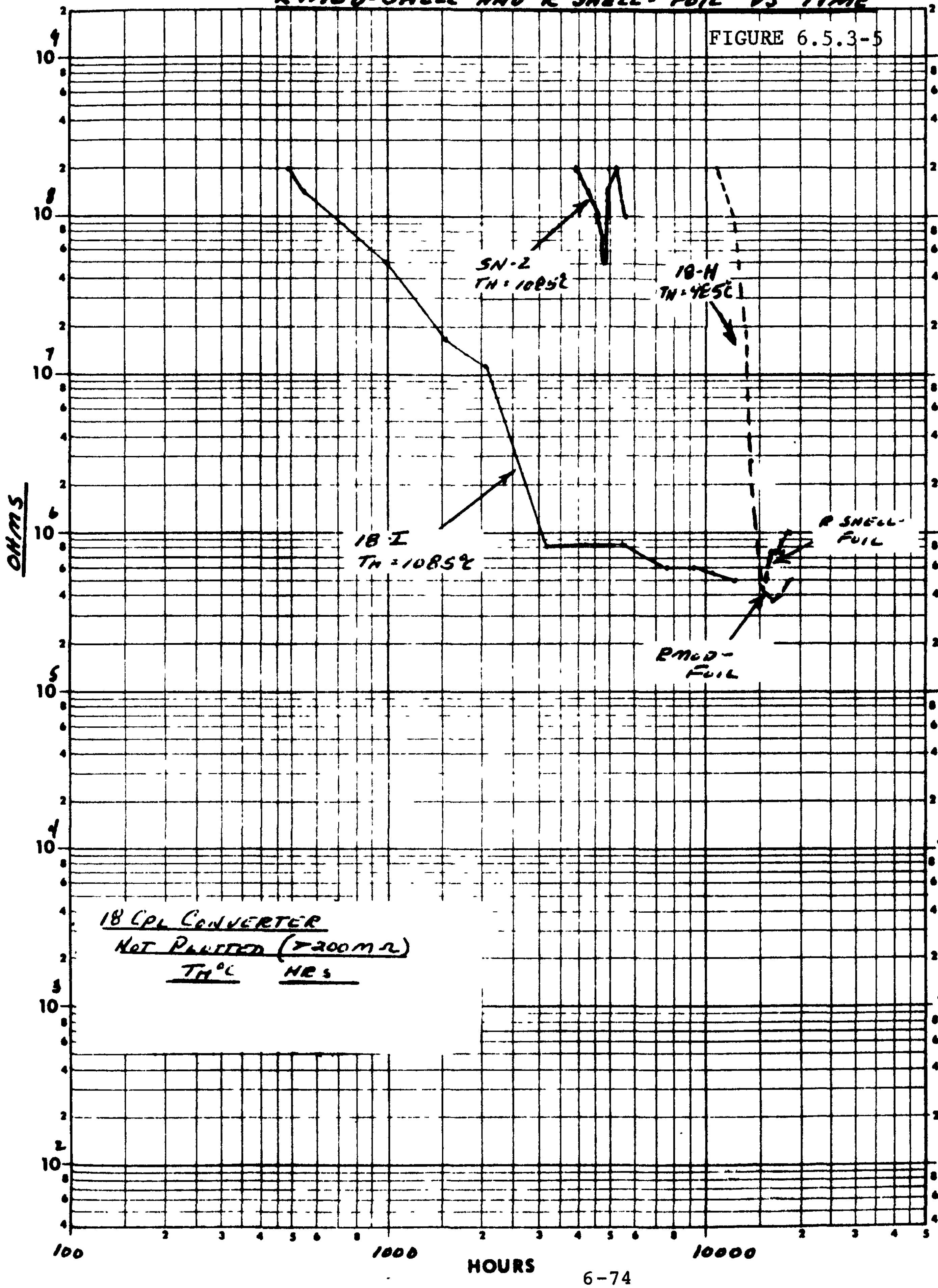

18-φ CONVERTER

LEAKAGE RESISTANCE VS. TIME AT TEMP.

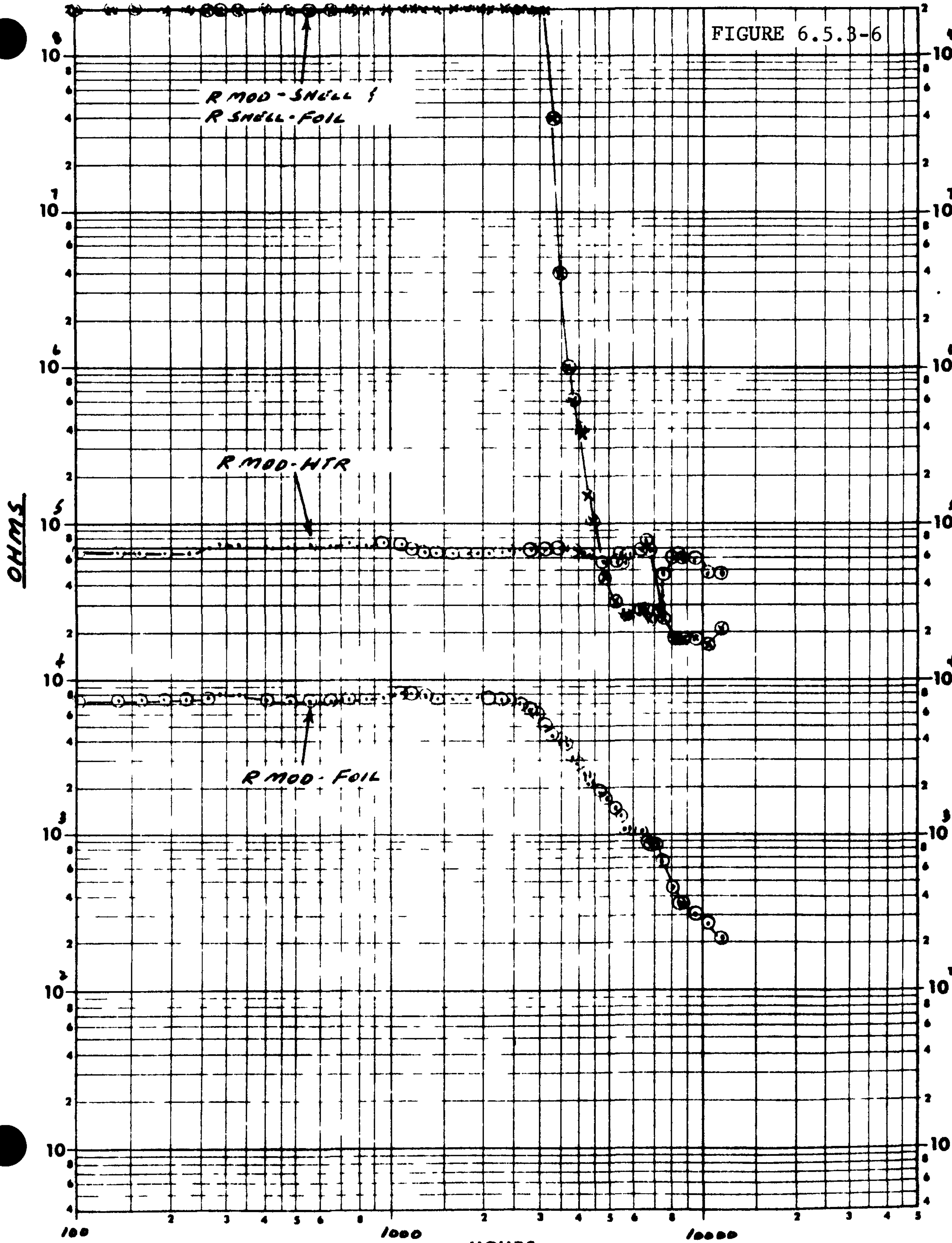

FIGURE 6.5.3-7

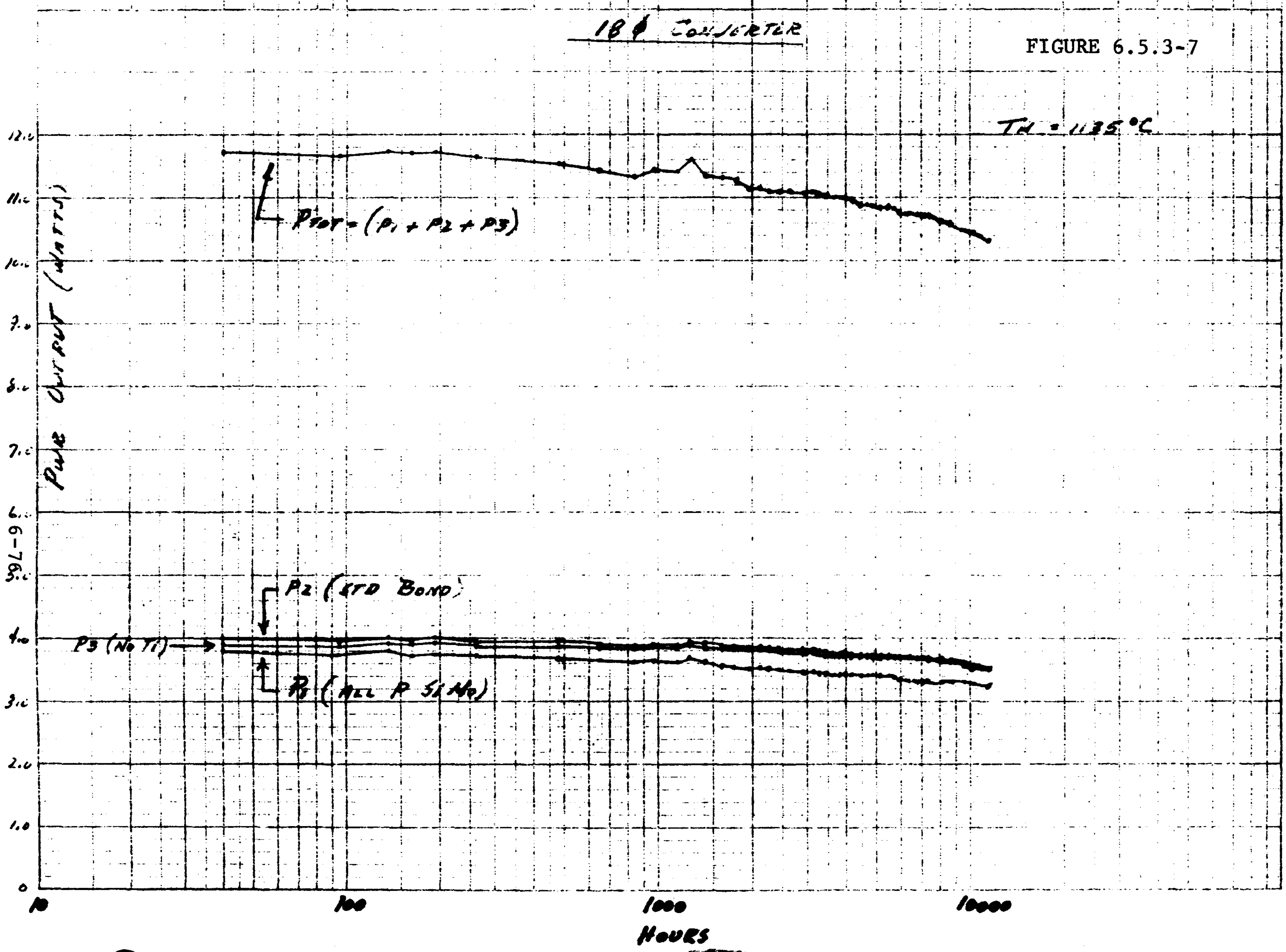
18 ϕ CONVERTER
TH = 1135°C
PTOT = (P1 + P2 + P3)
P2 (STD BOND)
P3 (NO TI)
P1 (ALL P SI NO)
PEAK OUTPUT (WATTS)
12.0
11.0
10.0
9.0
8.0
7.0
6.0
5.0
4.0
3.0
2.0
1.0
0
10
100
1000
10000
HOURS

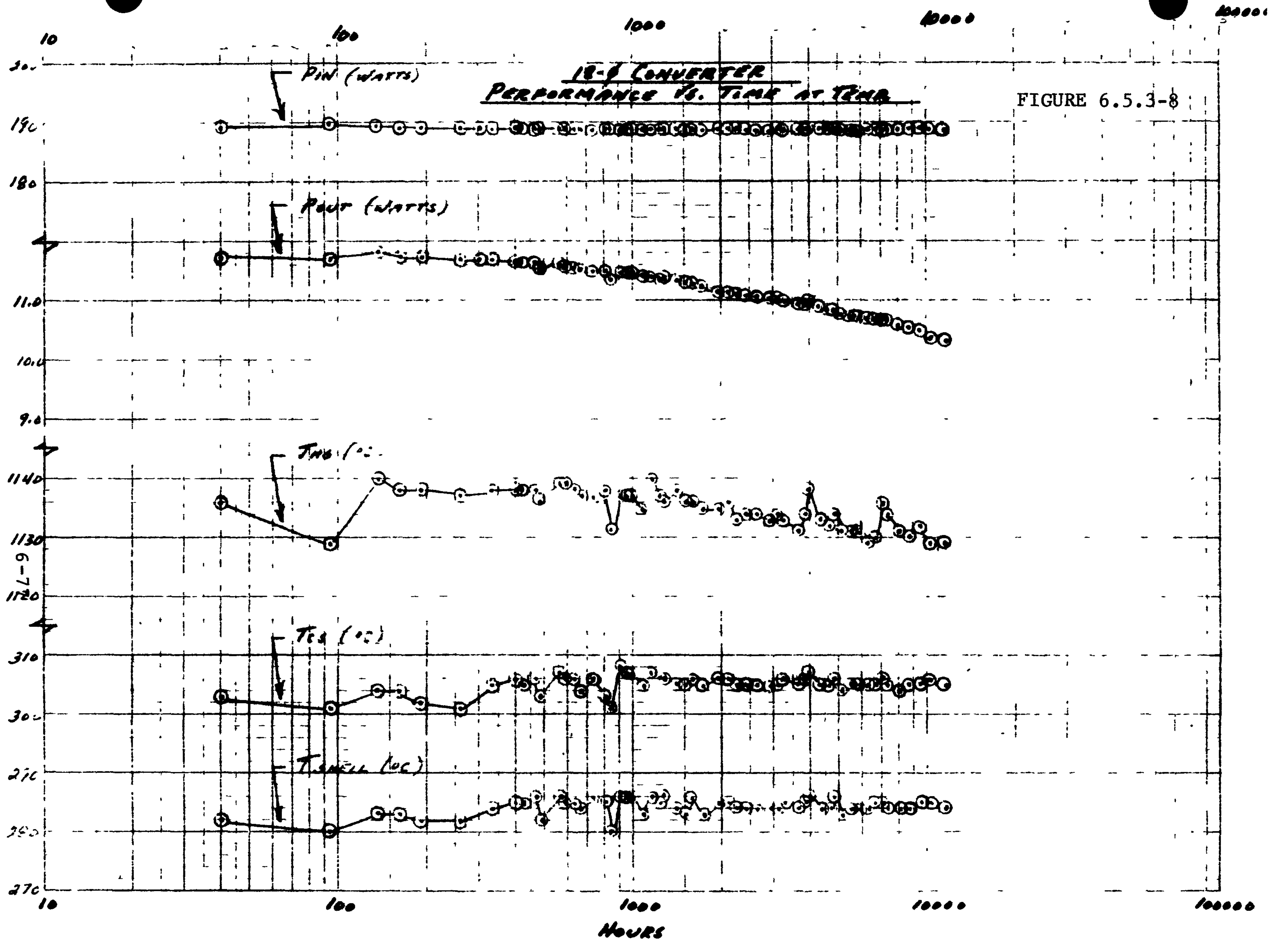
CONVERTER
PERFORMANCE VS. TIME AT TEMP
PIN (WATTS)
POUT (WATTS)
TCS (°C)
HOURS
10
100
1000
10000
100000
180
11.0
10.0
9.0
1140
1130
310

FIGURE 6.5.3-8

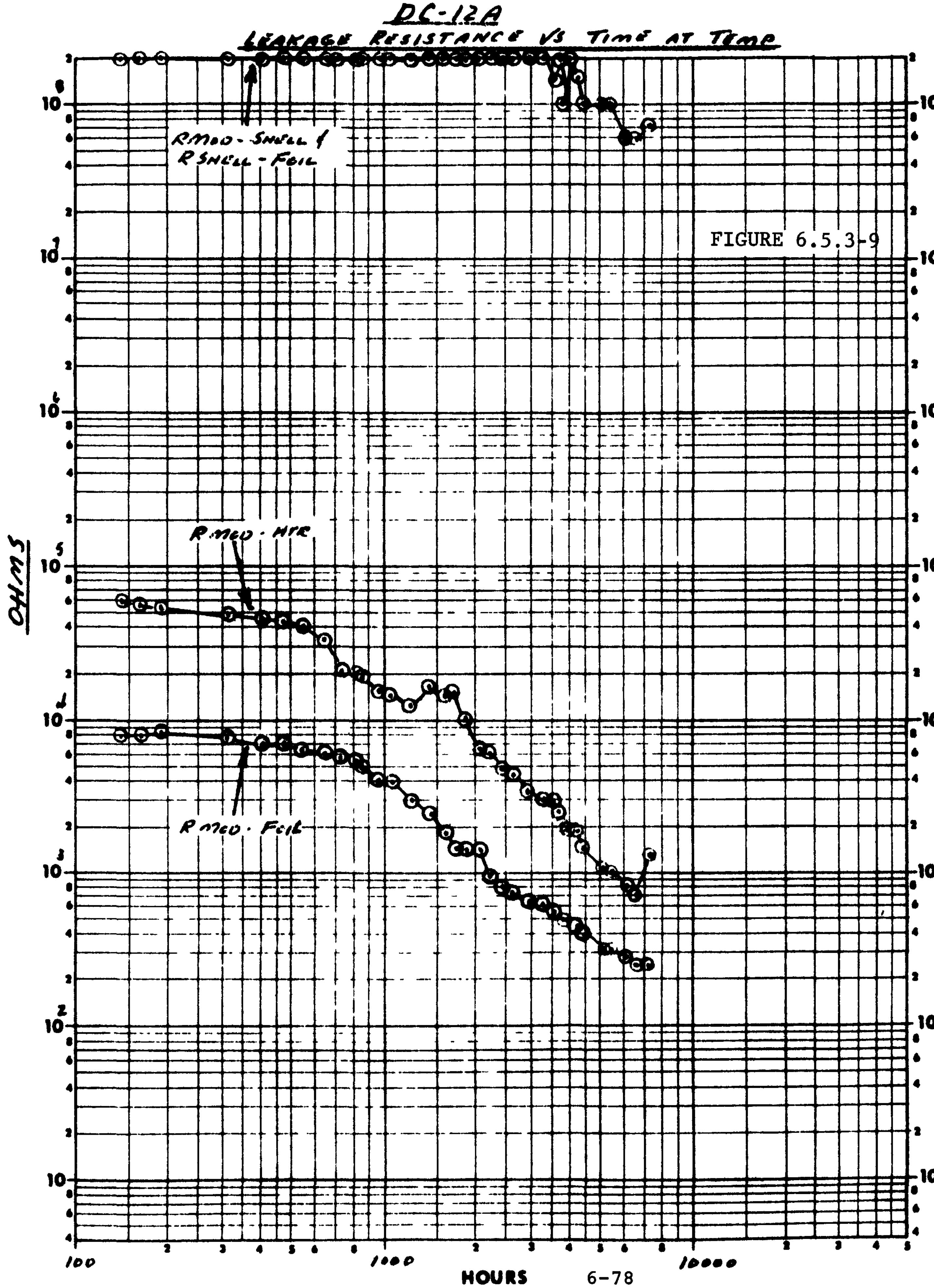
DC-12A
LEAKAGE RESISTANCE VS TIME AT TEMP
RMOD - SHELL &
RSHELL - FOIL
R MOD - HTR
R MOD - FOIL
OHMS
HOURS

FIGURE 6.5.3-9

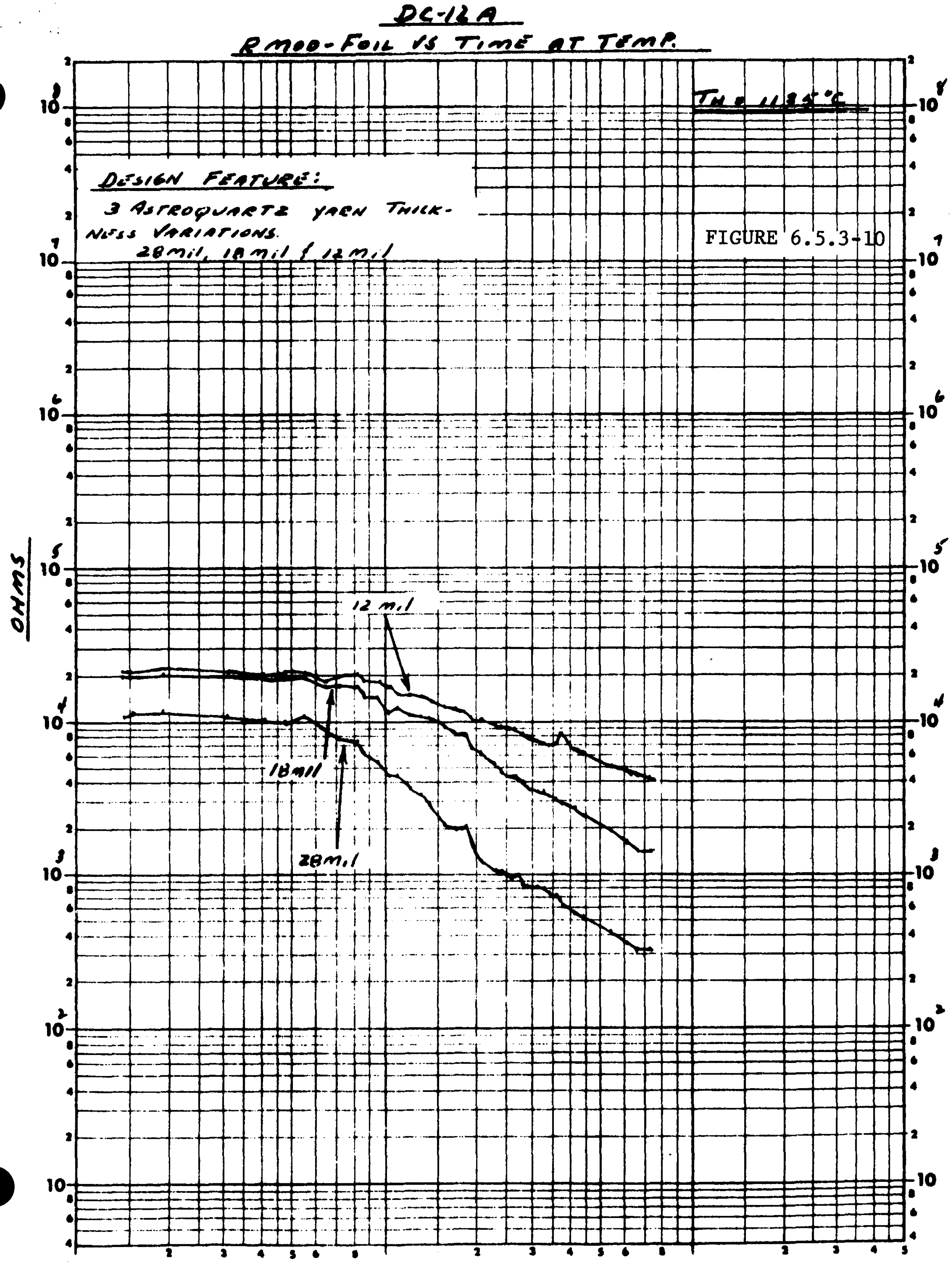

DC-12A
RMOD-FOIL VS TIME AT TEMP.
TH = 1135°C
DESIGN FEATURE:
3 ASTROQUARTZ YARN THICK-NESS VARIATIONS.
28mil, 18mil & 12mil
FIGURE 6.5.3-10
12 mil
18mil
28mil
OHMS
HOURS
100
1,000
10,000

FIGURE 6.5.3-11

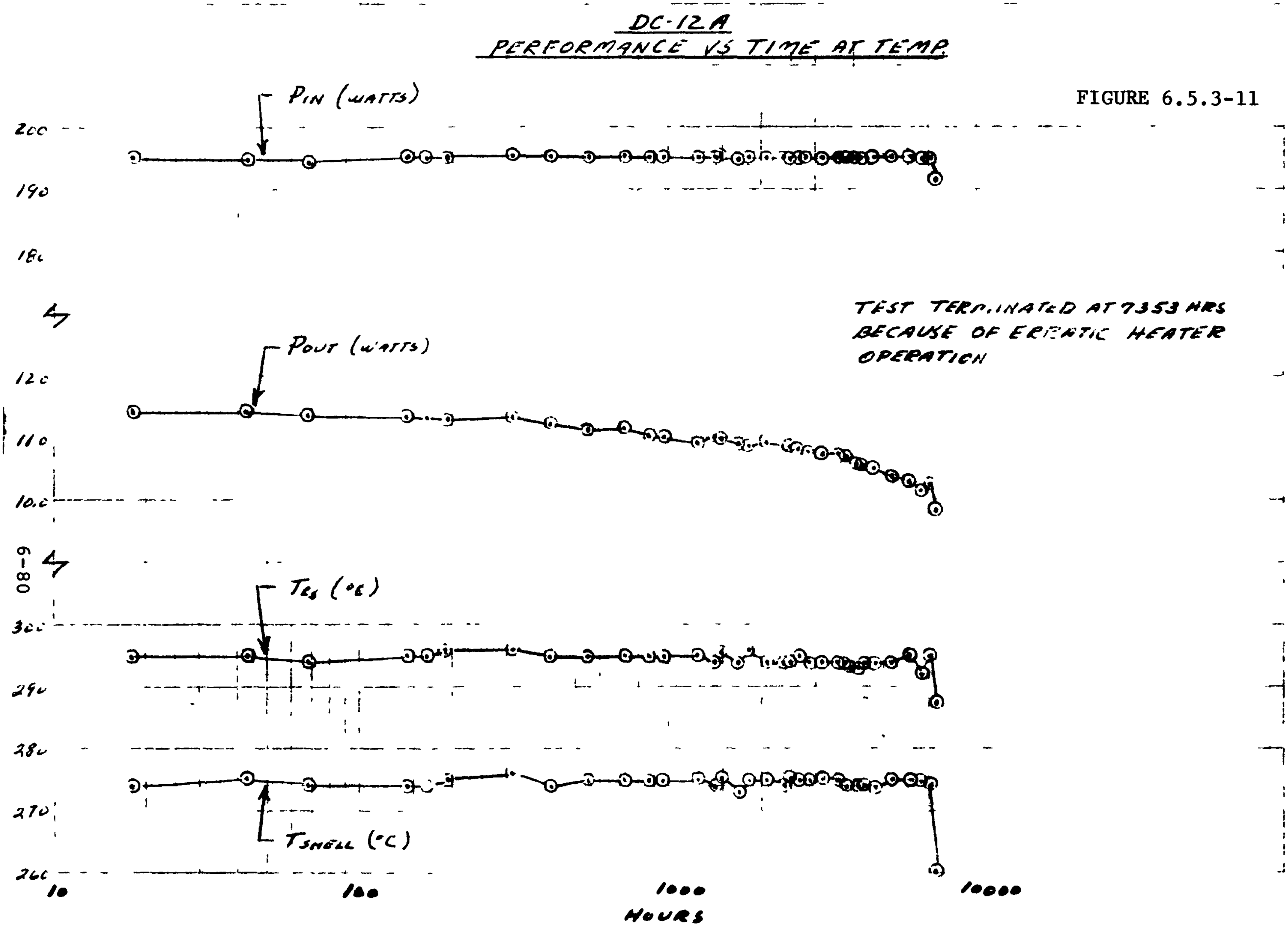

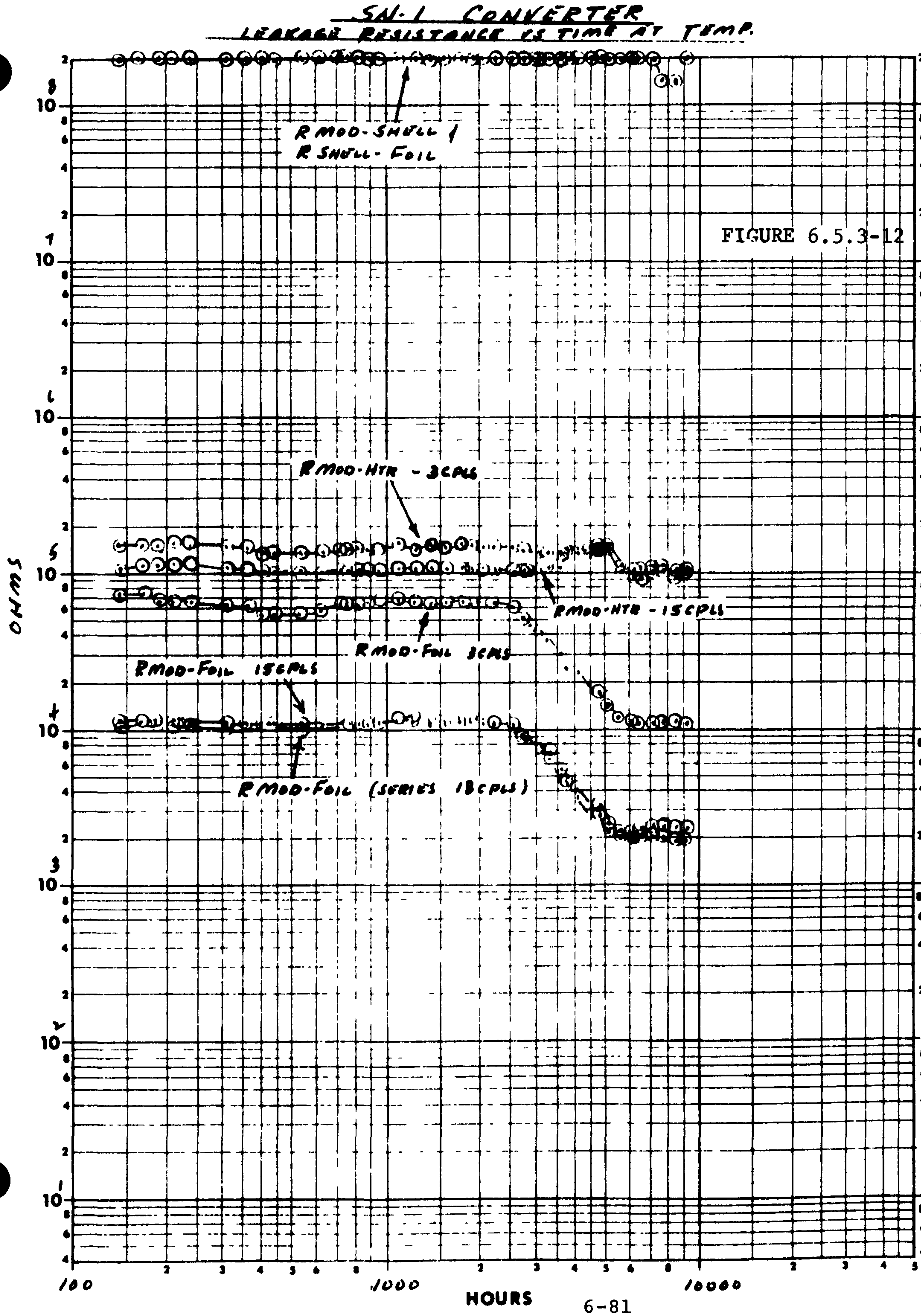

FIGURE 6.5.3-12

FIGURE 6.5.3-13

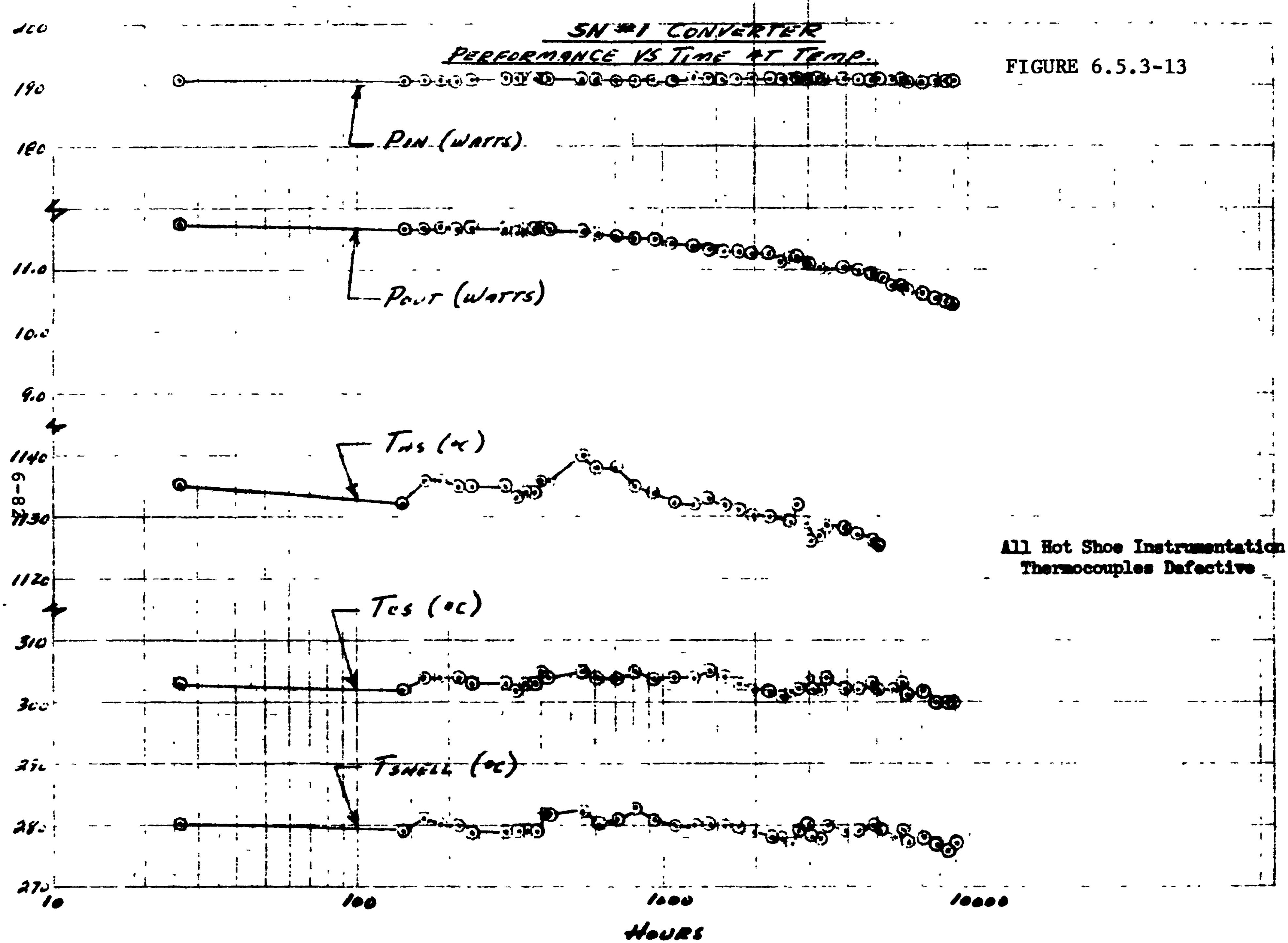

6-87

MOD - FOIL RESISTANCE

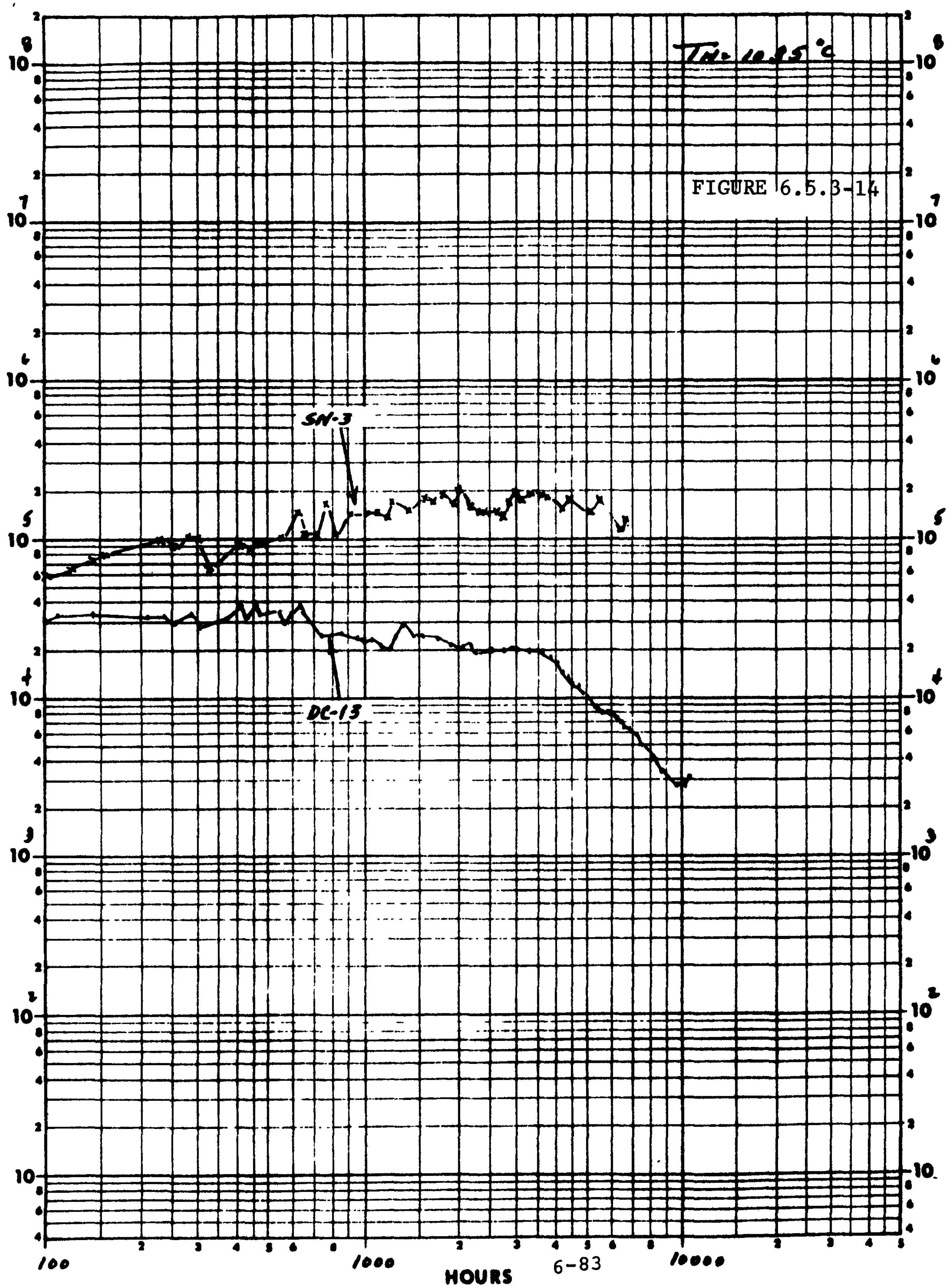

FIGURE 6.5.3-14

FIGURE 6.5.3-15

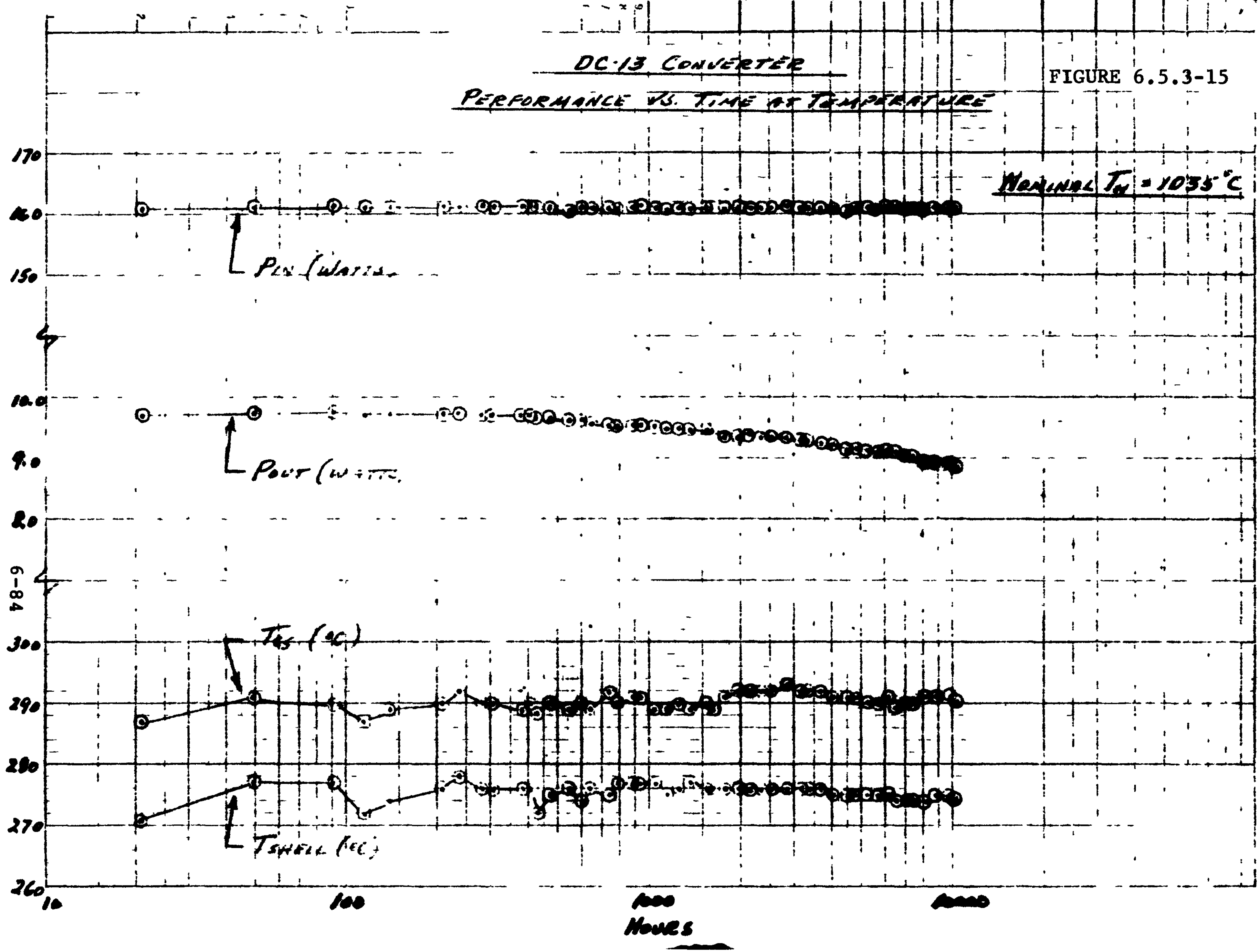

DC-13

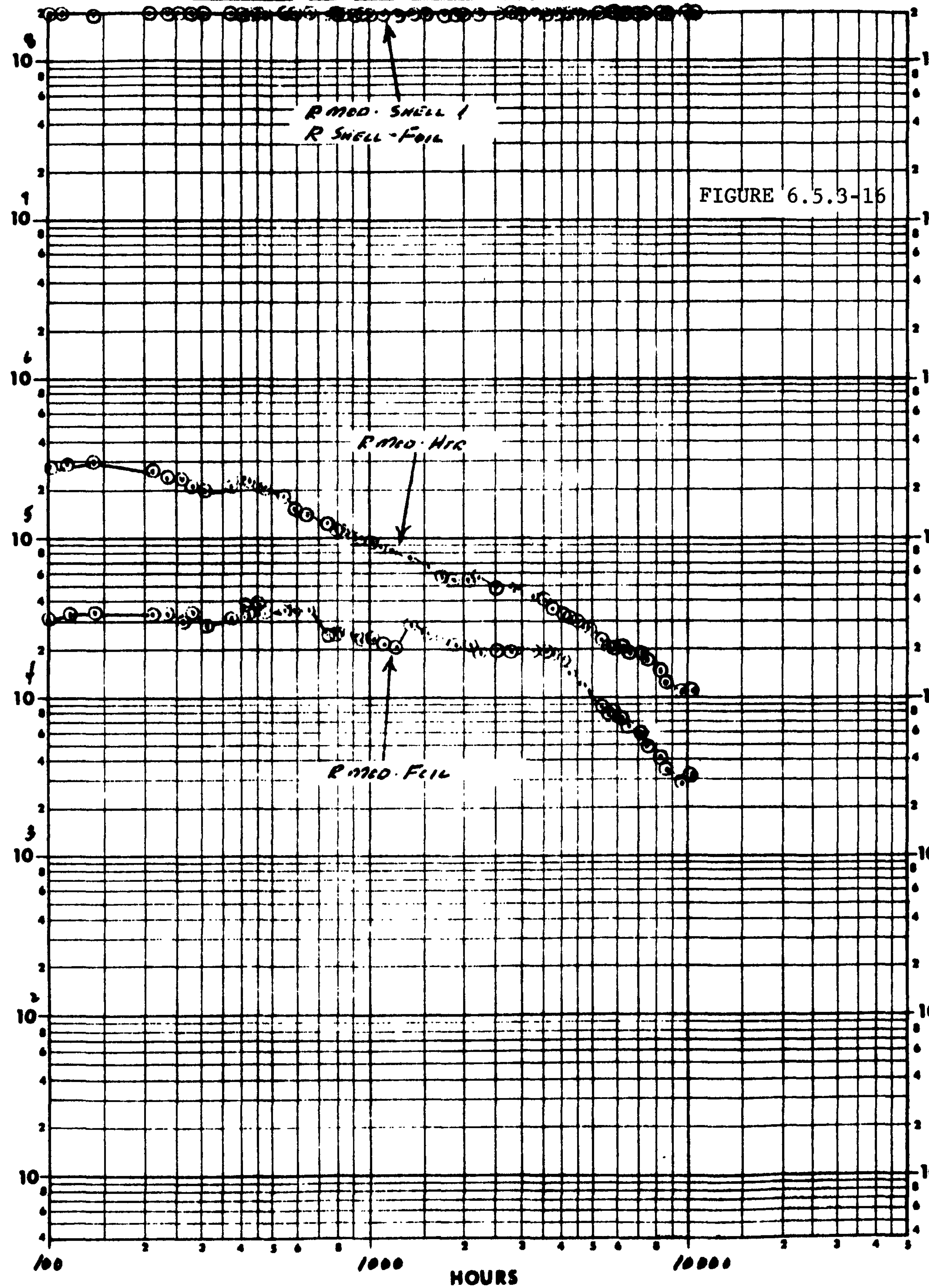

FIGURE 6.5.3-16

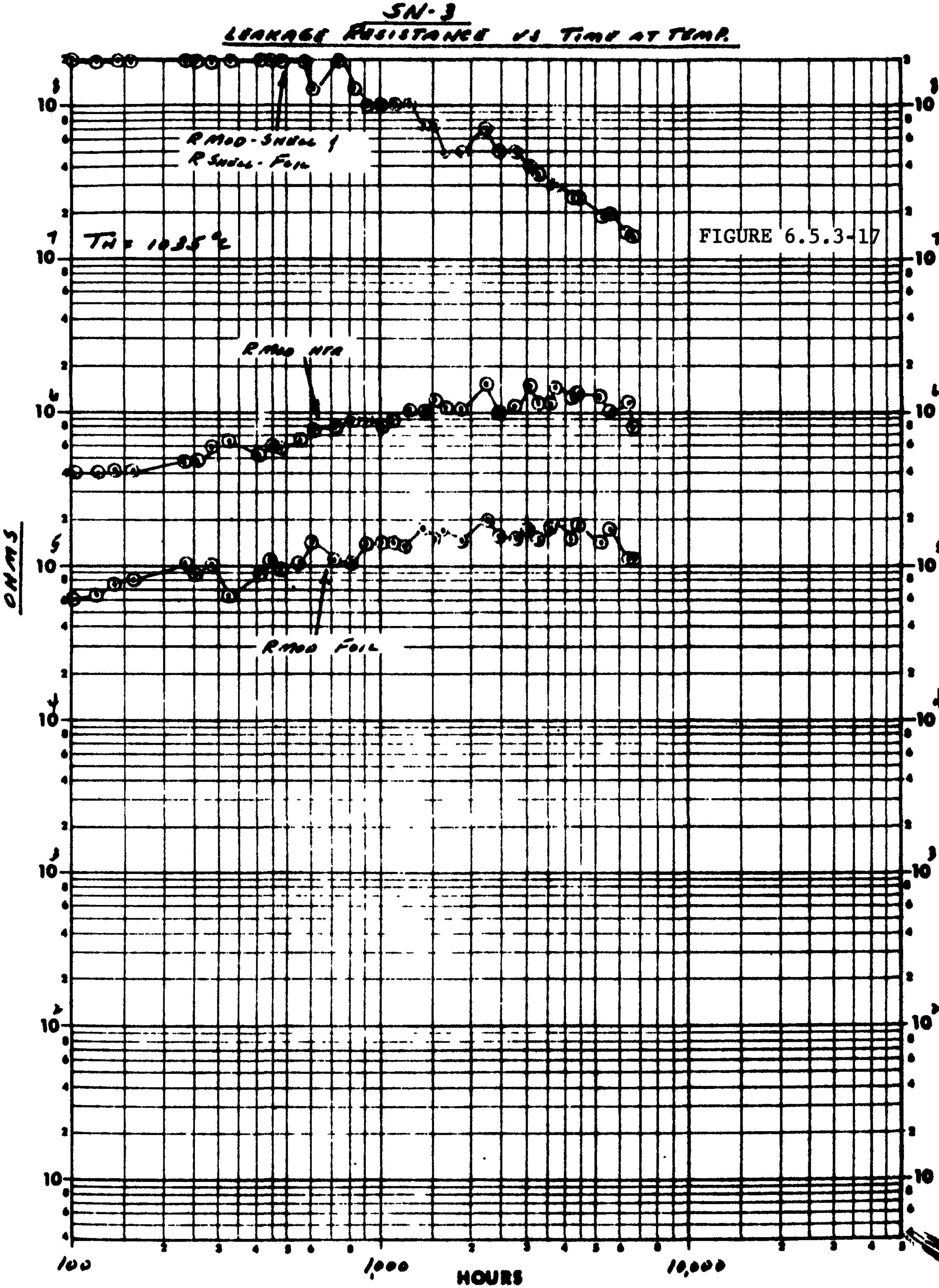

FIGURE 6.5.3-17

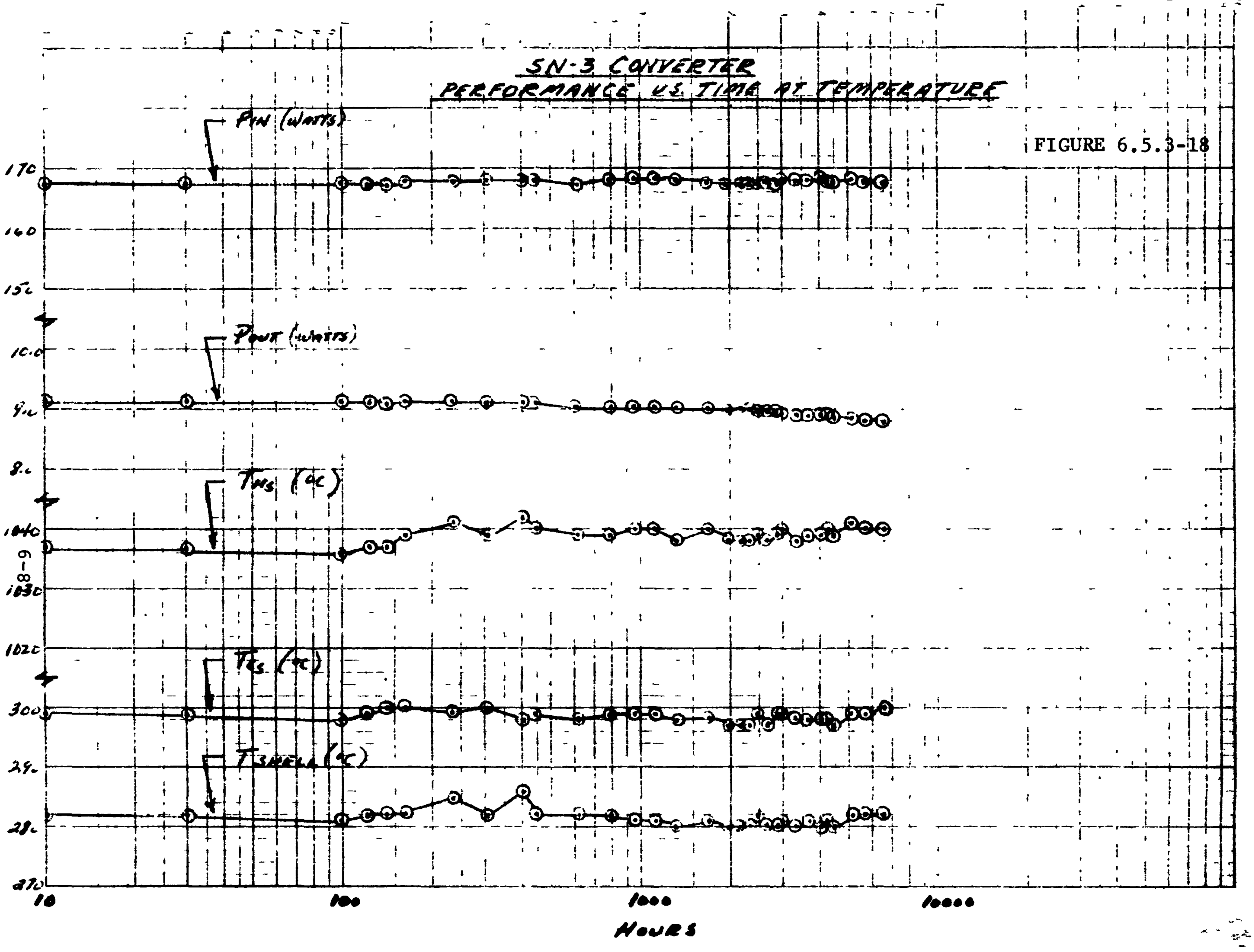

FIGURE 6.5.3-18

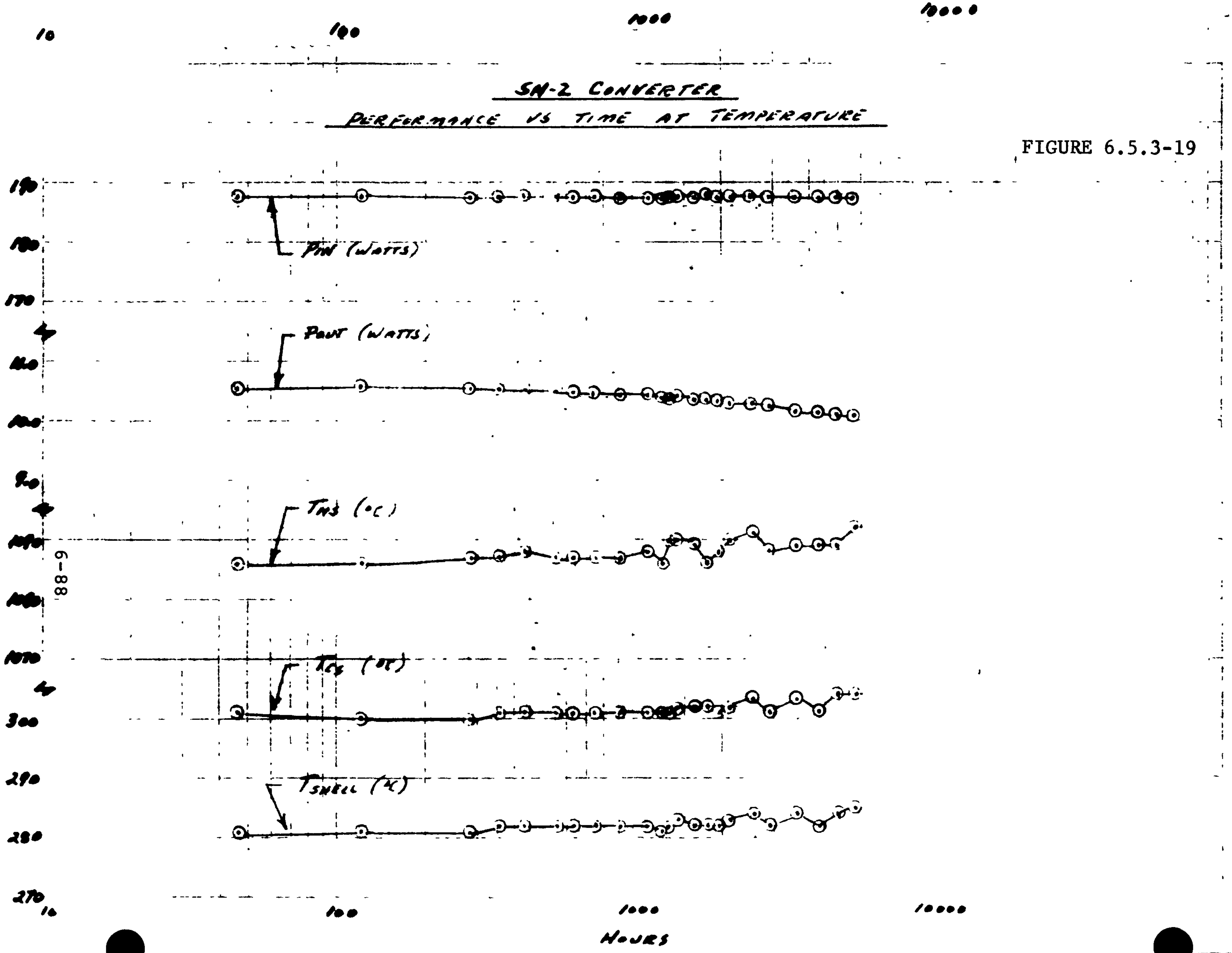

FIGURE 6.5.3-19

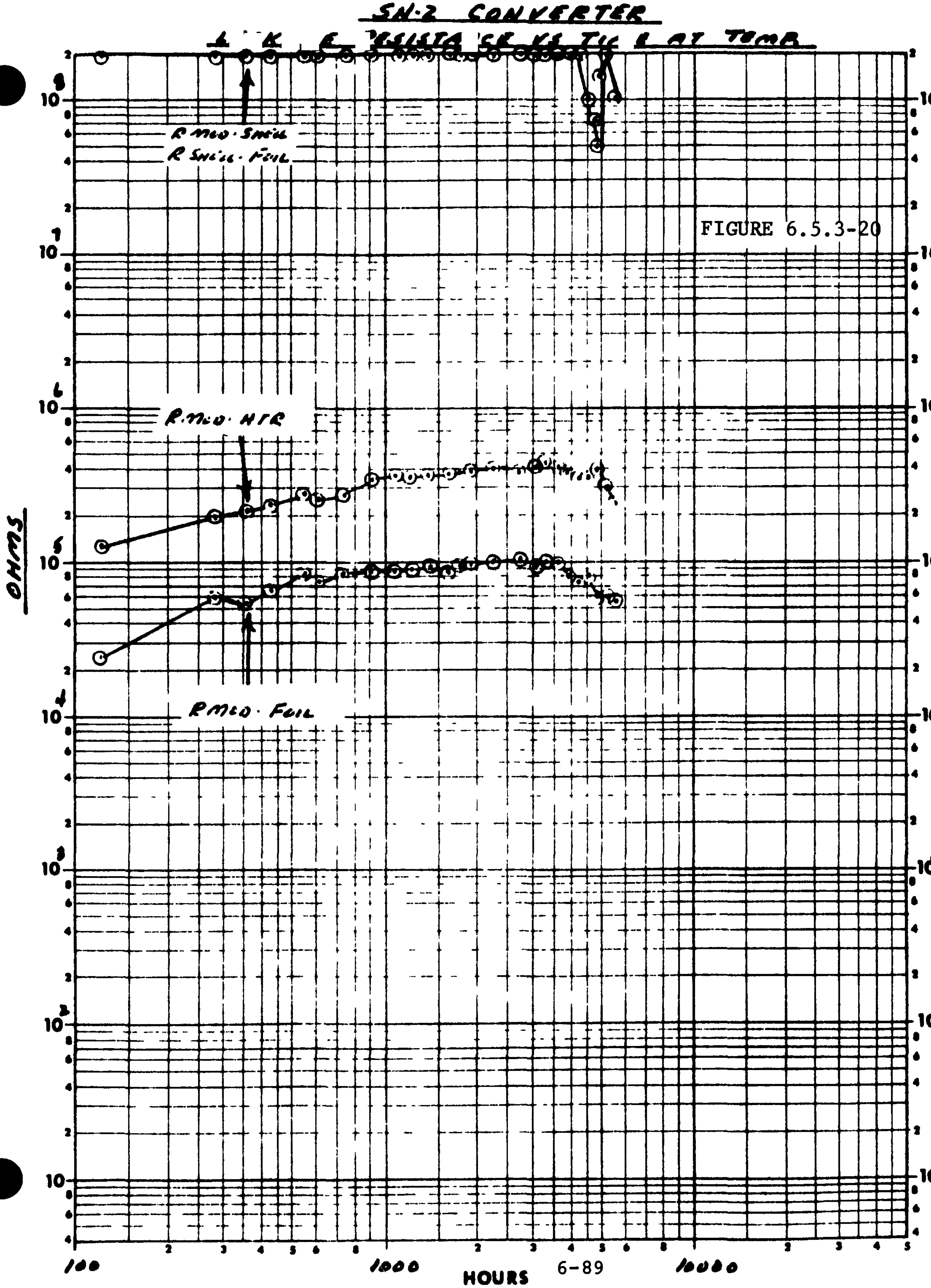
SN-2 CONVERTER
L K E RESISTA CE VS TI E AT TEMP
R MEO · SHELL
R SHELL · FOIL
R MEO · HTR
R MEO · FOIL
OHMS
HOURS
100
1000
10000
FIGURE 6.5.3-20

MOD. FOIL RESISTANCE

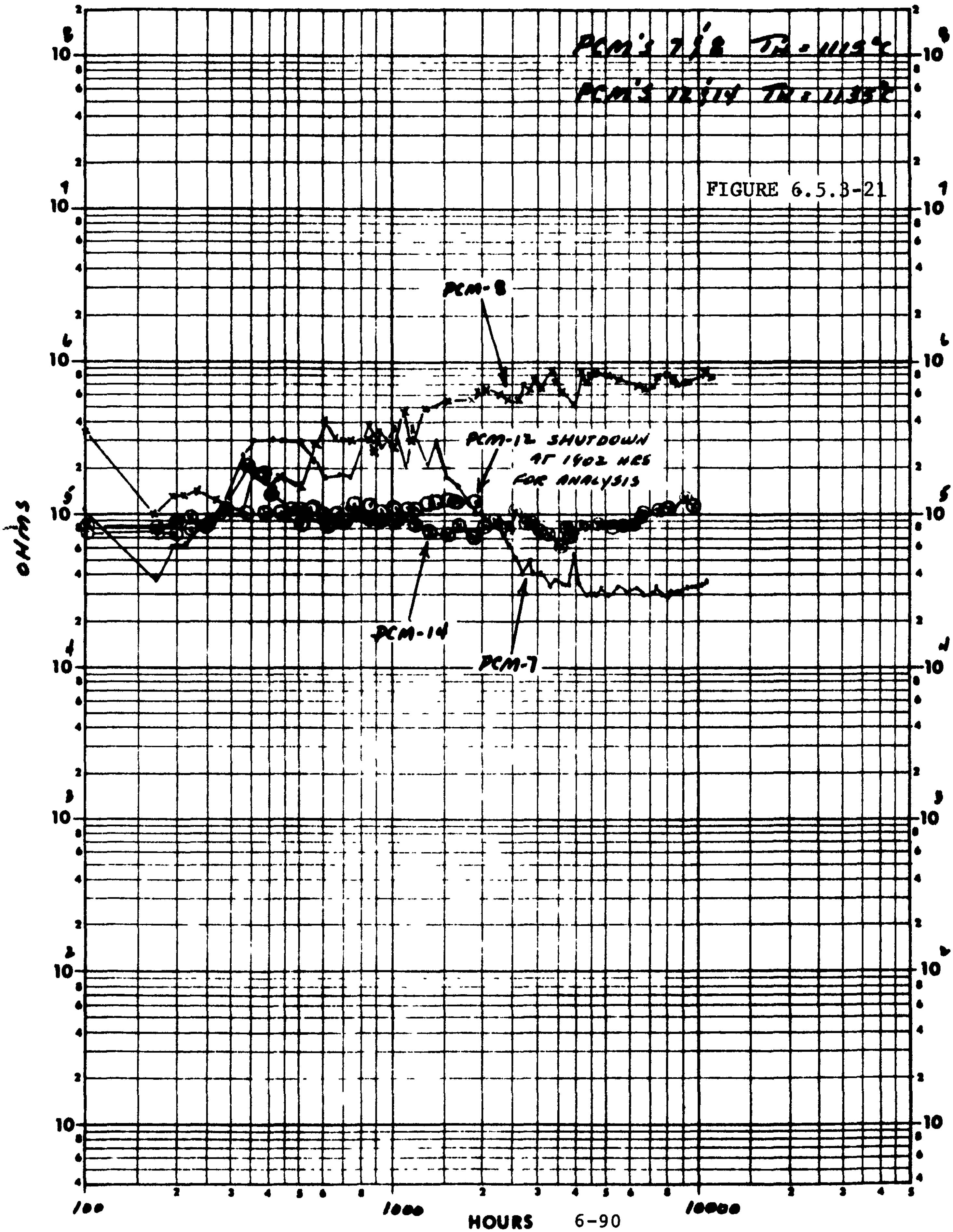

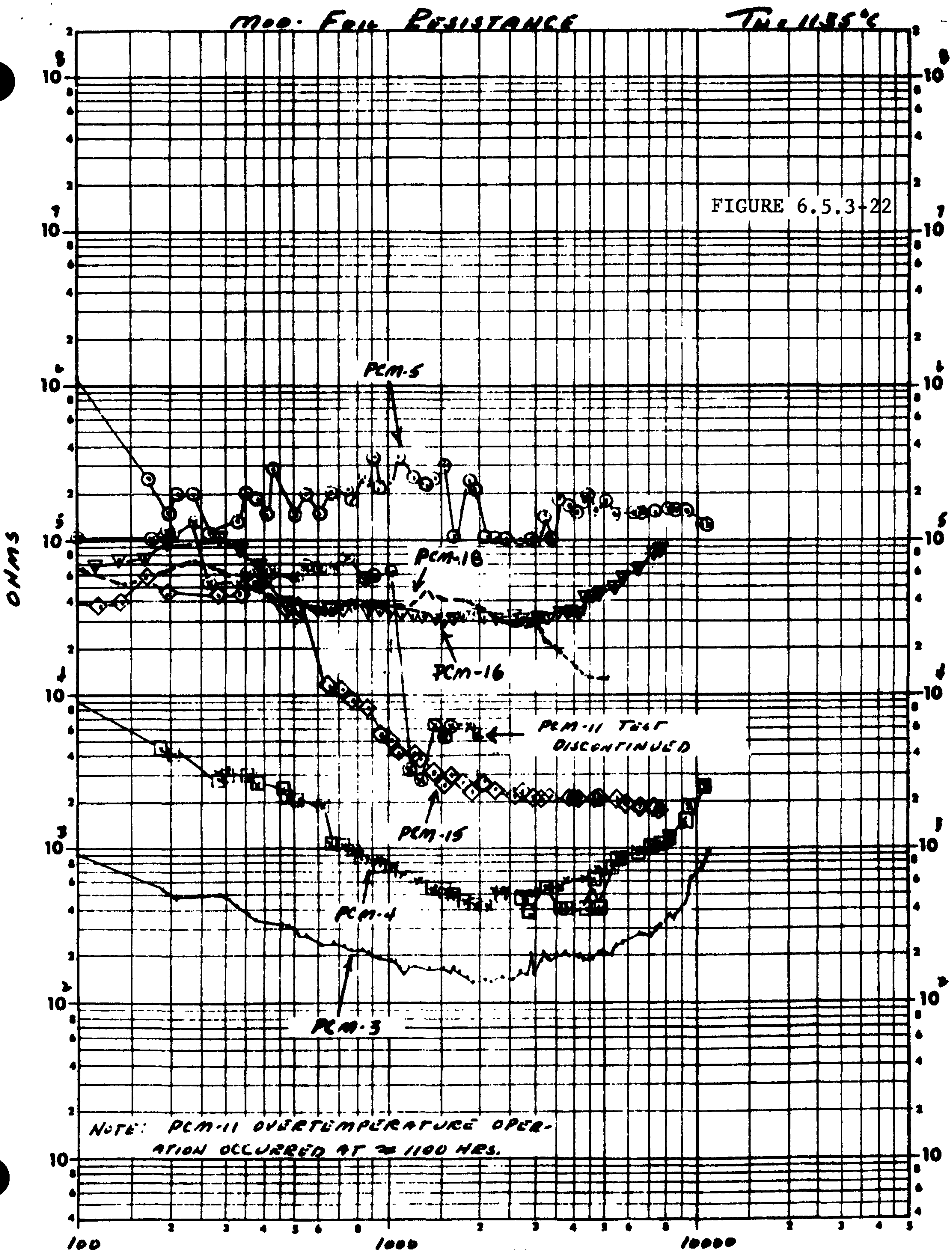

x--x--x PCM 4A INSTRUMENTED
□-□-□ PCM 4B UNINSTRUMENTED

PCM-17

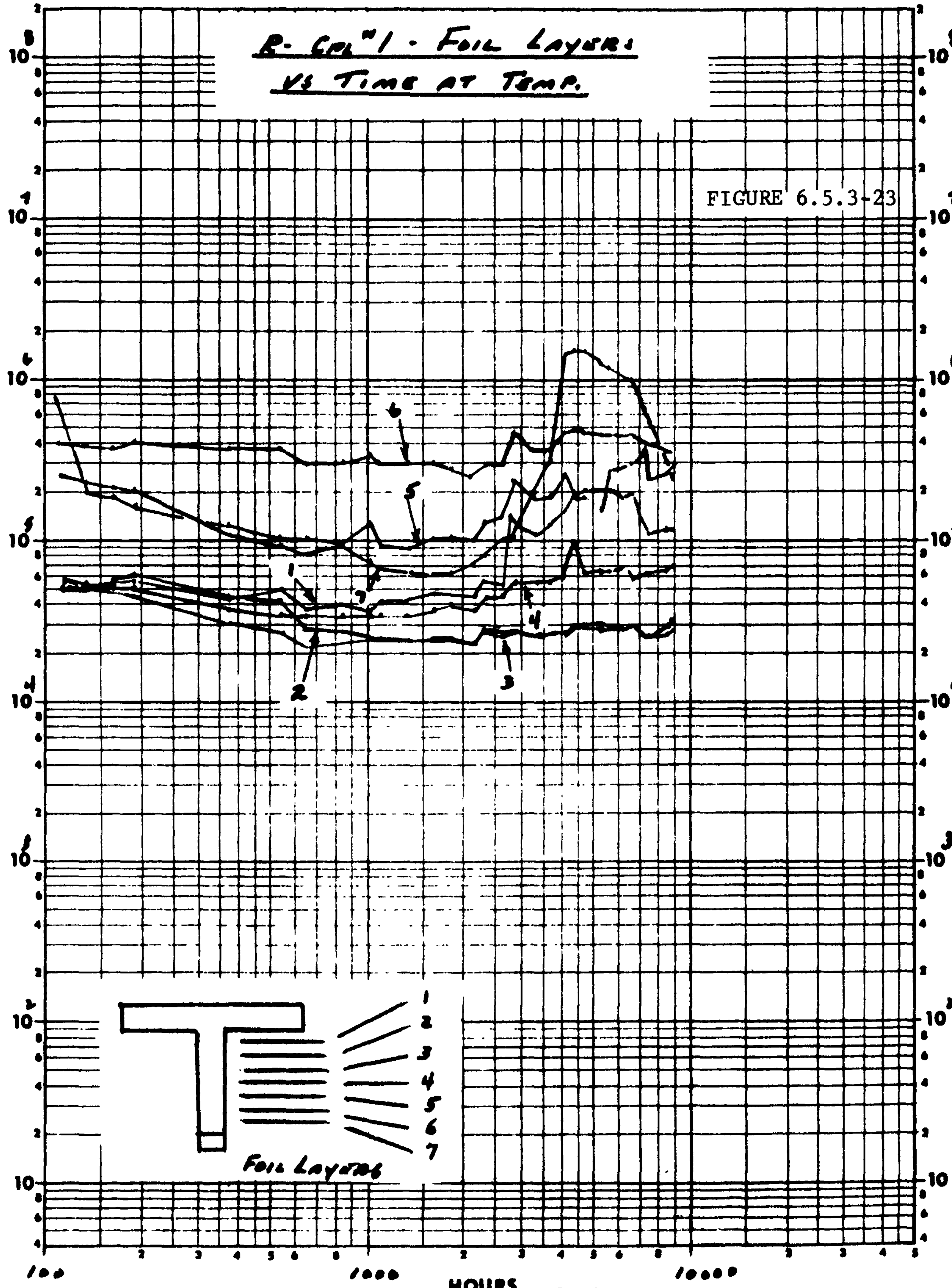

FIGURE 6.5.3-23

PCM-17

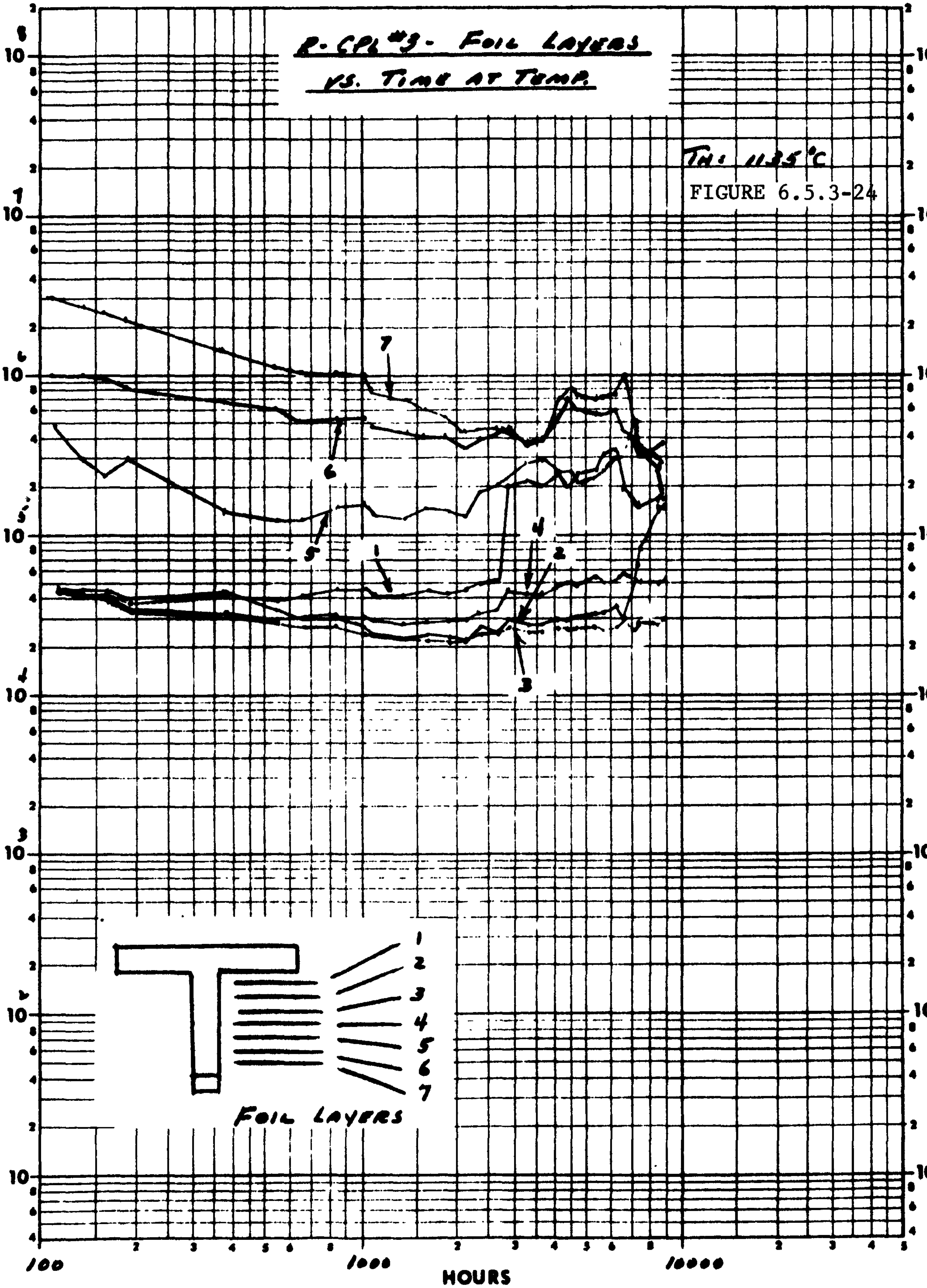

FIGURE 6.5.3-24

MOD - FOIL RESISTANCE

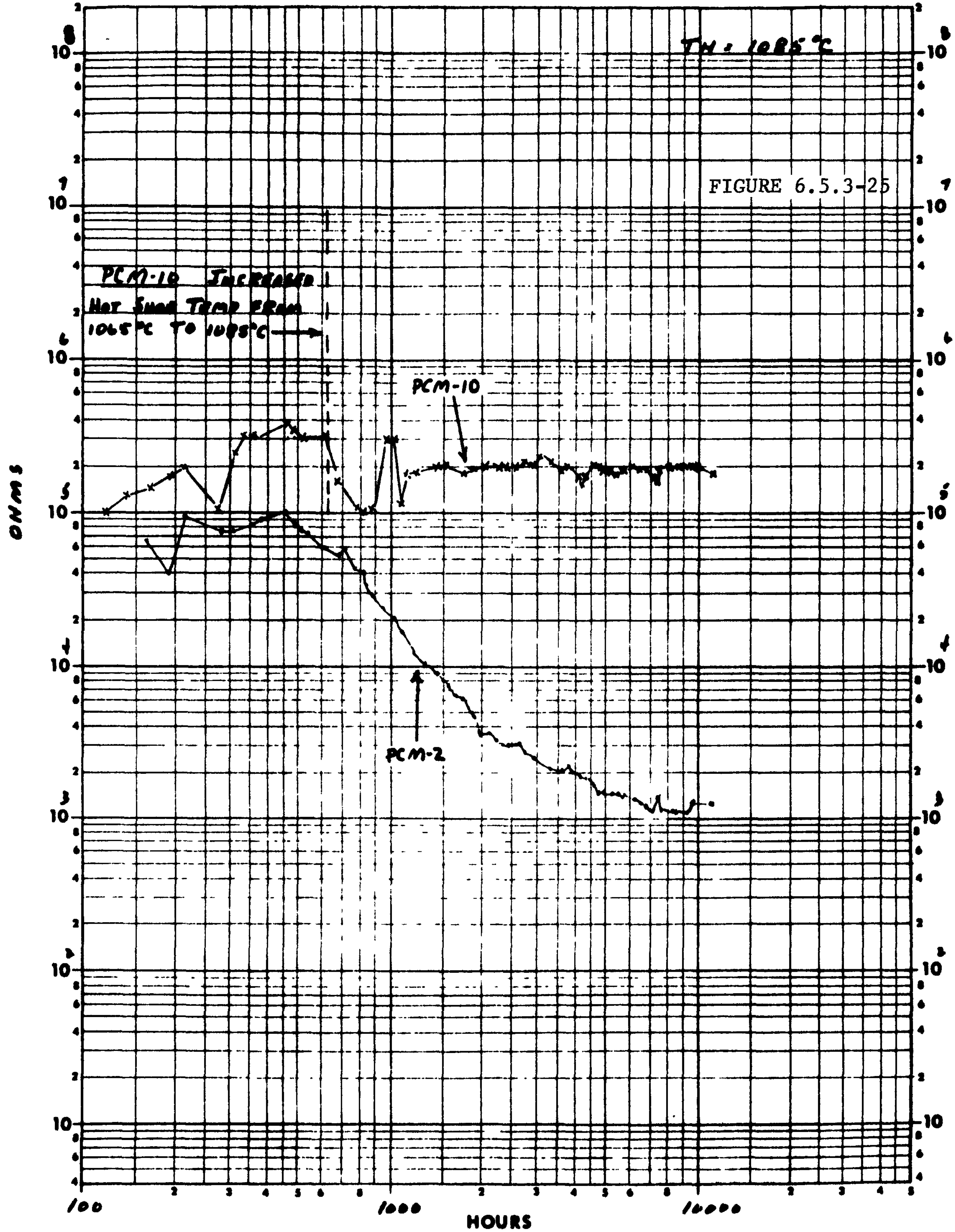

MOD- FOIL RESISTANCE

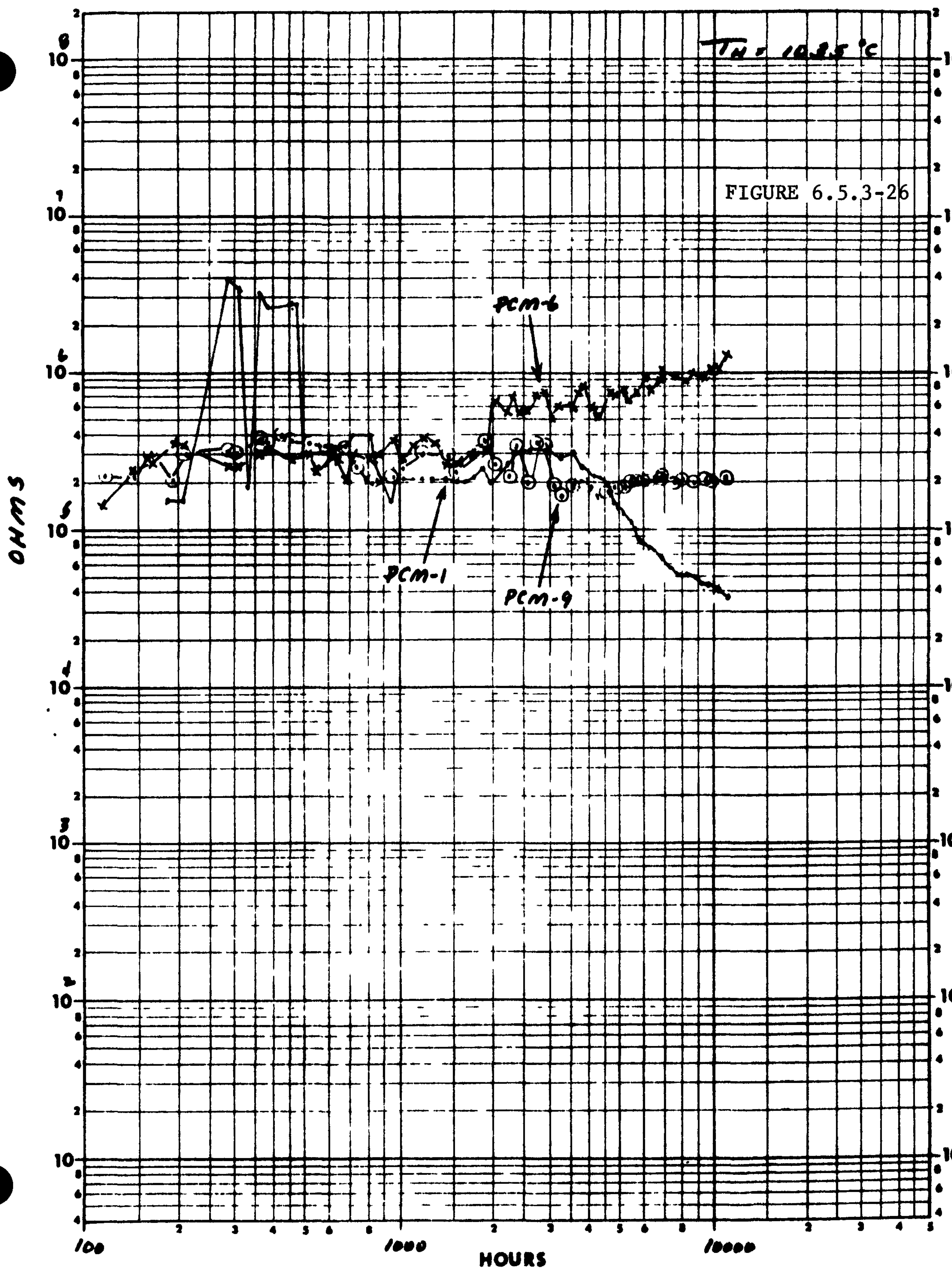

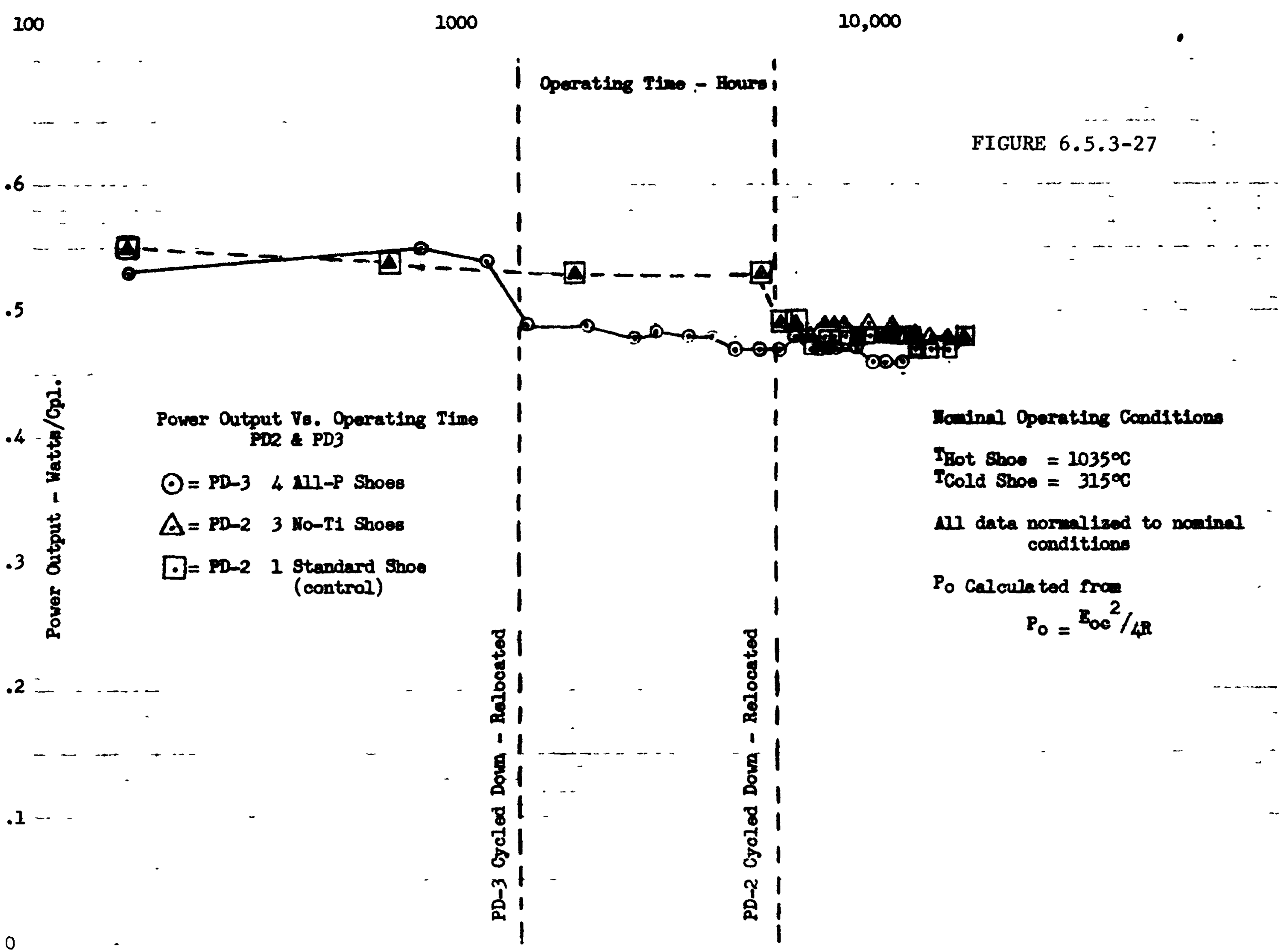

FIGURE 6.5.3-27

The testing of 18-couple converter DC-12A was terminated because the operation of the heater became very erratic. The unit was shipped to G.E. for post-test tear-down analysis. It should be noted that increasing resistance of the heater with operating time is normal, and that failure of the DC-12A heater had been predicted to occur about the present operating time. The performance curves for DC-12A, shown in Figure 6.5.3-9, show the expected improvement in Module-to-Foil resistance with the use of finer astroquartz yarns which provide denser wrap. However, use of smaller diameter astroquartz results in much greater incidence of yarn breakage in wrapping and a less rugged wrap.

Some difficulty was experienced in bringing SN-5 and SN-6 to operating temperature, in that the cold side temperatures ran approximately 40°C higher than desired. The problem was traced to a change in the cleaning schedule for the radiator plates, which resulted in a lower emissivity for the radiators. This had been corrected by coating a portion of the radiators with a high emissivity coating. As shown in Table 6.5.3-1, SN-6 has now reached operation temperature with the proper cold side temperature. SN-5 is still being brought to temperature, but the cold side temperaturesare tracking properly.

One of the heaters in the SNAP-17A module operating in air (MTA9-1) burned out. The heaters are being replaced and the module returned to operating temperature.

6.5.3.2 Converter Processing

Converter Q-2 was processed during the reporting period, and shipped to G.E. on August 22, 1975.

Processing proceeded normally and performance in all respects compares favorably with previous converters, see Table 6.5.3-4. The leakage resistance performance of Q-2, in marked contrast to that of the previous converter F-13, is the best observed to date. Since the low levels of leakage resistance observed on F-13 were ascribed to high humidity during the period of assembly operations and similar conditions prevailed during assembly of Q-2, Q-2 was held in vacuum at room temperature in the processing station for approximately 36 hours before start of the normal processing sequence. While a definite cause and effect relationship can not be proved, it is believed that this additional room temperature outgassing contributed to the superior leakage resistance of Q-2.

TABLE 6.5.3-4

CONVERTER PERFORMANCE AT DESIGN CONDITIONS

	F-1A	F-2	F-3	F-4	F-5	F-13	Q-2	Specification
Power In - Watts	2400.0	2402.6	2400.3	2401.5	2396.2	2402.1	2402.1	2400 ± 5
Power Out - Watts	158.2	159.0	159.5	159.2	159.0	158.2	158.8	155 minimum
Output Voltage - Volts	30.1	30.1	30.2	30.0	30.0	30.0	30.0	30 ± 1
T/P Shell Resistance - Ohms	15.0 K	14.5 meg*	8.5 K	10.0 K	14.5 K	7.4 K	19.7 K	2 K minimum
T/P Foil Resistance - Ohms	4.5 K	4.3 K	4.1 K	5.3 K	7.5 K	2.4 K	12.3 K	2 K minimum

* Instrumentation Fault

6.5.4 Product Assurance

6.5.4.1 Reliability

6.5.4.1.1 Major Design Changes

There were no major configuration changes made during this report period.

6.5.4.1.2 Failure Reports - None

6.5.4.2 Configuration Management

The following specifications have been revised through approval of ECN's:

ECN No.	Engineering Data No.		Description
AT(29-2)2831-994	RQ24A1	Rev. E	Product Acceptance of Si_3N_4 Coat 1st Bond.
AT(45-15)3066-013	RA2B1	Rev. C	Diffusion Bond of 1st Bond Assembly Process Procedure.
AT(45-15)3066-015	RG21A2	Rev. H	Converter Processing Procedure.
AT(45-15)3066-016	RA6E1	Rev. L	Thermopile Assembly Fabrication Procedure (Phase II)
AT(45-15)3066-017	RA6F1	Rev. D	Thermopile Assembly Fabrication Procedure (Phase III)
AT(45-15)3066-018	RA18B1	Rev. C	Mounting Converter Assembly into Shipping Container

6.5.4.3 Quality Assurance

6.5.4.3.1 Quality Assurance Progress

6.5.4.3.1.1 Prime Converter Assembly

Flight Model F-13 and MJS Qualification Model Q-2 were shipped to G.E. on July 8, 1975 and August 22, 1975, respectively.

MJS Engineering Model, E-5, is in Thermopile Assembly Fabrication.

6.5.4.3.2 Nonconforming Reports

6.5.4.3.2.1 MRB Actions

Table 6.5.4-1 lists the Nonconformance Reports (NR's) issued during the report period for MRB Authorization to use the noted discrepant items.

6.5.4.3.2.2 Nonconformance Report Sheet (NRS) Summary

Disposition of defective items found at inspection is obtained through approvals contained in Nonconformance Report Sheet (NRS). The summary of items placed on NRS is shown below and in Table 6.5.4-2. These are defective pieces for all causes that must be dispositioned for use, such as, submit to MRB Action, rework, or reject for prime hardware. They do contain rejects from lots that have been accepted or supplier-known rejects that must be submitted since the material was RCA-supplied. Since the lot is dispositioned by defect, a single NRS may have multiple dispositions. Thermopile and Converter Assembly is not included in this summary, since the information is contained in the Fabrication History Logbook for the unit.

Number of NRS's and Their Disposition

Month	No. of NRS's	Submit to MRB	Return to Vendor	Rej. for Prime Hardware	Rework to Spec.	ECN Required
July	47	0	1	44	2	0
August	66	0	0	66	0	0
Totals	113	0	1	110	2	0

TABLE 6.5.4-1

NONCONFORMANCE REPORTS REQUIRING MRB ACTION

RCA NR #	GE NR #	ITEM	Spec. #	Discrepancy	Disposition	Problem Cause
1327	43125	ETG Conv. Assly F-13	47J302596G4	Thermopile to Shell Resistance was 6.8 K	Use as is with additional 24 hours of processing at temperature.	Humidity during fabrication
1329	43126	Machined Electrical Insulator	P4F3	AL995 body mixed in with AL300 Ceramic	X-Ray Fluorescence test all items of Lot 03-0056	Vendor Problem
1330	-	Unicouple Assembly	A3H1	Use for Engineering Test	Use for 18-Couple Module SN-4	None
1331	42273	Unicouple Assembly	A3H1	Use for Engineering Test	Use for 18-Couple Module SN-4	None

TABLE 6.5.4-2

NRS NONCONFORMANCE SUMMARY BY PARTS - JULY 1975

ITEM	DWG. #	# LOTS INSPECTED	# LOTS W/DEFECTS	% OF PARTS INSPECTED W/DEFECTS	PROBLEM AREAS
PARTS					
Radiator Attachment Assembly	A12A7	13	8	6.2	None
Cold Stack Assembly	A19A3	5	1	3.1	None
Pellets "N"	P1G25	2	2	13.0	Chips
Pellets "P"	P1G26	3	3	9.3	None
Segments "N"	P1G27	1	1	17.7	Chips
Pellets (Rough) "N"	P1T1	2	1	0.7	None
Pellets (Rough) "P"	P1T2	3	2	0.2	None
Formed Plate	P8B4	2	2	100.	Dimension
Machined Radiator Attachment	P11C2	9	3	1.5	None
Hot Shoe (Rough)	P11G2	5	3	25.0	One lot rejected for--Resistance
Hot Shoe	P11G4	3	2	3.0	None

UNICOUPLE ASSEMBLIES		No. Rejected for Prime Hardware
First Bond	A26A2	33
Coated First Bond	A30A6	0
Second Bond	A3C1	13
Preassembly	A2C1	4
Unicouple	A3H1	0
Wrapped Unicouple	A8E1	0

TABLE 6.5.4-2 (CONT.)

NRS NONCONFORMANCE SUMMARY BY PARTS - AUGUST 1975

PARTS	DWG #	# LOTS INSPECTED	# LOTS W/DEFECTS	% OF PARTS INSPECTED W/DEFECTS	PROBLEM AREAS
Radiator Attachment Assembly	A12A7	14	9	11.4	Bond voids and damaged heat shunts.
Cold Stack Assembly	A19A8	6	2	1.9	None
Compensator	P1F5	3	2	0.8	None
Pellets, 'N'	P1G25	1	1	18.8	Chips
Pellets, 'P'	P1G26	3	3	9.2	None
Pellets (Rough),'N'	P1T1	3	3	1.5	None
Pellets (Rough), 'P'	P1T2	4	4	4.0	None
Electrical Connector	P3H1	1	1	7.5	None
Electrical Insulators	P4F3	14	13	13.9	Engineering Test
Heat Shunts	P7C15	10	1	10.0	None
Machined Radiator Attach.	P11C2	19	1	0.3	None
Hot Shoes	P11G4	3	3	2.3	None
Hot Shoe Spacers	P20H1	3	1	0.6	None

MATERIALS	DWG #	No. LOTS REJECTED	PROBLEM AREAS
78 % SiGe 'N' Vacuum Hot Press	P1R5	1	Multiple Cracks
63.5% SiGe 'P' Vacuum Hot Press	P1R8	1	Multiple Cracks
SiMo, 'P' Vacuum Hot Press	P1R10	1	Multiple Cracks

UNICOUPLE ASSEMBLIES	DWG #	NO. REJECTED FOR PRIME HARDWARE
First Bond	A26A2	47
Coated First Bond	A30A6	0
Second Bond	A1C1	2
Preassembly	A2C1	3
Unicouple	A3H1	11
Wrapped Unicouple	A8E1	5

6.5.4.3.3 Problem Areas

Western Gold and Platinum Company (WESGO) Metallized Electrical Insulators which had AL995 body ceramics mixed in with the specified AL300 ceramic body were tested to screen out the undesired ceramics. All Unicouples, Cold Stack Assemblies, and Machined Electrical insulators made from ceramic Lot 03-0056 were tested using X-ray fluorescence to separate the AL300 ceramics from the AL995. About 3 to 4% of the assemblies contained AL995 ceramics.

Chlorine content of the silicon nitride Coated First Bond Assemblies for eleven (11) coating runs was found to exceed the specification limit. Assemblies from these runs were segregated and held by Quality. Design Engineering is investigating the cause of the problem. A Nonconformance Report (NR) is being prepared for submittal to MRB. The process specification is being amended to increase the frequency of test so as to prevent a repeat of a large accumulation of product before the problem is detected.

6.5.5 Converter Design

6.5.5.1 Specification Modifications

The following specifications were reviewed and revised as required to reflect actual experience into the specifications:

RA15C3 - Converter Assembly Fabrication Procedure
RG21B1 - Preparation for Converter Processing

A New Specification RG21B2 - Preparation for Converter Processing was prepared for E-5. The following specifications were reviewed and revised, as required, to incorporate actual experience into the specifications.

RA6E1	Thermopile Assembly Fabrication Procedure Phase II
RA6F1	Thermopile Assembly Fabrication Procedure Phase III
RG21A2	Converter Processing Procedure
RG18B1	Procedure for Mounting Converter into Shipping Container

6.5.5.2 Tooling and Equipment

Several tools and fixtures were designed and fabricated to allow x-ray inspection of cold stack ceramics.

The additional tooling required for processing the E-5 Converter has been designed and fabricated. Also, the Unicouple Concentricity Fixture and the First Bond Assembly Sanding Fixture were checked out and reworked.

6.5.6 Material Analysis and Thermopile Characterization and Testing

6.5.6.1 Use of Astroquartz Cloth in 1st Bonding

The use of Astroquartz Cloth in place of the Dynaquartz Pad promises a significant long term improvement in 1st bond yield.

Throughout the history of production First Bonding, the major reject category has been voids in the leg-to-shoe bonds. The level of the shrinkage has fluctuated, sometimes correlating with the degree of skill of the 1st bond operator. Clip bonding is being investigated to resolve this problem; see below. In addition, a review of the 1st bond process revealed the dynaquartz pad used between the end of the N and P pellets and the graphite fixture as a possible factor.

An engineering test was run in which the dynaquartz pad was replaced with astroquartz cloth. Since the cloth has a more controlled structure than the bulk dynaquartz material, it was postulated that the cloth would allow less movement of the parts during bonding. The test showed better results with the astroquartz cloth. Although the sample size was small in relationship to the level of defects being encountered in production, the engineering test appeared to support the postulation of more controlled results from the astroquartz cloth. Since the chemistry of the astroquartz and dynaquartz is the same, an ECN was written and approved allowing the use of either material in production. This made possible the conduct of a relatively large scale test, using both materials in parallel under actual production conditions.

Results from the larger scale examination clearly demonstrated the superiority of the astroquartz cloth approach, and all fabrication has been switched to use of the cloth.

6.5.6.2 Clip Bonding

Work has been initiated in the evaluation of tungsten clips in lieu of tungsten weights which are used to maintain pressure on the thermoelectric parts during the 1st bond operation.

The recent experience in increased shrinkage attributable to a personnel change in bonders, and the associated training period, again pointed up the high degree of sensitivity of the 1st bond operation to the operator skill. The objective of this work is to reduce the dependency on operator skill by establishing a more positive holding technique through the use of spring clips. The clips should afford better retention of the parts during assembly and firing, thereby alleviating the most significant problem for rejects, i.e., parts movement during set-up, furnace loading, and firing. Other advantages anticipated from clip-bonding are: (i) further improvement in fabrication yield due to compensation of any slight imperfections encountered in set-up or parts; the compensation is realized from the higher pressure exerted by the clips, and (ii) to offset the higher pressure, a lower bonding temperature may be used which will result in less degradation of the N-P SiMo bond.

The method being evaluated for 1st bond clip bonding uses the same tungsten chips presently in use for fabrication of 2nd bonds. The graphite fixture currently used for 1st bonding is retained, so that all other conditions, including thermal mass, are retained, minimizing introduction of other changes. Only slight modifications have been made to the graphite fixture to accommodate the use of tungsten clips.

A limited parametric study was conducted to determine the best temperature for bonding with clips. Since it was expected that bonds satisfactory in all respects could be made within the present allowable bonding temperature range, only this range has been explored to date. As expected, acceptable bonds could be made at temperatures near the low end of the range. At temperatures near the high end of the range, the minor normal reaction between hot shoe and molybdenum reflector became more pronounced. Based on these results, a control test of 12 standard process and 12 clip bond couples was performed using temperatures near the low end of the temperature range for the clip bonds, and normal temperatures which would have been selected for the standard process bonds. Hot Shoe, N-leg, and P-leg materials were from the same lots for all 24 couples in this control test.

Yield results were encouraging showing no bond or dimensional rejects for the clip bond couples and 4 out of 12 for the standard process couples. Breaking strength tests for the N-P bonds showed a slight improvement for the clip bonds over the standard process, while metallographic examination showed no significant difference between the two processes.

After second bond, the clip bonded couples showed an average total resistance approximately 0.4 milliohms lower than the standard process bonded couples using the same material lots.

In view of the results to date, present plans are to continue a low level development effort on clip bonding. Bonding at lower temperatures will be performed to determine the optimum bonding temperatures for clip bonds. It is expected that the optimum temperature will be slightly lower than present specification limits. This will require a slight reduction in the lower total resistance limit for 2nd bonds and subsequent assemblies, because of the effect of the lower bonding temperature on the amount of phosphorus in solution in the N 78% SiGe material. The implication of a minor decrease in room temperature resistance against power output at operating temperature must be evaluated.

6.5.6.3 Alternate Source of Ceramic Insulators - P4G2

In light of the continuing difficulties experienced with the only qualified vendor for metallized ceramic insulators, effort has been initiated to secure alternate sources. Several approaches are being pursued as tabulated below:

	Alumina Body			Metallizing
	Vendor	Type	% Al_2O_3	Vendor
a.	Frenchtown	4462	94	Frenchtown
b.	Frenchtown	4462	94	RCA Lancaster
c.	Frenchtown	2082	96	Frenchtown
d.	Frenchtown	2082	96	RCA Lancaster
e.	American Lava	AlSi Mag 771	94	RCA Lancaster
f.	Wesgo	AL300	97.6	RCA Lancaster

Initial engineering tests have been completed for approaches a, b, c, and e above. All of those combinations show superior strength over the present qualified product and all meet other specification requirements except for several minor deviations, which can be accepted.

6.5.6.4 Measurement of Si_3N_4 Coating Thickness

The measurement of Si_3N_4 coating thickness using simulated 1st bond samples which were fabricated of single crystal silicon by optical means has been continued. One 'dummy' 1st bond is measured for every six coating runs. A summary of the measurements made to date is given in Table 6.5.6-1. These measurements were on a Model DB-GT Beckman Spectrophotometer. Because of the wavelength limitation, 0.2-0.8 microns (Ultra-Violet) of this instrument, which affects the measurement accuracy of thicker coatings, the use of a model DK2A Beckman Spectrophotometer, which has a wavelength capability of 0.2 - 3.0 microns (near-Infra-Red) is being investigated. Pending resolution of the measurement techniques, this method would be prepared as an alternate to the SEM thickness measurement.

6.5.6.5 Silicon Nitride Coating Process

ECN 994, which delineates the chlorine level of the silicon coated wafers processed in the 1st bond coating runs, was approved, and these limits have been incorporated into the Product Acceptance Specification for Coated First Bonds. These limits are as follows:

	8-Couple Runs	16-Couple Runs
Max Chlorine Level, ppm	850	550

These limits were based on runs from the initiation of the coating process thru L-306. Analysis of subsequent runs, L-312, L-318, L-324, L-330 and L-335 revealed that L-324, L-330 and 335 were higher than the specified limits. Accordingly, all runs from L-319 to L-335 were analyzed for chlorine level; results are summarized below.

Run No.	Chlorine Content, ppm	Run No.	Chlorine Content, ppm
L-312	450	L-326	490
L-318	488	L-327	480
L-319	740	L-328	580
L-320	380	L-329	600
L-321	320	L-330	675
L-322	500	L-331	750
L-323	660	L-332	680
L-324	622	L-333	730
L-325	490	L-334	670
		L-335	700

An investigation of the coating process and equipment resulted in identification of a defective component. This was replaced and the chlorine content in subsequent engineering coating runs returned to normal levels. Production runs of coating first bonds have resumed. As a result of this occurrence, process control limits have been established, and the chlorine level of each coating run will be measured, rather than one run for every six coating runs. An ECN incorporating these changes has been approved.

TABLE 6.5.6-1

SPECTROPHOTOMETRIC MEASUREMENTS OF Si_3N_4 COATING THICKNESS

Couple No.	Coating Run No.	Couple Position	S_1	S_2	S_3	S_4	S_5	S_6
1	L-280	5	15,517	12,220	16,137	6,518	6,391	16,320
2	L-280	12	15,471	11,938	16,527	7,590	7,528	15,006
3	L-295	5	15,311	12,149	17,230	7,666	7,702	17,192
4	L-295	12	15,266	12,053	15,930	7,812	7,863	16,749
5*	L-304	5	15,585	11,681	16,653	7,800	7,873	16,397
6	L-304	12	15,197	11,875	15,633	7,887	7,861	18,786
7	L-314	5	15,791	12,398	16,833	7,699	7,677	16,883
8	L-315	5	16,095	12,465	17,472	7,738	7,726	16,769
9	L-328	5	15,769	12,193	16,697	7,157	7,291	16,819

NOTE: * Couple No. 1 acid etched and re-used.

8.0 PRODUCT ASSURANCE

8.1 CONFIGURATION MANAGEMENT - LES 8/9

During this reporting period 20 Alteration Notices (AN's) were processed on GE-issued drawings and specifications, while 17 Engineering Change Notices (ECN's) were processed on RCA-issued drawings and specifications.

8.2 QUALITY ASSURANCE - LES 8/9

The Pre-Shipment Buy-off Reviews were completed for RTG's F-2, F-4, and F-5. The data reviews included the following items:

- Open NR Status
- Log of NR's written during RTG Processing
- Class I NR Status
- NR Summary by Category
- FRB Status
- Conditional C of I Status
- Ship Loose Status
- Product/Configuration Definition List
- Historical data package containing all NR's and C of I's pertinent to the RTG

Quality Assurance continued test support and test monitoring activities on a round-the-clock basis as necessary to support RTG testing.

8.3 CONFIGURATION MANAGEMENT - MJS

For the MJS Program, 100 AN's were processed and three Program Change Proposals (Nos. 25, 26, and 27) were submitted.

8.4 QUALITY ASSURANCE - MJS

The MJS Quality Program Plan was submitted for approval. Minor changes and corrections were made at the request of SNS, and the plan was released for final distribution.

Major effort continues in the inspection area associated with preparation of parts and sub-assemblies for assembly into RTG's. Emphasis is being given to improving the rate of acceptance of C of I's being submitted.

Figure Nos. 8-1 and 8-2 show Non-Conformance Report activity for the months of July and August, respectively. The greatest category for rejection in inspection still continues to be Dimensional Discrepancy. Most of these items have been dispositioned "Accept-as-is". This indicates that the nature of the discrepancy is minor, and also indicates that the original drawing tolerances are perhaps not really required.

FIGURE 8-1 - MHW NON-CONFORMANCE REPORT ACTIVITY & STATUS - JULY 1975

	TYPE OF NON-CONFORMANCE					DISPOSITION				
	DIMENSIONAL	PROCESS	TEST	WORKMANSHIP	MISC.	ACCEPT AS IS	REWORK	RETURN TO VENDOR	SCRAP	TOTAL
LES 8/9										
GE-SSO	3	1	4	8	2	8	8		2	18
ALL OTHER SUPPLIERS	3	2		2		2		4	1	7
MJS										
GE-SSO	5	7	2	6		13	3		4	20
MOUND LABS	6	1				7				7
ALL OTHER SUPPLIERS	11	2		7	1	15		6		21
TOTALS	28	13	6	23	3	45	11	10	7	73

FIGURE 8-2 - MHW NON-CONFORMANCE REPORT ACTIVITY & STATUS - AUGUST 1975

	TYPE OF NON-CONFORMANCE					DISPOSITION				
	DIMENSIONAL	PROCESS	TEST	WORKMANSHIP	MISC.	ACCEPT AS IS	REWORK	RTV	SCRAP	TOTAL
LES 8/9										
GE-SSO	2		16	8	3	17	9		3	29
SUPPLIERS				1			1			1
MJS										
GE-SSO	1	4		3	2	6	3		1	10
MOUND LABS	4	1		1		4	2			6
RCA	2	3				4	1			5
ALL OTHER SUPPLIERS	13	3	1	9	2	11	3	14		28
TOTALS	22	11	17	22	7	42	19	14	4	79

10.0 HARDWARE FABRICATION

- Q2 converter hardware was processed and delivered to RCA for assembly.
- E5 and F6 converter hardware is in process for delivery to RCA in the September-October period.
- A potentially serious schedule and cost impact was sustained at Speedring Industry, Division of Schiller Industries, when a crack was accidentally induced in the F7 Be converter shell during machining operations. This shell is scrap and all efforts are aimed at reduction of schedule impact while assuring that a quality shell is produced.
- All "rigid design" PRD vent tube assemblies were fabricated in this period.
- PMD assembly and test is proceeding thru the shop and test areas.
- The IHS graphitic parts were shipped to MRC for assembly with Q2 heat source.
- Frit vents were shipped to MRC to cover F6 requirements.
- Q1A and F1E converters were machined in NuMac in Cleveland and safely returned to VFSC to continue with modification.
- Pressure domes for Q1A, F1E, and E5 were shipped to Gulton Industries for connector assembly/welding in early August.

11.0 ACCEPTANCE TESTING

11.1 ETG ACCEPTANCE TESTING

11.1.1 F-1 ETG

The unit remained in storage in its Converter Shipping Container (CSC) in Bldg. B throughout the reporting period.

11.1.2 F-5 ETG

11.1.2.1 ETG Disassembly

As previously reported, the F-5 ETG had been installed into LAS #1 on 6/30/75. The flight power output cable was received on 7/1 and after removing the GSE power output cable, which had been installed on 6/17, the flight cable was installed onto the F-5 ETG. The installation of this flight power output cable prior to securing the chamber had been a constraint of the Segment Readiness Review also held on 7/1.

After securing the chamber, pumpdown was initiated early 7/2, with argon backfilling and scrubbing operations being completed late 7/2. The forward dome and spool piece were removed and the EHS was then hoisted out of the converter 7/3. Visual examination of the internal case showed no apparent abnormalities.

See Section 11.2.4 for the F-5 RTG operations.

11.1.3 F-13 ETG

11.1.3.1 Receiving Inspection Operations

After receiving the F-13 ETG from RCA, initial inspection operations began on 8/9/75 at Bldg. B. After the Converter Shipping Container (CSC) was opened, visual examination showed no superficial defects. The ETG was then hoisted out of the CSC and installed onto a handling base plate on a work table.

The Gas Service Cart was setup and interconnected with the ETG for a "cold" pressure decay test which was completed on 8/9 and yielded a pressure increase of 0.06 psi/6 hours.

Circuit resistance and isolation measurements were performed on 8/9. The thermopile circuit measured 2.140 ohms as compared to the RCA pre-ship measurement of 2.122 ohms. Isolation measurements between thermopile to case and to foil basket indicated greater than 1 megohm at 50 VDC potential.

The installation of the 2805G5 RTD instrumentation cable and the 2806G5 power output cable was completed on 8/12/75. Circuit resistance and isolation measurements on the installed power output cable were acceptable, as were the circuit resistance measurements of the RTD cable. However, isolation measurements of the RTD circuits from the converter case showed an anomalous indication of less than 0.5 megohms at RTD #1 to case. NR-43278 documented this (less than the required one megohm minimum isolation) and the initial disposition was to continue testing, with final disposition to be determined at the conclusion of all RTG acceptance testing.

The RTG and IHS pneumatic flex hoses and the PRD support bracket were also installed on 8/12. Installation of the ETG into its CSC then began and was completed mid 8/13.

11.1.3.2 ETG Disassembly

With the LAS #1 preparations completed, the F-13 ETG was routed from storage to the Bldg. 800 floor area late 8/21 where the CSC was opened and the ETG transferred to the slide tray assembly. After interconnecting the RTG and power out cables and the IHS and RTG flex hoses, the unit was installed into LAS #1.

The Segment Readiness Review to allow the continuation of operations was held at 2000 hours, 8/25. After the bakeout and storage container was installed into the LAS #1 load lock, chamber evacuation began at 0045 hours, 8/26. By 1615 hours, 8/26, chamber vacuum had achieved 1×10^{-5} torr and backfilling operations were initiated, being completed at 1645 hours. "Scrubbing" via the facility gas purification system then began and acceptable chamber atmosphere purity levels were achieved by 1100 hours, 8/27. The bakeout can was then opened, the forward and aft end cap assemblies were built-up and the ablation sleeve was installed into its holding fixture.

After the vacuuming of the converter's external surfaces was completed, the process valve and its tubulation were disassembled from the spool piece and the forward dome was removed. Visual examination showed no apparent abnormalities at the forward end of the converter interior. The EHS power leads were disassembled from their interconnection at the EHS and the EHS thermocouples were then snipped at their spool piece connector interface, this effort being completed by 0330 hours, 8/28.

Screw removal at the spool piece/case interface began at 0400 hours, Two screws had seized, but were subsequently broken free by using vise-grip pliers at their heads.

When an attempt was made at removing the insulation retainer from the preload screw at 1030 hours, 8/28, it was found that the screw was turning along with the retainer. The method of retainer removal was then changed; a nut, with a washer under it, was installed onto the preload screw to secure it to the preload bushing and the retainer was then easily removed from the screw.

During the load lock operations at 1630 hours, 8/28, to pass out the spool piece and other miscellaneous hardware from the chamber, the facility gas purification system sounded an alarm. Subsequent purity level readings taken on the chamber atmosphere indicated that the O_2 level had reached 535 PPM. The roughing pump system was brought online at 1815 hours, 8/28, and after evacuation, the chamber was backfilled with fresh argon. "Scrubbing" was initiated at 0150 hours, 8/29, reaching acceptable chamber purity levels by 0330 hours.

After loosening preload from the support system, the forward end enclosure assembly was rotated slightly to free its bearing points from the six case brackets and the EHS was hoisted out of the converter at 1020 hours, 8/29. It was then found that the shaft of the EHS lifting adaptor had seized into the EHS.

Repeated attempts were made at freeing the lifting adaptor from the EHS, but proved futile. A hacksaw was then passed into the chamber and sawing at the shaft began at 2210 hours. The shaft was cut through by 2320 hours, 8/29, and the lifting adaptor was removed.

The chips from the cutting operation were vacuumed from the forward end enclosure assembly and the end enclosure was removed from the EHS at 0230 hours, 8/30. A visual examination was performed on the forward end enclosure assembly and it was found that the moly-foil end cap was torn in several areas, especially at the clearance holes where the EHS power leads fed through. In addition, several of the staples which secure the foil layers together were broken; NR-43339 was then written to document this condition. Disposition of that NR was that the moly-foil end cap condition was acceptable after the broken/loose staples were removed.

The bakeout can containing the EHS was transferred out of the LAS #1 load lock at 0430 hours, 8/30. Operations then resumed at the converter and the aft end cap assembly was installed by 0730 hours.

See Section 11.2.5 for the F-13 RTG operations.

11.2 RTG ACCEPTANCE TESTING

11.2.1 F-2 RTG

11.2.1.1 Rework Operations

As previously reported, the F-2 RTG had been removed from storage on 6/27 to allow a visual examination of the damaged threads on the outlet port of the RTG-GMV and then returned to storage in its SC on 6/28. The unit remained in storage until 8/5, when it was again transferred to the Bldg. 800 test area.

An IHS gas sample was taken on 8/6 and the F-2 RTG was then removed from the SC and installed onto the slide tray assembly for rework operations on the damaged RTG-GMV. The threads on the damaged valve port were renewed by chasing a die over them to remove galled/displaced metal. As the newly designed fitting saver, 3639G2, and the RTG flex hose were not immediately available to complete the rework operations, the RTG was placed into LAS #2 on 8/7, to await these items.

The new hardware was received on 8/9 and after the fitting saver and flex hose were mated to the RTG-GMV, evacuation and leak-up tests were performed to verify the integrity of the interconnections. These tests yielded acceptable evacuation and leak-up rates and showed that the rework operations on the RTG-GMV had been successful.

Also on 8/9, the PRD bracket which had been installed on the F-2 RTG in April was exchanged for one which was to the latest configuration (slotted mounting holes).

An air performance/pressure decay test was run on the F-2 RTG prior to exchanging the forward dome for one with a PRD. During the initial set-up for this test on 8/12, when the pneumatic lines between the gas service cart and RTG-GMV were being evacuated, the lines could not attain a vacuum below the 90 micron level. The fitting saver to GMV connection was retorqued to 140 inch-lbs and the lines to the RTG-GMV then attained an acceptable evacuation level of 50 microns. NR-43264 documented this operation.

After the interconnection system evacuation was completed, the RTG-GMV was opened and RTG pressure measured 24.35 psia. This indicated that RTG internal pressure had not degraded since 6/10/75 when the unit had been pressurized to 25 psia at Lincoln Laboratory. An RTG gas sample was then collected in an evacuated 500-ml bottle and subsequent mass spectrographic analysis showed this sample to have 2.5% helium and negligible CO and N_2, with the remainder as the basic argon fill gas.

After the load was switched from short-circuit to the loaded mode, the unit was thermally stable for the start of a 12-hour air performance/pressure decay test mid 8/12. Output power over the 12-hour test duration averaged 80.4 watts and the rate of pressure decay showed an increase of 0.12 psi/12 hours. The pressure increase is attributed to a rise in gas bulk temperature as seen on the fin RTD temperature increasing by $5^{\circ}C$ due to a change in ambient temperature in the LAS.

Segment Readiness was completed at 1500 hours, 8/13, to allow the start-up of the LAS #2 operations for the forward dome exchange. Chamber evacuation began shortly thereafter and the chamber had been backfilled with argon and gas purification completed by 1000 hours, 8/14.

The forward dome was removed from the converter case early 8/15 and given to manufacturing for the installation of a PRD. After an expeditious turn-around, the refurbished forward dome was received at Bldg. 800 at 1800 hours, 8/15, and transferred back into LAS #2. The dome was positioned onto the case with a new P5 "C"-seal in place and screw torqueing sequences began at 2400 hours, 8/15, and continued through 1500 hours, 8/16. After approximately 15 torqueing sequences over this period, the specified less than 2-mil gap at the dome/case interface could not be attained. NR-43268 was written to cover this discrepancy and its preliminary disposition was to continue on with the next operation, which was pressure decay testing. The RTG was pressurized with argon to 25 psia and the pressure decay test which started at 0200 hours, 8/17, yielded a leak rate of 0.0 psi/six hours.

LAS #2 was opened and the RTG removed on the slide tray assembly at 1330 hours, 8/17. After successful mating of the PRD tube to the support bracket, the installation of the RTG into its shipping container (RTG-SC) began at 1600 hours, 8/17. Shortly thereafter, it was found that the SC vent valve fitting was severely galled and would not accept a pneumatic connection. RTG operations were suspended until 0130 hours, 8/19, to allow the SC vent valve replacement. Installation into the SC was then completed at 1100 hours, 8/19.

11.2.1.2 Pre-Vibration Air Performance/Pressure Decay Test

Transfer of the F-2 RTG from Bldg. 800 to Bldg. 400 was completed at 1500 hours, 8/19. The unit then remained in its RTG-SC while awaiting the facility set-up for the pre-vibration performance testing. Early 8/23, the unit was removed from the RTG-SC and after it was installed in the handling sling, another torqueing sequence was performed at the forward dome/case interface per a secondary disposition on the previously mentioned NR-43268. There was no improvement (lessening) in the gap which still ranged up to 5 mils. The final disposition of this NR, after completion of pressure decay testing, was to accept the condition "as is".

The RTG was hoisted out of the handling sling cradle and positioned on the vibration slip table at 1400 hours, 8/23. Operations on the RTG were then suspended until 8/27, while the check-out of the newly designed "G2" Readout Console (ROC) was completed.

The electrical cables and pneumatic flex hoses were interconnected with the RTG early 8/27. During a routine scan on the "G2" ROC's Digitrend Data-Logger, it was noticed that the Digitrend's reference voltage gave an improper indication. A decision was made shortly thereafter to replace the "G2" ROC with a "G1". After the exchange and check-out of the "G1" ROC, Segment Readiness to allow the start of performance testing was completed at 1500 hours, 8/28.

RTG load was switched from short-circuit to loaded mode and stability at 30 volts load for the start of the air performance/pressure decay test was achieved early 8/29. Output power over the 48-hour test duration averaged 82.1 watts and rate of pressure decay was 0.07 psi/48 hours.

11.2.1.3 OA Vibration Test

The F-2 RTG had been set-up on the vibration slip table in the X-axis orientation prior to the start of the above air performance/ pressure decay test. Upon completion of that test, the clevis blocks were torqued to the slip table plate and vibration testing was ready to begin.

The vibration cycle in the X-axis, consisting of a 1/2G sine sweep from 20-2000 Hz, a 15-to-20-second burst of random vibration at 3.18G (rms) overall level for system equalization and a 60-second burst of OA random vibration at 9.54G (rms) overall level, was performed over the period 0935 to 1040 hours, 8/31.

After verifying that there was no thermopile circuit or structural degradation due to the X-axis vibration application, the RTG was rotated on the slip table to the Z-axis. The clevis blocks were torqued to the vibration plate and the Z-axis vibration cycle (same sequence as the X-axis above) then ran from 2030 to 2140 hours, 8/31. There were no anomalous indications during the vibration application and post-test data scanning and visual examination showed no degradation.

11.2.2 F-3 RTG

11.2.2.1 Storage Operations

As previously reported, the F-3 RTG had been received from Lincoln Laboratory, Lexington, Mass. on 6/18/75 and placed into storage in Bldg. 800.

The unit remained in storage in its RTG-SC until 7/14 when it was transferred to the Bldg. 800 test area for the taking of RTG and IHS gas samples. During the operation of connecting the pneumatic line from the gas service cart to the RTG vent valve port on the shipping container, it was found that the threads on the vent valve fitting were severely galled. A management decision was made shortly thereafter to postpone the gas sampling until just prior to the forthcoming dome exchange. F-3 was then returned to storage early 7/15.

On 7/17, the shipping container pressure was reduced from 8.0 psig to 5.5 psig so as to maintain an approx. 2.5 psi pressure delta between the RTG and the SC. RTG internal pressure was 8.5 psig at that time and could not be readily increased due to inability of mating the gas cart to the RTG vent valve port. These operations were performed again on 7/31, when the SC pressure was reduced to 4.2 psig with RTG pressure at 6.7 psig and on 8/19, when the SC pressure was reduced to 2.6 psig with RTG pressure at 5.1 psig.

11.2.3 F-4 RTG

11.2.3.1 OA Vibration Test

As previously reported, the F-4 RTG had been set-up in the Bldg. 400 vibration facility on the slip table in the X-axis configuration. The pre-vibration air performance/pressure decay testing had been completed on 6/29 with the RTG load voltage at 26 volts rather than the specified 30-volt load due to a gradual increase in helium concentration in the converter.

After the clevis blocks were torqued to the slip table at 0130 hours, 7/1, the vibration testing was ready to begin.

The vibration cycle in the X-axis, consisting of (1) a 1/2G sine sweep from 20-2000 Hz, (2) a 15-to-20-second burst of random vibration at 3.18G (rms) overall level for system equalization and (3) a 60-second burst of OA random vibration at 9.54G (rms) overall level, was performed over the period 0320 to 0450 hours, 7/1.

After verifying that there was no thermopile circuit or structural degradation due to the X-axis vibration application, the RTG was rotated on the slip table to the Z-axis. The clevis blocks were torqued to the vibration plate and the Z-axis vibration cycle then ran from 1900 to 2115 hours, 7/1. There were no anomalous indications during the vibration application and post-test data scanning and visual examination showed no degradation.

With the completion of the lateral axes testing, the RTG was hoisted from the slip table and set-up on the exciter head for the longitudinal (Y-axis) vibration. The Y-axis vibration cycle was performed over the period 1415 to 1630 hours, 7/2, with no degradation to RTG integrity.

During the course of the vibration test cycle, there had been recurring problems in evacuating the pneumatic flex hose up to the RTG-GMV. The requirement of a less than 100 microns evacuation level and less than 100 microns/minute leak-up rate was just marginally being met. Initially the difficulty was thought to be caused by a faulty "O"-ring at the quick-disconnect at the RTG flex hose to GSC flex hose interface. This "O"-ring was replaced early 7/2, after the Z-axis vibration, but there was no improvement in the ultimate vacuum level achieved.

A helium mass spectrometer was used on 7/2 to ascertain where the leakage points were in the RTG flex hose interconnections. The above mentioned quick-disconnect interface showed negligible leakage, while the connection at the RTG flex hose to RTG-GMV interface showed a positive leakage indication. A plan was formulated to add a fitting saver at this interface to eliminate the leakage. This fitting saver had just been recently designed for the salvaging of the damaged RTG-GMV on the F-2 RTG and would be installed on F-4 after it was transferred to Bldg. 300.

A management decision was made to postpone the post-vibration 48-hour air performance/pressure decay test until after the transfer of the F-4 RTG to Bldg. 300 for thermal-vacuum testing. An abbreviated pressure decay test of 9-hour duration was performed while the unit was still on the vibration exciter head, but this test was run under unstable conditions. Pressure decay indicated 0.32 psi/9 hours; however, the room temperature heat sink dropped from 88°F to 81°F over this time frame, causing a case temperature drop of 3°C. This drop in case temperature contributed significantly to the high leak rate.

The F-4 RTG was hoisted from the vibration exciter head and installation into the RTG-Shipping Container began at 0915 hours, 7/3. Installation operations were then completed at 0100 hours, 7/4.

11.2.3.2 Preparations for Post-Vibration Air Performance/ Pressure Decay Testing and Thermal-Vacuum Testing

The F-4 RTG remained in storage in its shipping container in the Bldg. 400 vibration facility until early 7/10, when it was transferred to the Bldg. 300 Long Life Lab. The operations of removing the RTG from the SC then began. During the course of these operations, IHS and RTG gas samples were taken for mass spectrographic analysis. The removal from the SC was completed with the RTG installed in the handling sling on the platform outside of the Long Life Lab at 1500 hours, 7/11.

Prior to transferring the RTG to thermal-vacuum chamber #3, a fit check was performed at the RTG's uniballs using a Lincoln Lab truss yoke and three clevi. There were no difficulties encountered in making this hardware interface gauging.

The RTG was moved from the handling sling to the portable lift truck and routed to T/V chamber #3, where it was installed onto the chamber's support frame at 0200 hours, 7/12.

The fitting saver was received early 7/16 and installed at the RTG-GMV to RTG flex hose interface. No improvement was then seen in the evacuation level of the RTG pneumatic lines. During 7/16, the fitting saver to flex hose interface was torqued to 100 inch-lb. and then 120 inch-lb. with still no improvement in evacuation level, which was running at approximately 250 microns. Operations were suspended late 7/16 to await further MRB direction.

At 1000 hours, 7/17, this direction was received. The fitting saver was removed from the RTG-GMV and a visual inspection showed that its "MS" ferrule was not properly set. A helium mass spectrometer test on the fitting saver was then performed and indicated excessive leakage at the "MS" ferrule. The fitting saver was then reworked by a proper pre-setting of the "MS" ferrule and the saver and RTG flex hose were re-installed onto the RTG-GMV at 2200 hours, 7/17. The evacuation level of the RTG pneumatic lines improved from the previously-attained 250 microns level to 125 microns. The fitting saver to RTG-GMV interface was then torqued to 120 inch-lb. (initial installation had been 80 inch-lb.), but there was no subsequent improvement in the evacuation level, which remained at approximately 125 microns.

Early 7/18, the fitting saver was again removed from the RTG-GMV. Its end was plugged and an evacuation test on the fitting saver yielded 70 microns. The fitting saver and flex hose were again installed onto the RTG-GMV and the same as earlier 120-to-130-micron evacuation level was attained.

As the RTG internal pressure had not been monitored for several days, the pneumatic lines were backfilled to 25 psia and the RTG-GMV was opened at 1400 hours, 7/8. RTG pressure indicated 20.35 psia, which was a pressure decrease of 4.66 psi/181 hours.

Based upon all of the investigations related to the 125-micron ultimate evacuation level in the pneumatic lines going to the RTG-GMV, there was a suspicion that there was leakage across the GMV's seat. Plans were made to continue with the diagnostic testing after the completion of thermal-vacuum testing.

Direction was given to proceed with the preparations for the post-vibration air performance/pressure decay test. During the evacuation of the pneumatic system between the Gas Service Cart and the RTG-GMV, early 7/19, it was determined that the chamber penetration fitting between the internal and external backfill solenoid valves was leaking. These two solenoid valves were for the automatic backfilling of the RTG in the event of a loss-of-vacuum in the chamber. Since there is a manual system in parallel with the automatic system, approval was received late 7/19 to perform subsequent testing with the two backfill solenoid valves deactivated (via the removal of their electrical connectors). This effectively isolated the leaking section of the pneumatic system and precluded air in-leakage at the backfill valve chamber penetration fitting from reaching the RTG.

11.2.3.3 Post-Vibration Air Performance/Pressure Decay Test

The chamber #3 door was secured and the shroud was set-up for an 80°F heat sink at 2300 hours, 7/19. Conditions were stable for the start of the 48-hour test at 0100 hours, 7/20. Output power averaged 69.7 watts over this duration and the rate of pressure decay was 0.86 psi/48 hours.

11.2.3.4 Thermal-Vacuum Performance Test

Chamber evacuation for the start of the F-4 RTG T/V test was initiated at 1800 hours, 7/23. After the chamber had attained below 100 microns, the RTG evacuation through the Gas Service Cart began and by 2130 hours, 7/23, chamber pressure was 2 x 10^{-4} torr with RTG internal pressure at approximately 1000 microns. By 0400 hours, 7/24, RTG internal pressure had been reduced through the Gas Service Cart to 350 microns and after isolating the cart, pulse venting of the RTG's remaining gas load into the chamber began. Chamber pressure increased from the high 10^{-5} torr range into the low 10^{-4} torr range. Since there was no progress in the RTG venting operation, a decision was made to reduce the IHS internal pressure, as it was believed to be contributing to the large RTG gas load. By 0900 hours, the IHS internal pressure had been reduced from approximately 16 psia to 1.75 psia. RTG evacuation through the Gas Service Cart resumed and after attaining the 80 micron level, the RTG was vented directly into the chamber at 1400 hours, 7/24.

Chamber pressure held in the high 10^{-5} torr range after the above RTG venting and slowly dropped into the mid and then the low 10^{-5} torr range over the period to 1100 hours, 7/28. Numerous attempts had been made at bringing the chamber's ion pump on-line in parallel with the roughing pump in order to reduce chamber pressure into the 10^{-6} torr range. Finally at 1100 hours, 7/28, the ion pump cavity could remain open without the pump being saturated and chamber pressure then quickly dropped to the mid 10^{-6} torr.

Thermal-vacuum performance testing ended at 1500 hours, 7/28, with RTG output power stabilized at 157.6 watts.

11.2.3.5 Post T/V Air Performance/Pressure Decay Testing

Segment Readiness Review to allow the backfilling of the F-4 RTG to end T/V testing was held at 1800 hours, 7/28. After the Health Physicist had obtained an acceptable IHS radiological sample, the IHS pressurization with helium to 9 psia, its first backfilling plateau, began. Shortly after the start of IHS backfilling, chamber pressure increased into the 10^{-4} torr range and effected a loss-of-vacuum signal. The RTG was immediately backfilled with argon to 17 psia. The cause of the increased chamber pressure is attributed to the increased rate of helium leakage into the chamber after the IHS backfilling began. Throughout the T/V test cycle, the IHS had been leaking into the F-4 converter and then into the chamber via the open venting valve.

With the RTG already backfilled to 17 psia via the emergency system, the IHS was pressurized to 16 psia at 0600 hours, 7/29. The RTG pressure was subsequently increased to 25 psia and chamber backfilling with dry N_2 to one atm was completed at 1100 hours, 7/29.

The chamber shroud, which had been running at 100°F for T/V testing, was adjusted to 80°F for "air" mode testing and the unit was allowed to thermally stabilize. Thermal stability was achieved at 1630 hours, 7/29, for the start of the 48-hour post-T/V air performance and pressure decay test in the closed chamber #3. Testing was completed at 1630 hours, 7/31, and yielded a rate of pressure decay of 0.87 psi/48-hours. Power output at the start of this period was 79.26 watts and decreased to 77.56 watts after 48 hours due to the helium build-up from the leaking IHS which changed foil conductance.

11.2.3.6 Post Acceptance Test Operations

The chamber door was opened at 2130 hours, 7/31, and the task of RTG removal from the chamber and installation into the RTG-SC began then and was completed at 2330 hours, 8/1. The transfer of the F-4 RTG to the Building 800 storage area was completed at 0100 hours, 8/2.

On 8/7, the RTG-SC containing F-4 was moved to the Building 800 test area for the obtaining of an IHS gas sample and additional diagnostic testing to determine the source of leakage at the RTG-GMV.

Early 8/8, the RTG-SC was opened to allow access to the IHS-GMV. After opening the IHS-GMV, IHS pressure indicated 21.75 psia as read on the 3499G1 gas tap adaptor. An IHS gas sample was collected in the evacuated sample bottle and the IHS was then repressurized with helium gas to 16 psia.

The RTG was removed from the SC and set-up in the test area, suspended from the RTG-SC lid, for the start of the diagnostic testing. Sniffing operations using the helium mass spectrometer showed insignificant external leakage at the pneumatic connections to the RTG-GMV.

A 6-hour pressure decay test on the RTG was initiated late 8/8. This decay test was different from previous tests in that the pneumatic line to the RTG-GMV was bled down to 14.7 psia (after the GMV was closed to isolate the RTG) between decay measurements so as to have a 10 psi delta across the RTG-GMV seat. This test yielded a leak rate of 0.52 psi/6-hours as opposed to the test completed on 7/31 which yielded a rate of 0.87 psi/48-hours. The 10-psi delta across the RTG-GMV seat was the difference between the two decay tests and with there being a significant difference in their leak rates, the suspicion that there was leakage across the RTG-GMV seat was virtually confirmed.

The operations of installing the F-4 RTG into its SC were completed at 1400 hours, 8/9, and the unit was placed into the Building 800 storage area.

On 8/14, preparations were started for shipment of the F-4 RTG to Mound Laboratory for storage. After the RTG was partially hoisted out of the SC and the IHS-GMV closed, the RTG was secured into the SC. A final RTG gas sample was then taken late 8/15.

The ERDA SST van arrived early 8/16, but problems with its air conditioning system delayed the loading of the F-4 RTG until 8/18. The F-4 RTG was secured into the van late 8/18 and approval was given to transfer the unit to Mound Lab for storage purposes until it is shipped to the Cape for launch activities.

11.2.4 F-5 RTG

11.2.4.1 F-5 RTG Assembly and Processing Operations

The S/N-5 IHS, in its SPC, was installed into the LAS #1 load lock late 7/7. After the SPC dome removal was completed, the disassembly of the tripod and valve assemblies and vent tube straightening were completed 7/8.

The IHS was hoisted out of the SPC late 7/8 and after dimensional gauging operations proved acceptable, the gantry position was changed from the 0° to the 90° LAS station and the installation of the ablation sleeve was completed.

The IHS was routed to its position over the converter and after establishing IHS/converter concentricity, the IHS was lowered and seated into the converter without incident early 7/9. The forward graphite end cap was seated onto the IHS and the forward end enclosure assembly was installed. Preliminary preloading of the support system was accomplished mid 7/9, and after achieving thermal stabilization, final preloading of 29.5 mils dial indicator deflection was completed early 7/10. Final support system operations -- preload screw packing, retainer installation and preload screw/bushing lockwiring -- were also completed early 7/10. IHS vent tube forming, routing and interconnection to its case feed-through fitting were completed and an IHS gas sample was then obtained mid 7/10. The IHS was pressurized with helium to 19 psia for a short pressure decay test which yielded an IHS leak rate of 0.02 psi/one-hour. This test was then repeated and yielded a rate of 0.03 psi/one-hour.

Preparations were then made for the RTG processing cycle in the LAS. After the IHS pressure had been reduced to 2 psia, chamber evacuation for the start of processing began at 0900 hours, 7/11. The first IHS gas sample was taken at 8 hours after the start of chamber evacuation, and subsequent samples were taken at 14, 20, 27, 35, 58 and 84 hours (1800 hours, 7/14).

During the above period of processing, the chamber pressure had been running in the low 10^{-4} torr range, which was approximately two decades higher than normal. Coupled with the inability to achieve the desired vacuum (less than 1×10^{-5} torr), there were spurious electrical discharges within the chamber whenever the chamber's ion gauge filament was on. It was believed that these discharges were ionized gas molecules randomly striking the metal surfaces of the chamber and its fixturing. The phenomenon had not previously been experienced on the MHW program, since there had never been a prolonged period of 10^{-4} torr vacuum level with an ion gauge filament energized.

Approval was given to suspend the vacuum processing in order to investigate for the source of chamber leakage and the chamber was backfilled to one atmosphere of argon at 2000 hours, 7/15. The suspected source of leakage was at either the inlet or outlet valve isolating the chamber from the facility gas management system. Both of these valves were cycled several times and indications were that faulty valve seating had indeed been the problem and the situation had been corrected. The roughing pump system was again opened up to the chamber to resume vacuum processing at 2100 hours, 7/15. However, the chamber had to almost immediately be backfilled with argon again as there was an indication that the roughing pump was starting to seize-up. The LAS #1 was maintained under a "scrubbed" argon environment while repairs were made to the pump.

Repair of the seized roughing pump was completed at 1500 hours, 7/16. Prior to again initiating chamber evacuation, IHS gas sample #8 was obtained and at 2130 hours, 7/16, pumpdown began, with the chamber attaining a vacuum level of 3 x 10^{-5} torr at 2400 hours, 7/16. IHS gas sampling was resumed at 0630 hours, 7/16, with sample #9 being drawn. Vacuum processing then continued until mid-7/26 with daily IHS sampling being performed, giving a total of 22 IHS gas samples being obtained since the start of processing on 7/11.

In addition to the gas sampling, the IHS was purged every 2-3 hours for the first 72 hours of processing and then once daily through termination. The purging cycles consisted of an evacuation of the IHS for a one-half hour period after the 1000 micron level had been achieved (usually attaining below 500 microns) and then backfilling with helium to 10 psia. A total of 62 purge cycles were performed over the processing duration.

Direction was received early 7/26 to terminate the vacuum processing. After the final IHS purge cycle at 1000 hours, the chamber was backfilled to one atmosphere of argon at 1300 hours, 7/26. Operations were then suspended until 7/28 with the facility gas purification system in the "scrubbing" mode.

After the Health Physicist had inspected the LAS atmosphere radiologically and given his approval to continue with operations, the IHS was pressurized to 19 psia late 7/28 and at 2000 hours, 7/28, an IHS pressure decay test was initiated, yielding a leak rate of 0.0 psi/one-hour.

The flight-configured forward dome was transferred into the chamber through the load lock at 2200 hours and placed onto the converter case. Dome screw installation began early 7/29. After ten screw-torqueing sequences, the less-than-2-mil gap at the dome/case interface could not be attained at a perimeter length covering 3 screws.

Late 7/29, after pressurizing the RTG to 25 psia, a 6-hour pressure decay test was started and yielded an acceptable 0.07 psi pressure delta which indicated that the above-mentioned greater-than-2-mil gap was not significantly degrading the leak rate.

LAS #1 chamber door was opened early 7/30, and the F-5 RTG was removed on the slide tray. After PRD-tube-to-PRD-bracket mating was completed, the operations of installing the RTG into the SC began at 1730 hours, 7/30, and were completed at 1445 hours, 7/31.

11.2.4.2 Mass Properties Testing

Transfer of the F-5 RTG from Bldg. 800 to Bldg. 400 was completed at 1000 hours, 8/1. Operations were then suspended until 8/4. Preparations for weight and CG measurement and the subsequent vibration test were completed mid-8/6 and the operations of removing the RTG from the SC began. Early 8/7, a significant problem was encountered during these operations. Upon attempting removal of the RTG-SC lid from the RTG mono-balls, after the RTG was installed onto the handling sling, it was found that one of the pins securing a mono-ball to a lid clevis had seized. Considerable effort was expended in the removal of this pin (along with excess exposure to personnel) and it finally had to be driven out. A design change in the method of attaching the RTG mono-balls to the SC lid clevi was subsequently initiated but hardware changes will not come into effect until SC use on MJS RTG's.

After the RTG removal from the SC was completed at 0700 hours, weight and center of gravity measurements were performed, being completed mid-8/7.

11.2.4.3 Pre-Vibration Air Performance/Pressure Decay Testing

The RTG was transferred from the CG fixture cradle and positioned on the vibration slip-table. After interconnection with the Readout Console and Gas Service Cart, the RTG load was changed from short circuit to loaded mode. Thermal stability at 30-volt load was achieved at 0500 hours, 8/8, for the start of the pre-vibration air performance/

pressure decay test. Output power averaged 81.6 watts over the 48-hour duration and rate of pressure decay was 0.03 psi/48-hours.

11.2.4.4 OA Vibration Test

The F-5 RTG had been set-up on the vibration slip table in the X-axis orientation prior to the start of the pre-vibration air performance/ pressure decay test. Upon completion of that test, the clevis blocks were torqued to the slip table plate and vibration testing was ready to begin.

The vibration cycle in the X-axis, consisting of a 1/2G sine sweep from 20-2000 Hz, a 15-to-20-second burst of random vibration at 3.18G (rms) overall level for system equalization and a 60-second burst of OA random vibration at 9.54G (rms) overall level, was performed over the period 0920 to 1140 hours, 8/10.

After verifying that there was no thermopile circuit or structural degradation due to the X-axis vibration application, the RTG was rotated on the slip table to the Z-axis. The clevis blocks were torqued to the vibration plate and the Z-axis vibration cycle (same sequence as the X-axis above) then ran from 1920 to 2100 hours, 8/10. There were no anomalous indications during the vibration application and post-test data scanning and visual examination showed no degradation.

With the completion of the lateral axes testing, the RTG was hoisted from the slip table and set-up on the exciter head for the longitudinal (Y-axis) vibration. The Y-axis vibration cycle was performed over the period 0910 to 1030 hours, 8/11, with no degradation to RTG integrity.

11.2.4.5 Post-Vibration Air Performance/Pressure Decay Test

After the vibration testing was completed, the RTG remained on the exciter head (Y-axis orientation) for the post-vibration performance testing. This testing ran from 1630 hours, 8/11, until 1630 hours, 8/13. Output power average 81.6 watts over this time period and the rate of pressure decay was 0.07 psi/48 hours.

11.2.4.6 Preparations for Thermal-Vacuum Testing

Upon completion of the post-vibration air performance and 48-hour pressure decay test, the F-5 RTG was hoisted from the vibration exciter head and installation into its shipping container began at 2100 hours, 8/13; installation operations were then completed by 1400 hours, 8/14.

Transfer of the F-5 RTG in its SC to the platform outside of the Bldg. 300 Long Life Lab was accomplished at 1800 hours, 8/14. However, the unit had to be transferred back to Bldg. 800 late 8/15 in order to accomplish some rework that was required on the SC. This was the replacement of the IHS and SC vent valves on the shipping container, which had to be performed in a radiologically controlled, ventilated area. After valve replacement, the unit was again transferred to the Bldg. 300 Long Life Lab mid-8/18. Removal of the unit from its SC began at 2200 hours, 8/19, and the RTG was installed in the handling sling by 1430 hours, 8/20. In parallel with the above operations, the chamber, data acquisition system, Readout Console and general facility check-outs were completed.

The RTG was moved from the handling sling to the portable lift truck and routed to T/V chamber #3 where it was installed onto the chamber's support frame at 1700 hours, 8/20. Pneumatic flex hose and electrical cable interconnections between the RTG and chamber penetrations were completed and the Segment Readiness Review certifying test preparedness was completed at 2245 hours, 8/20.

After the gas service cart lines had been purged/evacuated, the IHS and RTG-GMV's were opened, the chamber door was secured and all preparations for chamber evacuation were completed at 0200 hours, 8/21.

11.2.4.7 Thermal-Vacuum Performance Testing

Chamber evacuation for the start of T/V testing on the F-5 RTG was initiated at 0340 hours and by 0700 hours, 8/21, a vacuum of 1×10^{-4} torr had been achieved. The RTG evacuation through the Gas Service Cart then began and at 1030 hours, 8/21, chamber pressure was 5×10^{-6} torr and RTG internal pressure was 70 microns. After isolating the gas service cart from the RTG, pulse venting of the RTG's remaining argon fill gas into the chamber began and by 1040 hours, 8/21, the venting valve could remain open. Chamber pressure then increased into the 10^{-5} torr range until 1130 hours, 8/21, when the 10^{-6} torr range was again achieved. The mid, then low, 10^{-6} torr range was held for the remainder of T/V testing.

After the Health Physicist had obtained an IHS radiological sample, the IHS was de-pressurized to 2 psia at 1400 hours, 8/22. With the decrease in IHS helium pressure, there was no distinct corresponding drop in chamber pressure as there had been on the F-4 RTG.

Stability was achieved at 1800 hours and the four-hour T/V performance test was completed at 2200 hours, 8/22. RTG output power was 159.5 watts at that time.

11.2.4.8 Post T/V Air Performance/Pressure Decay Testing

Segment Readiness Review to allow the backfilling of the F-5 RTG to end T/V testing was completed at 2300 hours, 8/22.

After the Health Physicist obtained an IHS radiological sample, the IHS pressure which had been at 2.32 psia just prior to sampling, was increased to its first backfilling plateau of 9 psia at 0100 hours, 8/23. Backfilling of the converter with argon then began and by 0400 hours, the first pressure plateau of 17 psia for the converter was achieved. The IHS pressure was increased from 9 psia to 16 psia and by 1400 hours, the converter had been pressurized to 25 psia.

Chamber backfilling with dry N_2 then began, and after attaining 13.6 psia, the chamber atmosphere was verified as being radiologically acceptable by the Health Physicist. He gave his approval to continue with the nitrogen backfill and chamber pressure was one atmosphere at 1900 hours, 8/23.

The chamber shroud, which had been running at 100^{o}F for T/V testing, was adjusted to 80^{o}F for "air" mode testing and the RTG was allowed to thermally stabilize. Thermal stability was achieved at 2300 hours, 8/23, for the start of the 48-hour post-T/V air performance and pressure decay test in the closed chamber #3. Output power over this test duration averaged 80.4 watts and the rate of pressure decay was 0.10 psi/48 hours.

11.2.4.9 Post-Acceptance Test Operations

The chamber door was opened at 0230 hours, 8/26, the task of RTG removal from the chamber and installation into the RTG-SC began then and was completed at 0200 hours, 8/27. The transfer of the F-5 RTG to the Building 800 storage area was completed at 0300 hours, 8/27.

11.2.5 F-13 RTG

11.2.5.1 F-13 RTG Assembly and Processing Operations

The S/N-1 IHS, in its SPC, was installed into the LAS #1 load lock late 8/30. After the SPC dome removal was completed, the disassembly of the tripod and valve assemblies and vent tube straightening were completed 8/31.

The IHS was hoisted out of the SPC late 8/31 and after dimensional gauging operations proved acceptable, the gantry position was changed from the 0° to the 90° LAS station for the installation of the ablation sleeve.

13.0 GROUND SUPPORT EQUIPMENT

13.1 POWER SUPPLY AND READOUT CONSOLES

- All design changes were completed to meet LES 8/9 and MJS program requirements and corresponding new drawings and drawing modifications were issued to incorporate these changes.
- Two RTG panels, one RTD panel and console wiring were modified and checked out to the new requirements.
- Calibration procedures were written for new RTG and RTD panel designs.
- Revisions were prepared and issued for the LES 8/9 Readout Console acceptance test procedure, system checkout procedure and operating manual.

13.2 RTG SHIPPING CONTAINERS

All units required for LES 8/9 have been updated to the latest AN and are available for use.

13.3 STORAGE AND PROTECTION CONTAINERS

Modification was completed on the first SPC for MJS, and this unit was shipped to MRC for use with the Q2 IHS.

13.4 LOADING AND ASSEMBLY STATIONS

13.4.1 LAS 1

The F5 converter was installed into LAS 1 on July 1 for loading/processing and evacuation was started at 0230 hours the next day with backfilling occurring at 1300 hours. By 2000 hours, purity levels were within specifications except for the H_2O content which was at 10 ppm; however, GE Engineering approved a procedure variation which permitted an immediate start of the operation to remove the dome.

The IHS was passed into the LAS on July 7, and after it was loaded into the F5 converter, the LAS was evacuated for RTG processing on July 11. During this evacuation cycle it was impossible to evacuate the chamber below the mid 10^{-4} range and subsequent investigation revealed an Argon leak was present across the inlet valve of the Gas Management System. Also associated with this pressure range was an arcing condition whenever the ion gage was turned on. On July 15, operations were started to backfill LAS 1 and, by cycling of the inlet/outlet valves of the GMS to attempt to obtain a better "Seat" of the leaky valve. A procedure was written to evaluate the degree of success obtainable, before re-evacuating LAS 1 again, which indicated a "gross" improvement in the seal. The re-evacuation had to be aborted as a Stokes pump failure occurred when the chamber was at approximately 100 microns pressure.

The failure of the Stokes pump was caused by a plastic bag which had been sucked into the pump, blocking an oil line to the pump bearing. This plastic was evidently a "left-over" from the occurrence reported in the last reporting period where debris was dumped into the loadlock. Repairs were completed by 1400 hours on July 16; and re-evacuation was started at 2130 hours.

On July 30, maintenance was performed on the GMS inlet/outlet valves. Inspection revealed that a small thread-like wire lying across the O-ring had caused the leak. All valves on both LAS 1 and 2 were dismantled and cleaned and all O-rings were replaced.

Also on July 30, F5 RTG was removed from LAS 1, which was not used again until August 21 when F13 was installed, with evacuation starting on August 26. At the end of this reporting period F13 was still in LAS 1.

13.4.2 LAS 2

On July 8, screens were installed in the pump-out line of the loadlock in LAS 2. This rework was performed to prevent a re-occurrence of debris being sucked into the pump as previously reported.

On July 19, work on LAS 2 was started in preparation for F2 rework. Pumpdown of LAS 2 was started on August 13; and at 1330 hours on August 17, F2 was removed from LAS 2.

13.4.3 General

On August 8, a new hook-up was made to the emergency power bus which provides power to the ion gage readout panel during power failure conditions.